

CHARACTERIZATION OF 2<sup>ND</sup> GENERATION BIOMASS UNDER  
THERMAL CONVERSION AND THE FATE OF NITROGEN

JACOPO GIUNTOLI

Process and Energy  
Faculty 3mE  
Delft University of Technology



Characterization of 2<sup>nd</sup> generation biomass  
under thermal conversion and the fate of nitrogen

**Proefschrift**

ter verkrijging van de graad van doctor  
aan de Technische Universiteit Delft,  
op gezag van de Rector Magnificus prof. ir. K. C. A. M. Luyben,  
voorzitter van het College voor Promoties  
in het openbaar te verdedigen op woensdag 17 november 2010 om 15.00 uur

door

Jacopo GIUNTOLI

Ingenere Energetico, Politecnico di Milano  
geboren te Florence, Italië

Dit proefschrift is goedgekeurd door de promotor:

Prof. dr. ir. A. H. M. Verkooijen

copromotor:

Dr. ir. W. de Jong

Samenstelling promotiecommissie:

Rector Magnificus	voorzitter
Prof. dr. ir. A. H. M. Verkooijen	Technische Universiteit Delft, promotor
Dr. ir. W. de Jong	Technische Universiteit Delft, copromotor
Prof. dr. D. J. E. M. Roekaerts	Technische Universiteit Delft
Prof. dr. G. J. Witkamp	Technische Universiteit Delft
Prof. dr. ir. G. Brem	Universiteit Twente
Prof. dr. M. Hupa	Åbo Akademi University, Finland
Dr. ir. J. H. A. Kiel	Energy Research Centre of the Netherlands

This research was funded by the European Commission's INECSE programme.  
Contract nr. MEST-CT-2005-021018.

ISBN 978-90-9025803-4

Copyright © 2010 by Jacopo Giuntoli<sup>1</sup>

Cover image © 2010 by Kira. E-mail: kira\_in\_da\_club@hotmail.com

All rights reserved. No part of the material protected by this copyright notice may be reproduced or utilized in any form or by any means, electronic or mechanical, including photocopying, recording or by any information storage and retrieval system, without the prior permission of the author. An electronic version of this dissertation is available at <http://www.library.tudelft.nl>

Printed by Ipskamp drukkers, The Netherlands.

<sup>1</sup> Author e-mail contact: [jacopo.giuntoli@gmail.com](mailto:jacopo.giuntoli@gmail.com) and [j.giuntoli@tudelft.nl](mailto:j.giuntoli@tudelft.nl)

To my family and my dear Mahsa



*“My heart has become capable of every form:  
it is a pasture for gazelles and a convent for Christian monks,  
And a temple for idols and the pilgrim’s Ka’ba and the  
tables of the Torah and the book of the Koran.  
I follow the religion of Love: whatever way Love’s  
caravan take, that is my religion and my faith”*

Ibn Arabi, Tarjumân Al-Ashwâq

*“Dude, let’s go bowling”*

Walter Sobchak, The Big Lebowski





---

## SUMMARY

---

This dissertation deals with the characterization of several biomass materials under thermal conversion conditions using small-scale equipment. The fuels are tested under the conditions of slow and fast heating rate pyrolysis and combustion, with the main goal of investigating the chemistry of fuel-bound nitrogen.

New energy policies put forward in almost every country in the world, and especially in the European Union, are strongly promoting the use of renewable energy sources. Decreasing the use of imported fossil fuels in favour of locally available renewables is the answer to many energy-related problems of the 21<sup>st</sup> century: global warming, security of supply and high energy prices among some.

Among renewable sources, biomass materials hold a special position because they can, in the short term, substitute or integrate fossil fuels in all of their applications applying comparatively few changes to the existing equipment. Biomass wastes, from agriculture or other processes, are convenient in more respects since their use would not only substitute fossil fuels but it would also valorize waste streams.

These materials, however, present several issues that are highly delaying their deployment on a large scale. Three of the most important problems are dealt with in this thesis: the heterogeneous nature of the materials, high amount of ash forming matter containing troublesome compounds such as K, Cl and P, and finally, high content of nitrogen.

First of all, many biomass residues contain a higher amount of nitrogen compared with woody biomass or even coal. This high content of fuel-N could directly translate into high NO<sub>x</sub> emissions in combustion conditions or into a high content of nitrogen containing gases such as NH<sub>3</sub> and HCN in the syngas from gasification. Primary measures, such as air staging, can be applied directly in the reactor in order to promote the reduction of NO<sub>x</sub> and NO<sub>x</sub>-precursors to molecular nitrogen. However, in order to apply such measures and optimize the syngas composition or minimize emissions without relying on expensive catalysts, a detailed knowledge of the mechanisms of fuel-N conversion is required. This thesis has as its main purpose to study the release of volatile nitrogen compounds under pyrolysis conditions and the analysis of the emissions of NO under combustion conditions from high-N fuels.

Secondly, as explained in the first two chapters of this dissertation, the definition of biomass is very broad and it includes materials with extremely different composition and characteristics. Additionally, the interest in exploiting

some of these materials, such as manures, for energy conversion has never been high enough to trigger substantial research. As a consequence, fundamental data such as reactivity and products distribution are almost completely lacking for many biowastes. One of the purposes of this thesis is, therefore, to gather extensive fundamental data for potential fuels, which have not yet fully characterized.

Finally, some elements such as K, Cl, P and S, contained in biomass materials, are known to cause several problems during boiler operation. At high temperatures alkali silicates with melting temperatures lower than the operating one are formed; these partly molten particles can then create issues like slagging, fouling, loss of fluidization and, when Cl is present, corrosion of the boiler surfaces. Together with specific research on boiler materials and optimization of operating conditions, possible pre-treatments used to remove these compounds from the fuel before entering the reactor could greatly enhance the overall process. In this thesis, the effects of a water-leaching pre-treatment on the fuels' reactivity and product yields during pyrolysis are explored.

After a general introduction, Chapter 2 has the purpose of providing the reader with an overview of definitions and concepts that are used in the rest of the dissertation. The main components of biomass are listed as well as their behavior under thermal conversion conditions. A special focus is given to nitrogen structures, such as proteins and heterocyclic compounds, and the mechanisms of their decomposition under pyrolysis conditions as reported in available literature studies. Finally, an overview of NO<sub>x</sub> formation mechanisms is given.

The materials studied in this work and the setups used are introduced in Chapter 3. The materials are divided into two main categories: agricultural residues, including wheat straw, olive residues and peach stones, and biomass waste streams, including dry distiller's grains, palm kernel cake and chicken manure. All these materials have a high nitrogen content and are not yet fully exploited because of the issues mentioned above. Several different small-scale setups have been used in this work depending on the conditions that needed to be studied.

Chapter 4, then, presents the results of measurements performed on agricultural residues under slow pyrolysis conditions. The measurements were carried out using a thermogravimetric analyzer (TGA) connected with a Fourier Transform InfraRed spectrometer (FTIR). All the fuels presented peaks of reactivity at approximately 330 - 360 °C associated with the decomposition of cellulose. A shoulder was also found at lower temperatures, approximately 290 - 310 °C, and was associated with the pyrolysis of hemicellulose. The main volatile species released resulted to be CO<sub>2</sub> for all the fuels followed by CO and methane. No nitrogen compounds were detected because of too little concentrations in the pyrolysis gases which could not be accurately detected by the FTIR. The kinetic parameters for the pyrolysis reactions were found us-

ing a Distributed Activation Energy Model (DAEM). This analysis revealed a common reaction path for the main structures (cellulose and hemicellulose) among the various fuels. The water-leaching pre-treatment seemed very effective in removing the troublesome inorganic elements from these fuels. The removed elements, furthermore, had a catalytic effect on the pyrolysis of the fuels; once removed, the samples reacted at higher temperatures and with less reaction paths. Only the peach stones sample, which already had a very low ash content, did not seem to be affected by the treatment.

Chapter 5 reports the results of a similar analysis to the previous one, that was performed on different biomass residues: dry distiller's grains with solubles (DDGS) and chicken manure. Also these fuels were found to react with two main peaks at about 280 °C and 330 °C. Accordingly, also the kinetic parameters resulted very similar to the ones of the agricultural residues, clearly indicating a similar decomposition path for common structures. For DDGS and chicken manure, an additional component was found to react at approximately 400 - 430 °C and it was assigned to proteinic structures decomposing. The main volatile nitrogen compounds were found to be NH<sub>3</sub> and HCN for DDGS with traces of HNCO. The manure released more of its fuel-bound nitrogen in volatile form and the main compound was found to be HNCO, followed by HCN and ammonia. The water leaching pre-treatment, similarly to what was found for the peach stones sample, did not seem to affect substantially the reactivity of the fuels nor their ash composition. The share of fuel-N released as light volatiles, however, increased for the washed fuels.

Building up on the results of the previous two chapters, Chapter 6 describes the results of fast pyrolysis measurements of DDGS and palm kernel cake. These tests were carried out on a heated foil reactor integrated with an FTIR using much higher heating rates, closer to industrial applications. A numerical model of the reactor has been developed in order to have a better insight into the temperature and velocity profiles in the reactor chamber. The simulations, in combination with non-contact temperature measurements, have indicated a significant difference between the expected foil temperature and the actual one. This has been corrected in the experimental campaign, granting a more precise knowledge of the actual conditions.

The fast pyrolysis measurements have shown an increased weight loss compared to slow heating rates. CO<sub>2</sub> resulted to be still the main light volatile at temperatures below 900 °C while CO became more relevant at high temperatures due to tar cracking in the hot area around the foil. Compared to low heating rates measurements of the DDGS sample, HCN was the main volatile nitrogen compound while the yield of NH<sub>3</sub> was much lower. The palm kernel cake sample only released detectable yields of HCN, nor ammonia nor HNCO were found. Even at high temperatures, approximately 10% of the initial N was retained in the char of DDGS. The water leaching pre-treatment again did not affect the weight loss behaviour neither the main gaseous product

distribution but the yields of light volatile nitrogen compounds increased for the washed samples.

After the pyrolysis behaviour of different nitrogen compounds has been analyzed, Chapter 7 presents the results of measurements under combustion conditions for several biomass residues. It is shown that the devolatilization profiles for carbon to CO + CO<sub>2</sub> and fuel-N to NO are very similar among very different fuels, implying that a common approach could be taken for their modeling and it could very well be acceptable as a first approximation. Moreover, the conversion of fuel-N to NO appeared to follow a decaying trend where the fuels with lower initial N content presented a higher conversion than fuels with higher nitrogen content. Fuels with high nitrogen content, in fact, are likely to release a larger amount of it in volatile form with a consequent larger amount of NH<sub>3</sub> radicals available for thermal De-NO<sub>x</sub> reactions. Finally, the release of carbon as CO<sub>2</sub> and nitrogen as NO during devolatilization was found to be proportional for temperatures around 800 °C while at 1000 °C almost all of the NO was released during devolatilization.

Finally, in Chapter 8 the main conclusions of the work described in thesis are drawn and recommendations for future research are expressed.

Jacopo Giuntoli

---

## SAMENVATTING

---

Dit proefschrift behandelt de karakterisering van verschillende soorten biomassa door middel van thermische conversie, gebruikmakend van kleinschalige apparatuur. De brandstoffen zijn getest onder condities van pyrolyse met zowel langzame als snelle verhitting, alsmede verbranding met als belangrijkste doel het bestuderen van de brandstofgebonden stikstofchemie. Nieuwe voorgestelde energiebeleidsmaatregelen in bijna elk land ter wereld en in het bijzonder in de Europese Unie bevorderen sterk het gebruik van hernieuwbare energiebronnen. De afname van het gebruik van geïmporteerde fossiele brandstoffen ten gunste van de inzet van lokaal beschikbare hernieuwbare energiebronnen is het antwoord op veel energie gerelateerde problemen in de 21<sup>e</sup> eeuw: de opwarming van de aarde, zekerstelling van de energievoorziening en hoge energieprijzen, om maar een paar te noemen.

Biomassa neemt een bijzondere positie in te midden van de hernieuwbare bronnen omdat het op de korte termijn fossiele brandstoffen kan vervangen of ermee geïntegreerd kan worden in alle toepassingen met relatief weinig aanpassingen aan de bestaande technologie. Biomassa residuen afkomstig uit de landbouw of andere processen zijn in meerdere opzichten geschikt aangezien hun gebruik niet alleen substitutie van fossiele brandstoffen omvat, maar ook een valorisatie van afvalstromen betekent.

Deze materialen, echter, geven aanleiding tot verscheidene problemen die hun toepassing op grote schaal sterk vertragen. Drie van de belangrijkste problemen worden in dit proefschrift behandeld: de heterogene aard van de materialen, de grote hoeveelheid asvormend materiaal dat probleemcomponenten als K, Cl en P bevat en tenslotte het hoge gehalte aan stikstof.

Allereerst vertonen veel biomassa residuen een hoger stikstofgehalte in vergelijking met houtachtige biomassa of zelfs kolen. Dit hoge brandstofgebonden stikstofgehalte kan direct aanleiding geven tot hogere NO<sub>x</sub> emissies onder verbrandingscondities of in een hogere concentratie van stikstofhoudende gassen, zoals NH<sub>3</sub> and HCN in synthesegas afkomstig van vergassing. Primaire maatregelen zoals getrapte luchttoevoer kan direct in de reactor plaatsvinden om reductie van NO<sub>x</sub> en precursors van NO<sub>x</sub> in moleculair stikstof te bevorderen. Echter, om zulke maatregelen toe te kunnen passen en de synthesegas samenstelling te optimaliseren zonder afhankelijk te zijn van dure katalysatoren, is een gedetailleerde kennis nodig van de mechanismes van brandstofgebonden stikstofconversie. Het belangrijkste doel van dit proefschrift is het bestuderen van het vrijkomen van vluchtige stikstofcomponenten onder pyrolyse condities alsmede de analyse van de NO emissies van brandstoffen met een hoog stikstofgehalte.

Ten tweede, zoals wordt uitgelegd in de eerste twee hoofdstukken van dit proefschrift, is biomassa erg breed gedefinieerd en omvat het materialen met extreem verschillende samenstellingen en karakteristieken. Daar komt bij, dat de interesse in de inzet van deze materialen, zoals mest, nooit groot genoeg is geweest om aanzet te geven tot substantieel onderzoek. De consequentie is, dat fundamentele data, zoals reactiviteit en productverdeling, bijna volledig ontbreken voor veel biomassa residuen. Een van de doelen van dit proefschrift is daarom om uitgebreid fundamentele data te verzamelen voor potentiële brandstoffen die nog niet volledig gekarakteriseerd zijn.

Tenslotte staan sommige elementen in biomassa, zoals K, Cl, P en S, bekend als veroorzakers van verscheidene problemen gedurende het bedrijven van boilers. Bij hoge temperaturen worden alkali-silicaten gevormd met smelttemperaturen lager dan de bedrijfstemperaturen; deze deels gesmolten deeltjes kunnen dan problemen veroorzaken, zoals verslakking, vervuiling, fluidisatieverlies en -wanneer Cl aanwezig is- corrosie van boileroppervlakken. Tezamen met specifiek onderzoek naar boilermaterialen en optimalisatie van bedrijfscondities, kunnen mogelijke verbeteringen, toegepast met het oog op verwijdering van deze componenten voordat de brandstof in de reactor wordt geïnjecteerd, de gehele procesvoering sterk verbeteren. In dit proefschrift worden de effecten op brandstofreactiviteit en product opbrengsten van voorbewerking middels uitloging met water bestudeerd.

Na een algemene inleiding heeft hoofdstuk 2 als doel om de lezer te voorzien van een overzicht van definities en concepten die in de rest van het proefschrift worden gebruikt. De belangrijkste componenten van biomassa worden beschreven, alsmede hun gedrag onder condities van thermische conversie. Speciale aandacht is er voor de stikstofstructuren, zoals eiwitten en heterocyclische verbindingen, en hun ontledingsmechanismes onder pyrolyse condities, zoals in beschikbare literatuurstudies beschreven. Tenslotte wordt een overzicht van NO<sub>x</sub>-vormingsmechanismes gegeven.

De in dit werk bestudeerde materialen en de daarbij gebruikte opstellingen worden geïntroduceerd in hoofdstuk 3. Biomassa wordt verdeeld in twee hoofd categorieën: agrarische residuen, zoals tarwestro, olijfresiduen en perzikpitten; anderzijds biomassa reststromen, zoals "dry distiller's grains", palmpittenkoek en kippenmest. Al deze materialen vertonen een hoog stikstofgehalte en zijn nog niet volledig benut vanwege de eerdergenoemde problemen. Verscheidene kleinschalige opstellingen zijn ten behoeve van dit werk ingezet afhankelijk van de condities die bestudeerd dienden te worden.

Hoofdstuk 4 geeft de resultaten weer van metingen die zijn verricht op basis van agrarische residuen onder condities van langzame pyrolyse. De metingen zijn uitgevoerd gebruik makend van thermogravimetrische analyse (TGA) geïntegreerd met Fourier Transform InfraRood spectroscopie (FTIR). Alle brandstoffen vertoonden reactiviteitspieken bij circa 330 - 360 °C, geassocieerd met decompositie van cellulose. Een schouderpiek werd ook gevonden bij lagere temperaturen, namelijk bij circa 290 - 310 °C, en deze was geasso-

cieerd met de pyrolyse van hemicellulose. De belangrijkste vluchtige componenten waren CO<sub>2</sub> voor alle brandstoffen, gevolgd door CO en methaan. Geen stikstofcomponenten werden gedetecteerd vanwege te lage concentraties in de pyrolysegassen, zodat accurate detectie door middel van FTIR niet mogelijk was. De kinetiekparameters voor de pyrolyse reacties werden verkregen door gebruik te maken van een "Distributed Activation Energy Model" (DAEM). Deze analyse bracht een gemeenschappelijk reactiepad aan het licht voor de hoofdstructuren (cellulose en hemicellulose) in de verschillende brandstoffen. De voorbehandeling door middel van uitloging met water leek erg effectief in het verwijderen van de problematische anorganische elementen uit deze brandstoffen. De verwijderde elementen hadden verder een katalytisch effect op de pyrolyse van de brandstoffen; eenmaal verwijderd, reageerden de monsters bij hogere temperaturen en volgens een verminderd aantal reactiepaden. Enkel het perzikipittenmonster, dat al een erg laag asgehalte vertoonde, leek niet beïnvloed te zijn door de voorbehandeling.

Hoofdstuk 5 rapporteert de resultaten van een vergelijkbare analyse als bovengenoemde, welke werd uitgevoerd voor verschillende biomassa residuen: "dry distiller's grains with solubles" (DDGS) en kippenmest. Ook deze brandstoffen reageerden met vertoning van twee belangrijke pieken bij circa 280 °C en 330 °C. In overeenkomst met de resultaten voor de agrarische residuen waren de kinetische parameters erg vergelijkbaar, zodat duidelijk is aangetoond dat er sprake is van een overeenkomend decompositiepad voor gemeenschappelijke structuren. Voor DDGS en kippenmest werd een additionele component gevonden die reageerde bij circa 400 - 430 °C en deze werd toegewezen aan de decompositie van eiwitstructuren. De belangrijkste vluchtige stikstofcomponenten waren NH<sub>3</sub> and HCN voor DDGS met sporen van HNCO. Bij de mest kwam meer brandstofgebonden stikstof vrij in vluchtige vorm en de belangrijkste component die werd gevonden was HNCO, gevolgd door HCN en ammoniak. De voorbewerking door middel van uitloging met water leek de reactiviteit van de brandstoffen en hun assamenstelling nauwelijks te beïnvloeden, hetgeen vergelijkbaar was met wat was gevonden voor het perzikipittenmonster. Het deel van de brandstofgebonden stikstof dat als lichte vluchtige gassen vrijkwam nam echter toe voor de uitgeloopte brandstoffen.

Voorbouwend op de resultaten van de vorige twee hoofdstukken, beschrijft hoofdstuk 6 de resultaten van metingen verricht voor pyrolyse onder snelle verwarmingscondities van DDGS en palmpittenkoek. Deze tests werden uitgevoerd gebruikmakend van een verhitte folie reactor ingebouwd in een FTIR, waarbij veel hogere opwarmingssnelheden werden toegepast, dichterbij industriële toepassingen. A numeriek model van de reactor is ontwikkeld om een beter inzicht te verkrijgen in de temperatuur- en snelheidsprofielen in de reactor. De simulaties in combinatie met niet-intrusieve temperatuurmetingen vertoonden een significant verschil tussen de verwachte en de actueel gemeten folietemperatuur. Dit is gecorrigeerd in de experimentele meetcampagne, resulterend in een nauwkeuriger inzicht in de actuele condities.

De pyrolysemetingen onder snelle verwarmingscondities lieten een vergroot massaverlies zien vergeleken met pyrolyse onder langzame verwarmingscondities. CO<sub>2</sub> was nog steeds de belangrijkste lichte vluchtige component bij temperaturen lager dan 900 °C, terwijl CO in relevantie toenam bij hogere temperaturen ten gevolge van teerconversie in de hete zone rond het folie. In vergelijking met DDGS pyrolyse bij lage verwarmingssnelheden was HCN de belangrijkste vluchtige stikstofcomponent, terwijl de NH<sub>3</sub> opbrengst lager was. Bij het palmpittenkoekmonster kwamen slechts detecteerbare hoeveelheden HCN vrij, en noch ammoniak noch HNCO konden worden gemeten. Zelfs bij hoge temperaturen werd slechts ongeveer 10% van de initiële brandstofgebonden stikstof in het vaste koolresidu van DDGS aangetroffen. De uitloging door middel van water beïnvloedde opnieuw noch het massaverlies gedrag noch de productverdeling van de belangrijkste gasvormige producten, maar de opbrengst aan lichte vluchtige stikstofcomponenten nam toe voor de uitgeloopte monsters.

Na analyse van het pyrolysegedrag van de verschillende stikstofcomponenten beschrijft hoofdstuk 7 de resultaten van metingen onder verbrandingscondities voor verschillende biomassa residuen. Aangetoond werd, dat de (oxidatieve) ontvluchtigingskarakteristieken voor koolstofomzetting in CO + CO<sub>2</sub> en brandstofgebonden stikstofomzetting in NO erg vergelijkbaar zijn voor de zeer verschillende brandstoffen, hetgeen impliceert dat een gemeenschappelijke benadering kan worden gevolgd voor hun modellering en dit kan als eerste benadering zeer acceptabel zijn. Bovendien bleek de conversie van brandstofgebonden stikstof in NO een afnemende trend te volgen, zodanig dat de brandstoffen met een lager initieel stikstofgehalte een hogere conversie lieten zien dan brandstoffen met een hoger stikstofgehalte. Het is aannemelijk dat voor brandstoffen met een hoog stikstofgehalte een groter deel hiervan bij vervluchtiging in vluchtige vorm vrijkomt met als consequentie een grotere hoeveelheid NH<sub>i</sub> radicalen die beschikbaar zijn voor thermische De-NO<sub>x</sub> reacties. Tenslotte werd gevonden, dat het vrijkomen van koolstof in de vorm van CO<sub>2</sub> en stikstof in de vorm van NO gedurende de (oxidatieve) ontvluchtiging proportioneel verliep bij temperaturen rond 800 °C terwijl bij 1000 °C bijna alle NO vrijkwam tijdens de ontvluchtiging.

In hoofdstuk 8, tenslotte, worden de belangrijkste conclusies van het werk beschreven in dit proefschrift weergegeven en worden aanbevelingen voor toekomstig onderzoek gegeven.

Jacopo Giuntoli



---

## CONTENTS

---

Summary	ix
Samenvatting	xiii
List of Figures	xx
List of Tables	xxv
1 Introduction	1
1.1 World and Energy: Past, present and future	2
1.1.1 The Energy Present	5
1.1.2 Sustainability and the Energy Problems	11
1.1.3 Energy policies and Energy Technologies: Solutions for a New Era	13
1.2 The role of Biomass	17
1.2.1 Biomass as an energy source	17
1.2.2 Biomass perspectives	19
1.2.3 The routes of biomass conversion	20
1.2.4 Technologies for thermal conversion of biomass	21
1.2.5 NO <sub>x</sub> emissions	28
1.3 Open issues	29
1.4 Research question	31
1.5 Methodology	31
1.6 Outline	33
2 Overview of biomass composition and nitrogen chemistry	37
2.1 Biomass and Fossil fuels (or “very old biomass”)	38
2.1.1 Main structures in biomass: Origins	39
2.1.2 Main structures in biomass: Characteristics	41
2.1.3 Nitrogen compounds in biomass	48
2.2 Solid fuel combustion	57
2.2.1 Char oxidation	59
2.3 NO <sub>x</sub> formation mechanisms	60
2.3.1 From air nitrogen: Thermal NO <sub>x</sub> and Prompt NO <sub>x</sub>	60
2.3.2 From fuel bound nitrogen: Fuel NO	61
2.4 Nitrogen precursors and nitrogen oxides from biomass and model compounds: a review	64
2.4.1 NO <sub>x</sub> precursors from devolatilization	66
2.4.2 Char-N	72
2.4.3 Some examples of NO <sub>x</sub> -precursors and nitrogen oxides from biomass samples	72
3 Materials and Methods	77
3.1 Fuels, equipment and methodology	78
3.2 Fuels	80

3.2.1	Pre-treatments	80
3.2.2	Agricultural Residues	81
3.2.3	Bio-wastes and residues	85
3.3	Slow pyrolysis equipment	90
3.3.1	Thermogravimetric Analyzer - Fourier Transform In- fraRed Spectrometer (TG-FTIR)	90
3.3.2	Literature review	94
3.3.3	Kinetic analysis of slow pyrolysis	95
3.4	Fast pyrolysis equipment	100
3.4.1	Integrated Heated Foil Reactor – Fourier Transform In- fraRed Spectrometer (HF-FTIR)	100
3.4.2	Setup improvements	104
3.4.3	Literature review	110
3.5	Combustion equipment	111
3.5.1	Single Particle Reactor (SPR)	111
4	TG-FTIR Characterization of Slow Pyrolysis of Agriresidues	113
4.1	Introduction	114
4.2	Experimental section	115
4.2.1	Equipment	115
4.2.2	FTIR spectrometer	116
4.2.3	Samples and pre-treatments	116
4.2.4	Procedure	117
4.3	Results and Discussion	117
4.3.1	TG and DTG	117
4.3.2	FTIR	122
4.3.3	Kinetic analysis	127
4.4	Conclusions	137
5	TG-FTIR Characterization of Slow Pyrolysis of Bioresidues	141
5.1	Introduction	142
5.2	Experimental	143
5.2.1	Equipment	143
5.2.2	FTIR spectrometer	143
5.2.3	Samples and pre-treatments	144
5.2.4	Procedure	146
5.3	Results and Discussion	147
5.3.1	TG and DTG	147
5.3.2	FTIR	149
5.3.3	Kinetic analysis	157
5.4	Conclusions	164
6	Characterization and modeling of Fast Pyrolysis of DDGS and PKC	167
6.1	Introduction	168
6.2	Experimental section	169
6.2.1	Integrated heated foil – FTIR setup	169
6.2.2	Pyrometer	170

6.2.3	Materials	172
6.2.4	Numerical model	173
6.3	Results and Discussion	176
6.3.1	Numerical model: Temperature and velocity profiles	176
6.3.2	Numerical model: Temperature validation	179
6.3.3	Experimental results	184
6.4	Conclusions	198
7	Combustion characteristics of bioresidues: fate of fuel N	201
7.1	Introduction	202
7.2	Experimental Section	204
7.2.1	Procedure	206
7.2.2	Fuels	206
7.3	Results and Discussion	206
7.3.1	Release profiles	208
7.3.2	Total Release	213
7.3.3	Devolatilization/Char partitioning	216
7.4	Conclusions	220
8	Concluding remarks	223
8.1	Conclusions	224
8.1.1	Slow pyrolysis measurements	225
8.1.2	Fast pyrolysis measurements	227
8.1.3	Modeling of heated grid reactor	228
8.1.4	Combustion tests	228
8.2	Recommendations for future research	229
8.2.1	Slow pyrolysis research and kinetic modelling	229
8.2.2	Fast pyrolysis research and modelling	230
8.2.3	Combustion research	231
8.2.4	Pre-treatments and fuels related research	231
	Bibliography	233
A	TG-FTIR Quantification method	267
A.1	General	268
A.2	Species and spectral regions	268
A.3	Calibration lines	268
	Nomenclature	275
	Acknowledgements	279
	Selected Publications	283
	Curriculum Vitae	285

---

## LIST OF FIGURES

---

Figure 1	Historical evolution of the primary energy mix for the world	3
Figure 2	Historical energy trend accounting for energy efficiency	5
Figure 3	World primary energy demand by fuel in the IEA reference scenario	6
Figure 4	CO <sub>2</sub> emissions by Region	6
Figure 5	World Total Primary Energy Supply in 2007	7
Figure 6	Share of bioenergy in the world primary energy mix, 2007	8
Figure 7	Gross inland energy consumption for EU-27 countries in 2007	9
Figure 8	Historical share of RES in the Gross Inland Energy Consumption for EU-27 countries	9
Figure 9	Primary energy production from renewable energy sources in EU-27 countries by source	10
Figure 10	Import dependence to 2030 for EU-27 countries	10
Figure 11	Projected GHG emission scenarios in the EU-15 countries	11
Figure 12	World abatement of emissions of energy related CO <sub>2</sub> -eq. gases by 2030	14
Figure 13	World primary energy demand in the 450 scenario	14
Figure 14	European Energy Technology Roadmap	17
Figure 15	Projected growth in renewable electricity in EU-25 countries	20
Figure 16	Projected growth in renewable heating and cooling in EU-25 countries	20
Figure 17	Conversion paths of biomass	21
Figure 18	Technology status of pyrolysis reactors	23
Figure 19	Applications for syngas from biomass gasification	24
Figure 20	Technology status of biomass gasification	25
Figure 21	Development status of biomass-to-power and heat or CHP technologies	28
Figure 22	Schematic of the outline of this thesis	34
Figure 23	Van Krevelen coalification diagram	39
Figure 24	Structure of cellulose and chain bridging	43
Figure 25	Sugar units typical of hemicelluloses	44
Figure 26	Structural units of lignin and an example of lignin structure.	45

Figure 27	Thermal decomposition in slow pyrolysis of the main components of lignocellulosic materials	49
Figure 28	Nitrogen content in different plant sections	50
Figure 29	Common nitrogen structures in biomass	51
Figure 30	$\alpha$ -amino acids	52
Figure 31	Nitrogen functionalities in coal	54
Figure 32	DNA heterocyclic bases	55
Figure 33	Nicotine and Strychnine: two typical alkaloids in biomass	56
Figure 34	Structure of chlorophyll-a	56
Figure 35	Schematic of the thermal conversion of a solid particle	57
Figure 36	Influence of flame temperature on the $\text{NO}_x$ formation mechanisms for coal	62
Figure 37	Fuel- $\text{NO}$ formation during thermal conversion stages of biomass fuels	62
Figure 38	Homogeneous reaction paths of HCN and $\text{NH}_3$ to $\text{NO}$	64
Figure 39	Fuel-N retention in char with devolatilization temperature for several biomass materials	65
Figure 40	Reaction path diagram for the Thermal De- $\text{NO}_x$ process at moderate temperatures and fuel-rich conditions	66
Figure 41	Primary pyrolysis decomposition pathways for proteinic biomass-N model compounds	68
Figure 42	Pyrolysis decomposition pathways for glycine	68
Figure 43	Thermal decomposition of DKP	69
Figure 44	Secondary decomposition reactions of the products of primary pyrolysis	70
Figure 45	Schematic of the methodology used in this dissertation	79
Figure 46	Schematic of the TG – FTIR setup	90
Figure 47	TG-FTIR setup at Process and Energy Laboratory	90
Figure 48	Example of thermogravimetric weight loss curves and analysis of DDGS	91
Figure 49	Example of FTIR absorption spectrum for DDGS slow pyrolysis	93
Figure 50	Example of measurement of volatile species during pyrolysis of wheat straw	93
Figure 51	Example of the application of three independent first-order reactions to the pyrolysis of olive residues	97
Figure 52	Samples of PKC and DDGS as used in the heated foil reactor	101
Figure 53	Heated foil setup at Process and Energy Department	102
Figure 54	Heated foil reactor + FTIR at Process and Energy Department	103
Figure 55	Schematic of the pyrometer and heated foil reactor.	104

Figure 56	Temperature measured by thermocouple and IR pyrometer with different emissivity values	105
Figure 57	Relation between the temperature measured by the pyrometer and the thermocouple	106
Figure 58	Steel foils at different degrees of oxidation	106
Figure 59	CO <sub>2</sub> concentration over time after CaCO <sub>3</sub> at 1200 °C	108
Figure 60	NH <sub>3</sub> concentration over time released from chicken litter fast pyrolysis at T = 800 °C	109
Figure 61	Mixing behaviour of different gaseous species released from fast pyrolysis of chicken litter at T = 800 °C	110
Figure 62	Single particle furnace at Åbo Akademi University and particular of the quartz sample holder	112
Figure 63	TG – FTIR setup at the Process and Energy Laboratory	115
Figure 64	TG and DTG curves for wheat straw untreated and leached	123
Figure 65	TG and DTG curves for olive residue untreated, leached, fractionated and fractionated + leached;	124
Figure 66	TG and DTG curves for peach stones untreated and leached	125
Figure 67	Wheat straw untreated: Superposition of DTG curve with the relative compounds analyzed by the FTIR	126
Figure 68	Wheat straw leached: Superposition of DTG curve with the relative compounds analyzed by the FTIR	127
Figure 69	Peach stones untreated: Superposition of DTG curve with the relative compounds analyzed by the FTIR	128
Figure 70	Distribution of activation energies for slow pyrolysis of agricultural residues	130
Figure 71	Wheat straw untreated: DTG and fit with 25 parallel first order reactions	131
Figure 72	Wheat straw leached: DTG and fit with 25 parallel first order reactions	132
Figure 73	Peach stones leached: DTG and fit with 25 parallel first order reactions	133
Figure 74	Wheat straw untreated: experimental and reconstructed DTG at heating rate of 100 °C/min	134
Figure 75	Wheat straw leached: experimental and reconstructed DTG at heating rate of 100 °C/min	135
Figure 76	Peach stones leached: experimental and reconstructed DTG at heating rate of 100 °C/min	136
Figure 77	TG-FTIR set-up at Process and Energy Laboratory	143
Figure 78	TG and DTG curves for DDGS untreated and leached	149
Figure 79	TG and DTG curves for chicken manure untreated and leached	150
Figure 80	DDGS untreated: Superposition of DTG curve with the relative compounds analyzed by the FTIR	151

Figure 81	DDGS untreated: Re-scaling of Figure 80 for the main nitrogen compounds	152
Figure 82	FTIR spectra from the DDGS untreated at different temperatures	153
Figure 83	Chicken manure untreated: Superposition of DTG curve with the relative compounds analyzed by the FTIR	154
Figure 84	Chicken manure untreated: Re-scaling of Figure 83 for the main nitrogen compounds	155
Figure 85	FTIR spectra from the chicken manure untreated at different temperatures	156
Figure 86	Distribution of activation energies for DDGS and chicken manure	159
Figure 87	DDGS untreated, DTG and fit with 25 parallel first order reactions	160
Figure 88	Chicken manure untreated, DTG and fit with 25 parallel first order reactions	161
Figure 89	DDGS untreated experimental and reconstructed DTG at heating rate of 100 °C/min	162
Figure 90	Chicken manure untreated experimental and reconstructed DTG at heating rate of 100 °C/min	163
Figure 91	Heated foil setup	171
Figure 92	Geometry of the heated foil reactor used in the numerical model.	174
Figure 93	Example of current intensity and thermocouple reading used as input in the model	177
Figure 94	Temperature distribution in the heated foil reactor	178
Figure 95	Velocity distribution in the heated foil reactor	178
Figure 96	Velocity magnitude and direction over the foil	179
Figure 97	Temperature measured by thermocouple and IR pyrometer with different emissivity values	180
Figure 98	Measured and predicted temperatures of the foil at different setpoints	181
Figure 99	Relation between the temperature measured by the pyrometer and by the thermocouple	182
Figure 100	Temperature distribution over horizontal and vertical medians of the foil at T=800 °C.	183
Figure 101	Weight loss in function of pyrolysis temperature for all the samples	185
Figure 102	Kinetic reconstruction of the reactivity of DDGS sample using kinetic data retrieved on slow pyrolysis measurements	187
Figure 103	Product distribution for all samples in function of foil temperature	189

Figure 104	Yield of main gaseous species for DDGS and PKC under fast pyrolysis conditions	190
Figure 105	Yield of nitrogen species for DDGS and PKC under fast pyrolysis conditions	195
Figure 106	Fuel-N conversion to NH <sub>3</sub> and HCN for all samples under fast pyrolysis conditions	196
Figure 107	Partitioning of carbon and nitrogen for DDGS and DDGS leached at final temperatures of 900 °C and 1200 °C	197
Figure 108	Single-particle furnace at Åbo Akademi University.	205
Figure 109	Release of carbon as CO + CO <sub>2</sub> from all of the fuels at 900 °C	209
Figure 110	Release of nitrogen as NO from all of the fuels at 900 °C	210
Figure 111	Nitrogen release profiles at 900 °C for all the fuels	212
Figure 112	Total amount of carbon released as CO + CO <sub>2</sub> and initial C content	213
Figure 113	Total amount of nitrogen released as NO and initial N content	214
Figure 114	Conversion of fuel nitrogen to NO versus fuel nitrogen content: comparison between this study and Winter et al. [362]	216
Figure 115	Nitrogen conversion to NO as a function of temperature.	217
Figure 116	Carbon partitioning between devolatilization and char oxidation.	219
Figure 117	Nitrogen partitioning between devolatilization and char oxidation.	219
Figure 118	Calibration line plot and data for the species: CO <sub>2</sub> Low.	268
Figure 119	Calibration line plot and data for the species: CO <sub>2</sub> Mid.	269
Figure 120	Calibration line plot and data for the species: CO <sub>2</sub> High.	272
Figure 121	Calibration line plot and data for the species: CO Low.	272
Figure 122	Calibration line plot and data for the species: CO Mid.	272
Figure 123	Calibration line plot and data for the species: CH <sub>4</sub> Low.	273
Figure 124	Calibration line plot and data for the species: H <sub>2</sub> O.	273
Figure 125	Calibration line plot and data for the species: HCN.	273



---

LIST OF TABLES

---

Table 1	Elemental analysis of various biomass fuels, bioresidues and coals	40
Table 2	Typical lignocellulose content of some plant materials	46
Table 3	Ranges of variation of the chemical composition of different lignocellulosic feedstock	46
Table 4	Composition of common raw materials for industrial production of starch	47
Table 5	Protein content in various biomass materials	51
Table 6	Thermal decomposition of some $\alpha$ -amino acids with aliphatic chains.	53
Table 7	Thermal decomposition of some $\alpha$ -amino acids with five- and six-membered rings in their side chains.	53
Table 8	Thermal decomposition of some acidic, basic and secondary $\alpha$ -amino acids.	53
Table 9	Yields of volatile-N compounds in biomass slow pyrolysis.	74
Table 10	Yields of volatile-N compounds in biomass fast pyrolysis.	75
Table 11	Conversion of fuel-N to NO in different biomass combustion applications.	76
Table 12	Pre-treatments applied to the agricultural residues	82
Table 13	Proximate and elemental analysis of the agricultural residues	83
Table 14	Elemental analysis of the ash forming matter in agricultural residues	84
Table 15	Pre-treatments applied to the agricultural residues	86
Table 16	Proximate and elemental analysis of the biomass residues	87
Table 17	Elemental analysis of the ash forming matter in biomass residues	88
Table 18	Temperature setpoints for the experimental campaign	107
Table 19	Details of the pretreatments applied to the samples studied in Chapter 4	118
Table 20	Proximate and elemental analysis of the fuels in Chapter 4	119

Table 21	Elemental analysis of the ashes of the fuels in Chapter 4	120
Table 22	Temperatures at maximum release rates and maximum yields of volatile species	124
Table 23	Kinetic parameters for Gaussian distribution. Main volatile species: WS.	134
Table 24	Kinetic parameters for Gaussian distribution. Main volatile species: WSL.	135
Table 25	Kinetic parameters for Gaussian distribution. Main volatile species: OR.	136
Table 26	Kinetic parameters for Gaussian distribution. Main volatile species: ORL.	137
Table 27	Kinetic parameters for Gaussian distribution. Main volatile species: PS.	137
Table 28	Kinetic parameters for Gaussian distribution. Main volatile species: PSL.	138
Table 29	Proximate and elemental analysis of the fuels studied in Chapter 5	146
Table 30	Elemental analysis of the ash forming matter in the fuels studied in Chapter 5	147
Table 31	TG-FTIR studies on amino acids decomposition found in the literature*.	152
Table 32	Temperatures at maximum release rates and maximum yields of volatile species	157
Table 33	Kinetic parameters for Gaussian distribution. Main nitrogen species: DDGS.	161
Table 34	Kinetic parameters for Gaussian distribution. Main nitrogen species: DDGS leached.	162
Table 35	Kinetic parameters for Gaussian distribution. Main nitrogen species: Chicken manure.	163
Table 36	Kinetic parameters for Gaussian distribution. Main nitrogen species: Chicken manure leached.	164
Table 37	Proximate and elemental analysis of the fuels studied in Chapter 6	172
Table 38	Pre-treatments applied to the fuels in Chapter 6	173
Table 39	Elemental analysis of the ash forming matter. Data are on a dry basis.	173
Table 40	Boundary conditions for the general heat transfer equation	174
Table 41	Boundary constants for the general heat transfer equation	175
Table 42	Boundary conditions for the conductive media equation	175
Table 43	Boundary conditions for the weakly compressible Navier-Stokes equations	176

Table 44	Activation energy distribution obtained at slow heating rates for DDGS	186
Table 45	Yields of main light volatile species in flash pyrolysis conditions	192
Table 46	Proximate and elemental analysis of the fuels studied in Chapter 7	207
Table 47	Calibration range of the different species	269
Table 48	Spectral regions and windows for the different species	270
Table 49	Calibration matrix to account for mutual overlapping	271



---

## INTRODUCTION

---

*This dissertation deals with important numerical and empirical studies on thermo-chemical conversion of biomass waste materials. Such resources have high potential to be exploited as fuels in the near future but, as I will introduce later, there are still many aspects to be investigated before they can be efficiently employed in a clean way. However, when discussing about energy and especially biomass for energy, all the other issues associated with this concept, not only technological but also social and geopolitical, cannot be left apart. Therefore, before starting to dig into the subjects that constitute the core of this dissertation, I will start with describing the technological and political context in which this research has been conceived, planned and funded, hoping that it will help the reader to place the achieved results into a broader context.*

## 1.1 WORLD AND ENERGY: PAST, PRESENT AND FUTURE

Energy supply has been at the core of the World's social, technological and economical system almost since the Industrial Revolution in the 18<sup>th</sup> century. Before that age, people were already using wood to warm up their houses and cook their food, but it was only after the development of the steam engine and, later, the discovery of oil that the now well-known fossil fuels' based economy was established.

*The fate of energy sources: the deterministic advent of a renewables based economy*

In 1977 Marchetti [256] tried to explore different methodologies for the prediction of the trends of energy demand and consumption. He treated primary energy sources as if they were commodities competing for a market share and applied a logistic approach to this market. This type of analysis states that the fractional rate at which a new commodity penetrates a market is proportional to the fraction of the market not yet covered. This concept is summarized in the expressions 1.1 and 1.2, where  $F$  represents the fraction of the market penetrated and  $\alpha$  and  $c$  are constant values characteristic of a particular commodity and market.

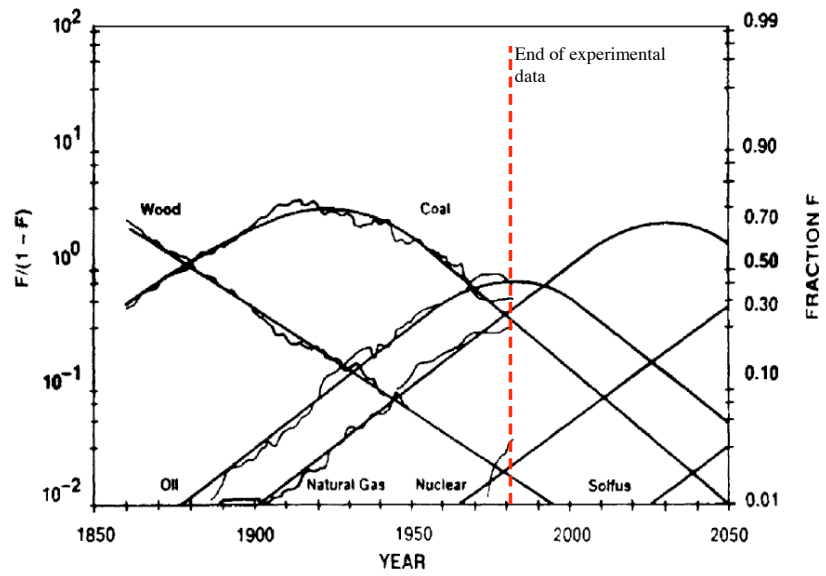
$$\frac{1}{F} \cdot \frac{dF}{dt} = \alpha \cdot (1 - F) \quad (1.1)$$

$$\ln \left( \frac{F}{1 - F} \right) = \alpha \cdot t + c \quad (1.2)$$

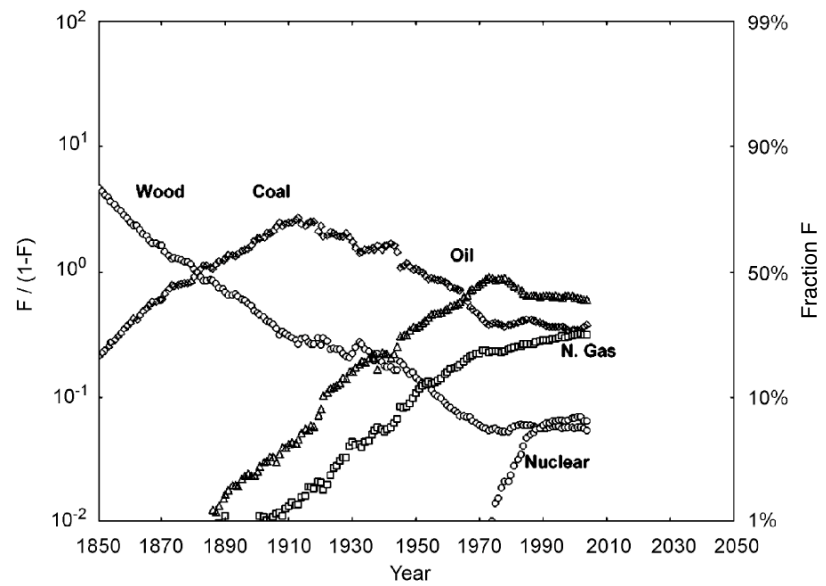
To his great surprise, more than a century of data could be perfectly fitted by such equations, unscathed by wars, depressions and oscillations in energy prices, as shown in Figure 1a. Such behaviour, such "cycles" of a duration of approximately 50 years are well known to economists as Kondratieff waves: these represent sinusoidal-like cycles in the modern capitalist world economy [135]. In subsequent works, Marchetti applied this model to several other social activities such as construction works but also violence and suicides, finding surprising correspondences in such cycles that brought him to coin the definition of a "fifty-year pulsation in human affairs" Marchetti [257].

According to Marchetti's model, therefore, also primary energy sources would take one long wave from their introduction to their maximum market share and another long wave to their phase-out.

A little knowledge of modern history, however, tells us that things did not evolve exactly as Marchetti had forecasted or, by now, as indicated in Figure 1a, we should have already seen a peak in oil consumption, a very strong decrease in coal usage and we would almost be ready to welcome nuclear



(a) Historical evolution of the primary energy mix for the world. Source: Marchetti [256]



(b) Historical energy trends with updated values to 2008. Source: Devezas et al. [137]

Figure 1: Historical evolution of the primary energy mix for the world.

fusion! Instead, somewhere around mid '80s, the predicted pattern seems to have been broken, shifting from a mechanism of source substitution to a more stable and heterogeneous energy mix (Figure 1b). After the oil crisis of 1973, in fact, many things happened that re-shaped the energy market to a form unknown before and similar to what we have today. Among these changes, great efforts started in the Western countries to apply policies to stimulate energy efficiency in order to be less exposed to the same oil price fluctuations as in '73.

Devezas et al. [137] in 2008, in a framework of wide resurgence of interest in long-waves studies [135, 136], decided to re-analyze the findings of Marchetti to determine whether a cyclical pattern could still be predicted with the current trends or if the method was substantially flawed. They maintained the same logistic model used by Marchetti but claimed that the differences were to be blamed on the boundary conditions of the system considered. In order to incorporate the new market developments, therefore, first of all they merged oil and natural gas into a single Fluid Fossil Fuels (FFF) category. This was considered reasonable because of the close nature of the fuels, the similar infrastructures used for their recovery and transport and the closely linked prices. Moreover, they used energy efficiency as a new source competing in the same market to account for the various energy conservation programmes introduced by many governments in the last 30 years. Figure 2 shows that the corrected model can indeed reproduce the behavior of the last 30 years, illustrating the presence of cycles resembling the Kondratieff cycles of innovation, deployment and investment [137].

Even before going deeper into technological advancements and breakthroughs, these data tell us that, as in many other aspects of human affairs, a recurring, mechanistic and pre-determined cyclical behaviour applies to energy sources as well as it does to economy, technology and biological systems [135]. Even without knowing the whys and hows, which will be explained in the following parts of this introduction, a simple analysis of historical data tells us that every new energy source and technology will need its necessary time for a significant market penetration and that the later such innovations are promoted and brought forward, the later they will actually impact the world's energy trends.

While the data introduced so far make it evident that it would actually be anti-historical if a change towards renewable sources was not to happen within the next century because of the natural substitution of energy sources, the rest of this introduction has the purpose of explaining why such a change would actually be beneficial for the economy and the environment under many aspects and what are the policies and technologies which will most likely be at the core of such change.



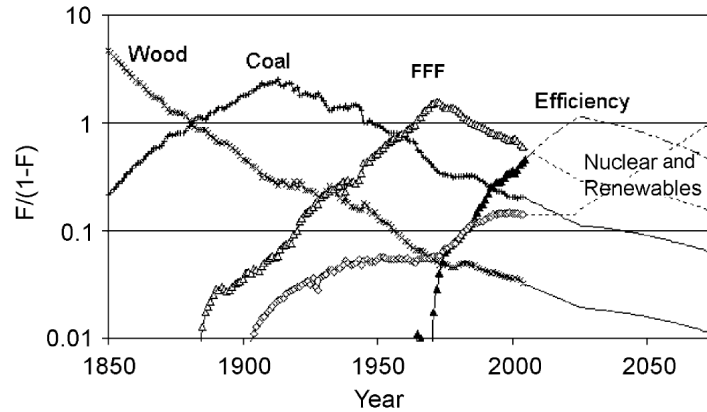


Figure 2: Historical energy trend analyzed according to the Marchetti model but accounting for energy efficiency. Source: Devezas et al. [137]

### 1.1.1 The Energy Present

#### *World Energy Outlook*

Before starting to explore the possibilities for future developments in the energy market, both in terms of technologies and policies, it is useful to give a brief introduction on the statistics of today's world energy sources consumptions and the future predictions. Many scenarios are available nowadays from different institutions and with slightly different perspectives and techniques [7, 12, 19, 29, 35]. Among these approaches, I chose to analyze the scenario described by the International Energy Agency in the latest World Energy Outlook 2009 [29] since it is used as reference by most policymakers in the world.

In the reference scenario, depicted in Figure 3, the projected Total Primary Energy Supply (TPES) is set to grow a stunning 40% above values of 2007, despite the first decrease in 30 years due to the financial crisis in 2009. Worth noticing is the fact that 90% of this growth is expected to take place in non-OECD countries [29].

It is worth reminding that the scenario considered here uses the assumption of oil prices increasing smoothly with time, reaching 115 \$ (value of 2008) in 2030. While it is impossible to accurately predict oil price due to its extreme volatility, such assumption seems reasonable considering the experience of the past years, when oil reached peaks of 120 \$ in 2007, and the persisting conditions of falling investments on exploration for new reservoirs [29, 123]. Therefore, in this scenario, the prices of imports will noticeably rise, granting OPEC countries a 30 \$trillion revenue from 2008 to 2030, almost a five fold increase over the past 23 years! [29]

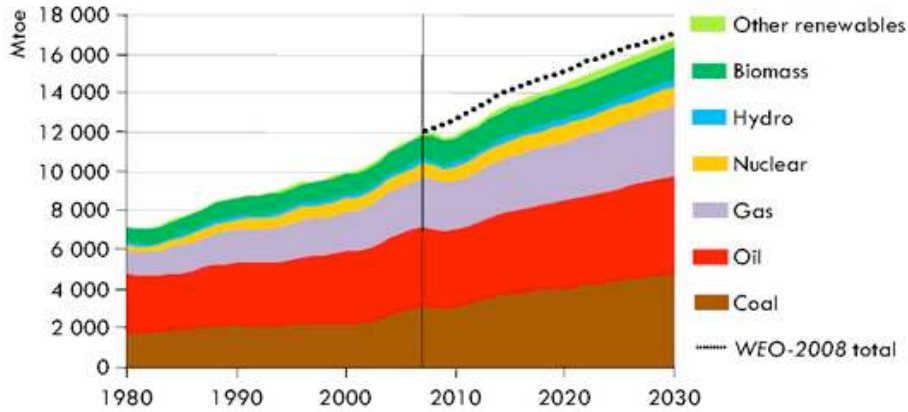


Figure 3: World primary energy demand by fuel in the IEA reference scenario. Source [29]

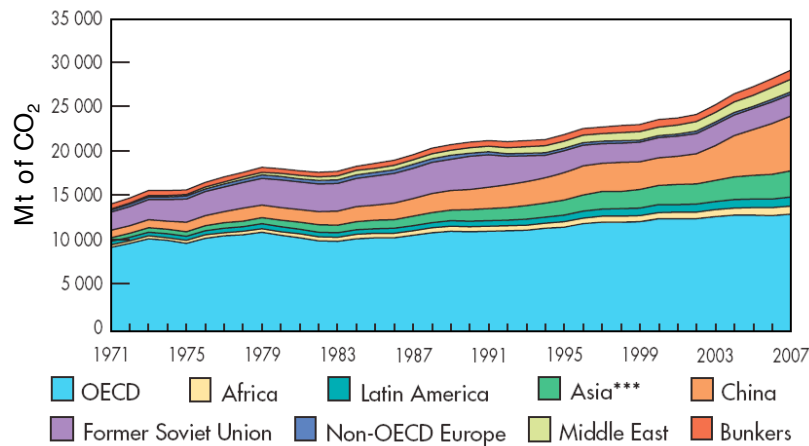


Figure 4: CO<sub>2</sub> emissions by Region. Source [25]

Figure 4 illustrates the development of global CO<sub>2</sub> emissions from fuels combustion in the last thirty years. Despite one global agreement (Kyoto Protocol) and many local policies, CO<sub>2</sub> emissions have globally constantly increased in the last years. The global economic crisis in 2009 is responsible for the first drop in global CO<sub>2</sub> emissions in 40 years (−3%) [29], but this effect will be only temporary. Emissions are predicted to rise up to 40.2 Gton CO<sub>2</sub> in 2030 [29] if there will be no change in global policies, increasing the atmospheric concentration of greenhouse gases to 1000 ppm<sub>v</sub> of CO<sub>2</sub>-eq. by the end of this century (from a value of 380 ppm<sub>v</sub> in 2008). Such rise will cause an increase of the Earth average temperatures of up to 6 °C with unpredictable consequences for the planet [29].

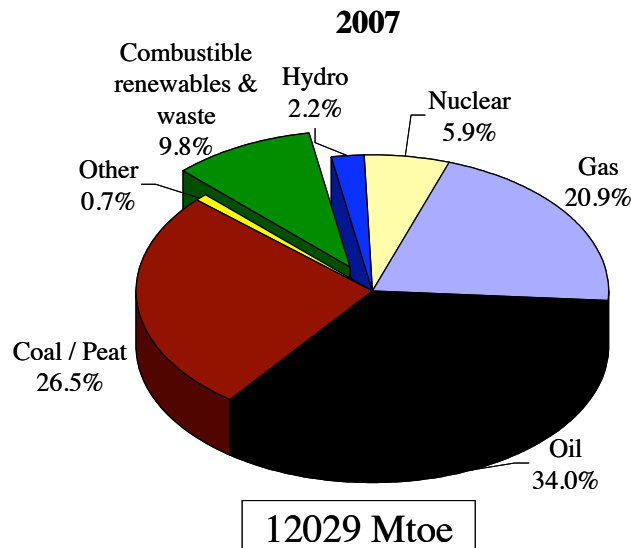


Figure 5: World Total Primary Energy Supply, 2007. Source [25]

IEA, moreover, assures that, even in the reference scenario, oil sources will be able to cover increasing energy needs well beyond 2030 [29]. However, other sources [322] indicate a likely peak in conventional oil production before 2030 (with chances of it happening even before 2020), making the needs for increasing the market penetration of low-carbon substitutes even more urgent.

In the section 1.1.3 I will briefly describe the possible ways to tackle issues like climate change, security of supply and high prices. However, as I have already shown how the role of renewable sources will be of primary importance in near and long-term future, I think it is appropriate to give an overview of the current situation in terms of supplies and consumption of renewable sources.

Figure 5 illustrates the composition of the World TPES in 2007. As seen in the chart, while fossil fuels make up for more than 80% of the total, the fraction of combustible renewables and waste covers almost 10% of the total supply and almost 80% of the renewable sources supply (Figure 6). Far from being a cheerful result, though, because most of this amount results from so-called traditional biomass. This definition usually refers to biomass resources used in rural or underdeveloped parts of the world, mostly in the form of wood or dried manure, combusted for the purposes of domestic heating or cooking. This source makes up for around 22% of the energy used in developing countries [92] and for almost 50% of the primary energy used in Africa [209] and it is often associated with health problems and pollution due to the incomplete combustion in closed spaces with serious risks of CO poisoning.

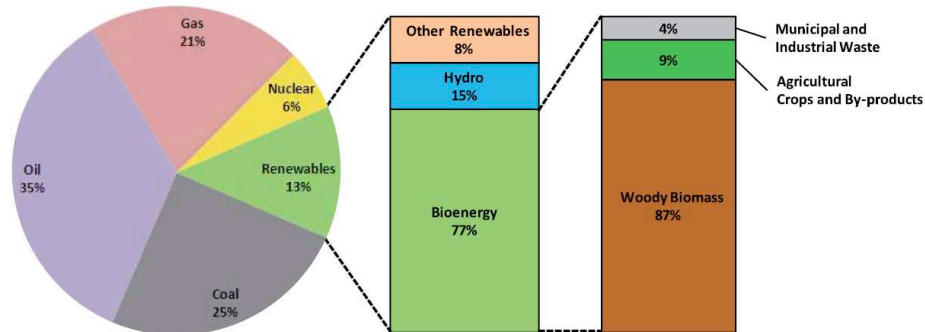


Figure 6: Share of bioenergy in the world primary energy mix, 2007. Source [92]

The use of biomass for energy purposes in OECD countries, and thus in more modern plants, accounts for only 3% of the primary energy supply [25]. This is usually called 1<sup>st</sup> generation biomass which includes thermal conversion of wood, wood cuttings, combustion of black liquor from the pulp and paper industry and incineration of municipal solid waste (only part of the MSW can be considered renewable). As it will be made clear in the next sections, this is quite an established technology.

### Europe

The energetic situation in Europe is illustrated in Figures 7, 8 and 9. The share of fossil fuels is still the most relevant, covering around 80% of total primary energy in 2007 (Figure 7). Renewable energy sources (RES) cover almost 8% of the total energy consumption.

Figure 8, moreover, shows how the share of RES is constantly increasing in the EU-27 area having more than doubled in the last ten years. Biomass accounts for most of the renewable energy sources used, covering more than 5% of the total energy consumption.

Figure 9 illustrates that among the biomass sources, wood and woody residues are still the main fuels used for thermal conversion and heating, together with the incineration of municipal solid wastes. Moreover, biomass already covers around 17% of the whole electricity produced from renewable sources.

As mentioned above, for some countries in the world, e.g. the U.S., energy import is forecasted to actually decrease by 2030 [29]. On the other hand, the energy dependence of the European Union is predicted to dramatically increase in the next decades, mostly because of depletion of indigenous sources, as seen in Figure 10. While today already 53% of the total energy consumed is imported, by 2030 the EU-27 could be forced to import up to 65% of its energy sources, with a peak of 93% for oil [13]. It is easily understandable that in this situation the risk of supply failure is constantly growing and that

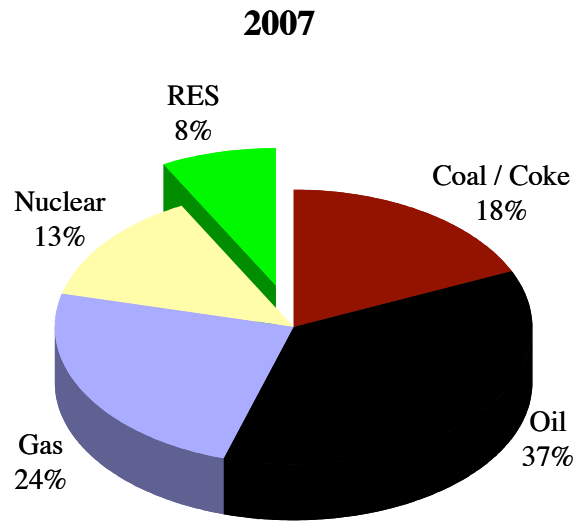


Figure 7: Gross inland energy consumption for EU-27 countries in 2007. Total 1825 Mtoe. Source: Eurostat [151]

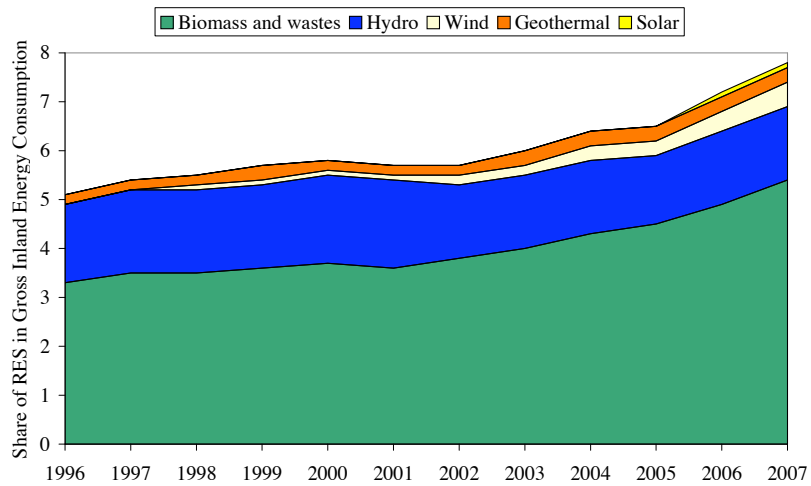


Figure 8: Historical share of RES in the Gross Inland Energy Consumption for EU-27 countries. Source: Eurostat [151]

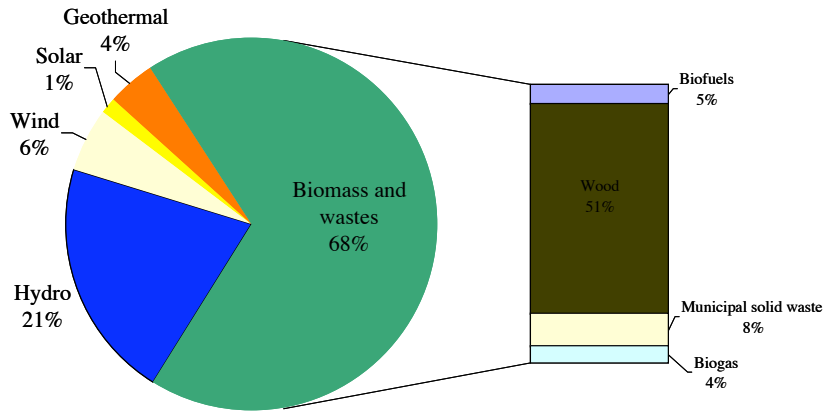


Figure 9: Primary energy production from renewable energy sources in EU-27 countries – breakdown by individual source, 2006. Source [27]

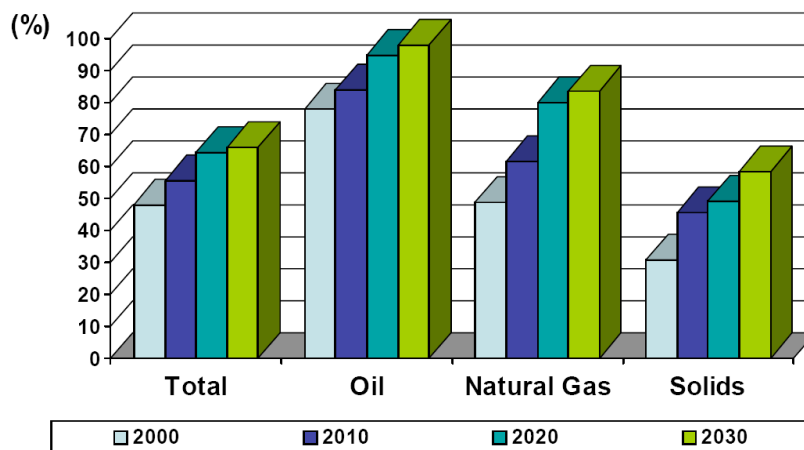


Figure 10: Development of import dependence to 2030 for EU-27 countries in the Base-line Scenario. Source [11]

the whole European economy will be more and more dependent on the prices of energy imports.

Figure 11, finally, shows the trend of Greenhouse gas (GHG) emissions in the EU-15 countries and the projection up to the year 2012, end of the Kyoto Protocol period (official data are available only up to 2007 ). It is evident that, while worldwide the trends are discouragingly increasing, mostly due to the contribution of developing countries like China, India and Brazil, the European Union is on track for a 5<sup>th</sup> year reduction in a row [22] and in line with its Kyoto targets.

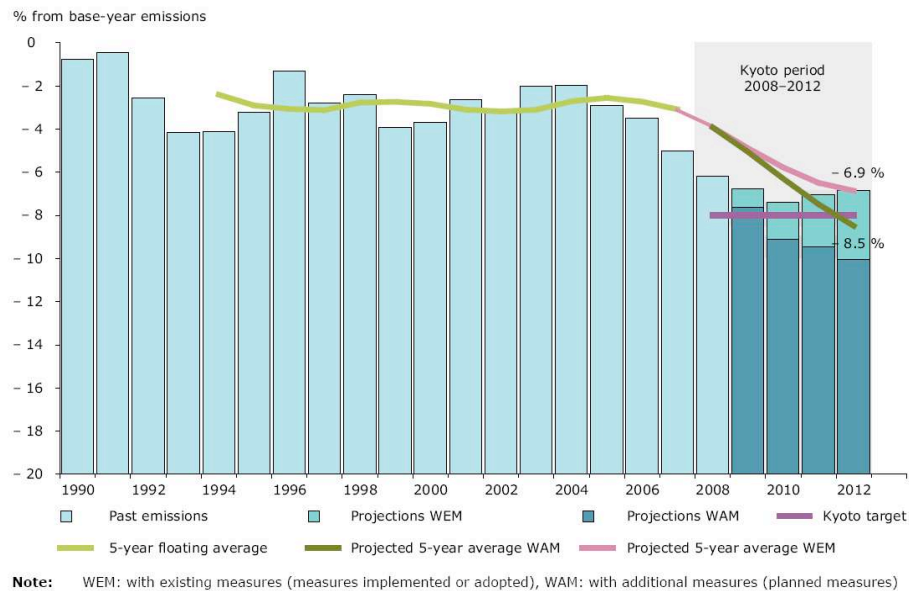


Figure 11: Projected GHG emission scenarios in the EU-15 countries. The data do not include Kyoto mechanisms but only actual emission reductions. Source [22]

### 1.1.2 Sustainability and the Energy Problems

“Development which meets the needs of the present without compromising the ability for future generations to meet their own needs” [1]

With these words the U.N. Brundtland Commission defined the term Sustainable Development in 1987.

In light of the trends described in section 1.1.1, it is easy to understand how the current path of development definitely does not comply with the definition of sustainability. Friedman [158] in a brilliant book on the effects of the convergence of over-population, climate change and globalization, identifies five worrying phenomena that characterize the current energy panorama:

- *Energy supply and demand imbalance.* On one side, population growth, growth of prosperity and the expansion of the world’s middle class through globalization will drastically increase energy demand in the next decades. On the other hand, the potential peak in production of oil and gas in many parts of the world and the consequent decline in oil supply will possibly limit the availability of conventional energy sources. These two phenomena would create a dangerous imbalance with the subsequent increase of prices, slowed-down progress, and eventually it

would prevent future generations from enjoying the same resources as we exploited.

- *Security of energy supply.* Data show that, in a BAU scenario, at least the EU, will have continuously increasing needs (and costs) for the import of energy sources. Most of those imports come from politically unstable areas of the world [27], thus creating serious risks of supply failures together with a continuous transfer of wealth towards many “petro-dictatorships” and pipeline owners.
- *Climate Change.* This is possibly one of the hottest topics of the past years (culminated with the Nobel Peace Prize to the Intergovernmental Panel for Climate Change (IPCC) and Al Gore in 2007) among scientists and common people and one of the main drivers for Governments to actually act, as I will show in the next section.

By now there is increased awareness and agreement concerning the anthropogenic origin of climate change [9]. More and more studies have helped to define the patterns of Earth’s climate, predict its evolution and, consequently, define the costs and the necessary means to avoid disastrous consequences [9, 326, 15]. The common understanding is that, in order to avoid catastrophic consequences, the average temperature of the Earth should not rise more than 2 °C over pre-industrial temperatures within this century. This, according to the latest predictions, would correspond to an atmospheric concentration of around 450 ppm<sub>v</sub> of CO<sub>2</sub>-eq. gases.

- *Energy Poverty.* In 2009, one person out of every four on the planet still did not have regular access to electricity [29]. Even in 2030, 1.3 billion people will still live in a permanent blackout. Electricity is a source for better medical treatments, better agricultural techniques, better education, access to information and promotion of freedom. Without access to the grid there will be no progress for a huge number of people, in plain contradiction with the Millennium Development goals [26].
- *Biodiversity loss.* There is a regular cycle on Earth of species disappearing and new ones being developed by evolution. But in the last years the number of species going extinct is dramatically increasing. Conservation International currently estimates that one species every twenty minutes is going extinct, a thousand times faster than in any other time on recent Earth’s history [158]. It is easy to blame human beings for such phenomenon: climate change, pollution of air and waters, overfishing, deforestation and habitat destruction are among many reasons. A planet made of steel and concrete is not what we should leave to future generations.

A proverb states that finding the problem is the first part of formulating a solution; the above-mentioned issues may seem to be impossible challenges



but I will show in the next section how a good mix of energy policies and energy technologies could transform great challenges into great opportunities.

### 1.1.3 *Energy policies and Energy Technologies: Solutions for a New Era*

The concept of Climate Change (or Global Warming or Enhanced Global Warming) is certainly not new (The United Nations founded the IPCC in 1988) and it has been strongly debated in the past due to the high number of factors determining Earth's climate and the consequent difficulty in achieving reliable predictions. However, this idea has gained extreme momentum in the last years when, assessment after assessment, the IPCC has come to state:

“Most of the observed increase in global average temperatures since mid-20<sup>th</sup> century is *very likely* due to the observed increase in anthropogenic GHG concentrations” [9]

Without entering the debate on climate change, for which books are written every day, the important concept behind it is the following: tackling climate change is giving governments around the world a reason to implement important energy policies that have the potential not only to mitigate anthropogenic climate change itself, but also to reduce pollution, allow abundant and affordable energy to grant progress for future generations, increase security of supply, protect the Earth's biodiversity and gain a dominant position for local enterprises in the newly developing, huge, and profitable market for green technologies.

#### *Bend the trend*

The latest World Energy Outlook [29], based on the available predictions and recommendations [9, 15, 326], gives a very concrete and detailed future scenario in which the concentration of GHG gases in the atmosphere is stabilized at 450 ppm<sub>v</sub> of CO<sub>2</sub>-eq., thus limiting the average Earth's temperature increase to 2 °C (compared to a possible increase of 6 °C on a BAU scenario) [9].

Figure 12 presents a comparison between the reference scenario and the 450 scenario in terms of CO<sub>2</sub> emissions from the energy sector. The role of energy efficiency is striking but not surprising, if one realizes that the cleanest energy is always the one that's not used. The second more important contribution is the one due to renewable sources, contributing to one fifth of the emissions' abatement. Figure 13 helps to picture the role of each fuel in this scenario: again it is evident that, among zero-carbon fuels, that should cover about 32 % of the world primary energy demand, biomass will hold a prominent role, with a potential to account for 40 % of the zero-carbon fuels mix and up to 14 % of the world primary energy demand.

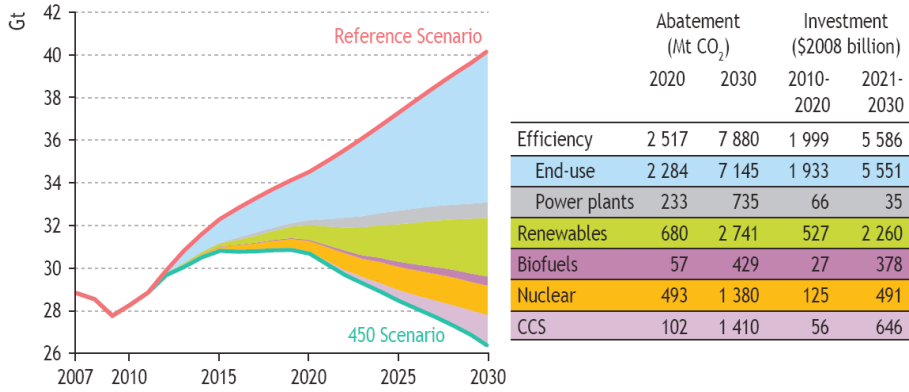


Figure 12: World abatement of emissions of energy related CO<sub>2</sub>-eq. gases by 2030. Source [29]

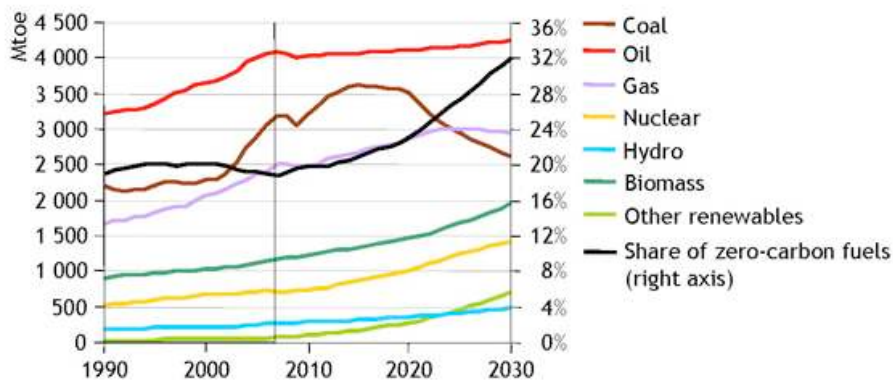


Figure 13: World primary energy demand in the 450 scenario. Source [29]

*Kyoto Protocol*

Now that it is obvious what should be the target for GHG emissions, the main question is how to reach it? How do we bend the trend?

As the term suggests, Global Warming is a global phenomenon and it has to be tackled as such. For this reason, in 1992, almost every country in the world signed the United Nations Framework Convention on Climate Change (UNFCCC), an international environmental treaty with the aim of reducing GHG emissions and thus limit the anthropogenic effects on the climate. The main historic result of this treaty has been the Kyoto Protocol, a legally binding agreement signed and ratified by 188 countries (by April 2010) and covering 64% of the world’s GHG emissions in 1990. You might wonder what happened to the remaining 36% of the global emissions of the year 1990; only one country among the developed ones did not ratify the protocol: the United

---

States of America, responsible for the remaining 36% of global emissions. Moreover, China and India that were not among the large emitters in 1990 but are now the first and third, respectively [21], are not included in the Annex I countries and thus not subjected to any mandatory reduction. These are the two biggest limitations to the actual success of the protocol but for the moment no additional global agreement has been signed and the Kyoto protocol still remains the best the United Nations have been able to achieve so far.

The protocol entered into force in February 2005 and it forces countries in the Annex I (most of OECD countries) to reduce their collective GHG emissions by at least 5.2% from the 1990 level within the year 2012. The protocol is based on three main mechanisms:

- *Emissions Trading*. Under the protocol, every country is allowed a certain amount of GHG emissions. When this level is exceeded, countries can purchase emissions rights from other nations which are instead under-emitting. The goal of this mechanism is to account for external costs (like climate change), which would otherwise be overlooked by the market, into the price of energy sources.
- *Clean Development Mechanism*. Through this mechanism, countries can acquire GHG emission credits by investing in emission-reduction projects in developing countries. This scheme is aimed at creating a sustainable development in developing countries through a continuous transfer of wealth and technology from developed countries.
- *Joint Implementation*: It suits the same purpose as the CDM but it allows developed countries to invest in other developed countries and gain carbon credits.

It is out of the scope of this dissertation to discuss the results so far achieved by the Kyoto Protocol, even though the data in Figure 4 stand out to highlight a partial failure of the protocol. However, a political institution has emerged as the more challenging and advanced in tackling climate change; not surprisingly, it is also the institution that has funded the project described in this dissertation.

#### *The European example*

The European Union has been at the front of the environmental debate since the Rio Conference in 1992; however, only with the increasing power conceded by the member states to the central government, the Utopia of an extensive and integrated energy policy for the whole union (27 Member states, almost 500 million people) has become reality [13].

Not only the EU-15, as signatory of the Kyoto Protocol, appears to be well on the way of complying with the limits imposed by the protocol [22], but in January 2008 the European Commission revealed a much more ambitious and comprehensive climate and energy package [14, 18].

The so-called “20 - 20 - 20 by 2020” package lays down the targets to be achieved within the year 2020 [18], while the “strategic energy technology plan (SET)” [14, 24] sets a roadmap for investments and deployment of low-carbon energy technologies to achieve such targets.

The targets laid out by the Commission are the following:

- A reduction of at least 20% in GHG emissions compared to the 1990-level by 2020 (The reduction in 2008 is predicted to be around -6.2% [22]). This commitment will increase to 30% in case an international agreement for the post-Kyoto period will be reached.
- A reduction of 20% of total primary energy consumption (compared to a business as usual scenario) by 2020 [13].
- A share of 20% of renewable energy sources in the EU Final Energy Consumption. Among the considered sources, a special target is assigned to biofuels which will have to cover at least 10% of the transportation fuels market by 2020. The share today is 9.2% [38]

To give an idea of the opportunities that such measures would create, the European Commission predicted that [13]:

- The measures would save at least € 50 billions in oil and gas imports by 2020 (with oil prices at € 61), thus protecting European industries and households from increasing energy prices;
- The increase in share of renewables and efficiency would create almost a million jobs in 2020 and many opportunities for European industries to achieve a leading role in the world market of low-carbon technologies;
- The increase in biomass use itself (including biofuels) is estimated in the direct creation of up to 300.000 jobs, most of which in rural areas [4].

To achieve such challenging objectives, the role of technologies is of primary importance. Several visions and roadmaps are being produced in these years [14, 24], covering many available and future technologies, from wind to nuclear fission and carbon capture and storage. From Figure 14, which summarizes some of these visions, it is possible to see that again, thermal conversion of solid biomass and biofuel production are considered key technologies for the achievement of the targets mentioned above.



- When carefully managed, biomass can be stored safely for long periods, so that biomass acts as a “natural battery” to store solar energy and can guarantee continuous generation of power and heat, as opposed to solar and wind;
- Biomass is the only energy source that can easily replace partially or totally fossil fuels in the short-term with few modifications to existing technologies: solid biomass fuels can substitute (or integrate) coal, bio-ethanol and bio-diesel can take the place (or integrate) of fossil gasoline and diesel, while syngas or biogas can substitute natural gas in many applications.
- Bioenergy is in theory “carbon neutral”: the CO<sub>2</sub> which is released during combustion had been previously fixed in the plant from atmospheric CO<sub>2</sub> and water (as explained better in Chapter 2). Biomass could function, theoretically, even as a “carbon sink” if the carbon released during thermal conversion was captured and stored.
- Bioenergy allows for valorisation of waste streams and byproducts into valuable power, heat and chemicals.
- Biomass use for bioenergy can promote development and additional sources of income for the rural areas of developed and developing countries and eventually offer a way to counteract the constant depopulation of such areas.

#### *Cons*

- Biomass matter has a low energy density, (about half the one of crude oil but close to the one of young coals, as explained better in Chapter 2) which makes logistics more difficult and expensive;
- Bioenergy is a renewable source but before the actual biomass source is ready for conversion, seeds need to be planted, fertilized, harvested and processed. These processes add not only costs to the initial biomass fuel (as opposed to solar and wind energy sources which are instead readily available), but also hinder the definition of carbon neutrality for biomass because of the fossil energy used during the whole life cycle of the biofuel [109].
- Biomass has a relatively limited availability due to the issues with logistics associated with its low energy density, and its impact on global energy supply can, thus, only be limited;
- Bioenergy involves policies and technical knowledge from many different backgrounds in order to optimize the whole life cycle from seeding to final conversion. Agronomy, bio-engineering, energy and chemical

process technology are only some of the fields involved in the study of bioenergy. Moreover, implementing effective policies is also complex: specific energy policies for biomass could conflict with other existing environmental or economic policies (such as the clash in Europe between biomass for energy policies and the Common Agricultural Policy).

- There has been and there are still concerns about possible negative side-effects of an extensive use of biomass for energy. Among such concerns can be named for example: possible scarcity of food if food sources are used to produce bio-fuels on a large-scale and consequent influence on food prices (biofuels are considered partly responsible for the food price spikes in 2008 [20]); the debate on the actual GHG savings and net energy balance from 1<sup>st</sup> generation bio-ethanol [109]; the concerns over possible deforestation in developing countries in favour of energy crops (e.g. Malaysia and Indonesia for palm plantations [367]); the concerns on the actual effects of ethanol-gasoline blends on tailpipe emissions [276].

### 1.2.2 *Biomass perspectives*

Despite the cons listed above, as underlined in the previous section, biomass sources for energy already have a prominent role in the European energy pool. And the role of bioenergy in the future is destined to be even bigger.

The European Environment Agency [6] estimated that the environmentally – compatible (no additional pressures on biodiversity, soil or water resources are exerted compared to a scenario without increased bioenergy production) primary energy obtainable from biomass in Europe could be around 190 Mtoe in 2010 and up to 295 Mtoe in 2030. This amount would be enough to cover around the 15 - 16% of the projected primary energy requirements of the EU-25 countries, in line with the declared targets [23]. It is important to note that one third of this potential would be covered by bio-wastes, including: solid agricultural residues, wet manures, the biodegradable part of MSW and black liquor. The use of bio-wastes is crucial because it not only carries out the disposal of waste material, but it upgrades such low-value substances to high-value energy carriers. Moreover, the use of biomass residues avoids the controversy of using edible materials for energy conversion [150, 307]. For these reasons most of the modern research is focused on the so-called 2<sup>nd</sup> generation biomass fuels, including biowastes, algae and hydrophytes.

Such increased use of bioenergy will involve all the sectors: transportation biofuels, electricity generation (through solid biomass, biogas and municipal solid waste combustion) and heating (Figures 15 and 16).

In order to be able to fully exploit the biomass potential there will be need for drastic improvements in biomass conversion technologies. Investments in research are considered essential to achieve such breakthrough and in fact, the budget allocated to the energy research by the EU, in its last Framework

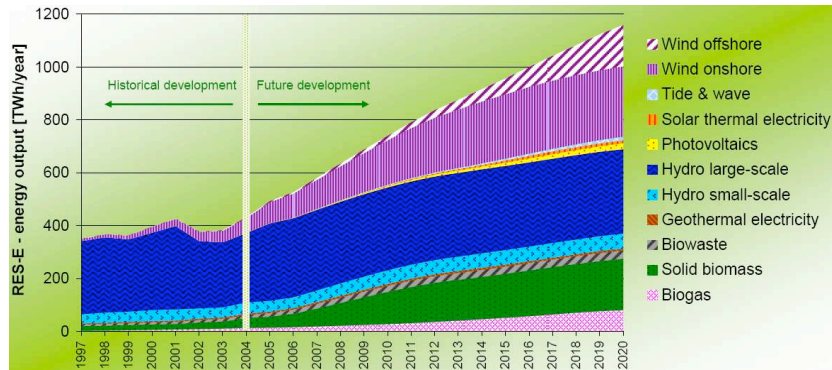


Figure 15: Projected growth in renewable electricity in EU-25 countries. Source [16]

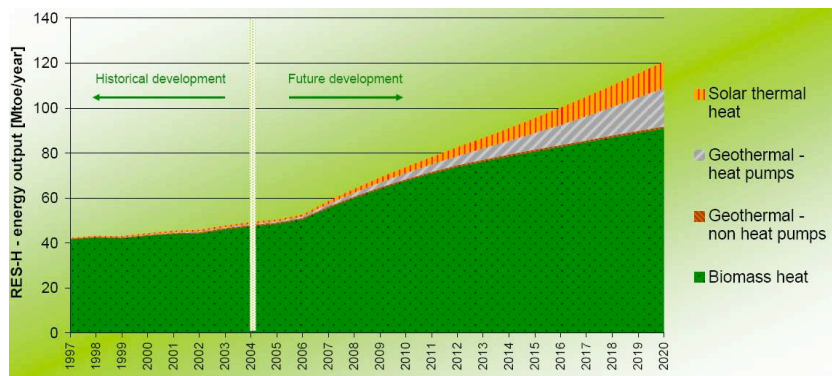


Figure 16: Projected growth in renewable heating and cooling in EU-25 countries. Source [16]

Programme 7, has increased to € 886 millions/year as compared to € 574 millions/year granted in the previous 7 years [17].

In the next sections I will give a brief overview of the possible conversion paths of biomass into energy (or energy carriers) and further I will dive into more details about technologies and issues in thermal conversion, which is the main topic of this dissertation.

### 1.2.3 The routes of biomass conversion

Figure 17 depicts the possible routes for the conversion of biomass materials into power and heat or other different energy carriers like bio-oil, bio-fuels and  $H_2$ . It is worth noticing that biomass sources are, in the short-term, the only ones capable of directly substituting fossil fuels in every application. Moreover, biomass materials are very rich sources of chemicals, as it will be explained in the next chapter. The concept of the bio-refinery has,



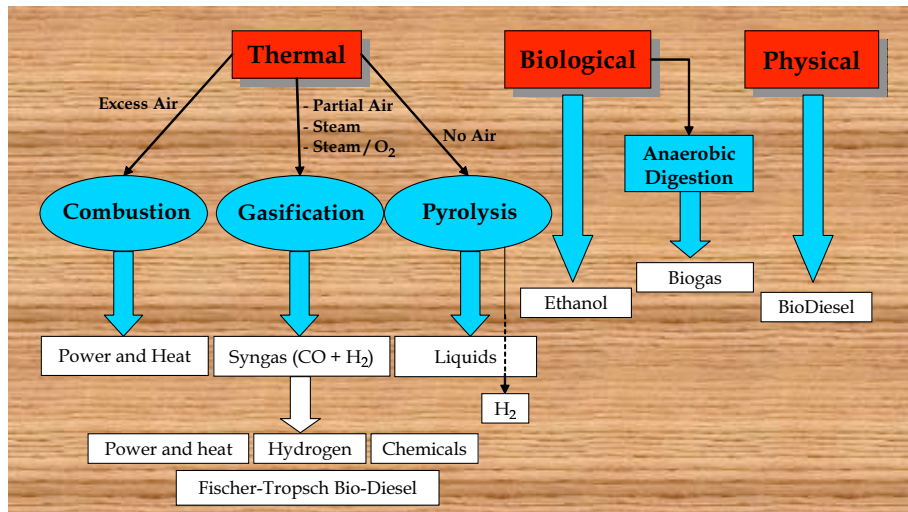


Figure 17: Conversion paths of biomass

in fact, raised again high interest among the research community. The main idea behind this concept is to extract different high-value products from biomass materials, including chemicals, fuels and, ultimately, heat and power [131, 184, 207, 228, 252, 305].

Many reviews and books are available on the synthesis of transportation fuels from biomass [81, 122, 130, 132, 188, 235, 237, 238, 288, 308], therefore it seems superfluous to try and sum up here such a vast concept.

Instead, since the work developed in this dissertation deals with the thermal conversion of biomass materials, a brief introduction to the current technologies is given. Additional details and information on biomass structure and mechanisms of thermal conversion are explained in Chapter 2.

#### 1.2.4 Technologies for thermal conversion of biomass

This section will provide a brief overview of the technologies currently used for thermal conversion of biomass and their role in the current markets.

The different technologies can be divided according to the applied oxidizer. It is important to notice that a fully integrated “biomass system”, including supply, processing and conversion of the material is still far from reality. Especially when dealing with wastes, whose composition and availability might change during the year, fuel flexibility is a crucial characteristic for a successful technology. Thermal conversion, compared to other conversion routes, already provides much higher flexibility since all the components of biomass are converted. However, this also has the drawback that different fuels possess

diverse characteristics making the characterization of each feedstock essential for an efficient use of these technologies.

#### *Pyrolysis (Inert atmosphere)*

Pyrolysis is the first step, after drying, in every thermal conversion process of solid fuel [114]. Pyrolysis dates back to at least ancient Egyptian times, when tar and certain embalming agents were produced by means of pyrolysis of wood [268].

As it will be described in details in Chapter 2, this process involves a decomposition of the solid fuel into volatiles and char, solely due to the effect of heat supply. The weight loss during the devolatilization of biomass is usually around 70 – 80 % of the initial weight [103, 159, 163], and therefore this step has a crucial role, not only on the control and stability of the whole conversion, but also on the total emissions and fuel reactivity.

Such process can also be employed as stand-alone in order to transform the original biomass into gaseous, liquid and solid products. Some biomass fuels, in fact, have a rather low energy density [147] and consequently, the transportation of the raw materials to the conversion site has a significant impact on their life-cycle emissions. Therefore, pyrolysis can be applied as a pre-treatment to upgrade a solid, low energy-density fuel, into a liquid, high-density bio-oil.

When biomass is heated up in the absence of oxygen, the distribution of its products varies greatly with the process conditions [115, 116, 268, 352, 365]:

- Low operational temperatures ( $\sim 300^\circ\text{C}$ ) and long residence times of vapors (i.e. low heating rates,  $\sim 10^\circ\text{C}/\text{min}$ ) favor the formation of charcoal (*carbonization*)
- High temperatures ( $\sim 700 - 800^\circ\text{C}$ ) and long residence times favor the formation of light gases (*gasification*)
- Moderate temperatures ( $\sim 500^\circ\text{C}$ ) and short residence times of the vapors promote the formation of liquids (condensable tars) (*fast pyrolysis*)

Despite some niche applications for charcoal production [67, 133], the current focus is mostly on the last option, targeted at the production of the so-called bio-oils [268, 365]. Two valuable reviews on pyrolysis technology development in the last 20 years and bio-oil characterization are the ones written by Bridgwater and Peacocke [116] and Mohan et al. [268]. Constantly up-to-date information can be found on the website of the IEA Bioenergy initiative, Task 34 for pyrolysis of biomass [42].

Pyrolysis has two evident advantages: first, almost any kind of biomass can be used and upgraded to liquid fuel; secondly, light gases and chars are used to sustain the temperature of the process and thus no side stream is produced. Moreover, the bio-oil produced has a high energy density (40 - 50 %

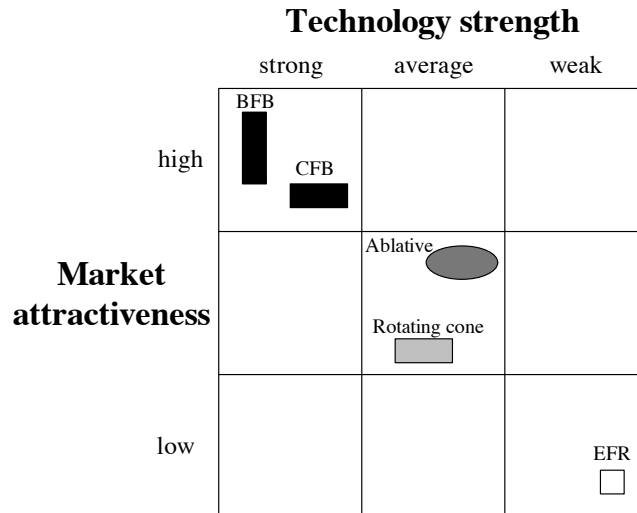


Figure 18: Technology status of pyrolysis reactors. BFB: Bubbling Fluidized Bed, CFB: Circulating Fluidized Bed, EFR: Entrained Flow Reactor. Source: [352]

of the value for hydrocarbon fuels [280]), it is storable and easier to transport than solids, it can replace fuel oil and diesel in some stationary processes and contains many high-value chemicals like pharmaceuticals and adhesives which can be extracted in a later stage [261].

The main drawbacks for such application at the moment reside in the high costs of the bio-oils, the high content of water, the presence of organic acids that are highly corrosive, the presence of solid particles, their high viscosity, the problems with long-term storage stability but, most of all, the inconsistent quality of the oils [261, 268, 280, 365]. In fact, although every biomass can be fed into a pyrolysis reactor, the composition of the resulting oils will differ substantially depending on the feedstock and the operating conditions [115, 268, 280, 281, 282].

Nowadays, the state of technology for the production of bio-oil by pyrolysis is between development and demonstration [42]. Figure 18 represents the current status of reactors used for pyrolysis. Fluidized beds are the most attractive option due to their fuel flexibility, ability to deliver high heating rates and short residence times of the gases [200]. The shortcomings of this technology reside in the limited understanding of the hydrodynamics and of the reaction kinetics [352].

#### *Gasification (Limited supply of oxidizer)*

The gasification of solid fuels is a known process since many years. Its capacity to convert solid fuels to combustible gas has attracted the attention of market and research since more than 150 years [152, 201].

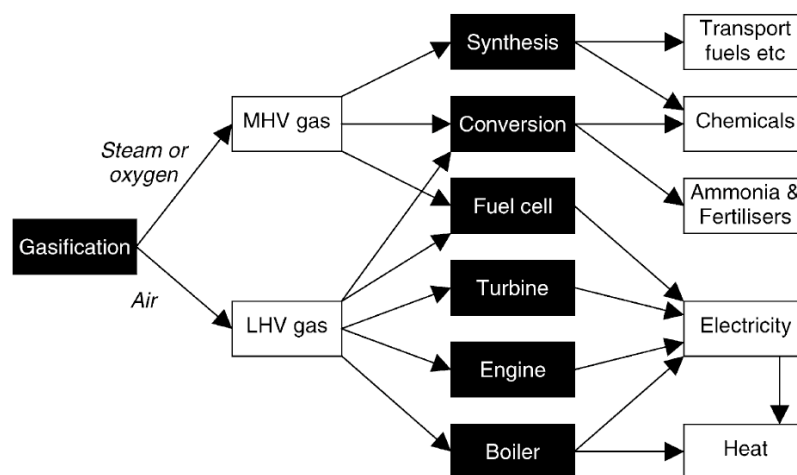


Figure 19: Applications for syngas from biomass gasification. Source: [115]

When providing a limited supply of oxidizer ( $\lambda \approx 0.3$ ) to the reactor at a temperature around  $800 - 1000^\circ\text{C}$ , the products of devolatilization and the residual char undergo only a partial oxidation. This produces a gas, called syngas, rich in  $\text{CO}$ ,  $\text{CO}_2$ ,  $\text{H}_2$  and  $\text{CH}_4$ .

As in pyrolysis, process conditions can define the distribution of products: gasification with air produces a very low-heating-value gas due to the dilution of  $\text{N}_2$ , while gasification with oxygen or steam provides a syngas with medium dry heating value. The promotion of the reforming reactions increases the amount of hydrogen in the gas at the expenses of methane.

The applications for the gasification gas, as illustrated in Figure 19, are multiple. Together with heat and power, the syngas can be used for the synthesis of various chemicals (among which ammonia and methanol [83, 145])[206] and also for bio-diesel production via a Fischer-Tropsch reaction. Moreover, applications for a hydrogen-rich gas in Solid Oxide Fuel Cells [71] and for the production of  $\text{H}_2$  for automotive applications are also under investigation [40]. Gasification is also considered the best option for the pre-combustion  $\text{CO}_2$  capture, which would lower the GHG emissions from biomass and, mostly, coal [32, 33, 34].

The current status of technology for biomass gasification is illustrated in Figure 20. As in pyrolysis, fluidized-bed reactors are the most attractive option for the market due to their fuel flexibility and their good scale-up potential, especially with woody biomass [115, 145, 201]. Pressurized technologies are at the moment almost abandoned because of the higher capital costs and technical problems with pressurizing the biomass feed flow. Entrained flow reactors are nowadays popular mostly for co-gasification of biomass and coal; their benefit is that they can be scaled-up to huge sizes ( $>1000\text{MW}$ ) and low or no

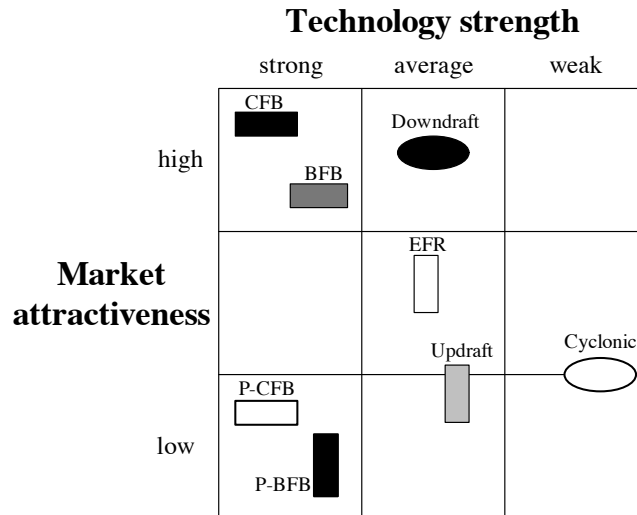


Figure 20: Technology status of biomass gasification. BFB: Atmospheric Bubbling Fluidized Bed, CFB: Atmospheric Circulating Fluidized Bed, P-BFB: Pressurized Bubbling Fluidized Bed, P-CFB: Pressurized Circulating Fluidized Bed, EFR: Entrained Flow Reactor. Adapted from: [115]

tars are generated because of the high temperatures involved. However, their fuel flexibility is quite limited because the fuel has to be reduced in very fine particles and the higher temperatures involved can cause more trace metals to go into the gas phase [201].

The production of heat and power through biomass gasification is used in large-scale plants achieving electrical efficiencies of up to 40% [152]. A review of demonstration and commercial plants can be found in de Jong [200, 201].

Integrated Gasification Combined Cycle (IGCC) plants fed with coal are a known technology, built since many years. However, the experience with these technology is still limited and hindered by some drawbacks [152].

Some of the main issues related to fluidized-bed gasification can be listed as following:

- The hydrodynamics of the system are highly influenced by the feedstock, especially by the inorganic matter which can cause agglomeration of the bed material and subsequently loss of fluidization [74, 85, 117, 218, 248, 249, 263, 275, 360].
- Knowledge of actual kinetics of fuel devolatilization and homogeneous gas reactions is essential in order to optimize the quality and quantity of product gas [115, 200] (maximize  $H_2$  and minimize heavy aromatic compounds called tars); this knowledge is still lacking for many bio-wastes.

- The cleaning of the syngas to a commercial utilization quality gas requires further investigation due to the high contamination of tars and solid particles at the exit of the reactor [266, 327, 337].
- The mechanisms of release of pollutants, such as S and N species, from the fuels is still highly unknown [200]. The formation of nitrogen species during gasification such as  $\text{NH}_3$ , HCN, HNCO and tar-N are of primary importance since they can have a significant impact on the  $\text{NO}_x$  emissions from gas turbines burning syngas [57, 187]. Moreover, while  $\text{NH}_3$  can act as a fuel in a SOFC system [71], the impact of HCN and tar-N on the catalysts used still needs to be fully investigated. Therefore, a thorough investigation of the chemistry of conversion of fuel-bound nitrogen is essential for an efficient deployment of these technologies.

#### *Combustion (Excess supply of oxidizer)*

Combustion is the complete oxidation of the fuel. Combustion of biomass for the production of heat and power has been proven and utilized already since many years and worldwide already provides over 90% of the energy from biomass [39], even though most of it comes from not efficient “traditional biomass” as described in section 1.1.1.

Biomass, in the form of wood fire, is the oldest fuel ever used by mankind, since the dawn of civilization, for cooking and heating. Fire in itself, from the myth of Prometheus on, has been associated with the power of the human mind and with science.

In a more modern meaning, small-scale domestic heating in open fireplaces or small furnaces is very common in countries like Germany, Sweden and Austria, even though with general low efficiencies, as low as 10%, and with considerable emissions [152]. Lately, however, in those countries, much improved technologies and standardized fuels have been developed, such as modern automatic pellet boilers with catalytic gas cleaning, that can reach overall energy efficiencies of 70 – 90% [30, 152]. District heating and CHP is also common in Northern-European countries like Denmark, which developed a major program for the utilization of straw with subsequent improvements in boiler design and fuel pre-treatments [152, 166].

Large-scale biomass stand-alone combustion is a mature technology when used for incineration of the organic part of Municipal Solid Wastes (MSW) and for the combustion of black liquor, a residue from the pulp and paper industry. Grate furnaces are usually applied for MSW incineration due to the capacity to burn many diverse wastes, while special recovery boilers have been developed for black liquor combustion [152, 232]. Typical electrical efficiencies for MSW incineration are around 20%<sub>el.</sub> but new plants are expected to reach efficiencies of about 30%<sub>el.</sub> [8, 152]. The use of fluidized-bed combus-

tors allows a dramatic scaling up of such technologies, up to  $500\text{MW}_{\text{th}}$ , with efficiencies of 30 to 40 %<sub>el.</sub> when using high-quality wood chips [8, 152].

The option of co-firing biomass in coal power plants is gaining more and more popularity among utilities. Co-firing is definitely among the lowest risk, least expensive, most energy efficient and shortest term options for biomass deployment in particular and renewable-based power and heat generation in general [39, 93]. Addition of biomass to coal-fired boilers, in fact, does not affect or only slightly decreases the overall conversion efficiency. At the same time, the biomass conversion efficiency ranges around values of 35 to 45 %, higher than in many dedicated biomass combustion systems.

The Netherlands have a long-term experience with co-combustion and co-firing is carried out in most coal-fired plant [139], with fuels ranging from clean wood to sludges, and manures [28, 139]. The share of fired biomass is usually around 1 to 20 %<sub>th</sub> [8, 93, 152], with most installations using values below 10 %<sub>th</sub>. With low shares of biomass, in fact, additional investments are low (even though additional operating costs still require subsidies to make co-firing economically viable [93, 61]) and there are high potentials for GHG and sulfur emissions mitigation due to the directly avoided emissions of coal. Due to the high share of coal in the world electricity production, in fact, even replacing only 5 % of coal would bring an immediate saving of 300 Mton/year of CO<sub>2</sub> emissions [28, 61]. The short-term co-firing potential worldwide has been estimated in more than 500 PJ. However, more and more plants in Denmark, Finland and The Netherlands are increasing the share of biomass in ranges of 25 to 70 %<sub>th</sub> with the flexibility to run on a 100 % biomass. An updated situation of co-combustion in Europe can be found in several papers and reports [28, 61, 93].

An IEA database accounts for 228 installations worldwide applying co-firing [39, 61], with many different boiler types and with capacities ranging from 50 to 700 MW<sub>e</sub>. Most of the coal combustion plants are based on pulverized fuel technology and therefore that is also the main technology where co-firing is applied. Fluidized-bed boilers are the second most diffused technology, followed by grate furnaces [251].

The effects and synergies of a high share of biomass on the process efficiencies and equipments are, however, not fully known for many bio-wastes as well as the effects of biomass on overall NO<sub>x</sub> and N<sub>2</sub>O emissions [39, 152, 360]. Therefore, research on coal – biomass co-firing is still highly necessary to increase even more the share of coal directly replaced and thus favour a faster and economically viable deployment of an integrated biomass system [8, 39, 93, 140, 218, 278, 336, 360].

Moreover, the effects of the different ash composition in biomass compared to coal require still deep investigation in order to avoid serious problems of fouling, corrosion and bed agglomeration [93, 360].

	Basic and Applied R&D	Demonstration	Early Commercial	Commercial
Biomass to Heat			Small-scale Gasification	Combustion (in boilers & stoves)
Combustion		Combustion in ORC or Stirling engine		Combustion+ Steam cycle
Gasification	IGFC	IGCC IGGT	Gasification+ Steam cycle	
Co-Firing		Indirect co-firing	Parallel co-firing	Direct co-firing

Biomass-to-Heat    
 Biomass-to-power or CHP

Figure 21: Development status of biomass-to-power and heat or CHP technologies. ORC = Organic Rankine Cycle, IGFC = Integrated Gasification Fuel Cell, IGCC / IGGT = Integrated Gasification Combined Cycle / Gas Turbine. Source [92]

The view of the experts in the IEA Bioenergy programme on the status of technologies for power and heat production with biomass is shown in Figure 21.

#### 1.2.5 $NO_x$ emissions

The definition of nitrogen oxides ( $NO_x$ ) includes mainly nitrogen dioxide ( $NO_2$ ) and nitric oxide (NO). Nitrous oxide ( $N_2O$ ) is another important nitrogen pollutant produced during the thermal conversion of fuels. These compounds are harmful for the environment and human health in several ways [134]:

- Nitrogen oxides react with water and oxygen in the atmosphere to form nitric acid, responsible, together with sulfuric acid, for acid rains.
- These acids can react to salts and form particulate matter in the atmosphere ( $PM_{10}$  and  $PM_{2.5}$ ) which is harmful to the human respiratory system.
- $NO_2$  is a serious respiratory irritant.



- NO is responsible for ozone formation on ground level.
- NO<sub>2</sub> deposited by rain in the waters can cause eutrophication: nitrogen is a nutrient for plant material, an excess of it in the water creates an overproduction of vegetation which cause problems for fish and other aquatic animal population.
- N<sub>2</sub>O is a strong greenhouse gas with a global warming potential (GWP) per molecule 300 times higher than CO<sub>2</sub> [10].

NO is mainly produced in combustion processes, both for stationary power and heat production but, mostly, in the transportation engines. NO<sub>x</sub> and N<sub>2</sub>O emissions are subject to regulation since many years and their limits have been constantly decreasing [134]. Consequently, technologies for NO<sub>x</sub> reduction are well established [134].

In common power plants, the main source of nitrogen oxides is the thermal mechanism [134], due to the high temperatures in the flame zones. However, in fluidized-bed combustors, the temperatures used are much lower and thus the thermal-NO mechanism is not important and the main source of NO (or NO<sub>x</sub> precursors in case of gasification) is the fuel-bound nitrogen. This mechanism will be better described in Chapter 2.

In air blown gasification processes, for example, the produced syngas contains relatively high concentrations of NH<sub>3</sub>, HCN and nitrogen-containing hydrocarbons [178]. When syngas is used in IGCC turbines, most of the NO emissions are caused by these compounds [218]. Gas cleaning is therefore required. However, most of the available techniques (primary and secondary removal) present heavy drawbacks and high additional costs for the plant operator [134, 200]. An increase of conversion of fuel-bound nitrogen to molecular nitrogen during gasification itself is therefore advantageous, both in technical and economical terms.

The nitrogen content in biomass matter varies greatly in quantity and structures with the different materials, as it will be explained in Chapter 2. As mentioned above, fluidized bed reactors are commonly chosen for their ability to handle a variety of feedstocks, but with varying feedstocks, the amount and origin of fuel-bound N also varies. This makes it hard, if not impossible, to predict and control the NO<sub>x</sub> emissions if the behavior of each fuel is not known in detail.

### 1.3 OPEN ISSUES

We have seen that, despite the increasing importance of bioenergy in all current energy policies, the majority of technologies for thermal conversion are still not mature. One of the main limitations of biomass stand-alone power plants is the availability of fuel. For this reason and for the experience accumulated in the last 30 years, fluidized-bed reactors are one of the favored

technologies. However, their use is still limited by some issues, some of which will be faced in this thesis.

1. ***Heterogeneous composition of biomass fuels.*** The definition of biomass for energy, given by the Directive 2009/28/EC is the following: “the biodegradable fraction of products, waste and residues from biological origin from agriculture (including vegetable and animal substances), forestry and related industries including fisheries and aquaculture, as well as the biodegradable fraction of industrial and municipal waste”. Chapter 2 will give a better insight into the physico-chemical nature of biomass; however, it is easy to understand that the term “biomass” includes many different materials. Moreover, these fuels are heterogeneous also in their own composition making it very hard to predict a priori their large-scale behavior.
2. ***Quality and quantity of inorganic material.*** The quantity and composition of inorganic matter varies greatly among different biomass fuels, as it will be explained in Chapter 2. While wood usually contains a very low amount of ash forming matter [147, 314], other residues, like straw or husks, present higher amounts of ashes (around 3 – 5 %<sub>wt</sub>). Sludges and manures are examples of extreme cases with ash content up to 50 %<sub>wt</sub>. However, quantity is not the only problem. Also the composition of such ash forming matter is troublesome. K, Cl and Na, together with Sulfur and Silica, contained in high concentrations in agricultural residues and other biomass materials, interact to form alkali silicates and alkali sulfates with melting points far lower than normal boiler temperatures (down to 700 °C). Such ash reaction gives rise to problems such as slagging, fouling, corrosion and, in fluidized-bed reactors, to the agglomeration of bed material and consequent loss of fluidization, as seen in previous sections.
3. ***Fuel-bound nitrogen chemistry.*** We have seen that fluidized bed boilers operate at temperatures well below the onset of thermal-NO<sub>x</sub> reactions. Therefore, the main source of NO<sub>x</sub> or NO<sub>x</sub>-precursors is the fuel-bound nitrogen. During years of experience with NO<sub>x</sub> abatement many primary removal techniques, directly applicable in the reactor, have been developed (e.g. low-NO<sub>x</sub> burners, air staging, flue gas recirculation and variations in residence time of the fuel) in order to reduce NO<sub>x</sub> precursors to molecular N<sub>2</sub>. In fluidized bed reactors, however, low-NO<sub>x</sub> burners cannot be used and neither can catalytic flue gas cleaning because of catalyst poisoning [165], so that the possibility of achieving NO<sub>x</sub> reduction in the reactor becomes essential for emission control. As explained in section 1.2.4, moreover, NO<sub>x</sub> emissions in co-combustion are difficult if not impossible to predict without a deep fundamental knowledge of the phenomena involved. This knowledge is still limited

---

for many biomass fuels and virtually absent for other potential biomass wastes.

#### 1.4 RESEARCH QUESTION

In view of the issues listed above, this thesis has the goal to answer the following main question:

“Which, how fast and how many nitrogen compounds are released during the thermal conversion of biomass wastes?”

The results obtained in this study will shed light on the mechanisms of devolatilization and combustion of some secondary fuels that have not yet been investigated. The outcome of this study will provide a deeper knowledge of the nitrogen chemistry of these fuels, under pyrolysis and combustion conditions, that will be essential to optimize the process conditions for maximal  $\text{NO}_x$  reduction. Furthermore, the kinetic parameters obtained with these measurements are almost totally lacking for these waste fuels and can, thus, be used in numerical models to optimize or to predict the chemistry of devolatilization in industrial applications. Finally, the tests on pre-treated biomass will provide important data to determine the effects of such pre-treatments on the fuels' composition and reactivity and eventually pave the way for an industrial application of these techniques.

The following sections will explain the methodology applied to the work carried out for this project and the collateral questions that will be answered while investigating the main one.

#### 1.5 METHODOLOGY

This work aims at characterizing the behavior of several biomass waste materials under thermal conversion conditions. The main focus is on the fuel-bound nitrogen structure and chemistry, but additional data regarding the kinetics of devolatilization and effects of the presence of inorganic materials are retrieved at the same time.

Investigations on fuel characteristics are usually carried out on large-scale or small-scale setups, or a combination of the two. Large-scale measurements can guarantee a direct comparison with real process conditions: the evaluation of parameters such as efficiency, emissions and operational problems can easily be applied to commercial-scale applications. However, when so many phenomena influence the outcome of a measurement, it is difficult to retrieve the fundamentals of such mechanisms. With small-scale experiments, instead, it is possible to control the process conditions and the outcomes of the measurements in a much more detailed way.

The results presented in this dissertation were obtained on small-scale setups. The measurements, as the chapters in which they are presented, were designed as follows:

1. **Slow pyrolysis measurements.** Pyrolysis is the first step in any thermal conversion of a solid fuel [114, 225, 251]. Its fundamental understanding is essential for interpreting and predicting conversion kinetics and emissions. Devolatilization happens in the range of milliseconds or few seconds, depending on particle size, in combustors or gasifiers, too fast for any reliable measurement of weight loss or gaseous release. For this reason, it has become common practice in the scientific community to perform slow pyrolysis tests, that is, with heating rates ranging from 1 to 100 °C/min. These tests were carried out in the present work using a Thermogravimetric Analyzer (TGA) connected with a Fourier Transform InfraRed (FTIR) spectrometer (described in Chapter 3). In such a setup, the sample is heated up in a controlled way in an inert atmosphere while its weight loss, together with the volatiles released, is continuously monitored. Kinetic parameters for the global devolatilization and the release of many gaseous compounds can be retrieved by applying a chemical kinetic model (as explained in Chapter 3). As stated above, the drawbacks of these measurements are that the conditions under which they are performed are very different from the ones encountered in industrial applications.
2. **Fast pyrolysis measurements.** In order to reproduce conditions more similar to the ones found in commercial applications, the fuels were tested in a heated foil reactor, capable of reaching heating rates of more than 1000 °C/s. The speed of such phenomena makes it impossible to monitor the detailed weight loss and volatile release. Therefore, such measurements were aimed at testing the influence of a much faster devolatilization on the release of volatile compounds, mostly NO<sub>x</sub> precursors, and global reactivity.
3. **Combustion tests.** Once the pyrolysis of the fuels was studied in its kinetics and verified at conditions closer to real applications, the materials were tested under combustion conditions. This was also performed using a small-scale reactor in which the oxygen concentration and the wall temperature were the control parameters. The release of NO and CO<sub>2</sub> was monitored through commercially available analyzers. The results from pyrolysis tests help understanding (and eventually modeling) the emissions under combustion or gasification conditions.

The above-mentioned experimental activities help to clarify the fundamental mechanisms of thermal conversion for the chosen biomass residues. They also provide data which can be used for future application on the modeling of large-scale processes [139, 200, 202, 204].

A CFD model of the heated foil reactor used for fast pyrolysis measurements was also developed in the framework of this project. Due to the speed of the phenomena involved in the reactor, in fact, many process conditions cannot be reliably measured (e.g. temperature and velocity distribution in the reactor volume). The CFD model, thus, makes it possible to simulate the physical conditions in the reactor in greater details, offering a precious tool for the interpretation of experimental results.

## 1.6 OUTLINE

Figure 22 helps to illustrate the outline of this thesis. This dissertation is divided into 8 chapters. Chapter 2 presents an addition to the definitions given and used in this introduction and in the rest of the thesis. This includes an overview of the structural compounds found in biomass materials and general composition of many materials, a theoretical background on thermal conversion of solid fuels and a review on literature investigating the mechanisms of nitrogen precursors and nitrogen oxides formation during thermal conversion of biomass fuels.

Chapter 3 introduces the fuels examined and the experimental setups used to carry out the measurements described in the following chapters. The materials chosen for the investigation were: wheat straw, olive residues, peach stones, dry distiller's grains & solubles (DDGS), chicken manure and palm kernel cake. Some pre-treatments such as water leaching and mechanical fractionation were carried out on the fuels in order to improve their ash quantity and quality. The experimental setups used were: Thermogravimetric Analyzer (TGA), Fourier Transform Infrared Spectrometer (FTIR), Heated Foil reactor (HF) and Single Particle reactor (SPR). The chapter provides a literature review on the origins of the fuels and their thermal conversion characteristics, as well as an investigation on previous works using the same type of setups. Finally, a detailed introduction is given on the kinetic models usually applied in biomass pyrolysis, specifically on the Distributed Activation Energy Model (DAEM).

Chapter 4 starts the description of the results of the measurements carried out in the framework of this project. As explained above, the results are presented in the direction of the most detailed experiments but farthest from real conditions (slow pyrolysis) to the most closely related to industrial conditions (combustion tests). Therefore, Chapter 4 reports the results of measurements carried out on a TG-FTIR setup under slow pyrolysis conditions. The fuels analyzed in this chapter are wheat straw, olive residue and peach stones and their pre-treated samples. Devolatilization profiles are given together with the kinetic parameters of global devolatilization. Moreover, kinetic parameters for the formation of light volatiles such as  $\text{CO}_2$ ,  $\text{CO}$ ,  $\text{CH}_4$ ,  $\text{H}_2\text{O}$ , are given. Finally, the effects of the pre-treatments on ash forming matter quantity and quality and on the reactivity of the fuels are explained.

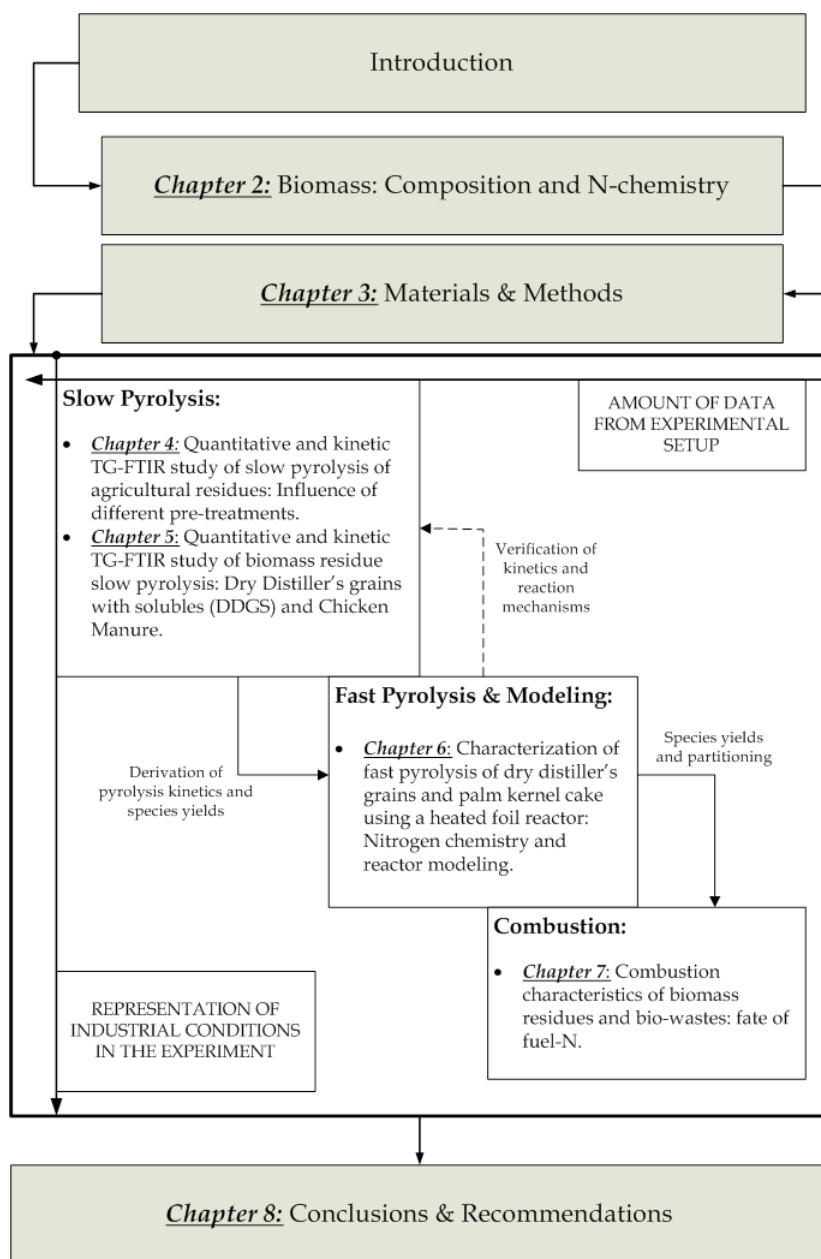


Figure 22: Schematic of the outline of this thesis

---

Chapter 5 illustrates the results of measurements similar to the ones described in Chapter 4. The fuels tested in this chapter are DDGS, chicken manure and their water-leached samples. The same typology of results is found as in the previous chapter and in addition,  $\text{NO}_x$  precursors are measured for these fuels. The kinetic parameters for the evolution of  $\text{NH}_3$ , HCN and HNCO during the slow devolatilization of these fuels are also presented.

Chapter 6 describes tests carried out using a heated foil reactor. Such tests provide results for the flash pyrolysis of DDGS and palm kernel cake. Final weight loss, final yields of light volatiles and nitrogen partitioning between char and volatiles are given. A comparison thereof with the results of the slow pyrolysis tests is described as well. A numerical model of the heated foil reactor is also introduced in this chapter and the temperature on the foil is verified via non-contact infrared pyrometer and compared with the simulations.

Chapter 7 presents the results of combustion tests performed in a single-particle reactor. Five biomass wastes are tested, among which, DDGS, chicken manure and palm kernel cake. Different oxygen concentrations and different final temperatures are analyzed. The final release of NO and  $\text{CO}_2$  from the fuels are given, as well as the profiles of release of such compounds. The partition between NO released during pyrolysis and char oxidation is presented for all the fuels.

Finally, in Chapter 8 the conclusions obtained in the previous chapters are summarized and by means of such conclusions, the main and secondary research questions are answered. Recommendations for future research work are also given.





# 2

---

## OVERVIEW OF BIOMASS COMPOSITION AND NITROGEN CHEMISTRY

---

*This chapter aims at expanding on some concepts which will be important in the rest of this dissertation: firstly, a description of the main structures present in biomass and their biological functions is given. Their thermal decomposition characteristics are also briefly introduced together with a summary of literature on the composition of various biomass fuels. Secondly the basics of solid fuels thermal conversion are explained. Finally, an overview of the main nitrogen structures present in biomass materials and the mechanisms of NO<sub>x</sub>-precursors and NO<sub>x</sub> formation is given. Throughout the chapter, moreover, several relevant references will be introduced to underline the state of the art knowledge on these topics.*

## 2.1 BIOMASS AND FOSSIL FUELS (OR “VERY OLD BIOMASS”)

The definition of biomass for energy given in the European Directive 2009/28/EC is the following:

“the biodegradable fraction of products, waste and residues from biological origin from agriculture (including vegetable and animal substances), forestry and related industries including fisheries and aquaculture, as well as the biodegradable fraction of industrial and municipal waste”.

This classification is very broad and it includes materials which, despite being accounted together as “biomass”, have little in common in terms of chemical composition and reactivity.

Figure 23 represents the Van Krevelen diagram of various types of coals and wood. Such diagram clearly underlines the relation between “young” fuels, like biomass, and older fuels like peat and coal. Biomass is characterized by a large content of oxygen which diminishes with the relative age of the fuels. The origin of coals and biomass is in fact similar and fossil fuels could well be defined as “very old biomass” fuels!

Once vegetable matter dies and it is covered by soil, it undergoes the process of coalification: under the mixed effects of pressure, heat and bacterial activity, the material is depleted of oxygen and hydrogen and is progressively enriched in carbon. In Figure 23 this process can be followed: in the top right part are young fuels like wood, rich in oxygen and hydrogen with gross heating values ranging from around 10 to 25 MJ/kg<sub>dry</sub>, as shown in Table 1. Moving to the left, peat is found: peat has been forming for around 360 million years [49] and during this process much of the water and of the biodegradable part from the original biomass material (trees, grasses, fungi and other organic remains) has been removed and the material that is left, consequently, has higher heating values in the range of 20 to 25 MJ/kg<sub>dry</sub> [147]. Moving on in history, lignite (or brown coal), is considered to be the youngest of coal types; it has a heating value of about 25 MJ/kg<sub>dry</sub> [147].

Finally, in the bottom left part of the diagram bituminous coals and anthracites are grouped. These materials present a carbon content of 80% or more and have heating values ranging around 30 to 37 MJ/kg<sub>dry</sub> [147] and are ranked according to their oxygen and hydrogen content [323].

A common classification for biomass and derived fuels is usually the following: wood and woody materials (e.g. hard and soft wood, demolition wood), non-woody biomass (e.g. agricultural residues, grasses and residues from industry), fruit and by-products of fruit industry, other residues and recovered materials (e.g. manures, sewage sludges, refuse derived fuels (RDF) and the organic part of MSW) [5].

All these materials present very different compositions and characteristics which make a detailed characterization, in terms of kinetics and emissions,

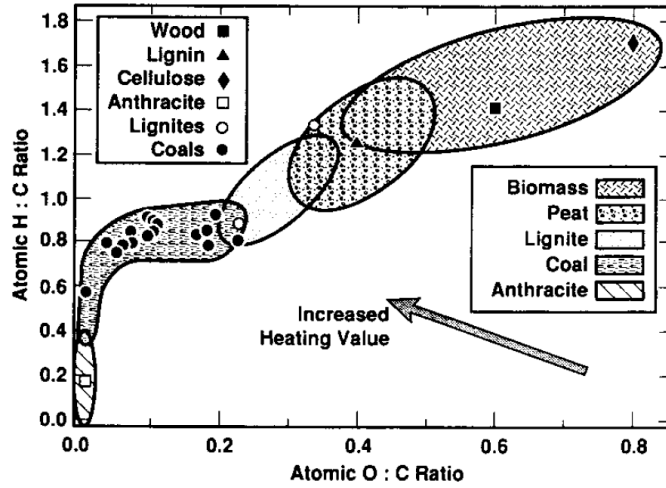


Figure 23: Van Krevelen coalification diagram. Source: Baxter [94]

essential for an efficient utilization. This is in fact the main purpose of this dissertation.

In order to present even a better idea on the heterogeneous nature of biomass materials, Table 1 summarizes the main characteristics of several biomass fuels in comparison with different coals.

### 2.1.1 Main structures in biomass: Origins

Despite the great variation in nature and composition of such materials, some common structures can be expected to be present in all such organic fuels, even though the amounts can vary with species, type of plant tissue, stage of growth and growing conditions [218, 314].

Biomass can be referred to as “nature’s solar battery” [92]: solar energy, in fact, is used by plants to synthesize their structural carbohydrates in the process of photosynthesis. Photosynthesis (from the Greek *photo* = light and *synthesis* = composition) is the process that converts carbon dioxide and water into organic compounds using photons from solar light to activate chlorophyll.

Even though the mechanism of the reaction is very complex and some photosynthetic processes are not yet fully understood [319], the overall reaction can be written as:

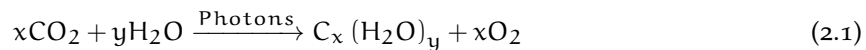
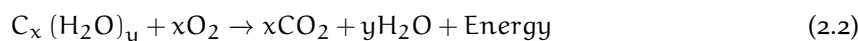


Table 1: Elemental analysis of various biomass fuels, bioresidues and coals. Data are on a dry basis.

FUEL	C	H	O	N	HHV	REFERENCES
Wood	52-49.4	6.9-5.2	42.1-39.7	1-0.33	20-18.5	[105, 338, 204]
Wheat straw	43.7-43.3	5.5-5.1	42-40.9	0.8-0.6	18.9	[90], This Work
Olive residue	54-47	6-5.4	34-31.7	3.2-0.9	21.7-18.1	[283, 338, 343], This Work
Miscanthus	48-47.9	5.6-5.3	42.8	0.6-0.54	17.9	[105, 204]
DDGS	49	6.3	32.6	4.5	19.8	This Work
Rapeseed cake	49.9-45.9	6.9-6.2	40.1-30.6	6.9-5.1	22.2-19.5	[341], This Work
Palm kernel cake	49-48.3	7.1-6.2	37.4-34.9	2.6-2.3	20.7-17.8	[338], This Work
Chicken manure	39.5- 32.8	4.4-4.1	34.9-15.6	5.9-3.3	14.9-13.3	[140, 338], This Work
Sewage sludge	33-26.5	5.9-4.4	19-17	4.4-3.2	12.1-11	[239], This Work
Meat and bone meal	43.1-40.2	6-5.8	20.8-15.6	9.2-8.5	18.6	[140, 338]
Brown coal	64.7	4.7	22.6	1.3	25.7	[147]
Bituminous coal	76.7	4.7	10.5	1.4	31.6	[147]
Anthracite	88.9	3.4	2.3	1.55	34.6	[147]

Photosynthesis is vital for life on Earth and it is responsible for it by balancing the amounts of CO<sub>2</sub> and O<sub>2</sub> in the atmosphere [50].

The carbohydrates that are formed are the main repository for energy for living beings; when their energy is released via oxidation (either with metabolic processes in the living tissues or combustion) the reaction is the following:



As it is evident from equations 2.1 and 2.2 the definition of “carbon neutral” applies perfectly to biomass materials since the carbon released in combustion is the same that was previously absorbed from the atmosphere. However, during the whole life cycle of biomass, fossil fuels are commonly used to: produce fertilizers and pesticides, grow and collect the plants, transport the harvested material and, finally, upgrade it to an actual fuel (e.g. biofuels production and pelletization). Due to all these energy-consuming side operations, biomass fuels are actually carbon neutral only in theory: for example, Wang et al. [355] calculated that even using a blend of 95 %<sub>vol.</sub> ethanol with gasoline, using the current technology for corn-based ethanol, the estimated reduction in GHG emissions would only be approximately between 21 and 27 %.

It is also interesting to notice that, being fossil fuels basically “really old biomass”, as explained in the previous section, the CO<sub>2</sub> released during their combustion was also previously absorbed from the atmosphere via metabolic processes and could also be defined carbon neutral. However, the fossil-carbon was fixed into organic matter hundreds of millions of years ago and would therefore be neutral to the pre-historic atmosphere and not to the present one!

#### 2.1.2 *Main structures in biomass: Characteristics*

The following section will define in more details the various main structures of which biomass is composed of and the characteristics of their thermal decomposition.

- **Cellulose:**

Cellulose is the most common organic compound on Earth and the most abundant biopolymer synthesized by Nature, approximately 10<sup>11</sup> ton/yr [208]. Cellulose is the main constituent of plants cell walls and is widely used in many common products such as paperboard and paper (from wood pulp), in the textile industry (cotton is composed for 90 % by cellulose [45]), for the production of other synthetic fibers like cellophane and Rayon and as a base for the production of celluloid (previously used as a photographic and movie film until mid '30s) [44].

Cellulose is a high-molecular weight (10<sup>6</sup> of molecular weight or more)

linear homopolysaccharide constituted of  $C_6$  sugars, namely D-glucopyranoside units, connected by  $\beta$ -glycosidic linkages [268, 314], as shown in Figure 24. The glucose units are polymerized into long, straight chains of 5000 – 10000 units. The basic repeating unit of the cellulose polymer consists of two glucose units and it is called cellobiose unit.

By forming intramolecular and intermolecular hydrogen bonds between the -OH groups within the same cellulose chain and the surrounding chains, the polymeric chains tend to arrange themselves parallel and to form a crystalline supermolecular structure which makes cellulose completely insoluble in normal aqueous solutions. Bundles of linear cellulose chains (in the longitudinal direction) tend to twist in space to make ribbon-like microfibrils structures which are oriented in the cell wall structure [82, 268].

This special configuration of cellulose makes it more resistant to thermal degradation than hemicellulose. Cellulose is known to decompose (in slow pyrolysis conditions, heating rates in the order of magnitude of  $10^\circ\text{C}/\text{min}$ ) following almost perfectly a 1<sup>st</sup> order reaction in a temperature range of 250 - 380  $^\circ\text{C}$  [66, 68, 103, 159, 163, 171, 186, 268, 278, 366]. However, the decomposition of cellulose in “real” biomass material can be different due to the influence of inorganic matter and linkages with the other structures [195, 345].

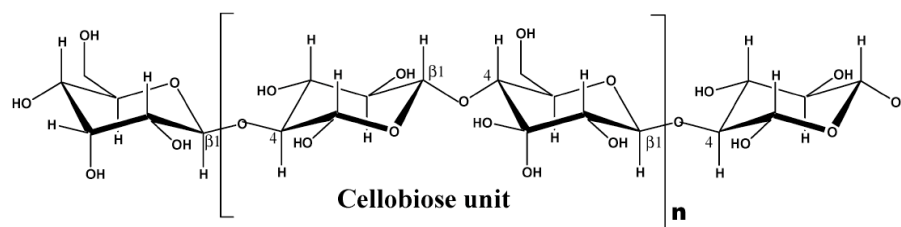
Cellulose fibers make up for around 40 to 50 %<sub>wt</sub> of dry wood. Other materials, especially bioresidues usually have a lower content of cellulose, but other lignocellulosic materials, like cotton, have a much higher content of cellulose fibers [82], as shown in Table 2 and 3.

- **Hemicellulose:**

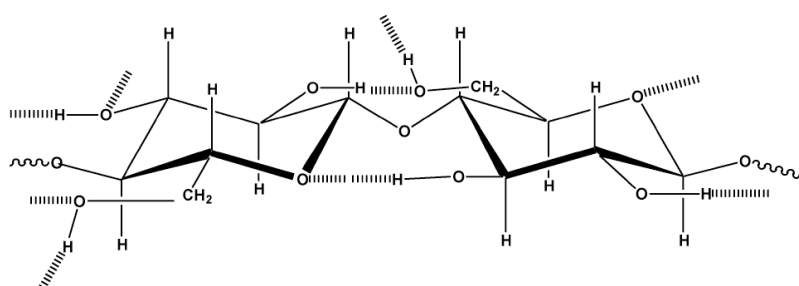
Hemicellulose (from the Greek: *hemisys* = half) is the second major constituent of biomass materials. Hemicellulose, with its amorphous structure, acts as a cement material in plant cell-walls holding together the cellulose micells and fibers.

Hemicellulose is a mixture of various polymerized monosaccharides such as glucose, mannose, galactose, xylose, arabinose and others which are summed up in Figure 25. Hemicelluloses consist of chains of lower molecular weight compared with cellulose and with repeating monomers in the order of 150 compared with the  $10^4$  of cellulose. The chains are, therefore, shorter and in some cases present side-chain branches. Hemicellulose, together with cellulose and pectin, belongs to the so-called “structural carbohydrates”, while other carbohydrates like saccharose and starch are called “storage” compounds [208].

Hemicelluloses exhibit different composition of sugars from species to species. For example, in deciduous woods, rye and oat it is mostly composed of pentosans, while in coniferous woods, wheat and barley, it is almost entirely composed of hexosans [208, 268]. Hemicelluloses are a



(a) Chemical structure of cellulose.



(b) Intrachain and interchain hydrogen-bonded bridging.

Figure 24: Structure of cellulose and chain bridging. Source: Mohan et al. [268]

rich source of monomeric sugars and base chemicals such as furfural [203, 254] and xylitol (sweetener used also in chewing gums), which make them precious in a future biorefinery concept [247].

Hemicellulose usually accounts for 25 to 35 % of dry wood, in softwoods and about 35 % in hardwoods. Content in other biomasses is shown in Table 2 and 3.

Hemicellulose is thermally less stable than cellulose. Measurements of xylan under slow pyrolysis conditions (10 - 20 °C) showed decomposition in two peaks closely situated in the range of temperatures of 200 - 350 °C [103, 159, 163, 186, 278, 345, 366].

- **Lignin:**

Lignin (from the Latin *Lignum* = wood) is a complex, heterogeneous polymer synthesized from the phenylpropanoid precursors shown in Figure 26a. These basic units are linked mostly by ether bonds but also carbon-to-carbon linkages exist, as shown in Figure 26b. The lignin matrix comprises many several functional groups such as hydroxyl, methoxyl and carbonyl [268].

Moreover, lignin is covalently linked to hemicellulose and cellulose, thus conferring mechanical strength to the whole plant [46, 82, 268]. Lignin is not digested by animal enzymes, it gives protection to the plant from bacteria, it helps water circulation in the vascular system of plants and

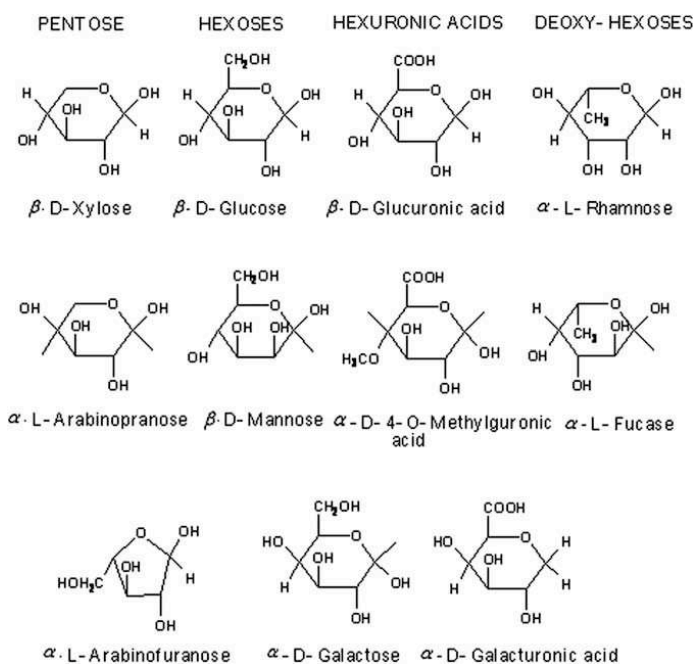


Figure 25: Sugar units typical of hemicelluloses. Source: Balat et al. [82]

is the least degradable part of dead plants making it the most important component of humus [46].

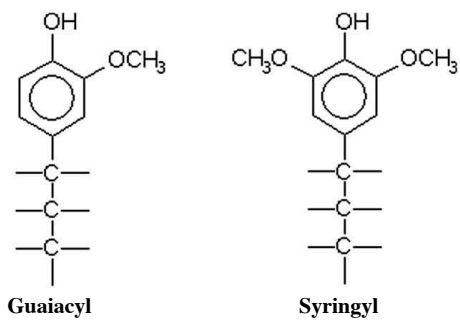
The heterogeneous nature of lignin and its strength is evident also in its thermal stability: many studies under slow pyrolysis conditions show that lignin reacts over a broad range of temperatures, starting at about 250 °C up to 500 °C [103, 186, 278, 366].

As for hemicellulose, quantity and quality of lignin changes with biomass materials and species: softwoods are more rich in “guaiacyl” lignin with a content of around 23 to 33 %<sub>wt</sub>, while hardwoods have a content of about 16 to 25 %<sub>wt</sub> of mostly “guaiacyl - syringyl” lignin. The content of lignin of different lignocellulosic materials is shown in Table 2 and 3. Lignin is nowadays mostly produced as a by-product in the pulp-and-paper industry where it is usually combusted for power and heat production. However, despite having a higher heating value than the other components of biomass, lignin can be used to produce other high-value products such as phenolic resins. Lignin also has a role in the rubber industry and in the production of antioxidants [293].

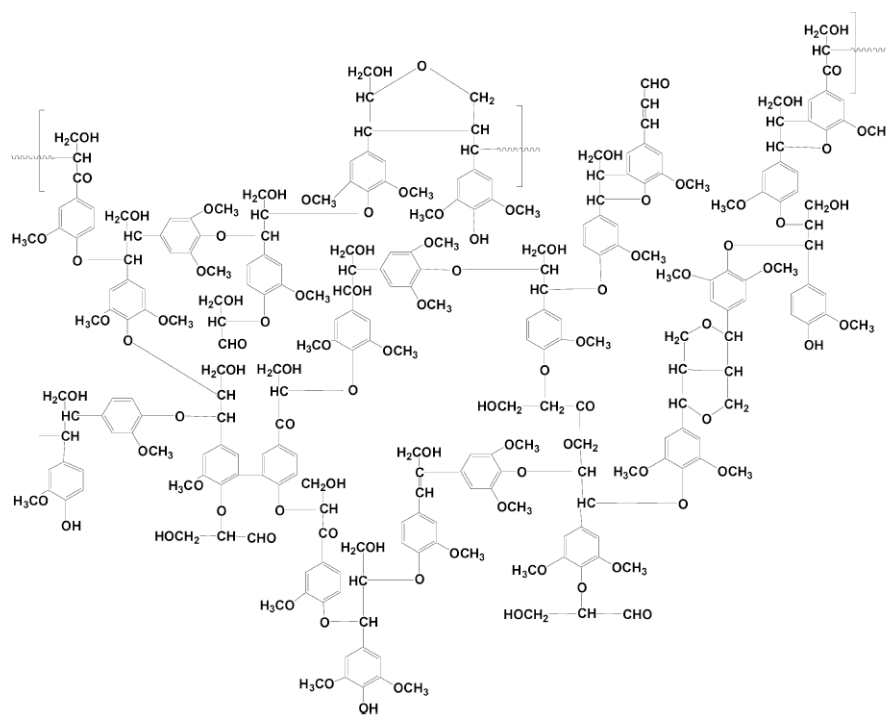
- **Starch:**

Starch, like cellulose, is a polymer constituted of glucose sugar units, but,





(a) Building units of lignin. Source: Balat et al. [82]



(b) Schematic of lignin structure. Source: Mohan et al. [268]

Figure 26: Structural units of lignin and an example of lignin structure.

Table 2: Typical lignocellulose content of some plant materials. Data are on dry basis.

PLANT MATERIAL	HEMICELLULOSE	CELLULOSE	LIGNIN
Orchard Grass <sup>a</sup>	40.0	32.0	4.7
Rice Straw <sup>a</sup>	27.2	34.0	14.2
Birchwood <sup>a</sup>	25.7	40.0	15.7
Poplar <sup>b</sup>	43	31	23
Oak <sup>b</sup>	35	32	26
Wheat straw <sup>b</sup>	32	37	18
Cotton <sup>c</sup>	91.2	0.8	0.4
DDGS <sup>d</sup>	16	13.5	n.a.

<sup>a</sup>Mohan et al. [268]<sup>b</sup>Kamm et al. [208]<sup>c</sup>ECN [147]<sup>d</sup>Kim et al. [220]

Table 3: Ranges of variation of the chemical composition of different lignocellulosic feedstock. Data are on dry basis. Source: Kamm et al. [208]

FEEDSTOCK	CELLULOSE (%)	HEMICELLULOSE (%)		LIGNIN (%)
		HEXOSES	PENTOSES	
Softwood	40-48	12-15	7-10	26-31
Hardwood	30-43	2-5	17-25	20-25
Cereal Straw	38-40	2-5	17-21	6-21
Maize Straw	35-41	2	15-28	10-17
Rape Straw	38-41	-	17-22	19-22
Recovered Paper	50-70	-	6-15	15-25

unlike cellulose, such units are linked together by  $\alpha$ -glycosidic linkages. Such bonds are weaker than the ones of cellulose, which makes starch digestible also by human enzymes. Starches are composed by two main molecules: the linear and helical amylose and the branched amylopectin. Most starches yield 10 - 20% amylose and 80 - 90% amylopectin [319]. As mentioned above, starch is one of the storage components used by plants to store energy in the form of glucose units which are easily accessible for the plant metabolism.

Table 4: Composition of common raw materials for industrial production of starch. Data are on wet basis. Source: Gröll et al. [173]

(%wt as received)	MAIZE	POTATO	TAPIOCA	WHEAT	RICE
Moisture	16	75	70	13	14
Starch	62	19	24	60	77
Protein	8.2	2	1.5	13	7
Ash	1.2	1.2	2	1.7	0.5
Sugars	2.2	1.1	0.5	8	0.3
Fiber	2.2	1.6	0.7	1.3	0.3
Fat	4.2	0.1	0.5	3	0.4

Starch is usually stored in the form of small granules and it is found in tubers, roots, seeds and fruits. It is commonly present in cereals and tubers like maize, potatoes, wheat and rice. The composition of some of the main feedstocks for the industrial production of starch can be found in Table 4.

Starch is a common feedstock for the 1<sup>st</sup> generation bioethanol: starch is first separated from the original cereal (e.g. corn, wheat, barley), then it is decomposed by enzymes into monomeric glucose and finally fermented by yeast into bio-ethanol [110, 197]. Starches are also widely used in the paper industry (to confer dry strength to the paper and for coating), textile, cosmetics, pharmaceuticals (as binding agent in tablets and pills) and food processing (as thickener and stabilizer) [51, 173].

Starches decompose, under slow pyrolysis conditions, in the range of temperature of 300 - 350 °C [58, 174, 185].

- **Other organic compounds (Fats and Extractives):**

Together with the above-mentioned structures, biomass presents other components such as extractives, oils and monomeric sugars. These compounds are widely used as food (e.g. olive or sunflower oil and sucrose from sugarcane) but also as lubricants, rubbers, pharmaceuticals (e.g. antibiotics and vitamins synthesis), dyes and even cosmetics (e.g. Jojoba oil) [106, 230]. However, they are also used as feedstocks for many 1<sup>st</sup> generation biofuels: vegetable oils, via the process of trans-esterification, are used for production of biodiesel (mostly from rapeseed and soybean oils) while monomeric sugars (mostly from sugarcane and sugar beet) are fermented to produce bioethanol.

- **Inorganic matter:**

The inorganic matter in biomass materials varies widely both in quantity

and quality among different plants and sources. Woody biomass, for example, presents very low amount of ash forming matter [147], while animal or industrial residues, like chicken manure or sewage sludge, contain very high amount of inorganic matter (up to 20 to 50% of the initial dry weight) [163, 164, 202, 338, 359]. Furthermore, agricultural residues and herbaceous matter are rich in silica and calcium (that give strength to the cell walls) as well as alkali metals (like potassium) and phosphorous (which are present in crystal salts and, P, also in the DNA of the plant). Chlorine is present in biomass matter in higher quantities than most fossil fuels (with the exception of marine coals) [76, 275] and Mg, contained in the chlorophyll, is also found in significant amounts, especially in green plants. Heavy metals are present in traces in biomass materials in amounts depending on their origins. Extensive reviews and data for different fuels can be found for example in Jenkins et al. [194], Vassilev et al. [351], Tortosa Masía et al. [338] and others [218, 289, 360].

- **Water:**

It might seem trivial but moisture is one of the main components of biomass and constitutes a main difference with coals. Water, in fact, is essential for every living tissue and it is fundamental in the process of photosynthesis, as mentioned above. The moisture content of fuels is very important for the stability of any thermal conversion process (e.g. wet bagasse from the sugar cane production [328]) and a very moist fuel might require to be dried before feeding into the reactor [359] or even require the application of a much different technology (e.g. supercritical water gasification for wet manures [231, 260]). Moisture in biomass varies greatly among the different materials but it is influenced also by the harvesting period and storage conditions [193, 340]. While woody materials and herbaceous biomass usually have a lower content of moisture, other residues like manures and sludges can contain more than 90%<sub>wt</sub> of water [147, 359].

### 2.1.3 Nitrogen compounds in biomass

Nitrogen content in biomass, as shown in Table 1, can vary considerably from less than 1% in wood, up to almost 10% in animal waste [351]. As described in Chapter 1, fluidized bed reactors work at temperatures considerably lower than the onset of thermal-NO<sub>x</sub> formation. The fuel-bound nitrogen becomes, therefore, the primary source of NO<sub>x</sub> in combustion and its precursors in gasification. Therefore, especially when analyzing high-N fuels like many bioresidues, a deep knowledge of nitrogen functionalities in biomass is essential to choose the optimal reactor conditions and eventual gas cleaning technologies.

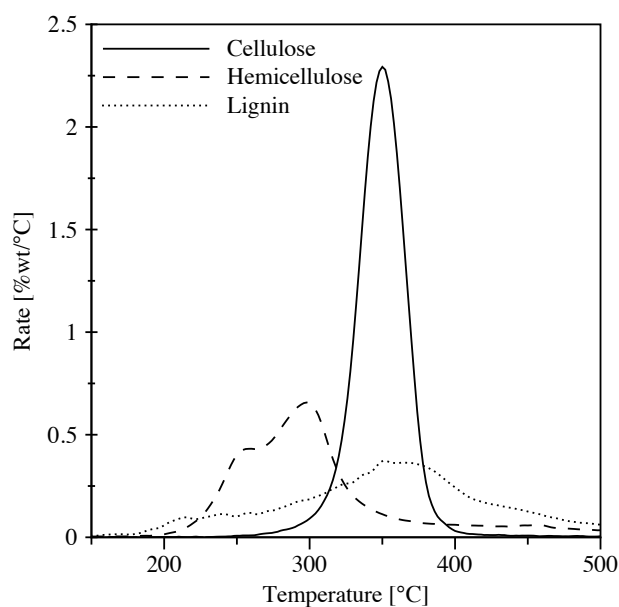


Figure 27: Thermal decomposition in slow pyrolysis of the main components of lignocellulosic materials. Heating rate = 20 °C/min in helium. Source: Heikkinen et al. [186]

To the author's knowledge, a systematic study to assess the origin of nitrogen functionalities has not been carried out on biomass, as it has been done, instead, on coal by Pels et al. [287]. Nitrogen is, with carbon and oxygen, at the very basis of every living being, plants as well as humans and animals. Nitrogen is found in many different structures and with many different functions:  $\alpha$ -amino acids, enzymes, proteins, DNA and many others [319]. A quite comprehensive review, from a bioenergy point of view, was compiled by Becidan [95] and a few concepts of it are summed up in this section.

#### 2.1.3.1 Total Nitrogen content

As indicated in Table 1, the total content of Nitrogen varies greatly among different biomass fuels, depending on its origin. However, the content of nitrogen is also influenced by the location in the plant (due to the organic function of the compounds), the season of harvest, the age, the resources availability (e.g. fertilizers and the type of water) and the stage of growth of the plant.

From Figure 28 it is possible to notice how the nitrogen content varies according to its biological function: it decreases, in wood, going deeper in the trunk as a result of cell maturation and at the same time it is most abundant in the seeds which contain nutritive (proteins) and protective (alkaloids for antifungal activity) compounds [95].

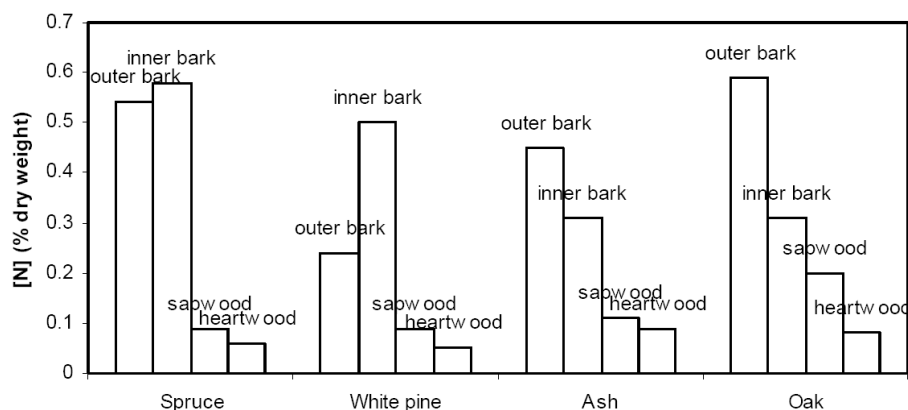


Figure 28: Nitrogen content in different plant sections. Source: Becidan [95]

### 2.1.3.2 Nitrogen functionalities

#### Proteins and $\alpha$ -amino acids

The main biomass structures in which nitrogen is found are proteins. Proteins are bio-macromolecules that consist of amino-acids joined by peptide bonds. As shown in Figure 29, an amino-acid is a compound which contains both amine and carboxylic acid functional groups. In nature, proteins are made out of 20 primary amino-acids called  $\alpha$ -amino acids which are depicted in Figure 30. Some of the amino-acids can be synthesized by all living organisms while others need to be taken in through diet and are called "essential amino-acids". Human beings, for example, cannot produce eight amino acids: Valine, Leucine, Isoleucine, Phenylalanine, Tryptophan, Threonine, Methionine and Lysine need to be assimilated through food. Insulin, hemoglobin and enzymes are examples of human proteins.

Studies in biomass have shown that most of the nitrogen is indeed either in the form of proteins or free amino-acids with quantities ranging from few percents to more than 35% of the initial weight. Table 5 summarizes some of the available results in literature.

The thermal history of proteins is usually investigated using as model compounds the basic  $\alpha$ -amino acids. Much literature is available on the slow pyrolysis of amino-acids and some of the main results are summed up in Tables 6 to 8.

Due to the more complex structure of proteins in the real biomass, it is very difficult to use results from model compounds as a predictive tool [95]. However, as it will be shown in the next sections and chapters, these results can give helpful information to analyze pyrolysis of biomass samples.

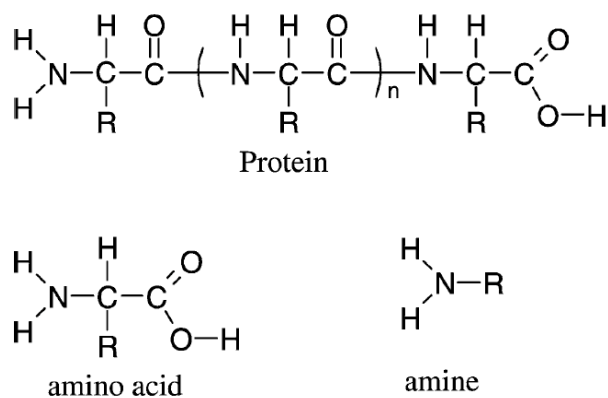


Figure 29: Common nitrogen structures in biomass. Source: Hansson et al. [180]

Table 5: Protein content in various biomass materials. Data on a dry basis

BIOMASS	PROTEIN CONTENT(%)	REF.
Softwood	0.2-0.8	[241]
Needles+Leaves	7-8	[241]
Corn	10	[126]
Corn stover	5	[126]
Soybean	40	[126]
Alfalfa	20	[126]
DDGS	25	[220]
Palm Kernel Cake	19	[294]
Cottonseed cake	40	[294]
Olive oil cake	6	[294]
Soybean cake	48	[294]
Rapeseed cake	36	[228]
Wheat straw	3-6	[147]
Chicken manure	47	[148]

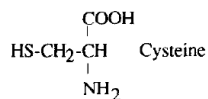
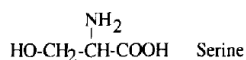
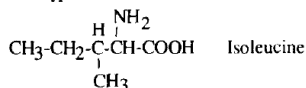
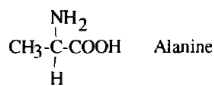
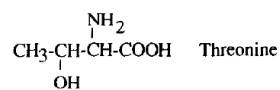
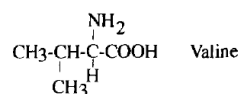
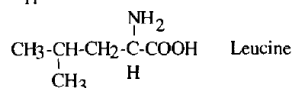
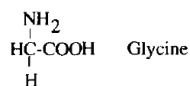
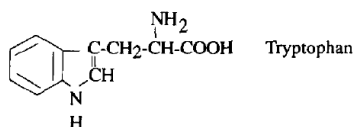
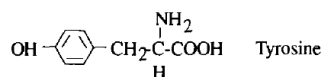
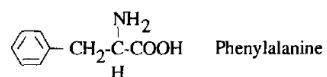
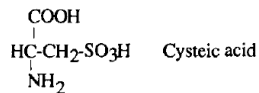
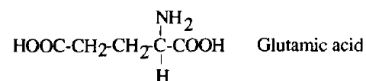
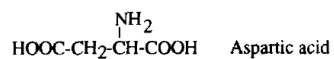
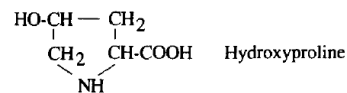
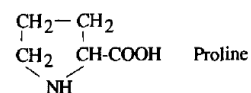
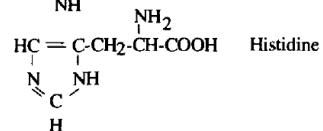
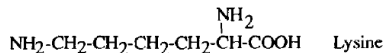
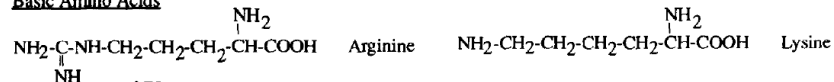
Neutral Amino AcidsAromatic Amino AcidsAcidic Amino AcidsSecondary Amino AcidsBasic Amino AcidsFigure 30:  $\alpha$ -amino acids. Source: Leppälähti and Koljonen [241].



Table 6: Thermal decomposition of some  $\alpha$ -amino acids with aliphatic chains.

MODEL COMPOUND	SETUP	HR (°C/MIN)	PEAK TEMPERATURE (°C)	REF.
L-Glycine	TG-FTIR	10-20	255-282	[244, 302]
L-Leucine	TG-FTIR	10-20	306-334	[243, 302]
L-Isoleucine	TG-DSC	10	301	[302]
D-Valine	TG-DSC	10	296-300	[302]
L- $\alpha$ -Alanine	TG-DSC	10	301	[302]
L-Threonine	TG-DSC	10	267	[302]
L-Methionine	TG-DSC	10	295	[302]
Serine	TG-DSC	10	235	[300]

Table 7: Thermal decomposition of some  $\alpha$ -amino acids with five- and six-membered rings in their side chains.

MODEL COMPOUND	SETUP	HR (°C/MIN)	PEAK TEMPERATURE (°C)	REF.
L-Phenylalanine	TG-FTIR	10-20	276/377- 291/404	[245, 302]
L-Tyrosine	TG-FTIR	10-20	318-334	[245, 302]
Tryptophan	TGA	10	297/395- 297/409	This work, [302]

Table 8: Thermal decomposition of some acidic, basic and secondary  $\alpha$ -amino acids.

MODEL COMPOUND	SETUP	HR (°C/MIN)	PEAK TEMPERATURE (°C)	REF.
L-Lysine	TG-FTIR	10	239/349/435	This work
L-Aspartic acid	TGA	10	240/264/397	[302]
L-Glutamic acid	TGA	10	197/284	[302]
Proline	TG-DSC	10	234	[300]

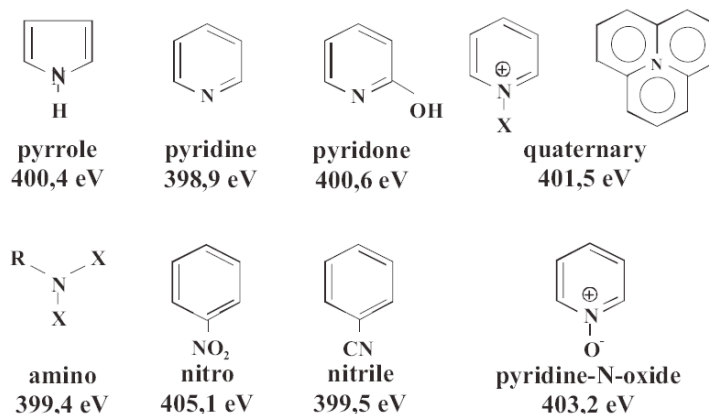


Figure 31: Nitrogen functionalities in coal and their XPS binding energies. Source: Di Nola [139]

### *Heterocyclic nitrogen*

While nitrogen in biomass is mostly in proteinic form, the main N-structures found in coal are, instead, aromatic, as shown in Figure 31 [139, 287]. The study of nitrogen functionalities in coal has been more successful than for biomass due to the crystalline structure of coal. This characteristic allowed measurement techniques like XPS, XANES and NMR to produce clear and easily interpretable signals, as seen in Figure 31. For biomass, unfortunately, this is not the case: even with much higher nitrogen concentrations, vacuum based techniques like XPS cannot be easily applied due to the volatility of the materials and  $^{15}\text{N}$ -NMR does not yield signals of clear interpretation. The “youngest” fuel to yield clearly interpretable signals appears to be peat and soils in general, for which a number of studies are available [62, 215, 223, 224].

Several investigations have been carried out to determine the nitrogen functionalities in different coals and, through the study of different model compounds [86, 287, 320], a clear picture is now available. The results of these studies [86, 118, 205, 213, 216, 269, 287, 354] show that most fuel-bound nitrogen in high-rank coals is in pyrrolic and pyridinic groups. However, other structures are present, like pyridone and the so-called quaternary nitrogen which is usually interpreted as a graphite-like structure with an N-bridge [287]. The works of Pels et al. [287] and Kelemen et al. [214] are the best sources for an in-depth study of the transformations of heterocyclic nitrogen structures during pyrolysis.

### *Heterocyclic-N in biomass*

Heterocyclic-N structures are present in biomass as well, even though in minor quantities compared to proteinic-N.

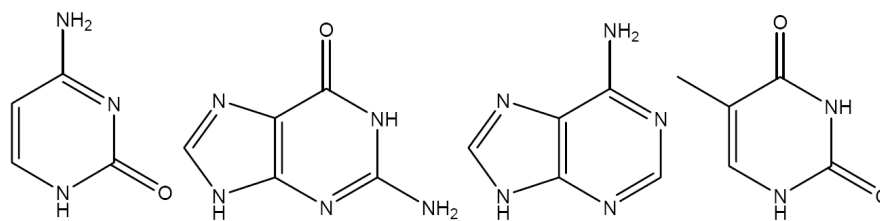


Figure 32: DNA heterocyclic bases: Cytosine, guanine, adenine and thymine. Source: Becidan [95]

**NUCLEIC** Among these structures are, for example, nucleic acids (e.g. DNA and RNA). Nucleic acids are the biomolecules containing the genetic information of living cells. Nucleotides are the building bricks of the macromolecules and are constituted by a nucleobase, a pentose and a phosphate or polyphosphates [95].

The four heterocyclic bases are shown in Figure 32.

No detailed study on the amount of nitrogen contained in biomass as nucleobases has been performed to the author's knowledge. However, Hansson et al. [180], based on the phosphorous content in several biomass samples, came to the conclusion that the content of DNA is not significant compared to other structures.

**ALKALOIDS** Alkaloids are extracted from several parts of plants, like bark, roots, leaves, berries and fruits. They are nitrogen-containing bases which react with acids to give salts (from which the name, because they behave alkali-like). The nitrogen atoms of most alkaloids is present in heterocyclic rings, even though, in a few cases, nitrogen can be present as primary amine or as an ammonium group. The variety of these substances amounts to thousands and their functions and effects on humans and animals vary greatly [319]. Some examples of notorious alkaloids are: *Strychnine* (a poison extracted from the seeds of the *Strychnos nuxvomica* plant), *morphine* and *codeine* (extracted from opium poppy), *nicotine* (extracted from the tobacco leaves) and *cocaine* (extracted from the leaves of the coca plant). Such compounds are used for many purposes but mostly in the pharmaceutical industry [95, 319]. Most of these compounds are very well known as well as their sources so they have to be taken into account when dealing with specific materials (e.g. residues from coffee [98] will have considerable amount of caffeine) but are not relevant in many other fuels.

**CHLOROPHYLL** As mentioned above, chlorophyll is an essential molecule for photosynthesis. The basic structure of chlorophyll is a porphyrin macro-

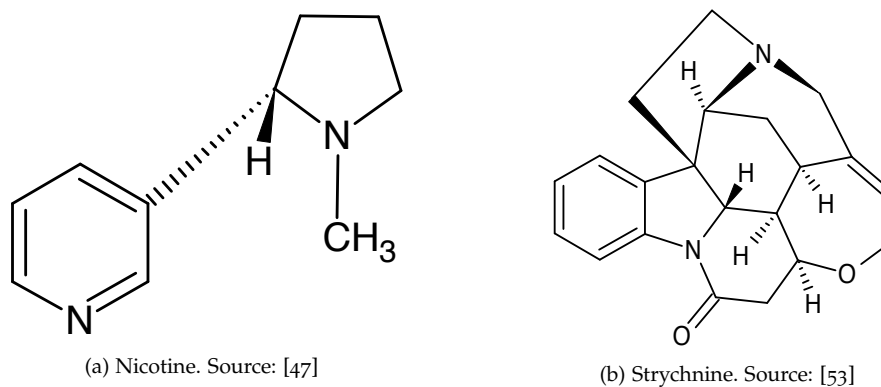


Figure 33: Two typical alkaloids found in biomass.

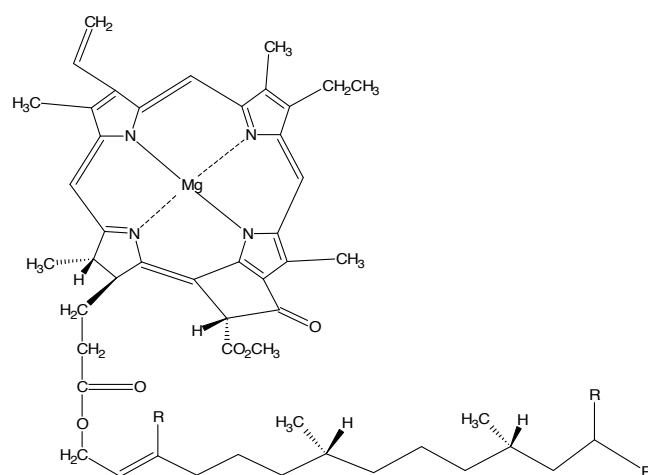


Figure 34: Structure of chlorophyll-a. Source: [319]

cycle (as in Figure 34) with a magnesium ion in the central cavity and various side chains [95, 319]. The amount of chlorophyll-N becomes significant when dealing with plant foliage and, in minor amounts, needles. For other biomass materials it is usually not relevant.

**OTHERS** Other N-compounds are present in minor amounts in biomass materials. Some species contain special amines, vitamins [95, 319], or amino sugars (such as *glucosamine*, found in chitin, a polysaccharide found in the shells of lobsters and crabs and skeletons of insects and spiders [319])[241] and inorganic nitrogen species such as nitrates, nitrites and ammonium. The latest ionic substances are a form of early intake of the plant through liquids and are then synthesized into proteins.

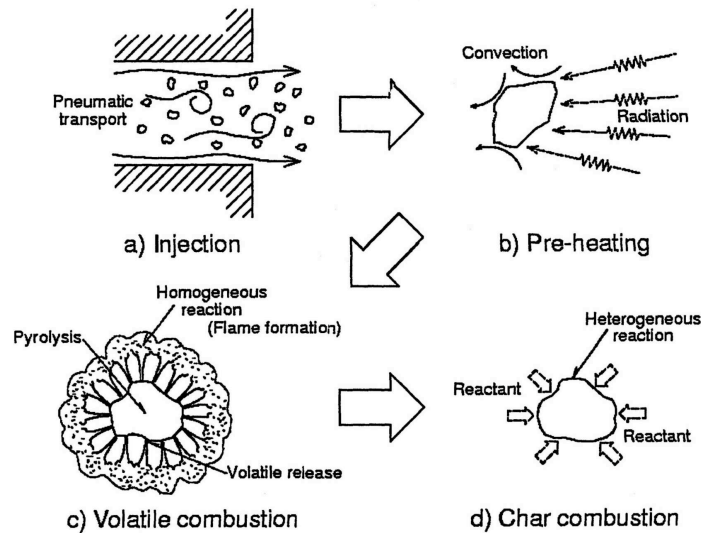


Figure 35: Schematic of the thermal conversion of a solid particle. The injection of the fuels varies depending on the technology used; pneumatic transport is used for pulverized fuel combustion. Source: Nogami [277]

## 2.2 SOLID FUEL COMBUSTION

The combustion of solid fuels is a combination of complex phenomena which happen in a very rapid succession or, in some cases, simultaneously. The three main steps can be summarized as following and are depicted in Figure 35:

- Drying
- Devolatilization + volatiles oxidation/gasification
- Char oxidation

### *Drying*

Any relatively small particle entering a hot reactor will be subjected to very high heating rates (in the order of  $10^3 - 10^4$  °C/s, upon which the fuel undergoes drying (Figure 35b). The moisture content of biomass can be, in some cases, critical for a stable combustion / gasification process, and very wet fuels, like sewage sludge or manures, need to undergo pre-treatments before entering the reactor [2]. Some new technologies, such as supercritical water gasification, are very promising for direct conversion of very wet feedstocks but they are still in a research and early development phase [231, 260].

*Devolatilization + volatiles oxidation/gasification*

The second stage is devolatilization or pyrolysis (from the Greek words *pyros* ("fire") and *lysis* ("decomposition")): as the term suggests, this process involves a decomposition of the fuel into volatiles and char, due solely to the effect of heat. Devolatilization is the first chemical step in every thermal conversion process of solid fuels independently from the local atmosphere, so both in gasification and combustion. However, as mentioned in Chapter 1, pyrolysis can also be achieved in an inert atmosphere and as a stand-alone process.

The changes that occur during pyrolysis under inert conditions can be listed as follows [268]:

1. Heat transfer from a heat source (usually the furnace) to increase the temperature inside the fuel particle ;
2. The initiation of primary pyrolysis reactions at this higher temperature breaks weaker bonds and functional groups which are released from the main structure and a more carbonaceous structure, called char, is left as the solid residue;
3. The flow of hot volatiles towards cooler solids results in heat transfer between hot volatiles and cooler unpyrolyzed fuel;
4. Condensation of some of the volatiles in the cooler parts of the fuel, followed by secondary reactions, can produce tar;
5. Autocatalytic secondary pyrolysis reactions proceed while primary pyrolytic reactions (point 2, above) simultaneously occur in competition;
6. Further thermal decomposition, reforming, water gas shift reactions, radicals recombination and dehydration can also occur and are a function of the process' residence time / temperature / pressure profile.

When devolatilization happens under combustion conditions, especially for biomass, secondary pyrolysis is usually less relevant since the volatiles released from the particle are quickly oxidized in a flame crown around the particle itself.

Devolatilization occurs in relatively short times compared to char oxidation, depending on the type of fuel and the process conditions (mostly on the particle size). For biomass fuels, as mentioned also in Chapter 1, the weight loss during the devolatilization process is usually around 70–80% of the initial dry weight [159, 163, 202, 278] but it can reach 95% for some fuels at high heating rates [139, 140]. Therefore, this step has a crucial role not only in the control and stability of the process but also in the global emissions and fuel reactivity.

The amount and composition of the volatiles, together with the structure of the remaining char, highly depends on the initial fuel properties but also on the process conditions such as heating rate, particle size, temperature and atmosphere [107].

Due to the heat supplied to the particle, the weaker bonds and functional groups present in the structures of the fuel are broken and gases are released. These gases consist of both high molecular weight compounds, called tars, and lower incondensable gases such as CO, H<sub>2</sub>, CH<sub>4</sub>, C<sub>2</sub>H<sub>6</sub>, but also H<sub>2</sub>O, CO<sub>2</sub> and nitrogen compounds such as NH<sub>3</sub>, HCN and N<sub>2</sub>. Tars are compounds which are released in gaseous form but condense at room temperature; tars from coal pyrolysis originate from the breakage of weaker bonds connecting aromatic structures [316], while in biomass they originate from the aromatic structures of lignin as well as from various oxygenated compounds released by cellulose and hemicellulose (such as levoglucosan and furans) [266]. The lighter volatiles in biomass pyrolysis originate mostly from the breakage of functional groups (e.g. amino group in proteins releasing ammonia) or the decomposition of the main polysaccharides listed in the previous sections.

Because of the extreme importance of pyrolysis in biomass conversion, in the last years many studies have been dedicated to this process. The pyrolysis characteristics of most of the biomass main structural components are listed in the previous sections and shown in Figure 27 and Tables 6 to 8.

Once the volatiles are released they will undergo homogeneous reactions of combustion or gasification depending on the oxidant atmosphere. The reaction mechanisms and kinetics of such reactions are quite well known [114]. Some mechanisms of homogeneous oxidation of nitrogen species are reported in the next sections.

### 2.2.1 Char oxidation

The next and last step of the conversion is, therefore, the char oxidation / gasification. This process is much slower than devolatilization because it is actually composed of different steps. In a simplified way, char conversion can be described as happening in three phases: first the oxidizing agent, O<sub>2</sub>, or the gasifying agents, CO<sub>2</sub> and H<sub>2</sub>O, need to diffuse from the surrounding bulk to the surface of the particle, then the heterogeneous reaction can take place and, finally, the products need to diffuse out of the particle. However, a more complex and detailed description of the phenomenon includes first a reaction of the carbon surface with the CO<sub>2</sub> produced during combustion to release CO. Carbon monoxide then diffuses towards the oxygen and at the reaction front a flame is developed where CO is oxidized to CO<sub>2</sub>. Clearly the global reaction rate will need to include not only the actual chemical rate but also the diffusion rate of the compounds to and from the solid particle.

As mentioned in the previous sections, the amount of residual char in biomass is much lower than for coal. Moreover, the reactivity is higher for bio-

mass chars compared to the ones from coal [107], one only need think of the wood charcoals used for barbeques for their ease of ignition and combustion [67]!

However, the particle dimensions to which coal can be reduced ( $\mu\text{m}$  range) cannot be obtained for biomass materials due to their fibrous structure and this can significantly slow the oxidation of biomass chars decreasing the specific surface area ( $\text{m}^2/\text{m}^3$ ) available for the reaction.

The nitrogen which is left in the char after devolatilization is released during this phase. To the author's knowledge, no systematic study on the structures of nitrogen in chars has been performed, moreover, it is difficult to assess the sole contribution of fuel-N to the global NO emissions: in fact when studying the pyrolysis of a fuel under inert conditions, the char produced will have a different structure from the char which would be actually produced under oxidant atmosphere and both kinetic and emission analysis will then be biased. Release of NO from combustion of biomass fuels will be presented in Chapter 7 of this thesis.

### 2.3 $\text{NO}_x$ FORMATION MECHANISMS

Before introducing the available literature and knowledge on  $\text{NO}_x$  emissions during biomass combustion and the formation of  $\text{NO}_x$ -precursors during pyrolysis and gasification, it is appropriate to give a brief introduction of the main mechanisms of NO formation during combustion.

#### 2.3.1 From air nitrogen: Thermal $\text{NO}_x$ and Prompt $\text{NO}_x$

The formation of  $\text{NO}_x$  from oxidation of molecular nitrogen at high temperatures is known as *thermal- $\text{NO}_x$* . This process is driven by the well-known Zeldovich mechanism [370]:



The so-called extended Zeldovich mechanism includes also the additional reaction:





The above-mentioned reactions are much dependent on temperature as clearly shown in Figure 36; especially reaction 2.3 has a high activation energy and is only important at temperatures above 1800 K [165].

The mechanism of *prompt-NO<sub>x</sub>* was described by Fenimore [153] as a reaction sequence initiated by the rapid reaction of hydrocarbon radicals with molecular nitrogen, leading to the formation of amines or cyano compounds that subsequently react to form NO, as in the following equations:



Prompt-NO<sub>x</sub> is formed mostly in fuel-rich zones next to the flame front and are mostly relevant for gaseous fuels combustion [264].

Following the considerations reported above and in Chapter 1, it is possible to state that at the temperatures at which biomass is usually combusted in fluidized bed and entrained flow reactors ( $\approx 800 - 1200^\circ\text{C}$ ) the mechanisms of thermal and prompt-NO are not relevant and do not influence the final NO<sub>x</sub> concentration.

### 2.3.2 From fuel bound nitrogen: Fuel NO

The main source of NO<sub>x</sub> emissions in biomass combustion is originating from the fuel-bound nitrogen. As mentioned in previous parts of this chapter, many biomass materials and mostly biomass residues, have a high content of N and therefore the danger of high NO<sub>x</sub> emissions might be concrete.

As shown in Figure 37, the primary devolatilization of the fuel distributes the initial nitrogen among volatile species, which are generally HCN and NH<sub>3</sub> [59, 264], nitrogen contained in large aromatic compounds (tar-N) and nitrogen remaining in the char matrix. The exact partitioning and composition of volatile gases, tars and char-N structures, varies greatly with different biomass fuels and process conditions such as temperature, pressure, residence time, heating rate and oxidizing agent [165]. For example, bituminous coals have been reported to release mostly tar-N which then quickly decomposes

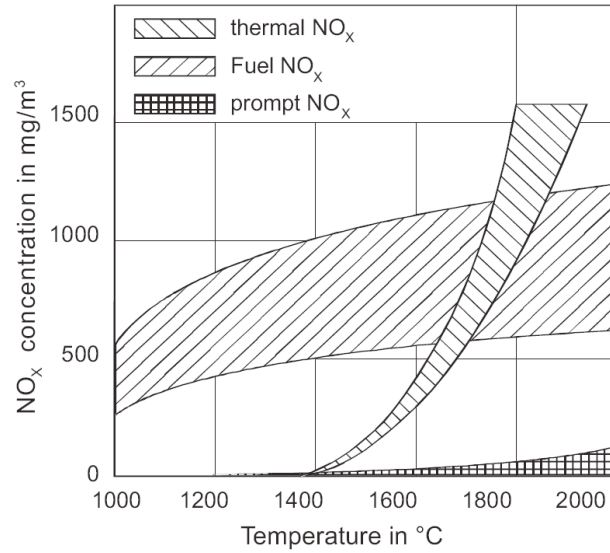


Figure 36: Schematic representation of the influence of flame temperature on the  $\text{NO}_x$  formation mechanisms for coal. Source: Zelkowski [371]

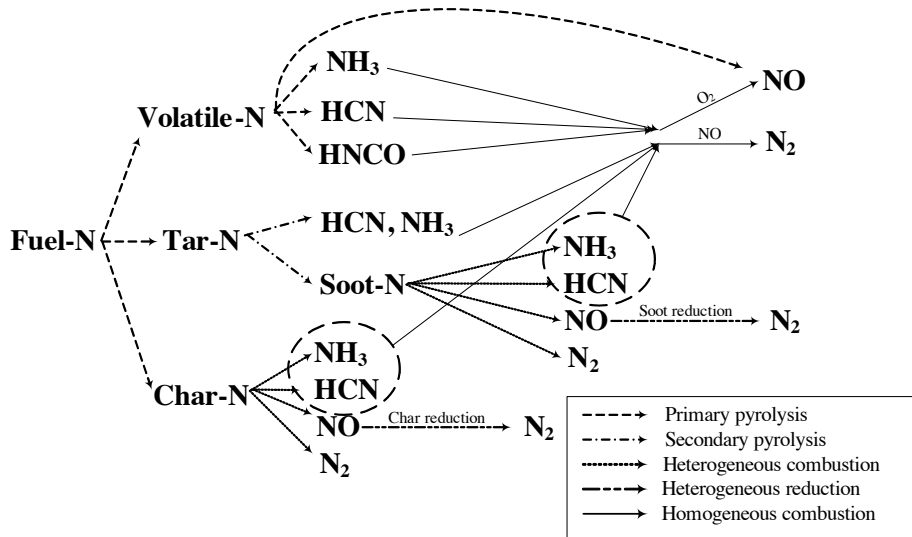


Figure 37: Schematic overview of fuel- $\text{NO}$  formation during thermal conversion stages of biomass fuels. Source: Adapted from Di Nola [139]

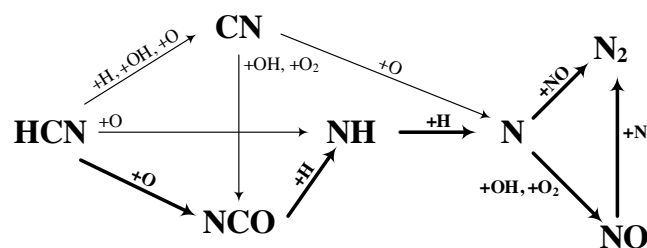
into HCN and soot-N [165]. Biomass is known to mostly release volatile-N in the form of  $\text{NH}_3$  [182] and HCN, but HNCO is sometimes also detected [98, 140, 182, 202]. Direct release of NO from biomass pyrolysis has also been reported and attributed to the high amount of oxygen present in the biomass [182, 299, 332, 377]. The partitioning between these species seems to depend on the process conditions, with  $\text{NH}_3$  being the main product at low heating rates, pressures and temperatures and HCN increasing, instead, with temperature and heating rate [165, 241]. The presence of inorganic matter such as Ca and K could promote the formation of ammonia and  $\text{N}_2$  and suppress HCN formation, while Fe could catalyze ammonia decomposition to molecular nitrogen [165]. A review of the experimental knowledge and proposed mechanisms for biomass materials will be given in the next section.

In a following stage, the volatile nitrogen species undergo homogeneous reactions of either oxidation to NO or reduction to molecular nitrogen. These mechanisms are well known and a detailed review of relevant reactions and their kinetic parameters can be found in Miller and Bowman [264]. Another important mechanism of homogeneous oxidation involves the reaction of volatile-N, mostly HCN and HNCO to  $\text{N}_2\text{O}$ , as investigated and detailed by Kilpinen and Hupa [219] and others [64, 199, 229]. The values of fuel-N conversion to volatiles (including  $\text{NH}_3$ , HCN and HNCO) range from 10 - 15% up to 70 - 80% [95, 139, 140].

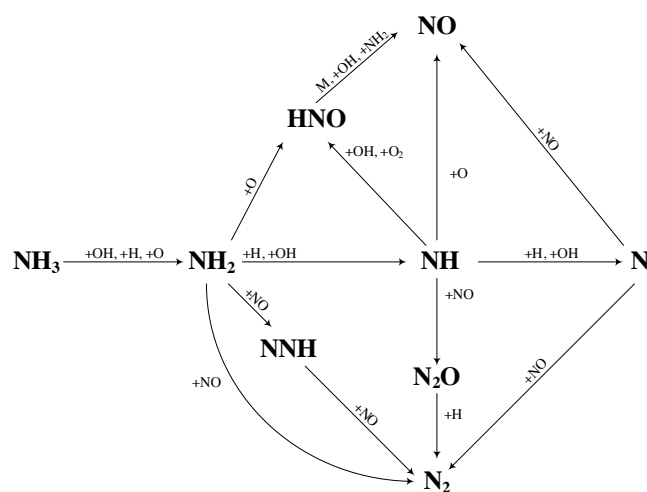
The nitrogen in tars, if it has the chance to further react and it is not quickly cooled and liquefied, will further decompose to volatile species or condense into soot, trapping the nitrogen into cyclic species that, via heterogeneous reactions, will then oxidize or reduce.

The nitrogen in the char is generally believed to undergo heterogeneous reactions which commonly yield either directly NO or HCN. Char-NO is a major contributor to the final NO emissions since the non catalyzed homogeneous chemistry of volatile-N is known in depth and primary DeNO<sub>x</sub> measures can achieve high conversions to molecular  $\text{N}_2$  [139, 200, 264, 272]. As shown in Figure 39a, the content of N in chars from straw decreases drastically with temperature down to about 25% of the initial N content in the range of 900 to 1200K. Most of the biomass fuels follow such a trend with temperature, even though different fuels might yield more char-N [101] or less [140] depending on the heating rate and the nature of the nitrogen structures [165, 180, 182, 236], as shown in Figure 39b.

Among the various NO<sub>x</sub> reduction techniques which have been developed already for many years [139, 200] such as burner modifications, staged combustion and selective catalytic reduction to name the most common ones, it is worth to mention in more details the mechanism of so-called *Thermal De-NO<sub>x</sub>*. This technique involves the injection of ammonia (or urea) into the boiler to reduce the already formed NO back to  $\text{N}_2$  via the reaction path illustrated in Figure 40. This mechanism becomes important in biomass fuels with high nitrogen content when much of the fuel-N is released as volatiles and many



(a) Reaction path diagram illustrating the reaction mechanism of conversion of HCN to NO and  $N_2$  in low-pressure flames.



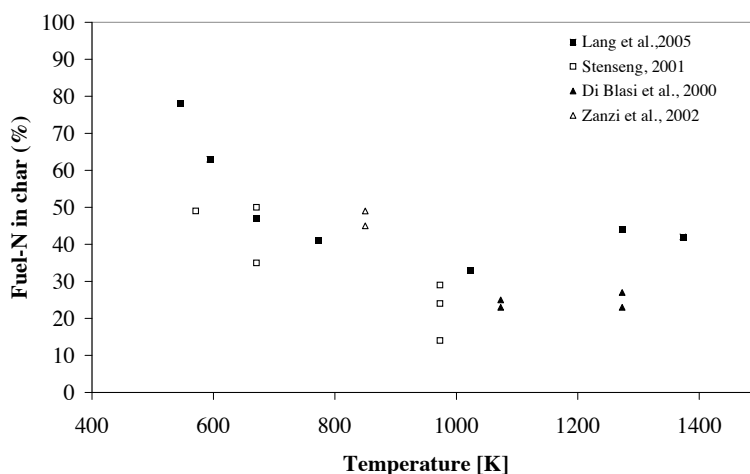
(b) Reaction path diagram illustrating the oxidation of ammonia in flames.

Figure 38: Homogeneous reaction paths of HCN and  $NH_3$  to NO. Source: Miller and Bowman [264]

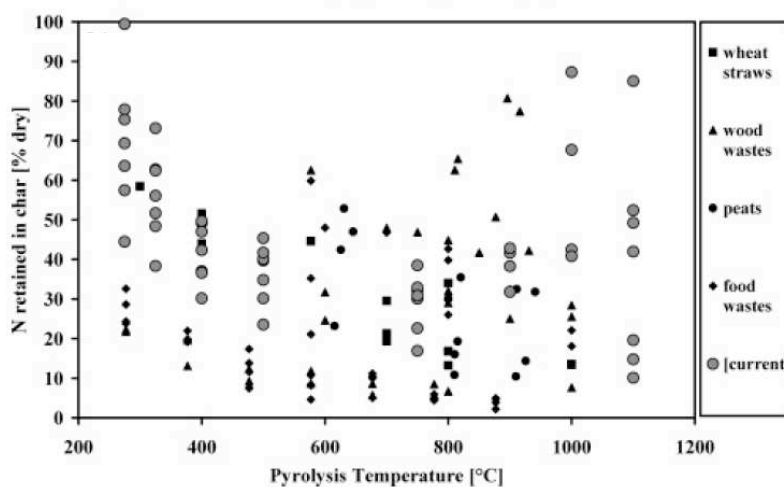
NH or  $NH_2$  radicals are available for the De- $NO_x$  process as discussed by Skreiberg et al. [315] and others [264, 265].

#### 2.4 NITROGEN PRECURSORS AND NITROGEN OXIDES FROM BIOMASS AND MODEL COMPOUNDS: A REVIEW

As mentioned in the previous sections, the mechanisms of oxidation and reduction of nitrogen oxides are well known and are precious in order to obtain optimal combustion conditions. However, in order to be useful, such kinetic schemes need to be provided with precise information on the primary volatile species which result from biomass pyrolysis and this is more complicated [182]. In fact, as reported above, the exact partitioning among volatile-N, tar-



(a) Variation of fuel-N retained in char with devolatilization temperature for various wheat straw samples. Sources: [108, 236, 324, 369]



(b) Retention of fuel-N in char with devolatilization temperature for various biomass samples. Source: Lang et al. [236]

Figure 39: Variations of the fuel-N retained in char with devolatilization temperature for several biomass materials and measurement techniques.

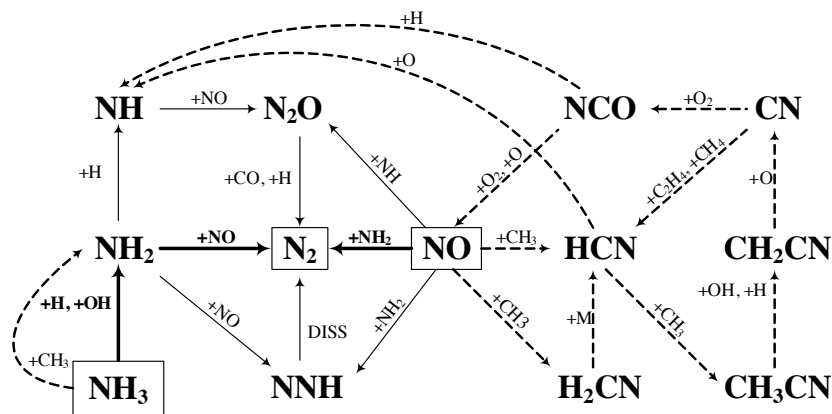


Figure 40: Reaction path diagram for the Thermal De- $\text{NO}_x$  process at moderate temperatures and fuel-rich conditions. The solid lines are the major reactions for  $\text{CO}/\text{H}_2$  as fuel; dashed lines are additional pathways when  $\text{CH}_4$  is present. Source: Skreiberg et al. [315]

N and char-N varies according to different process conditions and fuel composition, and so does the exact composition of the volatiles released.

For this reason a detailed characterization of each material is required in order to convert it efficiently. In this section the mechanisms of devolatilization of some model compounds for the nitrogen structures found in biomass are listed and described. Moreover, some results of previous studies on volatile-N partitioning are listed.

#### 2.4.1 $\text{NO}_x$ precursors from devolatilization

The results from many years of research on coal and many biomass materials sustain that the main nitrogen species released in volatile form during devolatilization are  $\text{HCN}$ ,  $\text{NH}_3$  and in minor amounts,  $\text{HNCO}$  and  $\text{NO}$  [59, 95, 182, 264].

##### 2.4.1.1 Amino acids and proteins

As mentioned above, it is well accepted that most of the nitrogen in biomass materials is in the form of amino-acids and proteins. Becidan [95] in his PhD dissertation gives a comprehensive review of the reaction mechanisms of pyrolysis known so far.

According to several studies, most of the volatile-N compounds are not primary products of pyrolysis but rather products of secondary decomposition.

*Primary pathways of decomposition:*

The main primary reaction pathways of decomposition of amino-acids and proteins are illustrated in Figure 41.

1. Formation of *amide* intermediaries [313];
2. *Decarboxylation* with subsequent formation of amines and CO<sub>2</sub> [295, 313];
3. *Dehydration* which causes the formation of polypeptide and consequently the formation of cyclic amides, among which the most commonly reported is 2,5-diketopiperazine (also called DKP) [180, 295, 310, 312, 313, 353];
4. Formation of the intermediary *α-lactam* [313].
5. *Cross-linking* of proteins' side groups to produce NH<sub>3</sub> and char-N [180]. This path is followed only by compounds with side chains, otherwise no char is reportedly formed [300, 301, 302].
6. *Deamination*, thermal loss of ammonia, is not considered to be significant for some substances [87, 295, 310, 313], but Li et al. [244, 245] in their studies on amino-acids pyrolysis, among which glycine, phenylalanine and tyrosine, found instead considerable amount of NH<sub>3</sub> being released as a primary product via deamination (Figure 42).

According to multiple studies, the most important primary pathways are decarboxylation and dehydration since they are favoured at high temperatures [95, 180, 244], but deamination has been proven to be of importance in slow pyrolysis of single amino-acids and dipeptides [244, 245]. Moreover, for polypeptides and proteins with side chains, it was suggested that the main primary conversion path would be number 5, with the formation of char and the release of ammonia [180, 182].

*Secondary pathways of decomposition:*

The five primary compounds described above undergo a secondary stage of decomposition which brings to the final composition of the volatile gases.

The main compound, as specified earlier, is DKP. DKP can undergo several cleavages:

1. The formation of different *nitriles* depending on the nature of the specific functional groups X and Y. For example, such reaction is responsible for the formation of HCN in glycine pyrolysis [244, 295];
2. The formation of intermediary *imines* which then decompose to HCN (or nitriles) and H<sub>2</sub> [180] or can react with amines to give ammonia and N-alkylaldimines [295];

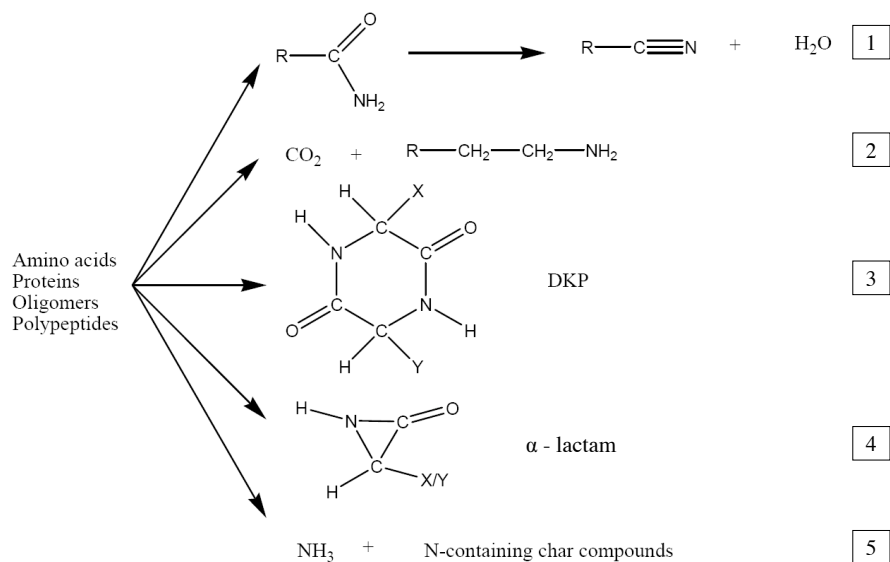


Figure 41: Primary pyrolysis decomposition pathways for proteinic biomass-N model compounds. Source: Becidan [95]

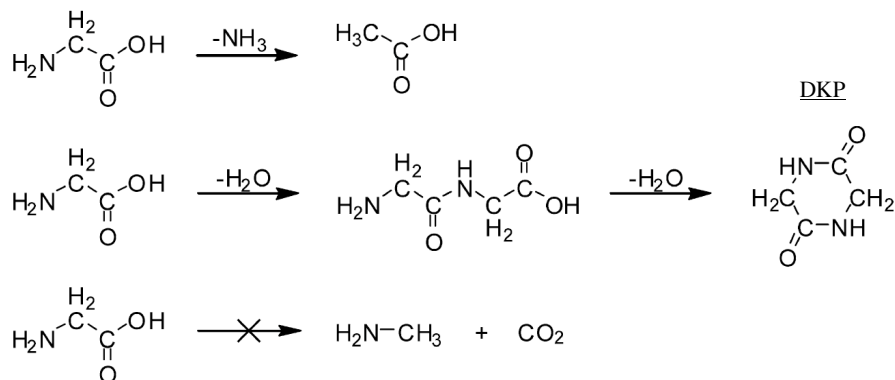


Figure 42: Pyrolysis decomposition pathways for glycine. Source: Li et al. [244]

3. The release of *HNCO* and *pyrroline* [87, 180];
4. Isomerisation to *hydantoins* (5-membered cyclic amides) before further decomposition to *HNCO* and *HCN* [88, 89];
5. Formation of the intermediary *α-lactam* before further cleavage [180, 313].

The importance of each pathway will vary with fuel and conditions. However, eventually, the DKP will decompose to *HCN*, mostly, and in minor



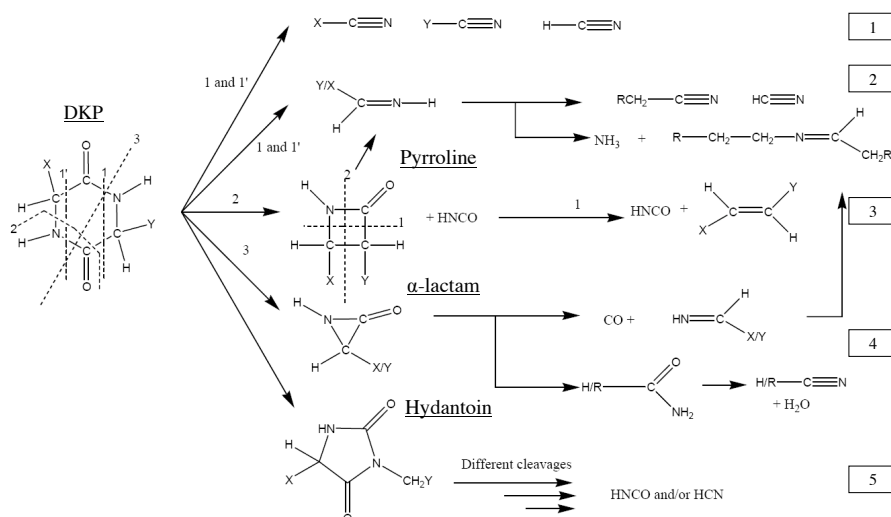


Figure 43: Thermal decomposition of DKP (formed in reaction 3 in Figure 41). X and Y may represent various functional groups. The dotted lines indicate the opening of the cyclic structure. Source: Becidan [95]

amounts to HNCO and  $\text{NH}_3$ . Johnson and Kan [198] reported conversions of DKP to HCN of about 38% at 700 °C while Hansson et al. [181] reported more than 80% conversion at 1000 - 1100 °C.

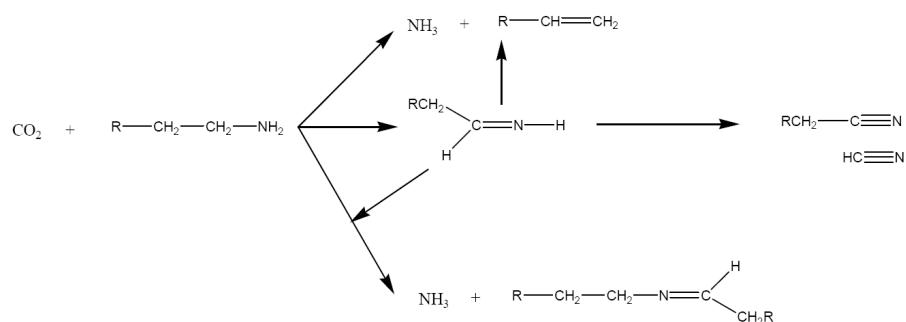
The decarboxylation reaction is the second most important pathway in primary pyrolysis of proteins and polypeptides. As seen in Figure 44a, the amines formed can decompose further into nitriles and / or HCN, or react with imines and yield ammonia and N-alkylaldimines [180, 313]. Another possible route is the direct thermal loss of  $\text{NH}_3$ .

Primary pyrolysis might also yield a compound called  $\alpha$ -lactam. When this pyrolyzes further, as seen in Figure 44b, it can decompose into an amide which can then evolve into nitrile and / or HCN with release of water [165]. Alternatively, it can form an intermediary imine and then proceed as explained earlier.

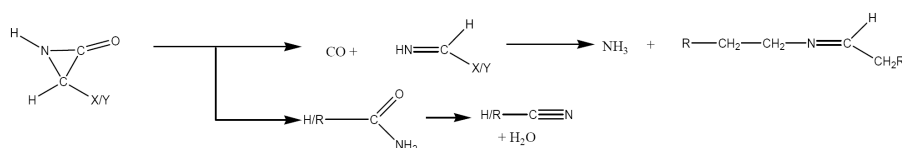
The reaction of the nitriles formed in reaction 1 of Figure 41 is shown in Figure 44c and it yields HCN.

Finally, the char-N formed via the reaction 5 in Figure 41 and only in presence of proteins with side chains, can decompose further to form hydantoin and eventually yield additional HNCO and / or HCN [88, 89] (Figure 44d).

From this brief prospect on the various reaction mechanisms disclosed so far, it is possible to see that the release of  $\text{NH}_3$ , HCN and HNCO during pyrolysis of biomass can be explained with the decomposition of its primary sources of N: proteins and polypeptides. However, the exact partitioning and amounts will undoubtedly depend on the exact composition of each mate-



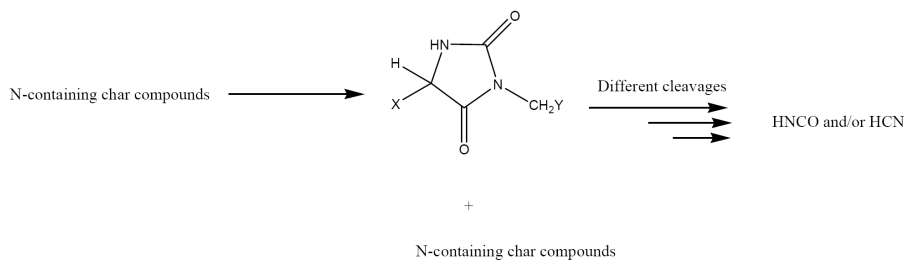
(a) Secondary decomposition of the amines formed after decarboxylation reaction (reaction 2 in Figure 41).



(b) Secondary decomposition of the  $\alpha$ -lactam formed in the primary pyrolysis (reaction 4 in Figure 41).



(c) Secondary decomposition of the nitriles formed in the primary pyrolysis (reaction 1 in Figure 41).



(d) Secondary decomposition of the char-N compounds formed in the primary pyrolysis (reaction 5 in Figure 41).

Figure 44: Secondary decomposition reactions of the products of primary pyrolysis.  
Source: Becidan [95]

rial: characterization is, again, an essential tool for deeper understanding and better performance.

#### 2.4.1.2 *Heterocyclic-N*

As explained earlier, together with proteinic-N, biomass might contain also heterocyclic nitrogen compounds, even though in much lower amounts except for particular materials. Considering that heterocyclic-N compounds are the main nitrogen compounds contained in coals [128], many studies exist in literature on the pyrolysis of pyrrole and pyridine structures [79, 143, 144, 179, 253, 331].

Pyrrolic structures are usually found to produce mostly HCN and various nitriles [79, 143, 242, 331] that can further evolve into additional HCN.  $\text{NH}_3$  was found only in minor amounts. Pyridinic model compounds are more stable than pyrroles and their decomposition occurs at higher temperatures [165]. Pyridines were found to release mostly cyanoacetylene which is then quickly converted into HCN [253]. However, contradictory results were also found: Hämäläinen et al. [179] tested heterocyclic N-structures with 5 and 6 elements rings and they found ammonia to be the main product when additional oxygen functional groups were present. Moreover, ammonia was detected in many studies on coal pyrolysis [59, 240, 242, 330]. Detailed kinetic mechanisms for the devolatilization and oxidation of these model compounds have been developed lately by Martoprawiro et al. [259] and Ikeda et al. [189].

Li and Tan [242] analyzing their own and the past results came to the conclusion that the formation of a significant amount of  $\text{NH}_3$  from the thermal cracking of pyrrolic or pyridinic rings in the gas phase is highly unlikely. They also stated that the indirect formation of ammonia via hydrogenation of HCN in the gas phase or on the char surface would not be sufficient to explain the yields of  $\text{NH}_3$  measured in pyrolysis of brown coal, which is rich in hydrogen and therefore even less likely for higher rank coals with lower hydrogen content. The mechanism proposed, therefore, is the direct hydrogenation of the nitrogen in the pyrolyzing char particle with the active hydrogen needed generated directly from the thermal cracking reactions within the particle itself.

However, pyrolysis of biomass happens at lower temperatures and with faster speed than for coal and with much higher amount of volatiles: these characteristics are less likely to favour serious interactions between the volatiles and the char. Therefore, the eventual presence of heterocyclic-N in biomass is most likely responsible for HCN release from the cleavage of the rings while proteinic-N is responsible for the ammonia release. According to the mechanism proposed by Li and Tan [242], moreover, faster heating rates would favour the presence of H radicals in coal and consequently favour higher ammonia formation, but this is the opposite of what is often seen for biomass fuels, as it will be explained in the next sections.

### 2.4.2 Char-N

Evaluating the actual oxidation of char-N is extremely difficult because such heterogeneous reactions are much influenced by the physico-chemical properties of the char itself and these characteristics (e.g. porosity, surface area, inorganic matter) change depending on how the char is obtained. For example, a char obtained in an inert atmosphere will not have the same characteristics of the actual char during oxidation.

There is general acceptance that coal char-N is mostly converted to NO in a range of 100 to 80% of the conversion [165] and in minor amounts to HCN and HNCO.

Glarborg et al. [165] described the accepted mechanism for coal char-N oxidation as follows:



Where C(N) and C(O) indicate the nitrogen and oxygen species, respectively, on the char surface.

Under fluidized bed conditions, moreover, considerable amounts of char-N could react to N<sub>2</sub>O via homogeneous oxidation of the HCN and HNCO released from the char or via the following heterogeneous mechanism [165]:



Here C(NCO) is an oxidized char nitrogen species, presumably an -NCO or -CNO type species.

Additionally, char plays an important role in the reduction of NO over its surface [55, 142, 321, 372, 377], especially in fluidized bed reactors when contact between gases and solids is extensive. Zevenhoven and Hupa [372] found that chars from peat and lignite are more reactive towards NO compared to chars from bituminous coals and wood. Moreover, a catalytic effect was found for calcium, magnesium and potassium, elements of which biomass chars are usually rich in [372].

### 2.4.3 Some examples of NO<sub>x</sub>-precursors and nitrogen oxides from biomass samples

The following Tables 9 and 10 summarize the results obtained in literature of slow and fast pyrolysis, respectively, of many biomass fuels. It is possible to see, as also mentioned by other authors in the past [95, 139, 240], that it

is difficult to find a general trend to explain the partitioning of volatile-N because it depends highly on the fuel type and on the reaction conditions.

Table 11, finally describes the total conversion of fuel-N to NO during biomass combustion in several different reactor configurations. It appears that under combustion conditions, instead, a general trend can be sketched, with the fuels with least N content releasing the most of it as NO and the fuels with high initial nitrogen content, instead, presenting only a little conversion of it to NO.

These trends will be explained in much more details in the next chapter of this dissertation.

Table 9: Yields of volatile-N compounds in biomass slow pyrolysis.

SAMPLE	HR (°C/MIN)	TEMPERA- TURE (°C)	FUEL-N (%WT <sub>DAF</sub> )	NH <sub>3</sub> (%WT <sub>DAF</sub> )	HCN (%WT <sub>DAF</sub> )	HNCO (%WT <sub>DAF</sub> )	N-TO- NH <sub>3</sub>	N-TO- HCN	N-TO- HNCO	REF.
Oriental tobacco <sup>d</sup>	30	900	2.78	0.3	0.4	1.0	8.9	7.5	11.7	[90]
Burley tobacco <sup>d</sup>	30	900	5.22	1.0	0.8	1.2	15.8	7.9	7.5	[90]
Wheat straw <sup>d</sup>	30	900	0.68	0.16	0.22	0.13	19.4	16.8	6.2	[90]
Wood pellets <sup>a</sup>	30	900	0.33	0.02	0.09	0.02	5.0	14.1	2.0	[204]
Miscanthus <sup>d</sup>	30	900	0.64	0.10	0.14	0.11	12.9	11.3	5.6	[204]
Chicken Litter <sup>d</sup>	30	900	5.35	1.04	1.10	1.73	15.7	11.3	11.2	[202]
Meat and Bone Meal <sup>a</sup>	30	900	11.03	2.2	1.1	0.5	16.0	5.3	1.5	[202]
DDGS <sup>a</sup>	10	900	4.84	1.4	1.3	0.45	23.8	15.9	3.0	[163]
DDGS washed <sup>a</sup>	10	900	4.83	1.9	1.9	0.5	32.4	20.4	3.4	[163]
Chicken Manure <sup>d</sup>	10	900	8.04	3.7	4.9	7.9	37.9	31.6	32.0	[163]
Coffee waste <sup>b</sup>	10	900	3.02	0.25	0.06	n.d.	6.9	1.0	n.d.	[98]
Brewer spent grains <sup>b</sup>	10	900	4.15	0.78	0.28	n.d.	15.7	3.5	n.d.	[98]
Fiberboard <sup>b</sup>	10	900	3.62	0.5	<0.07	n.d.	11.5	<1.0	n.d.	[98]
Pine bark <sup>c</sup>	10	900	0.4	0.05	<0.004	n.d.	10.2	0.5	n.d.	[240]
Sugarcane Bagasse <sup>d</sup>	6.7	1000	0.31	0.005	0.04	n.d.	1.5	7	n.d.	[242]

<sup>a</sup>Performed on a TG-FTIR setup<sup>b</sup>Performed in a Quartz tube furnace+FTIR<sup>c</sup>Performed in a Tube oven<sup>d</sup>Performed in a Drop tube reactor

Table 10: Yields of volatile-N compounds in biomass fast pyrolysis.

SAMPLE	HR (°C/s)	TEMPERA- TURE (°C)	INITIAL-N (%WT <sub>DAF</sub> )	NH <sub>3</sub> (%WT <sub>DAF</sub> )	HCN (%WT <sub>DAF</sub> )	N-TO-NH <sub>3</sub>	N-TO-HCN	REF.
Cane trash <sup>d</sup>	>17	900	0.31	0.09	0.13	23.9	21.7	[333]
Chicken litter <sup>b</sup>	1000	900	4.35	0.8	1.7	15.1	20.3	[140]
Meat and bone meal <sup>b</sup>	1000	900	11.17	3.8	4	28.0	18.6	[140]
DDGS <sup>c</sup>	600	900	4.84	0.07	0.6	1.2	6.4	[160]
PKC <sup>c</sup>	600	900	2.56	n.d.	0.4	n.d.	8.1	[160]
Coffee waste <sup>d</sup>	drop	900	3.02	1.39	0.82	37.8	14.1	[98]
Brewer spent grains <sup>d</sup>	drop	900	4.15	1.57	1.37	31.3	17.1	[98]
Fiberboard <sup>d</sup>	drop	900	3.62	1.58	0.63	36	9.1	[98]
Sewage sludge <sup>d</sup>	drop	900	5.47	3.37	0.91	50.7	8.6	[96]
Sugarcane bagasse <sup>e</sup>	drop	800	0.31	0.05	0.32	12.5	53.0	[242]

<sup>a</sup>Performed on a Fixed bed reactor

<sup>b</sup>Performed in a Heated grid reactor+FTIR

<sup>c</sup>Performed in a Heated foil reactor+FTIR

<sup>d</sup>Performed in a Quartz tube furnace+FTIR

<sup>e</sup>Performed in a Drop tube reactor

Table 11: Conversion of fuel-N to NO in different biomass combustion applications.

SAMPLE	SETUP	OXYGEN CONC. (%VOL.)	TEMPERA- TURE	FUEL-N	FUEL-N TO NO (% INITIAL N <sub>DAF</sub> )	REF.
Spruce wood	Fluid bed	10	800	0.22	22	[362]
Beech wood	Fluid bed	10	800	0.11	37	[362]
Alder wood	Fluid bed	10	800	0.26	31.7	[362]
Straw	Fluid bed	10	800	0.43	22.3	[362]
Malt waste	Fluid bed	10	800	4.99	11.6	[362]
DDGS	SPR	10	800	4.84	9.5	[164]
PKC	SPR	10	800	2.6	16.3	[164]
Rapeseed cake	SPR	10	800	5.45	10.4	[164]
Fermented sewage sludge	SPR	10	800	5.94	7.3	[164]
Chicken manure	SPR	10	800	8.04	7.5	[164]
Wood	Fluid bed	5	850	0.12	57	[226]
Demolition wood	Fluid bed	5	850	0.3	25	[226]
Rice straw	Fluid bed	5	850	0.69	33	[226]
Sewage sludge	Fluid bed	5	850	1	27	[226]



# 3

---

## MATERIALS AND METHODS

---

*Small-scale characterization is a useful method to investigate fundamental characteristics of solid fuels like devolatilization and combustion kinetics, as well as volatile composition and yields. The data gathered can then be used in models aimed at predicting behaviors in scaled-up installations.*

*This chapter introduces the properties and origins of the materials that were chosen for investigation: wheat straw, olive residues, peach stones, dry distiller's grains and solubles (DDGS), chicken manure and palm kernel cake. Furthermore, the setups that were used to obtain the results presented in the next chapters will be described, namely: thermogravimetric analyzer (TGA) and heated foil reactor (HF), both in combination with an Fourier Transform Infrared Spectrometer (FTIR), and, finally, a single particle reactor (SPR). The chapter also provides additional information on experimental practice, setup optimization and on the mathematical model used for the kinetic analysis of slow pyrolysis measurements. Finally, a brief literature review regarding previous studies on similar setups is introduced. More detailed information on previous literature and a comparison with results from this work can be found in the following chapters.*

### 3.1 FUELS, EQUIPMENT AND METHODOLOGY

As explained in the previous chapters, a great variety of materials can be classified as “biomass” and is available for use in power and heat production.

Among the various categories considered for industrial use, agricultural and process residues are extremely interesting because of their low (or even negative) values, their continuous production, wide distribution and their relatively high heating values. As mentioned in previous parts of this thesis, however, the composition of such materials poses many threats to proper plant operations: high nitrogen content might require additional gas cleaning units as well as high ash content might cause slagging, fouling, corrosion and loss of fluidization in the thermo-chemical conversion reactor.

All the materials tested in this work comply with such characteristics, both positive (cheap and distributed sources) and negative ones (high N, high K and Cl for example).

The thermal conversion of a solid particle, as described in Chapter 2, can be divided into three main steps: drying, devolatilization (or pyrolysis) and char oxidation/gasification. In order to realize a thorough characterization of the behavior of such materials, the experimental work of this dissertation was planned to follow the actual physical phenomena.

Figure 45 illustrates the approach followed. Starting from the top-left corner of the figure, the first measurements, described in Chapter 4 and 5, investigate the slow pyrolysis of the fuels. Such tests are extremely useful because the relative slowness of the phenomena involved (heating rates of 1 to 100 °C/min) allows for detailed measurements of the process temperatures, sample weight loss and gaseous compounds released. These tests are performed using a Thermogravimetric Analyzer (TGA) connected with a Fourier Transform Infrared Spectrometer (FTIR). Detailed gas composition, including volatile NO<sub>x</sub>-precursors, such as NH<sub>3</sub> and HCN, total gaseous yields and devolatilization kinetics are obtained through such measurements.

Even though these data are valuable themselves, the conditions of such experiments are very different from the ones in real applications, in which the heating rates are of the order of 10<sup>3</sup> to 10<sup>4</sup> °C/s. Therefore, to overcome this limitation, experiments are carried out using a heated foil reactor embedded in an FTIR spectrometer and the results are described in Chapter 6. This setup makes it possible to study the fuels under pyrolysis conditions with heating rates of approximately 10<sup>3</sup> °C/s. The most important data gathered from these measurements are the total weight loss and final yields of gaseous compounds, including NO<sub>x</sub>-precursors such as NH<sub>3</sub> and HCN, at different end temperatures and heating rates. However, the speed of the phenomena involved does not allow for detailed measurement of the temperature in the sample or for a continuous detection of the evolved gaseous compounds with an FTIR.

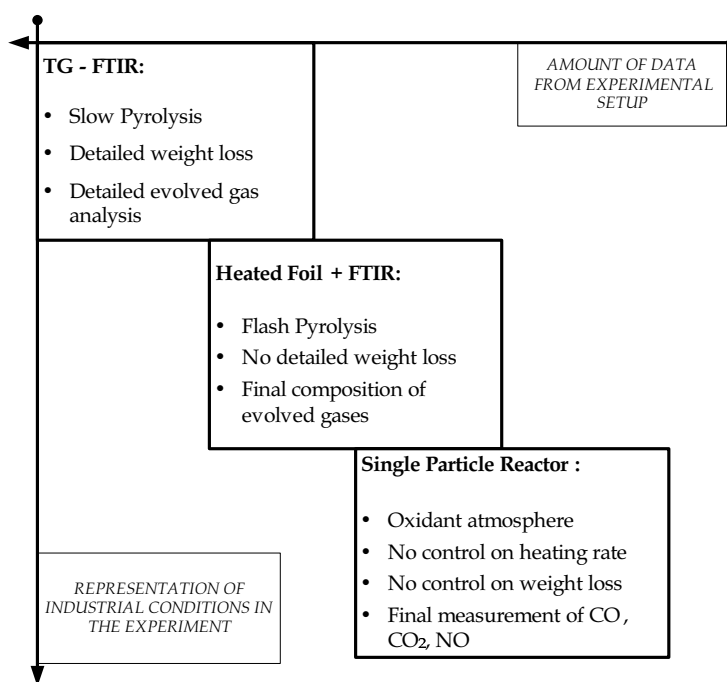


Figure 45: Schematic of the methodology used in this dissertation

For this purpose a numerical model, also presented in Chapter 6, was developed, in order to give a much better insight into the reactor conditions.

Finally, after the pyrolysis step has been thoroughly studied, the full process of combustion is investigated in a Single-particle Reactor. This equipment allows for the study of few milligrams of fuel under different oxidant conditions and different temperatures. Thanks to this reactor configuration it is possible to study the conversion of fuel-N to NO under conditions more similar to real combustion applications. However, no detailed weight loss or sample temperature are measured, making interpretation of the results more difficult. Nevertheless, with the aid of the results achieved from the other campaigns, it is possible to have a clear picture of the conversion of fuel-N to NO during every step of the thermal conversion.

The next section 3.2 will list the selected fuels, their properties and composition and give a brief description of their origin and current uses. Moreover, the pre-treatments which are applied on the fuels are introduced here.

In section 3.3, then, the various setups will be described together with a short literature review on previous studies carried out on similar equipments involving fuel characterization and especially biomass. For each setup some experimental practices and optimization are mentioned.

Finally, the mathematical model used to retrieve kinetic parameters from TG-FTIR measurements is introduced and explained in section 3.3.3.

### 3.2 FUELS

The fuels used in this work can be divided into two main categories: agricultural residues and residues from other processes. As explained in the Introduction, specific pre-treatments are applied to some of these samples in order to improve their ash quantity and quality. So, before the actual fuels are introduced, the next subsection will present a few words on these pre-treatments.

#### 3.2.1 *Pre-treatments*

As explained previously, not only the amount of ash forming matter in many biomass residues is relatively high, but also its elemental composition is critical for plant operation.

Arvelakis and Koukios [76], in fact, underlined how K, Cl and Na, together with sulfur and silicon, contained in high concentrations in agricultural residues, interact to form alkali silicates and alkali sulfates with melting points far lower than normal fluidized-bed boiler temperatures (even down to 600°C). The presence of a molten phase, then, gives rise to many problems such as slagging and fouling on the boiler's heat exchanger surfaces, but also corrosion if Cl is present (which is often the case for these materials). Additionally, in fluidized-bed reactors, agglomeration and loss of fluidization are caused when molten ashes act as binder of the bed materials [73, 77, 85, 218, 248, 249, 263, 275, 360]. More detailed information on this topic can be found, for example, in Glazer [166], Glazer et al. [167], Zevenhoven-Onderwater [373], Zevenhoven-Onderwater et al. [374, 375, 376] and Baxter [94].

Arvelakis and Koukios [76] proposed several types of pre-treatments which should improve the quantity and quality of ash forming matter in biomass residues and at the same time being easy to apply. The same procedures are used in this work. The pre-treatments that are applied to various fuels throughout this work are:

- **WATER LEACHING:** Before the leaching, the samples are ground and sieved to obtain a particle diameter smaller than 4 mm. They are then placed in a plastic grid, tied up and submerged in water for 24 hours. The mass-to-water ratio varied with the samples, as shown in the next sections.
- **FRACTIONATION:** The mechanical fractionation is performed using a mechanical shaker and using a 1 mm sieve. Only the coarse part is then kept for measurements, since the troublesome materials (such as mineral inclusions and salts) are mostly retained in the finer particles [76].

- **FRACTIONATION + LEACHING:** For few samples, a water leaching treatment is applied to the coarse fraction ( $D_p > 1$  mm) obtained from the fractionation pre-treatment.

Many other works can be referred to for more details on the procedures and discussions on the effectiveness of the pre-treatments for fluidized bed operation [72, 74, 75, 76, 77]. The effects of the pre-treatments on the reactivity, ash composition and nitrogen chemistry of the fuels studied in this work, instead, will be discussed in Chapters 4 and 5.

### 3.2.2 *Agricultural Residues*

The following samples are the subject of the study presented in Chapter 4:

- Wheat straw (WS)
- Wheat straw leached (WSL)
- Olive residues (OR)
- Olive residues leached (ORL)
- Olive residues fractionated (ORF)
- Olive residues fractionated + leached (ORFL)
- Peach stones (PS)
- Peach stones leached (PSL)

The details for the pre-treatments applied to these fuels are summarized in Table 12.

The properties of the fuels and the elemental composition of their ash forming matter are reported in Table 13 and 14, respectively. A detailed discussion on the effects of the pre-treatments on the ash forming matter in the fuels is presented more thoroughly in Chapter 4.

#### 3.2.2.1 *Origin of agricultural residues*

Straw is a residue from the harvesting of several cereal crops such as wheat, rye, barley and rice. Straw is thus available in many countries worldwide and in large quantities too, since it makes up for almost half of the weight of cereal crops [52]. Only in Europe more than 300 Mton of straw per year is produced [166]. The sample studied in this dissertation was received from Denmark.

Wheat straw is already used for power and heat production mostly in Denmark [166, 304] and mostly in co-firing or co-gasification with coal in medium and large-scale plants [3, 77, 193, 195, 196]. Usually, combustion efficiency

Table 12: Details of the pre-treatments applied to the agricultural residues

Sample	Sample Name	Particle Size Distribution	Water-to-Mass ratio	Time	Ref.
Wheat straw leached	WSL	$4\text{ mm} > D_p$	66.7 g/L	24 h	Arvelakis and Koukios [76]
Peach stones leached	PSL	$4\text{ mm} > D_p$	88.9 g/L	24 h	Arvelakis et al. [75]
Olive residue leached	ORL	$4\text{ mm} > D_p$	88.9 g/L	24 h	Arvelakis and Koukios [76]
Olive residue fractionated	ORF	$D_p > 1\text{ mm}$	-	-	-
Olive residue fractionated + leached	ORFL	$D_p > 1\text{ mm}$	88.9 g/L	24 h	Arvelakis [72]

Table 13: Proximate and elemental analysis of the agricultural residues. Data are on a dry basis.

	Wheat Straw	Wheat Straw Leached	Olive Residue	Olive Residue Leached	Olive Residue Fraction- ated	Olive Residue Fract+Leached	Peach Stones	Peach Stones Leached
Moisture <sup>a</sup>	8.1	5.75	9.5	11.1	8.8	6.6	8.5	12
Volatiles	76.0	80.6	76	78.7	77.9	83.3	81.3	81.6
Fixed Carbon	16.4	13.5	19.4	18.6	20.2	15.1	18.1	18.0
Ash	7.6	5.9	4.6	2.7	1.9	1.6	0.65	0.4
C	43.7	46.3	50.7	51.1	50.5	51.0	51.95	53.45
H	5.1	5.3	5.9	5.6	6.2	6.0	5.8	6.2
N	0.8	0.6	1.4	1.6	1.7	1.9	0.8	0.95
S	0.4	0.2	0.3	0.3	0.3	0.2	0.0	0.0
Cl	0.4	0.1	0.2	0.1	0.2	0.0	0.1	0.0
O (by diff.)	42.0	41.7	37.0	38.6	33.4	39.3	40.7	38.9
HHV (MJ/kg)	18.9	20.0	21.2	21.3	19.8	20.8	21.55	22.8

<sup>a</sup>as received basis.

Table 14: Elemental analysis of the ash forming matter in agricultural residues. Data are on a dry basis.

	Wheat Straw	Wheat Straw Leached	Olive Residue	Olive Residue Leached	Olive Residue Fraction- ated	Olive Residue Fract+Leached	Peach Stones	Peach Stones Leached
Al <sub>2</sub> O <sub>3</sub>	1.95	1.9	3.0	0.9	2.5	0.4	0.5	0.0
SiO <sub>2</sub>	39.2	49.8	32.6	39.3	31.9	40.95	6.0	10.5
CaO	14.4	15.3	10.2	23.9	9.8	36.8	7.1	19.3
MgO	2.7	2.5	3.8	0.9	3.3	4.1	2.7	2.5
Fe <sub>2</sub> O <sub>3</sub>	0.4	0.6	1.9	2.8	n.d.	1.9	0.5	0.1
K <sub>2</sub> O	15.9	10.9	27.2	10.0	34.8	4.2	38.45	21.2
Na <sub>2</sub> O	4.3	0.5	4.2	0.05	3.9	0.05	0.1	0.0
TiO <sub>2</sub>	0.1	0.1	0.1	0.2	n.d.	0.1	0.15	0.0
SO <sub>3</sub>	5.3	3.8	5.0	5.85	4.7	5.3	5.2	3.2
Cl <sup>-</sup>	2.7	1.8	1.4	0.0	1.4	0.1	0.1	0.0



and emissions are not particularly affected when the shares of straw are maintained below 20 - 25 %<sub>th</sub> [3, 360], however ash deposition, corrosion and bed agglomeration pose severe limitations to a wider use of this material.

The olive residue sample is a remainder from olive oil production. The sample was received from Greece and it contains: kernels, pulps, leaves, and limbs of the olive plants [73, 77, 159].

The peach stones sample came from Greece too. The sample contains residues of the production of juices and stewed fruits and it includes not only the stones but also the pulps of the peach fruits [75, 159].

Olive residues and peach stones are not yet widely used for energy supply, even though their potential in Mediterranean countries is high.

Due to their origin, the main structures in these fuels are generally hemicellulose, cellulose and lignin [72, 210, 343]. Among the available studies, Marcotullio et al. [258] provides the following composition for wheat straw: approximately 35 %wt<sub>d.b.</sub> of cellulose, 25 %wt<sub>d.b.</sub> of hemicellulose and 16 %wt<sub>d.b.</sub> of lignin, while the rest is mostly water.

The fuel-N content of these materials is generally higher than in other woody biomass but much lower than other bio-residues. Especially the peach stones sample is enriched in lignin due to the presence of the fruit kernels [72].

All the samples were pre-treated, according to the procedure described before, at the National Technical University of Athens by Dr. Arvelakis.

Several studies are available on the characteristics of co-combustion of agriresidues [77, 78, 193, 195, 212, 218, 336, 360, 364] but more details will be given in Chapter 4.

### 3.2.3 *Bio-wastes and residues*

The second group of materials that was chosen for this study includes residues of various processes. The fuels chosen are listed below, the chapter in which the fuels are studied is mentioned next to the fuel's name:

- Dry distiller's grains & solubles (DDGS) (**Chapters 5, 6 and 7**)
- Dry distiller's grains & solubles leached (**Chapters 5 and 6**)
- Chicken manure (CM) (**Chapter 5 and 7**)
- Chicken manure leached (**Chapter 5**)
- Palm kernel cake (PKC) (**Chapters 6 and 7**)
- Palm kernel cake leached (**Chapter 6**)
- Rapeseed cake (RC) (**Chapter 7**)
- Fermented sewage sludge (FSS) (**Chapter 7**)

Table 15: Details of the pre-treatments applied to the agricultural residues

Sample	Particle Size Distribution	Water-to-Mass ratio	Time
DDGS Leached	4 mm > D <sub>p</sub>	44.4 g/L	24 h
CM Leached	4 mm > D <sub>p</sub>	88.9 g/L	24 h
PKC Leached	4 mm > D <sub>p</sub>	88.9 g/L	24 h

Table 15 summarizes the pre-treatment conditions for the leached materials .

The proximate and elemental analysis of these fuels are reported in Table 16.

Finally, the elemental composition of the ash forming matter for the samples, for which such analysis is available, is summarized in Table 17.

### 3.2.3.1 Origin of biomass residues

Three of the chosen materials are by-products in different processes for the production of so-called 1<sup>st</sup> generation liquid biofuels: Dry distiller's grains and solubles (DDGS), palm kernel cake (PKC) and rapeseed cake (RC). Chicken manure (CM) is a waste of animal breeding and the fermented sewage sludge (FSS) is a residue of the anaerobic digestion of the original sewage sludge.

DDGS is a by-product of the dry-grind process to produce ethanol from cereals. The starch contained in the original cereal (commonly corn, barley or wheat) is separated from the rest of the material and hydrolyzed into its structural C<sub>6</sub> sugars which are then fermented, with the use of yeast, into ethanol and CO<sub>2</sub>. The residue of this process contains mainly proteins, cellulose, hemicellulose and lignin components from the original cereal, with the addition of residual starch and yeast [110, 220]. Once dried, this compound is called DDGS [110]. DDGS is commonly sold and used as feed for cattle due to its high protein content [220]. However, the production of bio-ethanol, mostly in the U.S., has seen an unprecedented growth in the last years, reaching a production of more than 10.5 billion gallons by the end of 2009 [36], doubled compared to values of 2006. The production of DDGS has, consequently, also doubled in the last three years. Up to now around 80% of the DDGS production is fed only to cattle [296] because of adverse effects of the poor balance of amino acids for swine and poultry [334]. The combination of growing supply and limited demand as cattle feed has created the need to investigate the possibility to use DDGS for the production of heat and power on-site at the ethanol mills. Tiffany et al. [335] modeled various scenarios for biomass energy integration in a 50 and a 100 million gallons/year corn-ethanol mills. They have shown that for most mills, the gasification or combustion of DDGS could fulfill the requirements of heat and power of the whole mill with additional power to be sold to the grid [334, 335]. The additional use of renewable

Table 16: Proximate and elemental analysis of the biomass residues. Data are on a dry basis.

	DDGS	DDGS Leached	PKC	PKC Leached	RC	FSS	CM	CM Leached
Moisture <sup>d</sup>	8.9	8.5	7.0	9.2	2.1	7.4 <sup>c</sup>	20.2	9.4
Volatiles	78.2	76.2	75.5	75.1	74.7	43.3	67.9	65.7
Fixed Carbon	14.7	17	18.4	19.5	18.8	10.6	5.5	9.6
Ash <sup>b</sup>	7.1	6.8	6.1	5.4	6.5	46.1	26.6	24.7
C	49.0	48.8	49.0	47.8	49.9	26.5	39.6	37.2
H	6.3	6.3	6.0	6.1	6.9	5.9	4.1	5.0
N	4.5	4.5	2.4	2.7	5.1	3.2	5.9	5.6
S	0.4	0.4	0.5	0.4	0.7	1.2	0.7	0.8
O (by diff.)	32.7	33.2	36.0	37.7	29.6	17	23.2	26.7
HHV (MJ/kg)	19.8	20.5	17.8	18.8	22.2	11	13.3	14.7

<sup>a</sup>as received basis

<sup>b</sup>Ashed at 600 °C, except for RC and FSS ashed at 550 °C

<sup>c</sup>Sample pre-dried in oven before combustion tests

Table 17: Elemental analysis of the ash forming matter in biomass residues. Data are on a dry basis.

	DDGS	DDGS Leached	PKC	PKC Leached	CM	CM Leached
Al <sub>2</sub> O <sub>3</sub>	0.2	0.4	4.4	5.2	0.6	0.8
SiO <sub>2</sub>	22.4	24.9	16.2	17.8	4.2	5.6
CaO	2.9	3.9	9.3	11.3	29.1	35.6
MgO	7.3	8.2	8.2	8.5	6.1	6.0
Fe <sub>2</sub> O <sub>3</sub>	0.4	0.5	11.5	12.4	0.6	0.8
K <sub>2</sub> O	22.7	22.4	14.0	12.3	15.3	13.9
Na <sub>2</sub> O	2.7	1.8	0.4	0.1	2.9	1.6
TiO <sub>2</sub>	0.01	-	0.1	0.2	0.04	-
SO <sub>3</sub>	9.5	2.0	9.2	2.4	6.0	2.1
Cl <sup>-</sup>	2.9	0.9	3.3	0.0	1.5	0.1
P <sub>2</sub> O <sub>5</sub>	29.0	32.4	23.7	25.4	21.3	22.0

sources in the production of bio-ethanol would, moreover, substantially raise its controversial energy ratio from 1.5 to 3.8 [334]. Furthermore, Wang et al. [356] calculated a reduction of 39 % in the Well-to-Wheel greenhouse gas emissions for bio-ethanol when a renewable source like DDGS is used to provide power and heat for the mill instead of natural gas and fossil electricity.

While bio-ethanol production is highly promoted in the U.S. due to locally available crops (corn) and favourable policies, biodiesel is the most common biofuel produced in Europe. Biodiesel production in Europe reached 7.8 Mton in 2008 with a 60% increase in the last two years [37]. More than 80% of this production was based on rapeseed oil as feedstock material and about 1 % on palm oil. While palm oil retains potential for biodiesel production, it is already an established product for soap production and food processing purposes. Malaysia and Indonesia share most of the palm oil market with a production of 35 Mton by 2008 [48]. PKC and RC are the solid residues left after the mechanical pressing of the seeds from the palm fruit kernels and rapeseeds, respectively. Both materials are rich in fibers and proteins [294] and are therefore commonly used as feed for livestock, even though they present limitations in their amino acid distribution which limits their market share in this sector. While several biotechnological and chemical applications could be suited for such materials in a biorefinery [228, 294], in many situations an efficient on-site combustion to provide the necessary power and heat to sustain the main process could be the most economical solution.

Chicken manure is waste which needs to be disposed of. However, disposal of this material is becoming increasingly difficult due to the raising consumption of chicken meat and eggs worldwide [361]. The CM sample studied in this work was scooped from the bottom of the cages where hens are kept for egg production. The sample, therefore, contains the excrements of the birds, together with urines, undigested food and organic parts of the birds themselves. CM is rich in nutrients like P, K and N, and it is therefore usually used as fertilizer and disposed on fields, directly or after composting. However, the amount of nutrients applicable on fields is limited by law due to possible eutrophication of the ground waters. Therefore, incineration is in many cases the cheapest way, not only to dispose of the waste, but to valorize it by producing power and heat. Despite presenting worse characteristics than the residues mentioned above, like higher ash content, high nitrogen content and lower calorific value, for some years CM has been used in large-scale combustors and data on pilot scale facilities are available in the literature [217, 246, 378]. Commercial-scale boilers are also starting to go online, like the 36 MW bubbling fluidized-bed combustor installed in Moerdijk, The Netherlands, which processes more than 30% of all the poultry litter produced in the country [41].

Sludge is formed during wastewater treatment. Werther and Ogada [359] gave a complete review of sludge composition and possible disposal techniques. Nowadays in Europe most of the sewage sludge is stabilized through digestion and then disposed either in landfills, as fertilizer on land, or incinerated. The fermentation process produces biogas that can be combusted to supply power and heat to the wastewater plant while the residue (FSS) is usually either composted and used as fertilizer or combusted. In The Netherlands the use of sludge in agriculture is forbidden already since 1995 [227] and it is foreseen that in the near future landfilling will become less and less popular while incineration will become the most common disposal technique.

The solid materials present in wastewater are mostly constituted by carbohydrates, fats, oils and proteins. The main source of nitrogen in wastewater are proteins and urea [359]. However, the FSS is a residue of a fermentation process and, therefore, it is to be expected that the biodegradable fraction of the fuel has already been released together with the weakly bound nitrogen. The residual material, thus, is expected to be mostly in the form of monomers and oligomers because of the effects of the enzymes action. The main N compounds are expected to be free amino acids. As for CM, experience with sludge combustion and co-combustion is quite substantial even though most of the data available rely on large-scale experiments and fundamental data are still largely lacking [56, 239, 306].

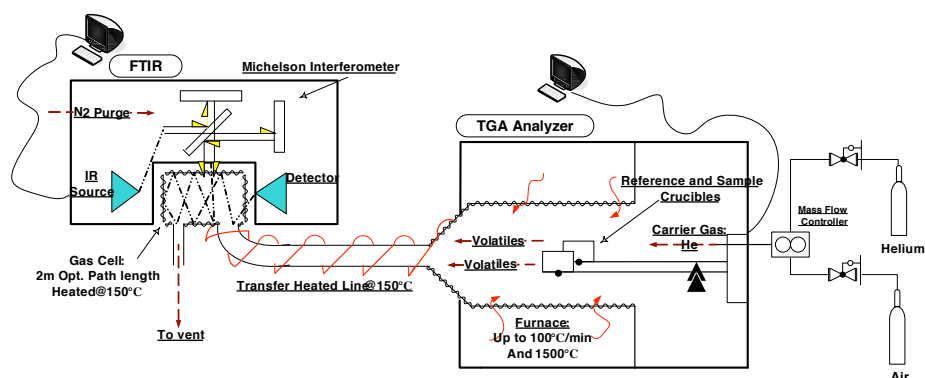


Figure 46: Schematic of the TG – FTIR setup

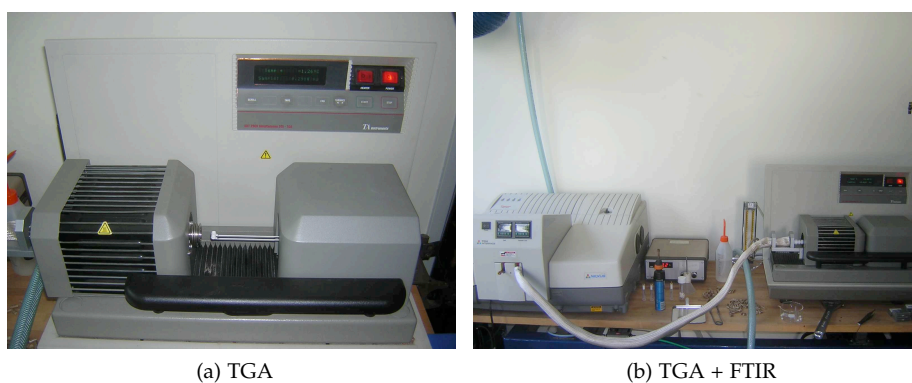


Figure 47: TG–FTIR setup at Process and Energy Laboratory

### 3.3 SLOW PYROLYSIS EQUIPMENT

#### 3.3.1 Thermogravimetric Analyzer - Fourier Transform InfraRed Spectrometer (TG–FTIR)

The experimental work described in Chapters 4 and 5 is carried out using the TG–FTIR setup shown in Figure 46 and 47.

Thermogravimetric techniques have gained a very important role in the past 30 years for solid fuel characterization. TG–FTIR equipments, in fact, allow almost full automatic runs with full and accurate control of process parameters such as heating rate, end temperature and process atmosphere. For example, from a simple TG–FTIR run it is possible to obtain the proximate analysis of the fuel (amount of moisture, volatile matter, residual char and ash content) but also devolatilization kinetics, char reactivities in gasification or combustion atmospheres, the heat of reaction and, finally, volatiles distribution and

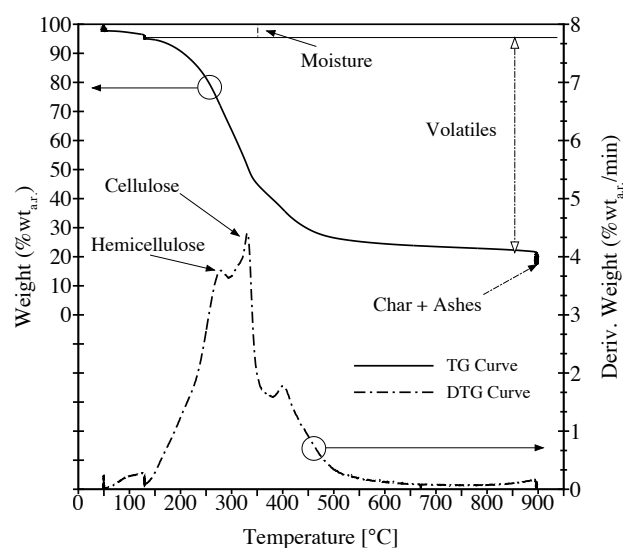


Figure 48: Example of thermogravimetric weight loss curves and analysis of DDGS at a heating rate of 10 °C/min; TG: thermogravimetric curve, DTG: Differential thermogravimetric curve.

yields. An example of thermogravimetric curves and partial information that can be obtained from this analysis is given in Figure 48.

The apparatus for the evolved gas analysis used in this work includes a thermobalance SDT 2960 from TA Instruments coupled through a short stainless steel heated line (heated at 150 °C) to an FTIR spectrometer NEXUS manufactured by Thermo Nicolet.

Measurements are carried out under an inert atmosphere using helium as a carrier gas with a volumetric flow rate of 100 mL/min, controlled by a mass-flow controller. This flow must be kept high enough to avoid long residence times in the oven and thus to prevent secondary reactions of the volatiles in the hot furnace. However, it must also be low enough to guarantee well detectable concentrations of the interesting species in the FTIR.

The TGA is composed mainly of a balance with a sensitivity of  $\pm 1 \mu\text{g}$  to which two beams are connected. One of the beams is used as reference while the other one is loaded with the sample. On the tip of the beams, right below the sample placement, a thin thermocouple is placed so that, at slow heating rates, it is possible to assume this temperature as the actual temperature in the sample. Both beams are inserted into a small ceramic furnace which is electrically heated. The whole process is remotely controlled via a PC.

Due to the small volumes involved, the control of the heating is very accurate and the setup can achieve precise heating rates from 1 °C/min to 100 °C/min. As it will be explained in the following sections and chapters, in order to per-

form a kinetic analysis of the pyrolysis process, experiments at multiple heating rates are required. In this work runs are performed at 10 - 20 - 30 °C/min in order to obtain proper kinetic parameters. These parameters are then extrapolated to 100 °C/min to verify their validity at least in this range of conditions.

The samples used in TGA measurements are usually ground and placed in small alumina cups in amounts ranging from 5 to 30 mg. Smaller sample sizes give more accurate analysis since heat and mass transfer limitations are minimized. However, since the FTIR measures volumetric concentrations, a too small sample decreases greatly the sensitivity of the FTIR analysis. In this work tests are performed both with low and high sample mass in order to verify whether significant changes are found in the retrieved kinetic parameters or not.

The inert helium gas carries the volatiles from the furnace, where they are released from the sample situated in the alumina crucible, to the gas cell of the FTIR which is also kept at 150 °C. This temperature must be high enough to avoid condensation of tars and ammonia adsorption [182] but not too high to avoid thermal cracking of the released compounds.

Two different gas cells are used in the FTIR for the campaigns described in Chapter 4 and Chapter 5. The work in Chapter 4 is carried out using a gas cell with an optical path length of 0.2 m, ZnSe windows, gold coated mirrors and an internal volume of 50 mL. The work described in Chapter 5 is, instead, carried out using a gas cell with an optical path length of 2 m, ZnSe windows, gold coated mirrors and an internal volume of 200 mL.

According to the vast experience acquired on this setup, the best compromise between signal-to-noise ratio and sampling time is obtained using a resolution of  $0.25\text{ cm}^{-1}$  co-adding 12 scans, for a total measurement time of 33.6 s.

The thermal history of the FTIR data can then be retrieved from the TGA data knowing the time delay due to the internal volume of the transfer line and gas cell. In our measurements this results in a delay of approximately 1 minute. The exact delay is then obtained by precisely overlapping the peaks obtained in the DTG curve of the TGA run with the peak of the absorbance curve obtained from the FTIR measurement.

A quantitative method is implemented on the FTIR by calibration of the following species: CO, CO<sub>2</sub>, CH<sub>4</sub>, H<sub>2</sub>O, NH<sub>3</sub>, HCN and HNCO. The method used in this work is an optimized version of the method presented by Di Nola [139]. The specific settings of the method are presented in the Appendix A. A common drawback of FTIR spectroscopy is that heavy molecules like tars cannot be analyzed nor quantified due to their broad resonance to InfraRed which makes it impossible to actually define an absorbance peak except for very specific compounds, as described by Defoort et al. [129]. Moreover, molecular compounds like H<sub>2</sub> and N<sub>2</sub> are not sensitive to InfraRed radiation and therefore cannot be detected at all. Tars and molecular compounds, which usually make up for 30 to 50 %<sub>w</sub>t of the mass balance from pyrolysis of biomass, can only be obtained by difference from the char and gas yields. An example of



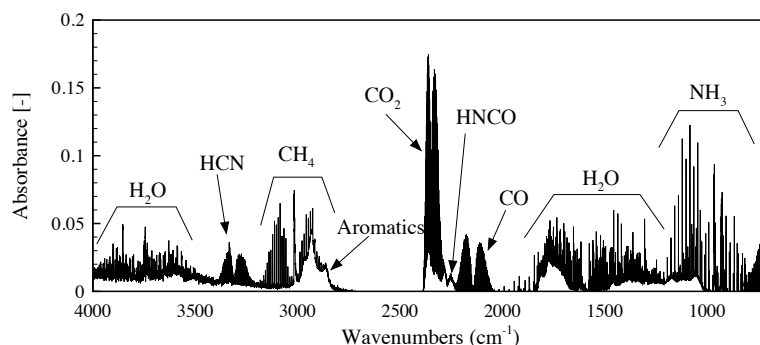


Figure 49: Example of FTIR absorption spectrum for DDGS pyrolysis with heating rate  $10^{\circ}\text{C}/\text{min}$  in He on a TG-FTIR setup.

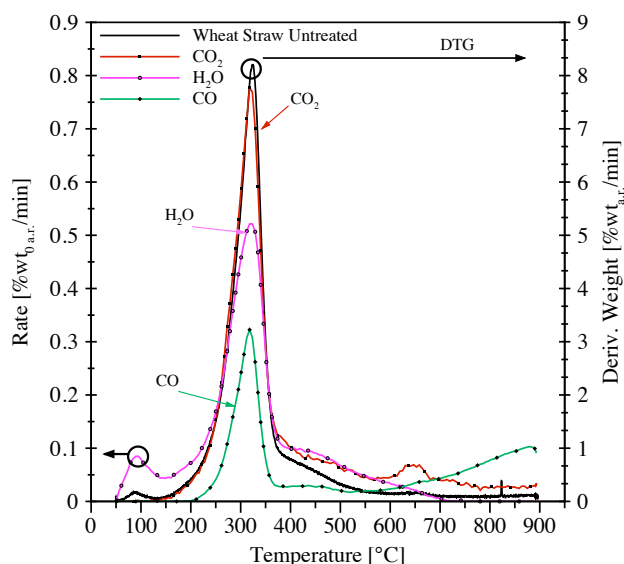


Figure 50: Example of measurement of volatile species during pyrolysis of wheat straw with heating rate  $10^{\circ}\text{C}/\text{min}$  in He on a TG-FTIR setup.

FTIR spectrum obtained in pyrolysis of DDGS is shown in Figure 49. During a whole measurements, a series of such spectra is taken at regular intervals of 33.6 s so that it is possible to obtain the release rate of specific gaseous compounds as indicated in Figure 50.

Some other limitations in our quantitative method could be considered as well: there are no calibration gases available for HNCO so that calibration lines can only be produced by means of urea decomposition following the procedure described by Di Nola [139]. Moreover, H<sub>2</sub>O calibration in vapor

phase is not performed by calibration bottles but using a flow of  $N_2$  saturated in water at well controlled conditions of pressure and temperature. In such way, the water vapor pressure is known and can be used as calibration value. The exact procedure is described in Di Nola [139].

On the other hand, tests performed with an ammonia releasing salt (Tetraamminecopper(II) Sulfate monohydrate, CAS 10380-29-7), whose thermal decomposition was described by Zivkovic [379], have given mass balance closures within 5 % for  $NH_3$  indicating the validity of our quantitative method for ammonia and the absence of significant adsorption phenomena in the reactors or transfer line.

The same technique was used for  $CO_2$  calibration verification using calcium carbonate ( $CaCO_3$ ) decomposition in the TGA. These tests also gave very good results, with mass balance closures within 5 %. For more information on the phenomena involved and on the principles of FTIR spectroscopy see for example Griffiths and De Haseth [170] and de Jong [200].

### 3.3.2 Literature review

This section presents several works carried out on thermogravimetric setups with the purpose of giving a brief overview of the large amount of data available in literature. However, a more detailed analysis of such data and comparison with the present results can be found in the appropriate chapters 4 and 5.

The popularity of TGA systems for solid fuel characterization has been steadily increasing with the increasing automatization of the systems themselves. Already 20 years ago Solomon et al. [316] published an extensive review on coal characterisation in which TGA was the main technique for the study of slow pyrolysis mechanisms.

When interest started to grow in biomass for energy, many studies began to appear on model compounds for the structural components of biomass. Antal and Várhegyi [68], Antal et al. [66], Grønli et al. [171] published several studies on cellulose thermal decomposition. Other works have focused on the study of hemicellulose model compounds (mostly xylans) and lignins [185, 191, 192, 255, 285, 344, 345]. Several authors, among which Biagini et al. [103], Jensen et al. [195], Yang et al. [366], also performed TGA measurements of hemicellulose, cellulose and lignin but they were also able to investigate the volatiles released by these model compounds with the use of an online FTIR spectrometer. Guinesi et al. [174] analyzed the thermal decomposition of various starches. Li et al. [243, 244, 245] investigated the pyrolysis of several amino acids on a TG-FTIR setup. Rodante et al. [300, 301, 302] described the thermal decomposition of dipeptides and Sharma et al. [311, 312] investigated the pyrolysis of peptides. Many studies are nowadays available on the thermal decomposition of biomass samples, of which just a few are reported

here: see for example Varhegyi et al. [346], Várhegyi et al. [345, 347, 348], Becidan et al. [100], Grønli et al. [172].

Together with important characteristics of thermal conversion of the fuels, such as the amount of volatile matter or onset temperature of devolatilization, TGA measurements can even provide data on the composition of a mixture of materials [186] or semi-quantitative data on the biomass structural composition [84, 285].

Thanks to the amount of parameters which are measured and controlled in a TGA, using the weight loss data obtained from different runs, it is possible to apply various kinetic models to the fuel devolatilization. The next subsection will give a brief overview of available models and describe the ones used in this work. Such models and parameters are essential in order to scale-up the results obtained under well controlled operation conditions to industrial applications, where many more parameters influence the final outcome [139, 200].

Furthermore, with the development of FTIR quantification methods, a new type of analysis has become available allowing detection and quantification of volatile compounds released during slow pyrolysis. Some of the most relevant TG-FTIR analysis for biomass samples are listed here: Bassilakis et al. [90], Biagini et al. [103], Giuntoli et al. [159, 163], de Jong et al. [202, 204], Wójtowicz et al. [363]. Applying kinetic models to the release of single species, then, allows for model predictions on speciation and yields of volatiles to conditions more relevant for industrial applications [139, 200, 202, 204].

### 3.3.3 *Kinetic analysis of slow pyrolysis*

In Chapter 2 it was shown how biomass materials are actually composed of many different structures. Therefore, in order to describe the kinetics of thermal conversion (devolatilization, homogeneous volatiles gasification/combustion, char gasification/combustion) there is the need for appropriate modeling. The kinetic analysis performed in this study is addressed, however, only to the devolatilization sub-process.

Global reactions cannot be represented by simple kinetic models, but a too detailed approach cannot be followed either because of the enormous number of reactions involved and their unknown mechanisms.

So the need to synthesize the data has been historically approached with linearization techniques [124, 157, 222] which use a logarithmic transformation of the data to obtain the necessary Arrhenius parameters (activation energy,  $E$ , and pre-exponential factor,  $A$ ) by a simple linear fitting.

A complex reaction can be treated as a pseudo-unimolecular reaction following the general kinetics described as:

$$-\frac{dx}{dt} = k(T) \cdot f(x) \quad (3.1)$$

Where  $x$  represents the unreacted fraction of the initial material and  $k(T)$  obeys the Arrhenius equation and it is a function of time because of the applied temperature profile:

$$k(T) = A \cdot \exp\left(-\frac{E}{R \cdot T(t)}\right) \quad (3.2)$$

$$\ln\left(\frac{H_r}{(R \cdot T_{max}^2)}\right) = -\frac{E}{(R \cdot T_{max}^2)} + \ln\left(\frac{A}{E}\right) \quad (3.3)$$

Equation 3.3, for example, illustrates the method developed by Kissinger [221, 222], called  $T_{max}$  shift method. It is a re-arrangement of the Arrhenius equation and uses the temperature of maximum reaction rate (obtained from DTG curves) at different heating rates to obtain the parameters  $A$  and  $E$  through linear fitting of the points obtained from experiments at a known heating rate ( $H_r$ ).

These methods are, though, limited and can only give approximate solutions for complex materials such as biomass. So, nowadays, Least Squares fitting methods of thermogravimetric curves from multiple experiments have become the most direct and widely used approach to analyze devolatilization results from thermogravimetric experiments [90, 111, 112, 125, 344].

This technique, even if criticized because of the non-normal distribution of errors in TGA measurements [350], has proven a more than useful tool if the data are analyzed accurately [120].

Actually, the main types of fitting analysis can be listed under two methods. The first one, followed by several authors [63, 66, 84, 262, 285, 344] and well described by Gómez Díaz [168], considers the three main components of biomass – cellulose, hemicellulose and lignin – as reacting independently under pyrolysis conditions. In this way the experimental Differential Thermogravimetric (DTG) curve can be fit with a weighted sum of three independent, first-order reactions (or “pseudo-components”) that will resemble the behavior of the actual main components.

$$\frac{dm^{calc}}{dt} = -\sum_{j=1}^M c_j \cdot \frac{d\alpha_j}{dt} \quad (3.4)$$

In Equation 3.4,  $dm/at$  represents the original data of weight loss from the TGA run,  $c_j$  is the weight factor, or amount, for each pseudo-component  $j$  and

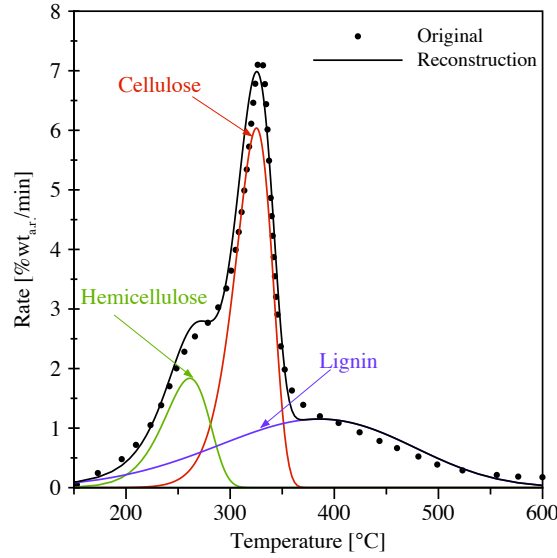


Figure 51: Example of the application of three independent first-order reactions to the pyrolysis of olive residues at 10 °C/min

$d\alpha_j/dt$  represents the reaction rate of each  $j^{\text{th}}$  pseudo-component according to:

$$\frac{d\alpha_j}{dt} = A_j \cdot \exp\left(-\frac{E_j}{R \cdot T}\right) \cdot (1 - \alpha_j)^{n_j} \quad (3.5)$$

This method gives accurate fits of the experimental data, as shown in the example in Figure 51. However, it is not uncommon that three pseudo-components are actually not enough to have a proper fit of the data for heterogeneous materials and multiple equations are required; for this reason the scope of comparison of the pseudo-components with the physical structures is indeed lost.

The second method is the one followed by Braun and Burnham [112] and many others [202, 204, 267, 339, 363]. In this case the process of devolatilization is modeled as an infinite series of parallel, irreversible, first-order reactions assuming that their activation energy follows a probability distribution. This model is called Distributed Activation Energy Model (DAEM) and was made popular by Anthony and Howard [69].

In this work we chose to follow the latter line considering the previous works from our group [139, 202, 204] and, mainly, the possible future applications of these data on an FG-Biomass model [318], which requires input data following this kinetic model [202, 204, 318, 339].

The distributed activation energy model can be expressed as follows, where  $x$  represents the unreacted fraction of the sample:

$$x = \int_0^{\infty} \exp \left[ - \int_0^t k(T) dT \right] \cdot D(E) dE \quad (3.6)$$

Where:

$$\int_0^{\infty} D(E) dE = 1 \quad (3.7)$$

The shape of the distribution  $D(E)$  is not known a priori and it depends on the composition and structure of the sample. It is common practice to assume  $D(E)$  as a Gaussian distribution with the expression in equation 3.8.

$$D(E) = (2 \cdot \pi)^{-1/2} \cdot \sigma^{-1} \cdot \exp \left[ - \frac{(E - E_0)^2}{2 \cdot \sigma^2} \right] \quad (3.8)$$

A valid alternative to this assumption is to choose a discrete distribution of activation energies: in this case the integral in equation 5.1 is substituted by the sum of a finite number of parallel reactions.

Using a discrete distribution for the activation energies introduces an additional degree of freedom in the analysis since this distribution does not need to be fixed in advance, as underlined also by Miura [267]. Moreover, the visualization of the results appears more effective when using this method, as it will be clear in Chapters 4 and 5. Even though it has been argued that the link between each reaction (characterized by an activation energy  $E_i$ ) and the decomposition of a single structure or functional group cannot be straightforwardly made [342], it will be shown in the next chapters that certain reactions are common to all the materials and can, therefore, be linked to the decomposition of specific structures.

For the analysis carried out in this dissertation, a FORTRAN based code is used which was developed by Dr. A.K. Burnham and Dr. R.L. Braun, called KINETICS05 [113, 119]. This software can analyze, simultaneously, measurements performed at different heating rates and fit them either with a discrete distribution or with multiple Gaussian functions.

When a discrete distribution model is chosen, up to 25 first-order reactions can be used, but all of them share the same pre-exponential factor. This is another common assumption using the DAEM model. In fact, due to the so

called “compensation effect”,  $A$  appears to depend on the activation energy through an expression of the following kind [273, 291]:

$$A = \alpha \cdot \exp(\beta \cdot E) \quad (3.9)$$

in which  $\alpha$  and  $\beta$  are arbitrary coefficients.

In the present work the common practice is followed and the pre-exponential factor is fixed to the value of  $2.2 \times 10^{13} \text{ s}^{-1}$  according to [202, 339] for several reasons. The main one is that in many publications describing kinetic analysis, the pre-exponential factor is indeed completely neglected and the activation energy is given almost as a “stand-alone” value. This is erroneous since the two values are closely related in determining the final reaction rate. On the other hand, many times, activation energy and pre-exponential factor are given as a couple but they vary on a wide range and because of the compensation effect non-unique solutions can be found when fitting both parameters [204, 202]. I think that, in order to have both a reliable comparison between different fuels conversion kinetics and a solid base for future applications, the physico-chemical meaning of the pre-exponential factor can be fixed into a reasonable value allowing instead the interpolation over the activation energies and the distribution shape. The well-known transition state theory, which gives a physical meaning to the empirical Arrhenius expression in general and to the pre-exponential factor in particular, states that the value of  $A$  should be between  $10^{11}$  and  $10^{16} \text{ s}^{-1}$  [102] and the value chosen in this work is included in this interval. Also is to note that when fitting three parallel first-order reactions, often for the lignin pseudo-component a pre-exponential factor of  $10 - 10^{-1} \text{ s}^{-1}$  is used [343], so that the actual meaning of the term is already lost since these values are not allowed by the transition state theory [102].

Finally, the approach used in this dissertation is to use a discrete distribution to model the devolatilization of the fuels because it is considered to be more suitable to represent the heterogeneous nature of the materials. On the other hand, one or more Gaussian distributions are used to analyze the volatile species released during pyrolysis. As described above, in fact, the TG-FTIR setup allows to follow closely the release of specific volatile species with increasing temperature and to attain a reaction rate profile for each species analogous to the DTG curve obtained for the whole fuel (see Figure 50). The use of three Gaussian distributions, thus, allows to describe the reaction of the pseudo-pools from which the compounds are released. The term precursor’s pool, as used in other works [202, 204, 318, 339], refers to a fictitious class of components in the original fuel which are supposed to release, during pyrolysis, the referred volatile species following the indicated kinetics.

The importance of the kinetic parameters obtained from such models lies in the fact that the data obtained in this work are directly applicable to other

network models, such as FG–Biomass [200, 202, 318]. Such models are essential in order to extrapolate these data (obtained in slow pyrolysis) to higher, more realistic, heating rates. Consequently, these models are gaining more and more importance because they can be used as pre-processors in CFD codes improving greatly the modeling of pyrolysis phenomena which are otherwise too simplified in commercial codes [139, 141, 185].

### 3.4 FAST PYROLYSIS EQUIPMENT

#### 3.4.1 *Integrated Heated Foil Reactor – Fourier Transform InfraRed Spectrometer (HF-FTIR)*

The experimental work described in Chapter 6 is carried out using the setup illustrated in Figure 53.

The apparatus was custom built and it has been previously described in the work of Di Nola [139]. The equipment has been analyzed and previously optimized in the work of Tamboer [329] but it has been further improved in the present work and the related work of Gout [169].

As it is visible in Figure 53, the setup consists of two different equipments: the proper heated foil reactor and the FTIR in which it is inserted. The main part of the reactor consists of a stainless steel cylindrical chamber of 60 mm diameter and 65 mm of height. A grid, or foil in this work, is placed between two electrodes in the center of this chamber. An S-type (Pt/Pt-Rh) thermocouple of 0.01 mm diameter is placed underneath the grid/foil in contact with it. Finally, the sample is placed on the center of the foil. The reactor walls are heated via resistive heating elements at a temperature of 110 °C, verified by an external K-type thermocouple, in order to avoid species condensation on the walls.

When electric current is passed through the electrodes, the foil is heated, via resistive heating, at very high rates of the order of 1000 °C/s. The control of the heating profile is done via the thermocouple and a fast acquisition card (Keithley KPCI-3108 with sampling frequency of 10<sup>3</sup> Hz) connected to a PC. The PC uses the thermocouple reading as input for the control and adjusts the electrical current input so that the actual temperature profile follows the programmed one. The control is done via the software Testpoint and the thermal history can be customarily defined via the parameters of heating rate, final temperature and holding time at final temperature. The software allows to input a maximum current intensity in order to protect the foil and smooth eventual overshoots in temperature.

The choice in this work was to use a foil of stainless steel AISI 304 (18Cr 9Ni) with a thickness of 0.05 mm and a surface of 8 × 14 mm. In previous works [139, 140, 329] both stainless steel and platinum grids were used; however, a foil seems to be more suitable than a grid because of several reasons: more homogeneous distribution of current (and thus temperature and heat transfer)





Figure 52: Samples of PKC and DDGS as used in the heated foil reactor

on the surface, there are no risks of reacting material loss through the mesh holes and, finally, modeling and validation is easier with a foil than a mesh geometry. The larger surface in contact between the sample and the foil, compared to a grid, however, could have a catalytic effect on the decomposition of the fuel.

As indicated in Figure 53, the system is flushed with helium for a sufficient time and the inlet and outlet valves are then closed to maintain the atmosphere in the reactor inert. After the valves are closed, the heating is started and the sample is heated usually with heating rates ranging between 600 to 1000 °C/s up to temperatures ranging between 500 °C and 1300 °C. The holding time at high temperature usually varies between 5 to 15 s.

As it was also found out by Di Nola [139] and Tamboer [329], compressing the sample powder into pills guarantees a more uniform heat distribution in the sample itself together with making char recovery and modeling easier. Therefore, the fuels are first ground by mortar and pestle. Consequently, 5 to 7 mg of sample are weighted and then pressed into thin discs of about 0.7 mm thickness and 3 mm diameter.

Once the gases are released from the sample, a volumetric pump, with a flow of 2.6 L/min, extracts them from the hot zone and circulates them into two transfer lines, heated at about 110 °C. The loop is closed by a final cylindrical tube encased among two ZnSe windows. This constitutes the actual gas cell of the FTIR and it has an optical path length of 0.2 m. The total volume of the reactor and circulation loop is 200 cm<sup>3</sup>. A filter of glass wool was inserted at the suction of the gases in order to absorb the tars produced during pyrolysis and not recirculate them through the pump volume and the FTIR gas cell.

The FTIR has been calibrated for the same species as the ones mentioned in section 3.3.1. The conditions of the scans are changed in order to have optimized measurements: the resolution is maintained at 0.25 cm<sup>-1</sup> but only 3 scans are overlapped for a total measurement time of 9 s. In order to guaran-

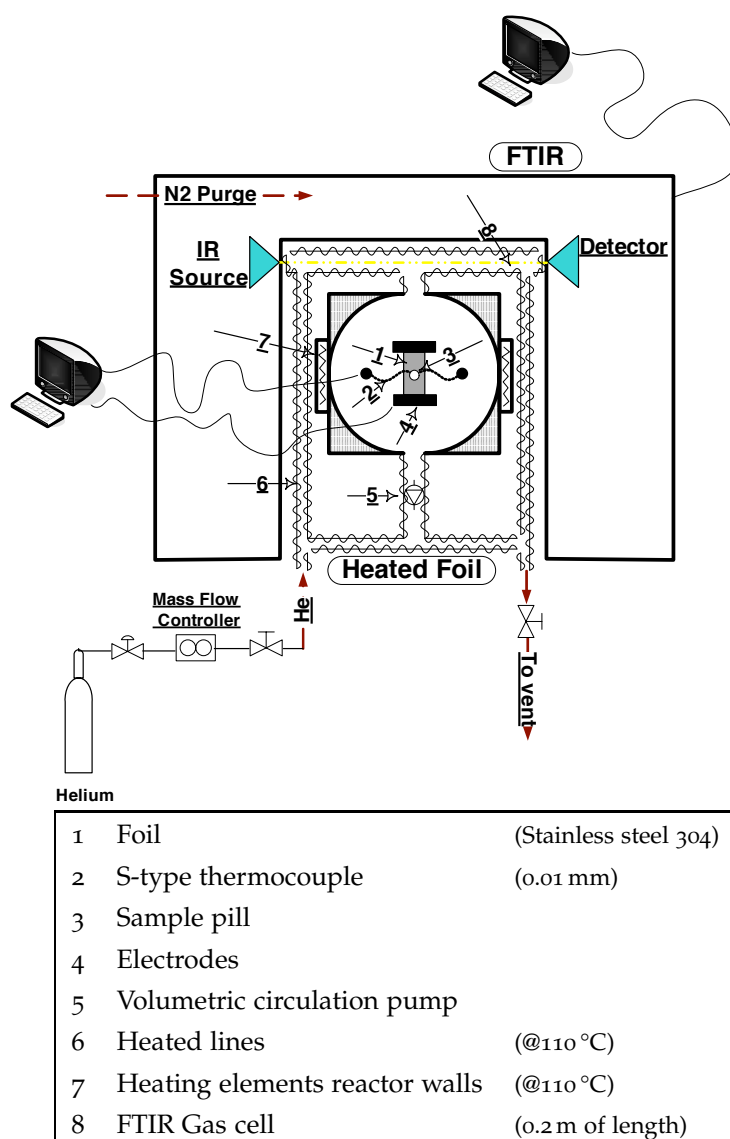


Figure 53: Heated foil setup at Process and Energy Department

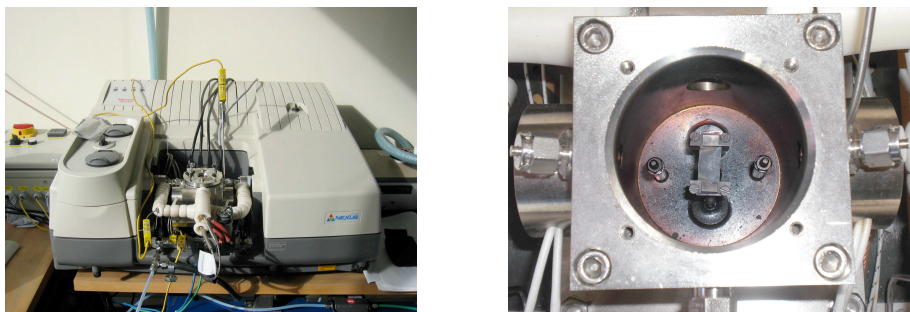


Figure 54: Heated foil reactor + FTIR at Process and Energy Department

tee a homogeneous distribution of the gases in the reactor volume, after the holding time at high temperature, the pyrolysis gases are circulated for about 2 minutes prior to the FTIR measurement, as it will be better explained in the next sections.

#### 3.4.1.1 Pyrometer

In order to validate the numerical model developed in this work and described in Chapter 6, an InfraRed pyrometer was used. The pyrometer is a IGA5 MB20 manufactured by the company Impac. This pyrometer can measure the IR radiation of a spot of 1.1 mm diameter when placed at a distance of 90 mm from the target. The pyrometer can measure temperatures in the range of 250 – 2000 °C in the wavelength range of 1.45 – 1.8  $\mu\text{m}$ . The uncertainty declared by the manufacturer is of 0.5% of the reading in °C+ 1 °C for temperatures lower than 350 °C and higher than 1500 °C. For intermediate temperatures the uncertainty is to be considered equal to 0.3% of the reading in °C+ 1 °C.

The pyrometer is mounted on two 25 mm travel motion control translation stages which can be adjusted on the x and y plane with a precision up to 25  $\mu\text{m}$ . The schematic of the setup is illustrated in Figure 55. The measurements of the foil temperature are conducted through the window on the lid of the reactor; this is not expected to influence the measurement since the material of the window, BK7, is for 99.9% transparent to the wavelengths detected by the pyrometer [31].

Another factor of uncertainty to keep in mind when dealing with an IR pyrometer is that, in order to translate the detected radiation into an accurate temperature reading, it is necessary to specify the emissivity ( $\epsilon$ ) of the surface. For more detailed information on the phenomena involved see for example Guo [175]. However, emissivity is not only a function of the material itself but also of temperature and surface conditions.

Therefore, in order to minimize the influence of the surface status, before any series of measurements, with or without sample, the “fresh” foil is heated up to 1100 °C for 1 minute under helium atmosphere. This is expected to create

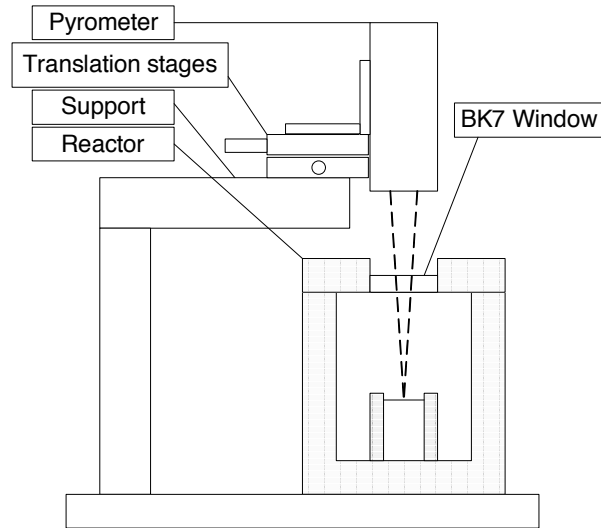


Figure 55: Schematic of the pyrometer and heated foil reactor.

the same surface conditions that the foil would encounter during normal pyrolysis tests. Moreover, eventual oxygen impurities would oxidize the steel surface and possibly reduce the catalytic effects of the foil on the fuel [176]. Successively, the emissivity of the pre-treated foil is calculated by placing the foil on a ceramic cooking plate and changing the emissivity itself until the temperature measured by the pyrometer coincides with the temperature indicated by a 0.1 mm K-type thermocouple in contact with the foil in the close proximity of the measurement spot of the pyrometer. The emissivity found with this experiment, at a temperature of about 300 °C, is equal to 0.75.

### 3.4.2 Setup improvements

#### 3.4.2.1 Temperature of the foil

In anticipation of the results that will be better explained in Chapter 6, this paragraph introduces the correction that is applied to the temperature reading from the thermocouple in the setup.

It has been suggested in previous works that measuring the grid/foil temperature with a thermocouple could introduce a significant error [175, 292]. This is mostly due to the temperature drain introduced by the thermocouple in the contact place (it is possible to see at naked eye a cold spot on the hot foil where the thermocouple tip touches the foil, in a temperature range of 800 to 900 °C), to the heat loss via the tip and wires of the thermocouple and to the non-perfect contact between the thermocouple and the foil.

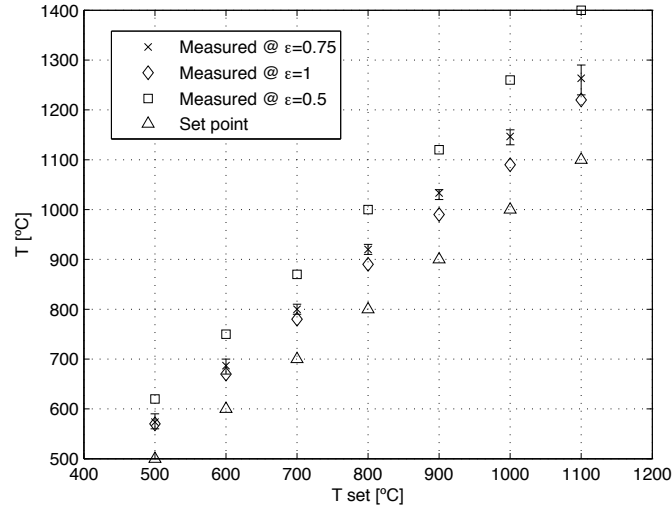


Figure 56: Temperature measured by thermocouple and IR pyrometer with different emissivity values

Guo [175] simulated the heat loss via a thermocouple (TC) in perfect contact with the grid surface and found out that, for a TC diameter of 0.1 mm already one can expect an error of 2 to 5 % of the grid temperature. Prins et al. [292], using laser thermometry, found out that the difference between the temperature measured by the thermocouple and the actual temperature on the grid ranged from 10 % up to 25 %.

In the present work, after the foil has been pre-treated in helium at 1100 °C for one minute, the pyrometer is used to measure the actual temperature on the foil surface; the results of this experiment are shown in Figure 56.

As mentioned in the previous section, the emissivity of the pre-treated foil is found to be equal to 0.75 at approximately 300 °C. In order to estimate the extremes of the possible error introduced for this value, measurements were done with emissivity values of 0.5 and 1. As it can be seen from Figure 56, at all temperatures the reading of the pyrometer resulted in values higher than the actual thermocouple setpoint, even considering an emissivity of 100 %. Such difference results in approximately 70 to 110 °C above the TC reading at 500 °C and even higher differences at 1000 °C, of about 100 to 250 °C. The case with  $\epsilon = 0.5$  needs to be considered, however, as an extreme since the emissivity is known to actually increase with temperature for the considered stainless steel AISI 304 [303].

In view of the results found, using the data with  $\epsilon = 0.75$ , the relation shown in Figure 57 is found between the actual temperature and thermocouple reading.

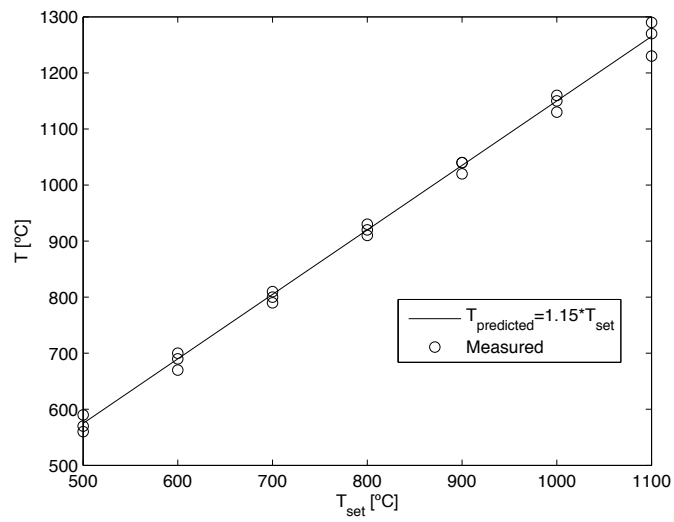


Figure 57: Relation between the temperature measured by the pyrometer with  $\epsilon = 0.75$  and the thermocouple

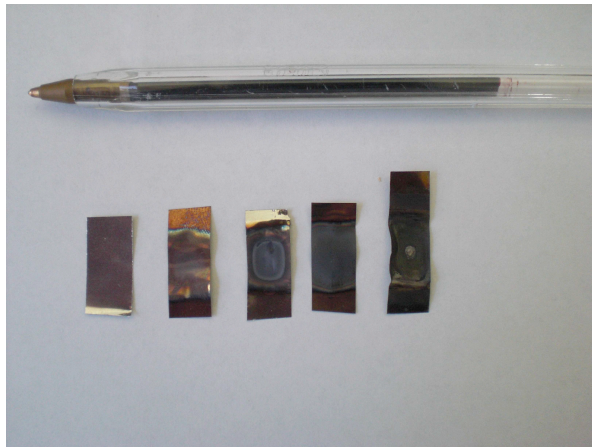


Figure 58: Steel foils at different degrees of oxidation without sample and with sample (last foil on the right)

Table 18: Temperature setpoints for the experimental campaign [in °C].

EXPERIMENT TEMPERATURE	SETPOINT TEMPERATURE
500	435
600	525
700	610
800	700
900	785
1000	870
1100	960
1200	1045
1300	1135

As it is evident from Figure 57, the temperature to be considered the real grid temperature is on average 15 % (in °C) higher than the thermocouple setpoint. For this reason, Table 18 indicates the setpoints used in the measurement campaign described in Chapter 6 to achieve the desired final temperatures.

#### 3.4.2.2 Ammonia absorption and FTIR quantification

Another critical point to be considered in the reactor is the possibility of ammonia absorption on the large stainless steel surfaces available. While the quantification method used to quantify the species in the reactor is the same as previously used and described by Di Nola [139], it was not possible to verify such calibration data as it was done with the TG-FTIR setup. In fact the measurements with the tetraamminesulfate salt did not yield any significant result because of a probable chemical interaction of the salt with the hot foil. This caused large part of the  $\text{NH}_3$  not to be released. However, when testing pills of  $\text{CaCO}_3$ , the mass balance closure for  $\text{CO}_2$  was found to be about 80 to 100 %.

The procedure used in previous studies consisted in quantifying the volatile species 30s after the end of the holding time at high temperature [139, 329]. However, during the present work it was found that the mixing of the species was not completed before 2 minutes.

Since no decomposition or absorption of  $\text{CO}_2$  is assumed to take place under such conditions, it can be seen from Figure 59 that after 2 minutes the concentration of carbon dioxide does not change anymore, indicating a complete mixing and homogeneous distribution in the reactor volume.

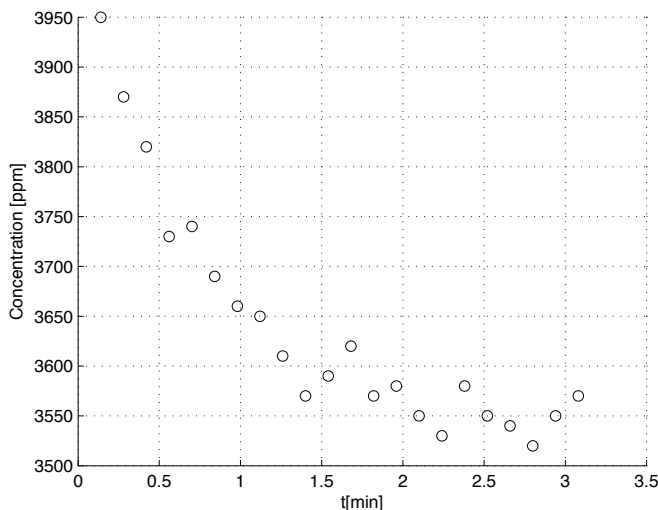


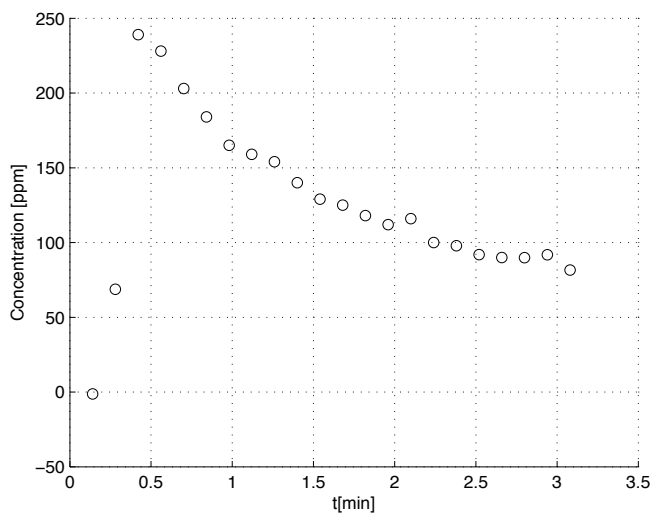
Figure 59: CO<sub>2</sub> concentration over time after CaCO<sub>3</sub> decomposition at 1200 °C. Heating started at t = 0 s

However, when the same plot is produced for NH<sub>3</sub> from a high-N fuel like chicken manure, it is possible to see that a steady concentration is not reached even after 3 minutes, as shown in Figure 60a. In order to test possible absorption of ammonia on the reactor walls, the reactor was flushed with a gas with a concentration of 1 %<sub>vol.</sub> NH<sub>3</sub> in He. After the flushing, the setup was made inert by purging with pure He for a sufficient time. Successively, another test was performed at the same conditions and, as shown in Figure 60b, the concentration of NH<sub>3</sub> decreased much less than in the previous measurement and after 1.5 minutes it actually started to increase again. This confirmed the hypothesis that absorption is actually ongoing in the reactor in the timescale of the measurements and that desorption is also a fast phenomenon.

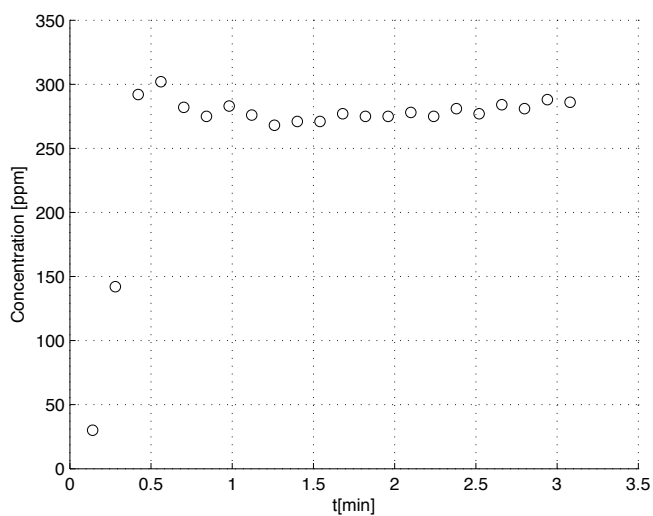
In order to overcome such limitation it was decided to assume the decomposition and mixing behaviour of NH<sub>3</sub> similar to the one of HCN, species which instead is not subjected to absorption or decomposition on the reactor walls, as shown in Figure 61.

Finally thus, the values used to quantify the final concentration of the species are the ones after two minutes from the end of the heating ramp for all the species except for NH<sub>3</sub> for which the value used is equal to 0.7 \* Peak value.





(a) NH<sub>3</sub> release before ammonia flushing of the system



(b) NH<sub>3</sub> release after flushing of the system with 1%vol. NH<sub>3</sub> in helium

Figure 60: NH<sub>3</sub> concentration over time released from chicken litter at T = 800 °C at heating rate of 600 °C/min and holding time of 15 s. The heating started at t = 10 s.

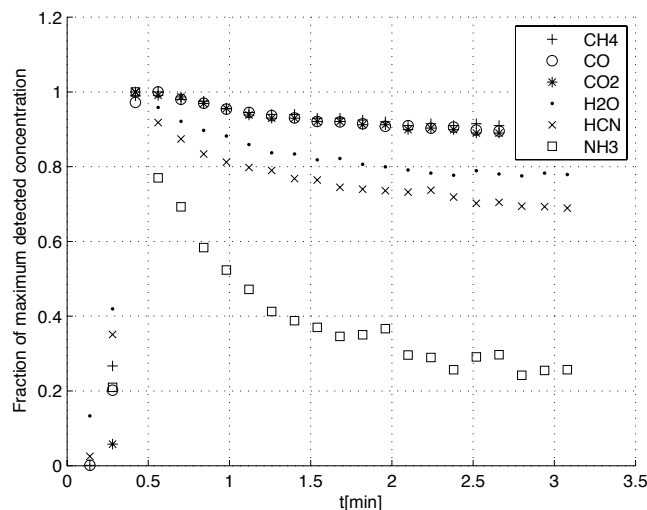


Figure 61: Mixing behaviour of different gaseous species released from pyrolysis of chicken litter at  $T = 800\text{ }^{\circ}\text{C}$  at a heating rate of  $600\text{ }^{\circ}\text{C}/\text{min}$  and holding time of 15 s. The heating started at  $t = 10\text{ s}$

### 3.4.3 Literature review

While thermogravimetric equipments are already commercially established technologies for fuel characterization at slow heating rates, heated grid/foil reactors (also called heated wire mesh reactors) are only one among many other techniques used for characterization of fast pyrolysis. A list of other available experimental techniques and previous literature can be found in the works of Bahng et al. [80], Di Nola [139] and Di Nola et al. [140].

However, the heated grid setup was introduced already more than 40 years ago by Loison and Chauvin [250]. It has, thereafter, been used in several works for the study of fast pyrolysis kinetics of coal and volatiles release, as in the works of Anthony et al. [70] and Solomon and Colket [317]. A comprehensive review of studies on fast pyrolysis setups can be found in Di Nola [139] and Di Nola et al. [140].

Studies on biomass or biomass model compounds have been less frequent and more recent; for example the ones performed by Hajaligol et al. [176, 177] on cellulose and, more recently, by the following authors: Stubington and Aiman [328], Drummond and Drummond [146], de Jong [200], Di Nola et al. [140], Bastiaans et al. [91], Tamboer [329].

Moreover, some attention has been dedicated to the detection and prediction of actual process conditions, as mentioned in the previous section, since the rate of the phenomena and the relative small dimensions of the setup make it hard to realize accurate measurements.

More detailed information on available literature involving heated grid reactors and comparison with the work presented in this dissertation can be found in Chapter 6.

### 3.5 COMBUSTION EQUIPMENT

#### 3.5.1 *Single Particle Reactor (SPR)*

The work described in Chapter 7 was performed at the Process Chemistry Centre at Åbo Akademi University, Turku, Finland. The setup used to carry out the measurement campaign is shown Figure 62. The equipment consists of a quartz tube reactor inserted in a electrically heated furnace. The feeding of the process gases is possible from the bottom and the middle of the reactor. The flow of the gases is controlled by mass flow controllers and the mixing of oxidizing (air) and inert (nitrogen) agents is achieved directly within the reactor. The average residence time for the process gases entering from the bottom of the reactor is around 20 s. If considering only the product gases from devolatilization / combustion of the fuel, released from the sample holder, the residence time at high temperature has to be considered equal to about 4 s. The temperature in the reactor is measured with a thermocouple inserted in the ceramic wall of the furnace, close to the surface of the quartz reactor in the proximity of the sample placement point.

An insertion probe allows the sample to be placed on the sample holder in a cold environment and to be then inserted in a fraction of a second into the hot reactor. For pulverized fuels, as the ones used in this study, a quartz sample holder with a porous bottom has been designed in order to allow the gases to flow through it.

The evolved gas analysis chain used includes three commercial analyzers for the measurement of O<sub>2</sub>, CO, CO<sub>2</sub>, NO and SO<sub>2</sub>. A chemiluminescence analyzer is used for NO detection; a non-dispersive infrared (NDIR) analyzer is used for CO + CO<sub>2</sub> measurement; and a combined infrared + paramagnetic analyzer is used for SO<sub>2</sub> and O<sub>2</sub> detection, respectively. The different internal volumes of the analyzers introduces a bias in the measured signals, so that the NO signal appears to be delayed and wider than the signal obtained for CO and CO<sub>2</sub>. This should not be attributed to a chemical phenomenon but rather to the longer residence time of the gases in the NO analyzer. However, the integral values of the released gases are not affected by this phenomenon, and, as it is explained in Appendix , data can be compared after proper fitting of the curves.

Before the work described in this dissertation, the single particle reactor has been mainly used to test samples of black liquor from the pulp and paper industry. These results are gathered in the following works: Forssén et al. [155, 156], Kymäläinen et al. [233, 234].

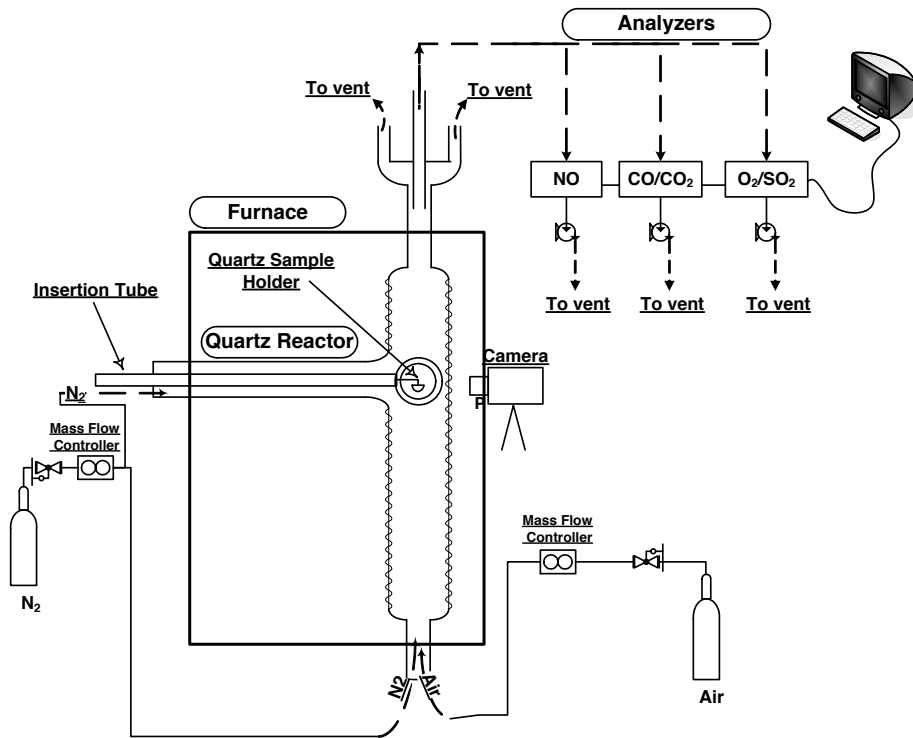


Figure 62: Single particle furnace at Åbo Akademi University and particular of the quartz sample holder

# 4

---

## QUANTITATIVE AND KINETIC TG – FTIR STUDY OF PYROLYSIS OF AGRICULTURAL RESIDUES: INFLUENCE OF DIFFERENT PRETREATMENTS

---

*This chapter presents the results of devolatilization studies of agricultural residues, untreated and pre-treated samples, in slow-pyrolysis conditions. As illustrated in Chapter 3, the TG-FTIR setup allows the recording of detailed mass loss profiles from fuels undergoing a defined thermal history. By applying a Distributed Activation Energy Model (DAEM) to such profiles it was possible to retrieve the kinetic parameters describing the devolatilization of wheat straw, olive residues and peach stones. These parameters are now available for future use on numerical models for large-scale predictions. Moreover, the devolatilization products were detected and quantified in a FTIR spectrometer. Based on these data, the kinetic parameters of slow pyrolysis were also retrieved for the gaseous compounds. Finally, the effects of different pre-treatments such as water leaching, mechanical fractionation and a combination of the two, were investigated in terms of ash composition and changes in the kinetic properties.*

The contents of this chapter were adapted from the work published in:  
J. Giuntoli, S. Arvelakis, H. Spliethoff, W. de Jong and A.H.M. Verkooijen,  
**"Quantitative and Kinetic Thermogravimetric Fourier Transform Infrared  
(TG-FTIR) Study of Pyrolysis of Agricultural Residues: Influence of Different  
Pretreatments"**

*Energy & Fuels*, 23(2009) 5695-5706 ; DOI: 10.1021/ef9005719

© 2009 American Chemical Society. Reprinted with permission.

#### 4.1 INTRODUCTION

Agricultural residues are produced continuously during the year and are abundantly available in rural areas where access to the electric grid can be difficult [43].

Moreover, more and more utilities around Europe and the world are starting to demonstrate in semicommercial scales the use of biomass fuels for electricity production, mostly in cogeneration with coal.

Despite being very promising resources, characterization is the first fundamental step when dealing with wastes in order to understand the conversion behavior and efficiently use these materials as fuels.

In this paper, the pyrolysis behavior of several agricultural residues from Mediterranean countries was studied in a TG–FTIR set-up. The fuels studied were wheat straw, olive residues and peach stones. A description of the origins and uses of these materials can be found in Chapter 3.

Unfortunately, the use on a large scale of such materials is hindered by their high contents of alkali metals and chlorine [193, 195, 297, 298, 346, 347]. Arvelakis and Koukios [76] underlined how K, Cl and Na, together with sulfur and silica, contained in high concentrations in agricultural residues, interact to form alkali silicates and alkali sulfates with melting points far lower than normal boiler temperatures (down to 700 °C) giving rise to problems of slagging, fouling, corrosion and, in fluidized bed reactors, to agglomeration of the bed material and consequent loss of fluidization [76, 77]. More information on these phenomena can be found in Chapter 1.

Zevenhoven-Onderwater et al. [375] tested the combustion of different biomass fuels in a pilot-scale pressurized fluidized bed gasifier and found that bed agglomeration was mainly due to formation of partly molten phases and that potassium played the main role interacting with silica-rich beds and forming low-melting potassium silicates.

Arvelakis and Koukios [76], moreover, proposed three pre-treatments in order to improve the ash quantity and quality of these particular fuels: water leaching, mechanical fractionation and a combination of the two. Arvelakis et al. [72, 74, 75, 77] tested the pre-treatments on the same samples used in this study during fluidized bed operation and found a greatly diminished agglomeration trend. Das et al. [127] compared different types of de-ashing methods on sugarcane bagasse samples, including water and acid leaching, and found that a 3 % HF solution achieved a nearly complete de-ashing of the sample together with a partial removal of extractives and hemicellulose but with no loss in heating value. Jensen et al. [195] studied the pyrolysis of biomass constituents and of untreated and water leached wheat straw on a TG–FTIR setup showing how the washed sample evidenced higher reaction temperatures, lower residual char and increased tar release, suggesting a catalytic effect of the minerals removed by the pre-treatment. Moreover, Giuntoli et al. [163], applied the leaching pre-treatment to more complex materials, like

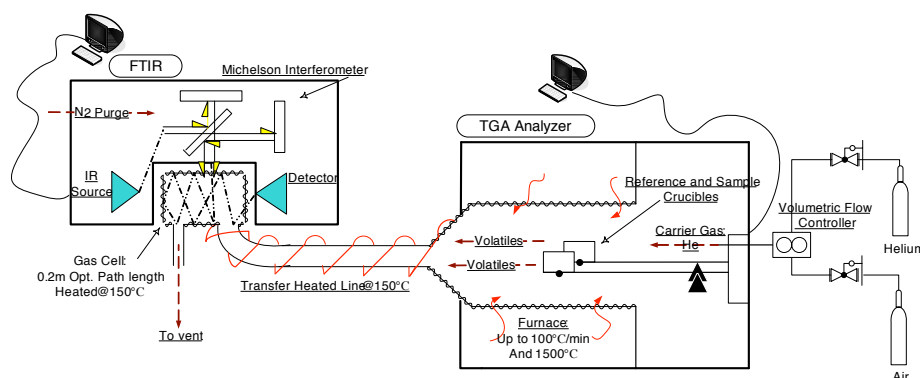


Figure 63: TG – FTIR setup at the Process and Energy Laboratory

dry distiller's grains and solubles (DDGS) and chicken manure, and found the reactivity of the washed samples to be almost unchanged.

In this chapter the three samples mentioned above underwent pre-treatments of water leaching, mechanical fractionation and a combination of the two. The pyrolysis of these fuels was then studied by means of a thermogravimetric analyzer (TGA). These measurements generated fundamental data on the kinetics of devolatilization of these secondary fuels. Moreover, by coupling a Fourier Transform Infrared Spectrometer (FTIR) to the TGA it was possible to characterize the main compounds released during the pyrolysis and their kinetic patterns. The kinetic data presented here are directly suitable for slow pyrolysis applications, like carbonization and biochar production [190], but also for modeling purposes using the appropriate tools (e.g. FG-Biomass) [318].

## 4.2 EXPERIMENTAL SECTION

### 4.2.1 Equipment

The experimental work described in this chapter was carried out using the TG-FTIR setup shown in Figure 108 and described in more detail in Chapter 3. The apparatus for the evolved gas analysis was composed by a thermobalance SDT 2960 from TA Instruments coupled through a short stainless steel heated line (150 °C) to an FTIR spectrometer NEXUS manufactured by Thermo Nicolet.

Measurements were carried out under an inert atmosphere using helium as a carrier gas with a flow of 90 cm<sup>3</sup>/min, controlled by a volumetric rotameter.

#### 4.2.2 FTIR spectrometer

The gas cell used in this work, differently from the set-up described in Giuntoli et al. [163], had an optical path length of 0.2 m, ZnSe windows, gold coated mirrors and an internal volume of 50 mL.

The best compromise between signal-to-noise ratio and sampling time was obtained using a resolution of  $0.25\text{ cm}^{-1}$  co-adding 12 scans, for a total measurement time of 33.6 s.

The thermal history of the FTIR data could then be retrieved from the TGA data knowing the time delay due to the internal volume of the transfer line and gas cell. In our measurements this resulted in a delay of approximately 1 minute that was then tuned by overlapping the FTIR absorption and the differential thermogravimetric curves.

A quantitative method on the FTIR was implemented by calibration for the following species: CO, CO<sub>2</sub>, CH<sub>4</sub>, H<sub>2</sub>O, NH<sub>3</sub>, HCN and HNCO. Calibration was carried out with calibration gas bottles, except for H<sub>2</sub>O, which was calibrated by means of establishing a saturated concentration in N<sub>2</sub>, and HNCO, which was calibrated through urea decomposition. Details of the method can be found in Di Nola [139].

The quantification method has been tested for CO<sub>2</sub> by using calcium oxalate, with mass balance closures within  $\pm 10\%$  for CO<sub>2</sub> singularly and within  $\pm 5\%$  for CO + CO<sub>2</sub>.

Despite the available calibration data, it was not possible to reliably quantify any of the nitrogen species due to their low concentrations in the samples studied.

#### 4.2.3 Samples and pre-treatments

The fuels studied in this work were agricultural residues common in many Mediterranean areas of Europe: wheat straw (WS), residues from olive oil production (consisting of kernels, pulps, leaves and limbs) (OR) and peach stones and pulps (PS), residues of production of juices and stewed fruits. All the fuels were provided from Greece.

Moreover, all the fuels underwent pre-treatments of leaching in water, and olive residues also the pre-treatment of mechanical fractionation and one sample underwent the combination of fractionation and leaching. A more detailed description of the samples, their characteristics and on the pre-treatments can be found in Chapter 3.

Proximate and ultimate analyses of the fuels are summarized in Table 20 for sake of clarity. Ash elemental analysis is summarized in Table 21 for the most relevant compounds. Table 19 summarizes the pre-treatments conditions.

We refer to other works [72, 74, 75, 76, 77] for more details and discussions on the effectiveness of the pre-treatments for fluidized bed operation. A dis-



discussion on the ash removal potentials and effects on the reactivity of the fuels will follow.

#### 4.2.4 Procedure

The fuels were ground and then placed in an alumina cup in amounts varying from 15 to 30 mg. The samples were kept at 50 °C for 45 minutes under a flow of 90 cm<sup>3</sup>/min of helium in order to properly flush the oven and the FTIR gas cell of atmospheric gases. After the isothermal period, the temperature was ramped up with three different heating rates (5 - 10 - 20 °C/min) to 900 °C where it was kept isothermal for 15 minutes. Heat and mass transfer phenomena are known to affect kinetic analyses when using thermogravimetric techniques [68, 171], but Stenseng et al. [325] reported that such phenomena were not relevant at conditions similar to ours for wheat straw. Moreover, additional measurements were run at higher heating rates, namely 100 °C/min, and were used to validate the predictive capacity of the retrieved kinetic parameters, as it will be shown in a following part of this chapter.

### 4.3 RESULTS AND DISCUSSION

#### 4.3.1 TG and DTG

Figures 64, 65 and 66 show the weight loss curves (TG) and differential thermogravimetric curves (DTG) for all the samples studied in this work at a heating rate of 10 °C/min.

Figure 64, in particular, illustrates the DTG curve of wheat straw: this presents a single, broad, peak of decomposition around 324 °C. This behavior is quite peculiar for biomass samples in which usually two separate peaks, attributed respectively to hemicellulose and cellulose decomposition, are identified [68, 163, 195, 347]. In this case the two peaks collide into a broader one.

Still, in Figure 64, the WSL sample, instead, shows a more common DTG curve with a sharp peak at 355 °C and a smaller shoulder at around 308 °C.

It is known in literature that K in wheat straw catalyzes devolatilization reactions [162, 195, 284, 297] such that, when KCl is added to a washed sample, the reaction temperature highly decreases and residual char yield raises. This is also the case for the samples studied here, for which a much lower residual char yield is found in the leached fuel than in the untreated one, with a difference that is far bigger than the simple ash removal would suggest (4.9 %wt<sub>a.r.</sub> difference in the residue, compared to 1.5 %wt<sub>a.r.</sub> in the ash content). In agreement with Jensen et al. [195], the leached sample appears, therefore, to react later but faster, showing a higher maximum reaction rate. A lower residual char yield is obtained because of the removal of minerals which catalyze char-forming reactions from organic volatiles. The values of

Table 19: Details of the pretreatments applied to the samples studied in this work and references to detailed descriptions

Sample	Sample Name	Particle Size Distribution	Water-to-Mass ratio	Time	Ref.
Wheat straw leached	WSL	4 mm > D <sub>p</sub>	66.7 g/L	24 h	Arvelakis and Koukios [76]
Peach stones leached	PSL	4 mm > D <sub>p</sub>	88.9 g/L	24 h	Arvelakis et al. [75]
Olive residue leached	ORL	4 mm > D <sub>p</sub>	88.9 g/L	24 h	Arvelakis and Koukios [76]
Olive residue fractionated	ORF	D <sub>p</sub> > 1 mm	-	-	-
Olive residue fractionated + leached	ORFL	D <sub>p</sub> > 1 mm	88.9 g/L	24 h	Arvelakis [72]

Table 20: Proximate and elemental analysis of the fuels. Data are on a dry basis.

	WS <sup>a</sup>	WSL <sup>a</sup>	OR <sup>a</sup>	ORL <sup>a</sup>	ORF <sup>a</sup>	ORFL <sup>a</sup>	PS <sup>b</sup>	PSL <sup>b</sup>
Moisture <sup>c</sup>	8.1	5.75	9.5	11.1	8.8	6.6	8.5	12
Volatiles	76.0	80.6	76	78.7	77.9	83.3	81.3	81.6
Fixed Carbon	16.4	13.5	19.4	18.6	20.2	15.1	18.1	18.0
Ash	7.6	5.9	4.6	2.7	1.9	1.6	0.65	0.4
C	43.7	46.3	50.7	51.1	50.5	51.0	51.95	53.45
H	5.1	5.3	5.9	5.6	6.2	6.0	5.8	6.2
N	0.8	0.6	1.4	1.6	1.7	1.9	0.8	0.95
S	0.4	0.2	0.3	0.3	0.3	0.2	0.0	0.0
Cl	0.4	0.1	0.2	0.1	0.2	0.0	0.1	0.0
O (by diff.)	42.0	41.7	37.0	38.6	33.4	39.3	40.7	38.9
HHV (MJ/kg)	18.9	20.0	21.2	21.3	19.8	20.8	21.55	22.8

<sup>a</sup>Arvelakis and Koukios [76]

<sup>b</sup>Arvelakis et al. [75]

<sup>c</sup>as received basis.

Table 21: Elemental analysis of the ashes. Data are on a dry basis.

	WS <sup>a</sup>	WSL <sup>a</sup>	OR <sup>a</sup>	ORL <sup>a</sup>	ORF <sup>a</sup>	ORFL <sup>a</sup>	PS <sup>b</sup>	PSL <sup>b</sup>
Al <sub>2</sub> O <sub>3</sub>	1.95	1.9	3.0	0.9	2.5	0.4	0.5	0.0
SiO <sub>2</sub>	39.2	49.8	32.6	39.3	31.9	40.95	6.0	10.5
CaO	14.4	15.3	10.2	23.9	9.8	36.8	7.1	19.3
MgO	2.7	2.5	3.8	0.9	3.3	4.1	2.7	2.5
Fe <sub>2</sub> O <sub>3</sub>	0.4	0.6	1.9	2.8	n.d.	1.9	0.5	0.1
K <sub>2</sub> O	15.9	10.9	27.2	10.0	34.8	4.2	38.45	21.2
Na <sub>2</sub> O	4.3	0.5	4.2	0.05	3.9	0.05	0.1	0.0
TiO <sub>2</sub>	0.1	0.1	0.1	0.2	n.d.	0.1	0.15	0.0
SO <sub>3</sub>	5.3	3.8	5.0	5.85	4.7	5.3	5.2	3.2
Cl <sup>-</sup>	2.7	1.8	1.4	0.0	1.4	0.1	0.1	0.0

<sup>a</sup>Arvelakis and Koukios [76]<sup>b</sup>Arvelakis et al. [75]

residual char at 630 °C for WS and WSL samples compares quite well with the values presented by Jensen et al. [195]: 21.6 %wt<sub>daf</sub> for WS and 18.2 %wt<sub>daf</sub> for WSL.

The leaching pre-treatment, thus, together with increasing the energy density of the fuel by removing inert material and thus enhancing the heating value of all the samples, increases the total amount of tars and volatiles produced during pyrolysis reducing the residual char, which is indeed a desirable effect in plant operation.

A common behavior to the one shown by wheat straw is observed in the next sample (OR) whose curves are represented in Figure 65. Here it can be noticed that the four samples clearly follow two separate trends: the non-leached samples (OR and ORF) react in a very similar way, showing one peak at 327 °C and a shoulder at around 270 °C, while the leached samples (ORL and ORFL) react similarly to each other but at higher temperatures, with a peak at 355 °C and a shoulder at around 300 °C. So, also for this fuel, the removal of alkali metals (−63 %<sub>ash basis</sub> of K<sub>2</sub>O for the ORL and −84 %<sub>ash basis</sub> of K<sub>2</sub>O for ORFL) causes the sample to react at higher temperatures.

The marked effect of leaching on the DTG curves of WS, though, implies that, despite the apparent lower removal of alkali compared to the OR sample, the minerals appear to have a more important catalytic effect on the devolatilization of WS and also a higher impact on the char-forming reactions. Jensen et al. [195] showed that by washing a wheat straw sample and then adding KCl, they were not able to reproduce the original DTG curve and still two separate peaks, for hemicellulose and cellulose, appeared. The authors suggested that K was not the only mineral washed away (mostly Na [346]), but also that not all the potassium in the sample was present as mineral inclusions but also organically bound in the structure of the straw. With some calculation it is possible to see that, indeed, in the WSL sample, potassium and chlorine are removed in the same proportion suggesting that the main effect of the leaching was the removal of mineral inclusions. This suggests that the simple addition of KCl to the washed structure was not able to reproduce the original behavior most probably because of the different mixing and morphology of the salt in the structure of the sample.

In the cases of OR and ORL samples, instead, the removal of potassium goes beyond the removal of KCl and probably other structures and minerals were also removed.

Moreover, the ORF sample, which did not go through a leaching treatment, despite the high reduction in its total ash content (−59 %<sub>d.b.</sub> ash content) does not show a significant difference in reactivity compared to the untreated sample. This appears clear looking at the values in Table 21 which show how actually the quality of the ashes in the ORF sample was indeed worsened by the pre-treatment, with a relative increase of K and unchanged content of Cl. This was also studied by Arvelakis et al. [74] who showed how the fractionation pre-treatment increased the operational time (free from agglomeration

problems) of a fluidized bed combustor, compared with the untreated sample, by only 20 minutes, compared to an improvement of over 900 minutes using the leached samples.

It is worthy noticing that among the olive residue samples, the ORF sample, despite being the one with the lowest content of ashes, presents the highest residual char, around 27%wt<sub>a.r.</sub>. This is in agreement with what is reported in literature: the alkali metals in the fuel, in this case even enriched compared to the original sample, catalyze char forming reactions giving rise to higher char residues.

The ORFL sample, lastly, shows a devolatilization behavior similar to the simply leached sample, ORL, but the ash quantity and quality appears much improved compared to all the other samples with a reduction of 66%<sub>d.b.</sub> of the total ash content and an even larger 94%<sub>ash basis</sub> decrease in K content in the ashes. Chlorine is also highly reduced by around 91%<sub>ash basis</sub>.

Figure 66, finally, illustrates the curves for the peach stones samples. The behavior of this material is more complex than the previous samples, with two very distinct peaks of reaction. The first peak, the one attributed to hemicellulose decomposition, appears at about 290 °C while the cellulose peak appears at around 360 °C. For PS and PSL there are no significant differences in reactivity except a slightly higher maximum reaction rate for the leached sample.

Moreover, the temperatures of the peaks are similar to the ones observed in the leached samples of the other fuels. This would imply a major role of KCl as catalyst for devolatilization reactions, seeing how the WS sample, having the highest Cl content, is also the fuel which reacts at lower temperatures and PS, with the lowest Cl content, at the highest temperatures.

The residue of pyrolysis for PS and PSL is around 24 – 26%wt<sub>a.r.</sub>, in the same range as the other agricultural residues and also for these samples the difference of 2%wt<sub>a.r.</sub> in the residual char is higher than the mere difference in ash content (0.21%wt<sub>a.r.</sub>). This implies that the leached sample has indeed a higher reactivity with a higher amount of volatiles and less residual char which would favor operations in thermal conversion, as shown by Arvelakis et al. [75].

#### 4.3.2 FTIR

As previously mentioned, the volatiles released from the samples during pyrolysis have been analyzed with an FTIR spectrometer so that the weight loss behavior studied in the previous section could be further investigated. In Figure 67 and 68 the signals from measurements for WS and WSL are plotted.

CO, CO<sub>2</sub> and H<sub>2</sub>O are the main products of the pyrolysis of biomass constituents (together with tars, which, due to their complex structures, cannot be identified by FTIR), thus they follow closely the trend of the main weight loss, introduced in the previous section.

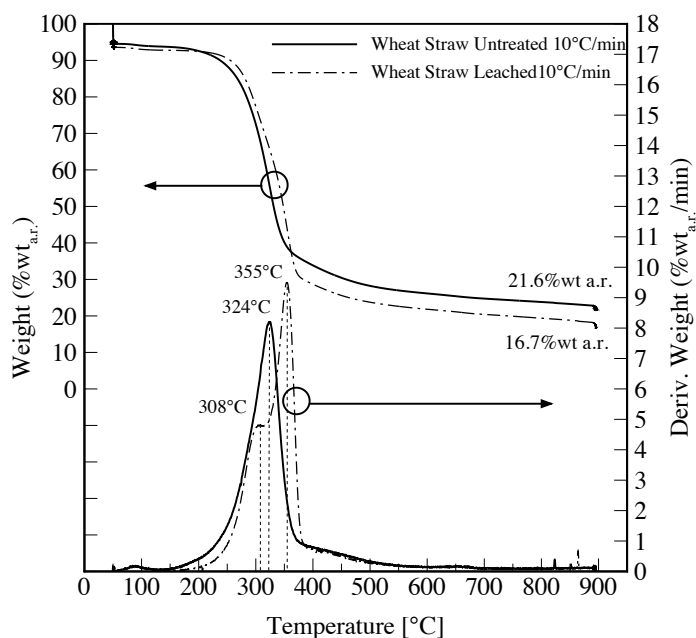


Figure 64: TG and DTG curves for wheat straw untreated (-) and leached (---); heating rate  $10^{\circ}\text{C}/\text{min}$  and He flow  $90\text{ mL}/\text{min}$ . Data are on an “as received” basis.

Comparing Figure 67 and 68 it is possible to notice how the curves of the untreated sample almost perfectly overlap, in shape, the ones of the leached sample, indicating indeed a superposition of the reactions in the untreated sample. In the WSL sample, instead, the removal of the minerals separates the decomposition of hemicellulose and cellulose and, as can be seen from Table 22 and as expected from the higher weight loss, seems to promote the release of light volatile compounds. Basilakis et al. [90] also studied the pyrolysis of wheat straw in a TG-FTIR setup; while the final yields of CO and  $\text{CH}_4$  are consistent with the ones found in this study ( $8.5\% \text{wt}_{\text{daf}}$  vs.  $7\% \text{wt}_{\text{daf}}$  for CO and  $1\% \text{wt}_{\text{daf}}$  for  $\text{CH}_4$ ) there is a marked difference in  $\text{CO}_2$  with a recovery of  $15.7\% \text{wt}_{\text{daf}}$  for our sample vs.  $10.5\% \text{wt}_{\text{daf}}$  for Basilakis et al. [90]. Closer values were found by Jensen et al. [195] which, on the same setup as Basilakis et al. [90], found a recovery of  $\text{CO}_2$  equal to  $12\% \text{wt}_{\text{daf}}$  at  $630^{\circ}\text{C}$  compared to  $13.6\% \text{wt}_{\text{daf}}$  recovery for the sample studied here. It is difficult to find a reason for this differences since Basilakis et al. [90] provided no ash elemental composition of the fuels.

The release of  $\text{CH}_4$  appears, also as a common feature among biomass samples, at higher temperature, peaking at around  $510^{\circ}\text{C}$ . From Table 22, it can be seen that this is a common characteristic for WS and OR samples and the leaching does not seem to affect it. This is due to the fact that  $\text{CH}_4$  is mostly

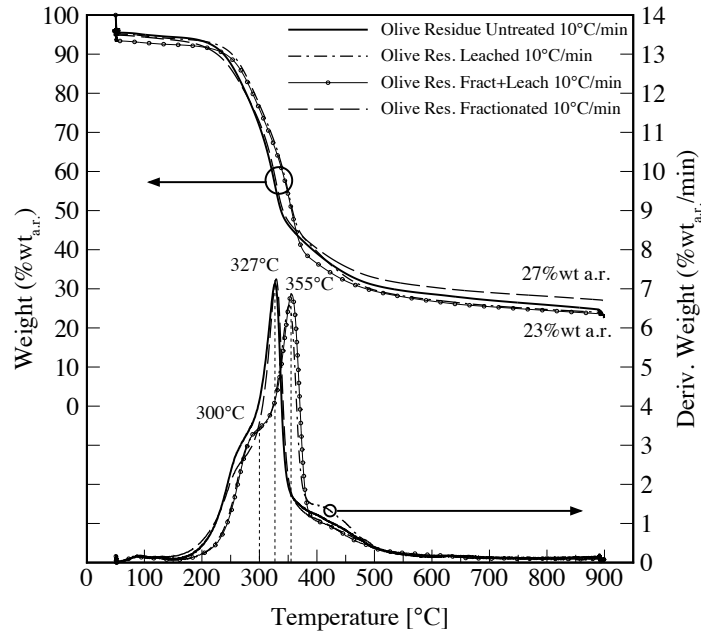


Figure 65: TG and DTG curves for olive residue untreated (-), leached (---), fractionated (-·-) and fract + leached (·-·-); heating rate 10°C/min and He flow 90 mL/min. Data are on an “as received” basis.

Table 22: Temperatures at maximum release rates for a heating rate of 10°C/min and maximum yields after holding times= 0s/15 min at isothermal conditions at 900°C, on a dry and ash free basis of the original fuel

	WS	WSL	OR	ORL	PS	PSL
CO <sub>2</sub>	324	355	327	351	292/354	291/358
% wt <sub>daf</sub>	15.7 / 16.8	16.0 / 18.3	13.1 / 13.6	12.7 / 13.4	13.4 / 14.6	10.3 / 10.9
CO	324	355	327	351	354	358
% wt <sub>daf</sub>	9.0 / 10.3	9.1 / 11.1	7.1 / 8.5	5.8 / 7.0	6.2 / 7.0	5.9 / 6.4
CH <sub>4</sub>	514	512	511	513	432/527	426/537
% wt <sub>daf</sub>	1.0	0.9	1.3	1.5	1.9	1.8
H <sub>2</sub> O	324	355	327	351	292/354	291/358
% wt <sub>a.r.</sub>	11.7	13.0	9.9	9.0	12.2	9.6



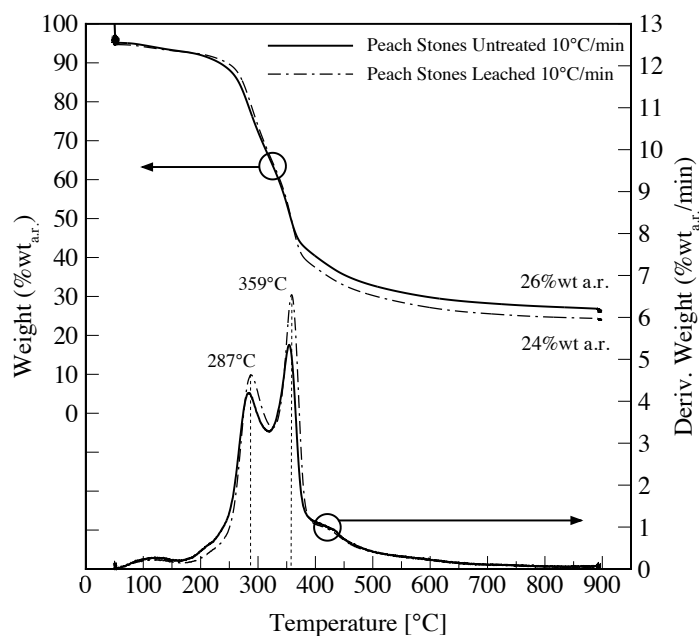


Figure 66: TG and DTG curves for peach stones untreated (-) and leached (---); heating rate 10°C/min and He flow 90 mL/min. Data are on an “as received” basis.

derived by the cracking of methoxyl groups in the lignin part of biomass [366] and Jensen et al. [195] showed that the washing did, indeed, not influence the methane release from lignin.

Yang et al. [366] investigated in details the pyrolysis of cellulose, hemicellulose and lignin with a TG-FTIR setup. They found the contribution of cellulose to the global release of CO and CO<sub>2</sub> to be limited compared to the release due to hemicellulose decomposition. This would seem to contradict the results in Figure 68 where the second peak at 355°C, attributed to cellulose pyrolysis, contributes substantially to CO and CO<sub>2</sub> release. But, on the other side, it is also well known that cellulose pyrolysis is highly influenced by the presence of inorganic catalysts in the sample [195, 346, 347] which greatly favor decomposition, thus increasing the release of light-weight molecules. This is also the reason why in real biomass samples the peak attributed to cellulose pyrolysis is usually at lower temperatures than expected from the single cellulose experiment [68, 163, 195].

The olive residues samples show a behavior similar to the one of WSL and there are no relevant differences among the untreated and washed samples, thus the plots are not reported here.

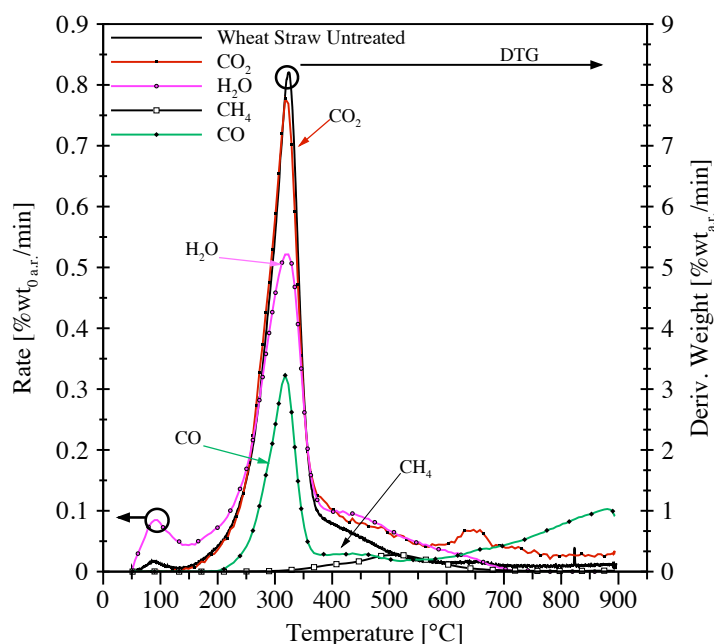


Figure 67: Wheat straw untreated: Superposition of DTG curve with the relative compounds analyzed by the FTIR; heating rate 10 °C/min and He flow 90 mL/min. Data are on an as received basis.

Peach stones FTIR curves are shown in Figure 69. CO<sub>2</sub> and pyrolytic water are the main products in the peak at 292 °C, while CO becomes important in the second peak at 354 °C.

The release of methane is, for this sample, somewhat different and shows two peaks at 432 °C and 527 °C and a much higher final yield equal to 1.9 %wt<sub>daf</sub>. This trend agrees with Jensen et al. [195] who studied the release of CH<sub>4</sub> from lignin and showed two separate peaks at around 430 °C and 560 °C. Yang et al. [366] also showed two separate peaks for CH<sub>4</sub> from lignin but at higher temperatures, which could be due to the different origins of the samples. CO and water are also released at the same temperatures as methane, most probably deriving from the cracking of methoxyl groups in the lignin part of the sample. The more marked impact of this high temperature tail is probably due to the nature of the sample which is mostly composed of peach stones and thus rich in lignin [72].

Moreover, all the samples show a release of CO at high temperature which continues even beyond the 900 °C used in this study. This behavior has been observed before [90, 104, 139, 163, 366], and it is generally attributed to the secondary cracking residues of the primary pyrolysis which has recondensed in the char.

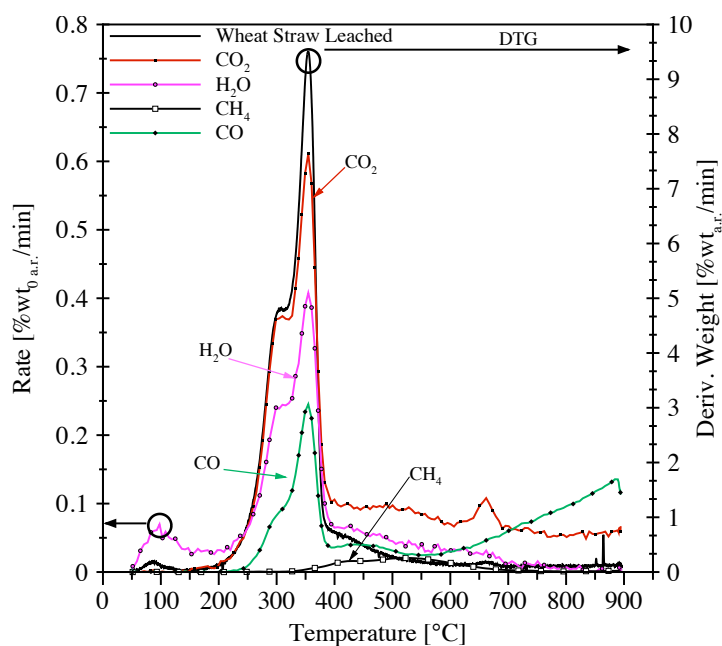


Figure 68: Wheat straw leached: Superposition of DTG curve with the relative compounds analyzed by the FTIR; heating rate 10 °C/min and He flow 90 mL/min. Data are on an as received basis.

The washing pre-treatment does not seem to particularly affect the yields of the main pyrolysis products in our samples. In literature, though, highly decreased yields of all main species are found in washed samples, and the difference is attributed to an increase in tar yield [195, 346, 348] sometimes up to even 50% [195].

All the fuels release about 18 - 25 %wt<sub>d.b.</sub> as light volatiles. All the fuels yield a comparable amount of tars (or undetected species) equal to about 52 - 56 %wt<sub>d.b.</sub>. When the data are analyzed in the same conditions as the ones used by Jensen et al. [195], 630 °C and on a dry and ash free basis, it is possible to notice that all the washed samples present a lower yield of residual char together with a lower yield of volatiles and, consequently, higher yields of tars, as suggested by Jensen et al. [195].

#### 4.3.3 Kinetic analysis

An excellent review of methods for kinetic analysis of global complex reactions can be found in Burnham and Braun [119]. A more detailed description of kinetic modeling of pyrolysis processes can be found in Chapter 3.

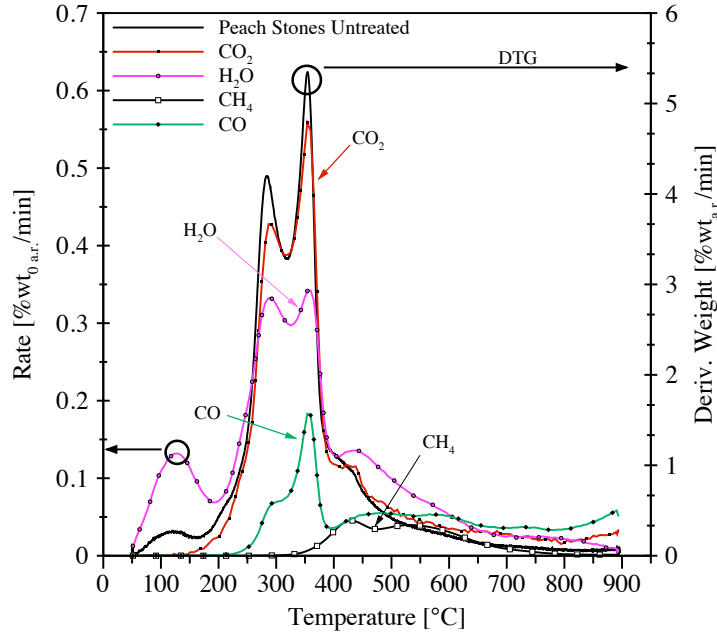


Figure 69: Peach stones untreated: Superposition of DTG curve with the relative compounds analyzed by the FTIR; heating rate 10 °C/min and He flow 90 mL/min. Data are on an as received basis.

As explained in Chapter 3, the DAEM can be formulated as follows where  $x$  represents the unreacted fraction of the sample (on ar basis):

$$x = \int_0^{\infty} \exp \left[ - \int_0^t k(T) dT \right] \cdot D(E) dE \quad (4.1)$$

In eq. 5.1  $k(T)$  obeys the Arrhenius equation and it is a function of time because of the applied temperature profile:

$$k(T) = A \cdot \exp \left( - \frac{E}{R \cdot T(t)} \right) \quad (4.2)$$

In eq. 5.2,  $A$  represents the pre-exponential or frequency factor,  $E$  is the activation energy,  $R$  is the universal gas constant and  $T$  is the absolute temperature and is function of time via the heating rate.

Moreover, in eq. 5.1:

$$\int_0^{\infty} D(E) dE = 1 \quad (4.3)$$

The shape of the distribution  $D(E)$  is not known a priori, and it depends on the composition and structure of the sample. As mentioned earlier, it is common practice to assume  $D(E)$  as a Gaussian distribution. A valid alternative to this assumption is to choose a discrete distribution of  $E$ , in which the integral in eq. 5.1 is substituted by a sum of a finite number of parallel reactions.

We decided to study our samples applying the DAEM model and, in particular, we applied a Gaussian distribution model for the main species obtained from FTIR measurements, while we applied a discrete distribution model to the global devolatilization curves. This allowed us to provide data which are ready to use for the main pyrolysis species, as found in Tables 23 to 28, but at the same time, through the discrete model, we were able to study in more details the differences among the samples and the influence of the pre-treatments on the reactivity [163].

For our analysis we used a FORTRAN based code, developed by Burnham and Braun, called KINETICS05 [113, 119] that can analyze, simultaneously, measurements performed at different heating rates and fit them with 25 first-order reactions sharing the same pre-exponential factor.

We chose to follow the common practice, anyway, and we fixed the pre-exponential factor at the value of  $2.2 \times 10^{13} \text{ s}^{-1}$  according to [202, 339], as explained in Chapter 3.

Figure 70 shows the discrete distributions of activation energies for all the 8 samples studied in this work. What can be easily noticed is that the main reaction in the decomposition, attributed to the pyrolysis of the cellulose component of the sample, appears for WS, OR and ORF samples at 176 kJ/mol. This is a consistent value in our measurements and it was found to be the main reaction pathway also for two completely different fuels like DDGS and chicken manure [163] suggesting a common nature of this constituent among the analyzed samples. Moreover, this component appears to be the most influenced by the water leaching, shifting the reaction to 184 kJ/mol. As found by Jensen et al. [195], pure crystalline cellulose reacts with a peak at around 650 K, which is a much higher temperature than the peak found in biomass samples. This has to do with the effect of the minerals present in the biomass samples, but not in the pure cellulose, which catalyze cellulose decomposition. This would also explain the increase in reacting temperature and activation energy for the same component when the mineral matter is leached away, as shown also by Antal and Várhegyi [68].

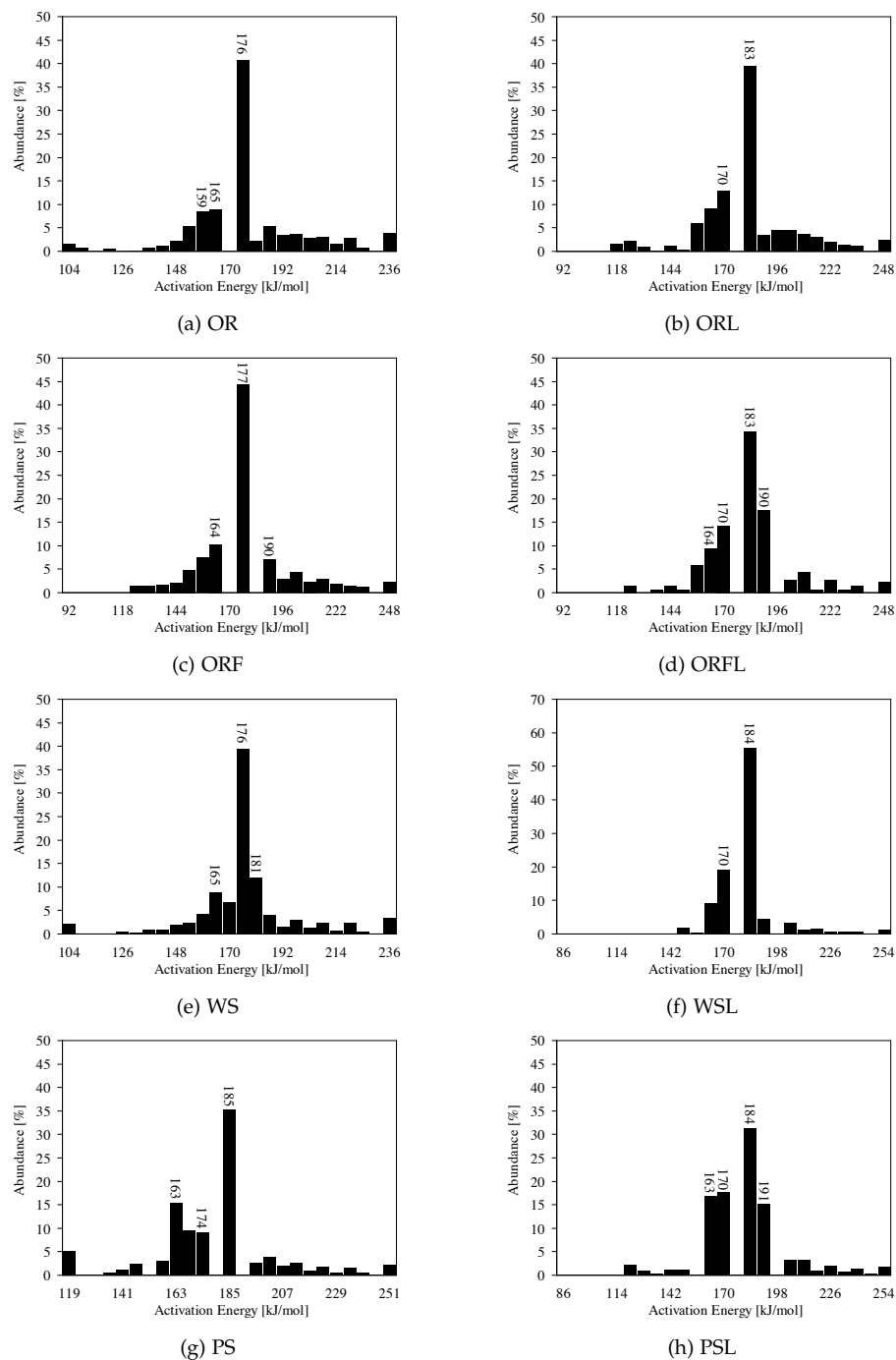


Figure 70: Distribution of activation energies using a pre-exponential factor  $A = 2.2 \times 10^{13} \text{ s}^{-1}$ .

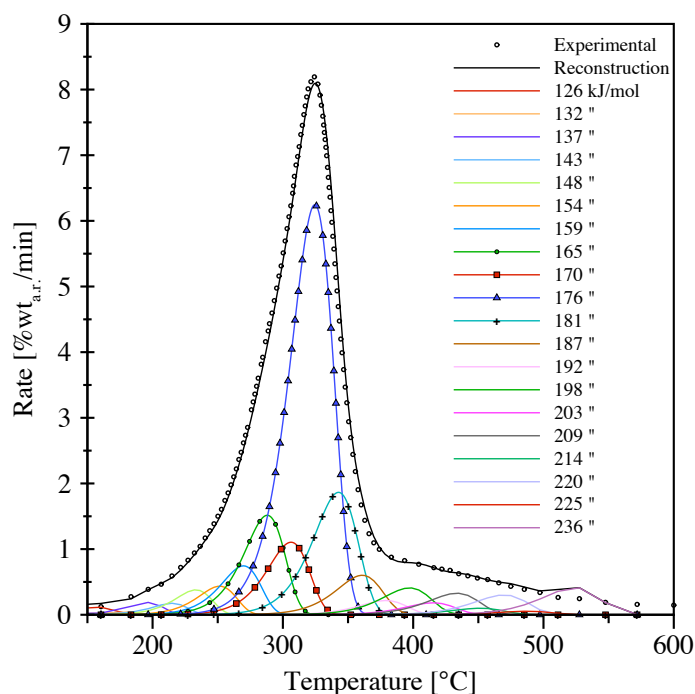


Figure 71: Wheat straw untreated at 10 °C/min: DTG and fit with 25 parallel first order reactions.

The hemicellulose component in the samples, instead, appears to react at around 165 kJ/mol and also increases to 170 kJ/mol when the sample is leached. This is also consistent with what found in other samples [163].

Figure 71 and 72 can assist in understanding the physical meaning of the kinetic parameters retrieved above. In Figure 71 the DTG curve of the wheat straw untreated sample is decomposed into the first-order reactions obtained from the DAEM model: it can be seen that, together with a main decomposition reaction with activation energy of 176 kJ/mol, three more reactions are relevant at 165, 170 and 181 kJ/mol. Together with these reactions, many more parallel reactions play a role in the decomposition of this sample. Figure 72 shows, instead, the WSL sample: here it is clear the smaller amount of relevant reactions, the more important being the one at 184 kJ/mol. In this sample, also, it is clearly visible a separate contribution from hemicellulose at 163 and 170 kJ/mol. The results found so far indeed show a strong catalytic effect of the mineral matter in the wheat straw sample.

The leaching pre-treatment appears to have the same effect on the olive residue sample, as can be seen in Figure 70a and 70b, while the fractionation appears not to affect the reaction kinetics substantially, as seen from the TGA curves, so that the relatively higher amount of K and Na does not affect the re-

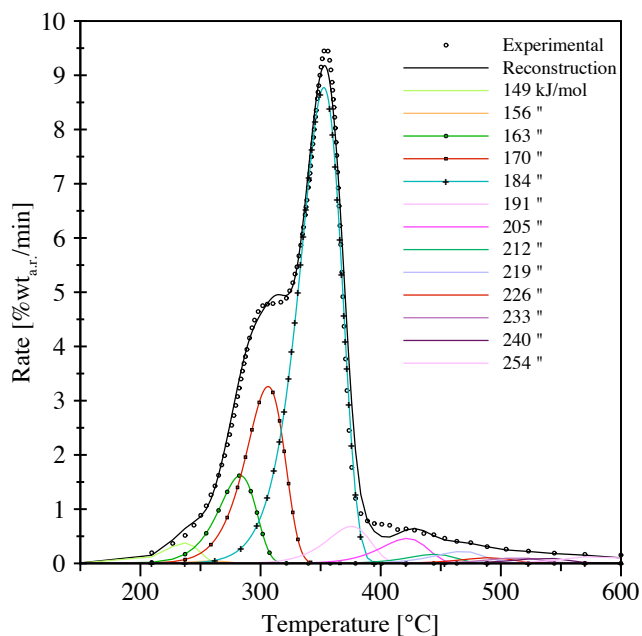


Figure 72: Wheat straw leached at 10 °C/min: DTG and fit with 25 parallel first order reactions.

activity of the sample, implying that it is the absolute amount of the minerals that matters.

The peach stones samples, in Figure 70g and 70h and in Figure 73, show a different behavior from the other samples studied in this work. The main reaction pathway appears to be the one at 185 kJ/mol which is not affected by the leaching pre-treatment at all. The hemicellulose decomposition happens around 163 – 170 kJ/mol and it is also only slightly influenced by the leaching.

As mentioned in previous sections, PS and PSL are the samples with the lowest Cl content, so that, even if the content of K is definitely bigger than in all other samples, this is not present as mineral inclusions of KCl but, most likely, bound to the organic structure of the lignin constituent, so that this does not affect the decomposition and also the effect of the leaching is limited.

Tables 23 to 28 show the results of the DAEM model when using a Gaussian distribution over the reactivities of the main species of pyrolysis. As explained in the previous section, the release of molecules follows closely the weight loss behavior of the whole sample, thus also the kinetic parameters mirror the ones obtained for the whole samples. From these data it is possible to notice a third component (or rather a pseudo-pool, referring to a fictitious class of components in the original fuel which are supposed to release, during pyrolysis, the referred volatile species following the indicated kinetics [202,



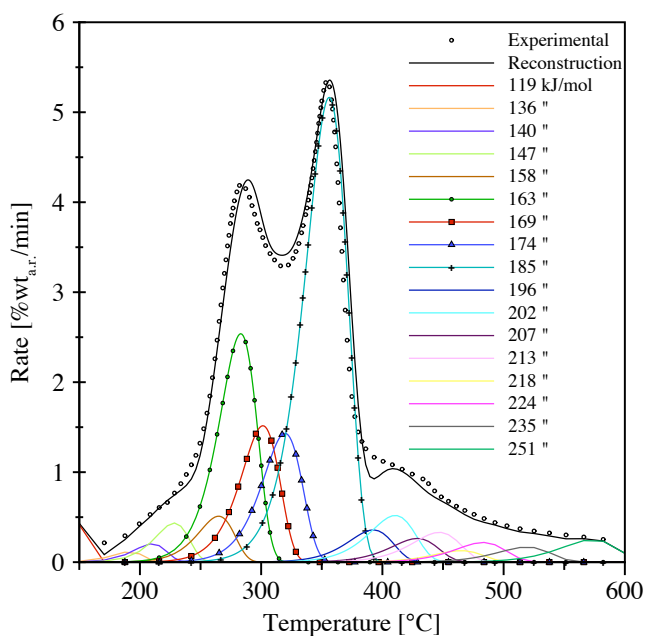


Figure 73: Peach stones leached at 10 °C/min: DTG and fit with 25 parallel first order reactions.

204, 318, 339]) for all the samples, with very high activation energy and high variance: this component is representative of the long tail of devolatilization due to the broad temperature gap in which the lignin decomposes [195, 298, 350]. In fact, methane, which is mostly a product of lignin pyrolysis, also reacts through similar pathways and activation energies like the third component of the CO and CO<sub>2</sub>.

Kinetic parameters retrieved by TGA measurements, and thus with slow heating rate measurements, are always subject to critics of being too specific to the single measurements and not having properties of general validity [68, 171, 350].

In order to prove the validity of the kinetic parameters, at least in a significant range of heating rates in which reaction mechanisms are not expected to change, and to verify the kinetically controlled conditions of the experiments, we ran measurements at heating rate of 100 °C/min and compared the experimental results with the DTG curves resulting from the extrapolation of the kinetic parameters obtained at slower heating rates.

As can be seen in Figure 74 to 76, the kinetic parameters appear to hold validity for WS and WSL samples, thus capturing also the characteristics of the pre-treated samples. For more complex materials, as PS, the extrapolation is not so straightforward but the main characteristics of the reaction, the two

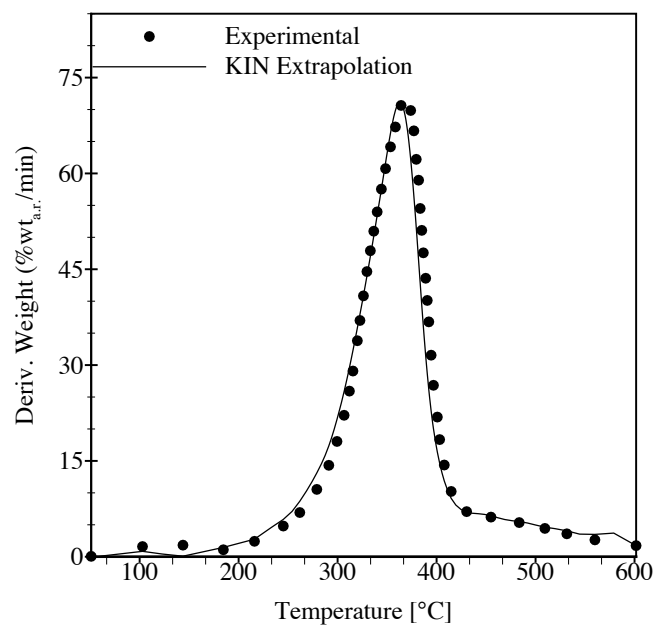


Figure 74: Wheat straw untreated: experimental and reconstructed DTG at heating rate of 100 °C/min. Discrete distribution was used for extrapolation.

Table 23: Kinetic parameters for Gaussian distribution. Main volatile species: WS.

Precursor pool	A (s <sup>-1</sup> )	E <sub>0</sub> (kJ/mol)	σ (% of E <sub>0</sub> )	Yield <sup>a</sup> (100%)
1 - CO <sub>2</sub>	2.2 × 10 <sup>13</sup>	170	6.2	44.8
2 - CO <sub>2</sub>	2.2 × 10 <sup>13</sup>	174	1	22.6
3 - CO <sub>2</sub>	2.2 × 10 <sup>13</sup>	201	17	32.6
1 - CO	2.2 × 10 <sup>13</sup>	173	4.1	36.7
2 - CO	2.2 × 10 <sup>13</sup>	176	0.05	24.2
3 - CO	2.2 × 10 <sup>13</sup>	206	18.2	39.1
1 - CH <sub>4</sub>	2.2 × 10 <sup>13</sup>	233	10.6	100

<sup>a</sup>The yield in the table indicates the relative amount (%) of each pool on a base of 100% for the considered pool.

separate peaks, peak temperatures and the temperature interval of reaction, are represented by the extrapolation.

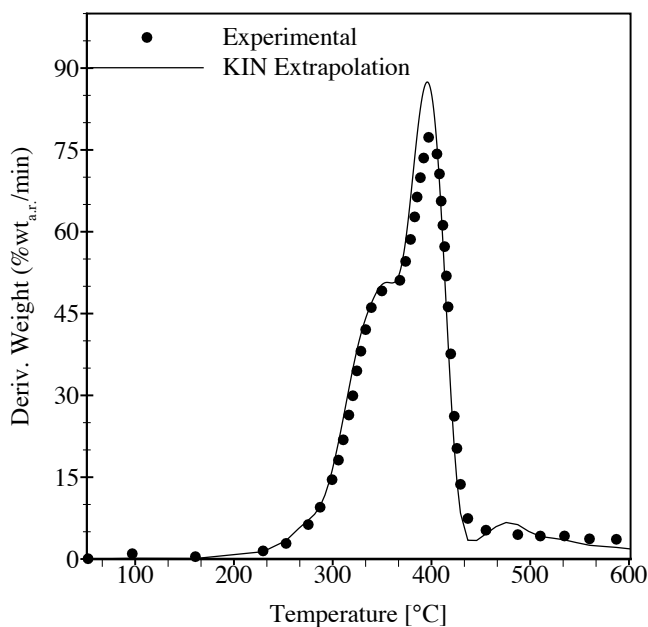


Figure 75: Wheat straw leached: experimental and reconstructed DTG at heating rate of 100 °C/min. Discrete distribution was used for extrapolation.

Table 24: Kinetic parameters for Gaussian distribution. Main volatile species: WSL.

Precursor pool	A (s <sup>-1</sup> )	E <sub>0</sub> (kJ/mol)	σ (% of E <sub>0</sub> )	Yield <sup>a</sup> (100%)
1 - CO <sub>2</sub>	2.2 × 10 <sup>13</sup>	168	2.7	24
2 - CO <sub>2</sub>	2.2 × 10 <sup>13</sup>	184	0.8	34.7
3 - CO <sub>2</sub>	2.2 × 10 <sup>13</sup>	210	15.5	41.3
1 - CO	2.2 × 10 <sup>13</sup>	167	1.5	12.3
2 - CO	2.2 × 10 <sup>13</sup>	183	0.6	44.1
3 - CO	2.2 × 10 <sup>13</sup>	218	12.7	43.6
1 - CH <sub>4</sub>	2.2 × 10 <sup>13</sup>	203	3.1	10.8
2 - CH <sub>4</sub>	2.2 × 10 <sup>13</sup>	238	8.6	73.5
3 - CH <sub>4</sub>	2.2 × 10 <sup>13</sup>	267	19.6	15.7

<sup>a</sup>The yield in the table indicates the relative amount (%) of each pool on a base of 100% for the considered pool.

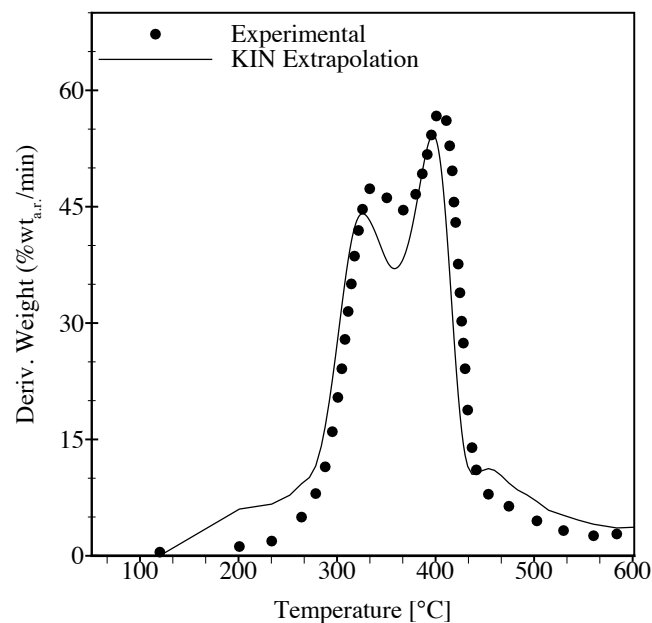


Figure 76: Peach stones leached: experimental and reconstructed DTG at heating rate of 100 °C/min. Discrete distribution was used for extrapolation.

Table 25: Kinetic parameters for Gaussian distribution. Main volatile species: OR.

Precursor pool	A (s <sup>-1</sup> )	E <sub>0</sub> (kJ/mol)	σ (% of E <sub>0</sub> )	Yield <sup>a</sup> (100%)
1 - CO <sub>2</sub>	2.2 × 10 <sup>13</sup>	160	3.5	26.6
2 - CO <sub>2</sub>	2.2 × 10 <sup>13</sup>	176	0.04	33.9
3 - CO <sub>2</sub>	2.2 × 10 <sup>13</sup>	196	16	39.5
1 - CO	2.2 × 10 <sup>13</sup>	160	0.05	10.2
2 - CO	2.2 × 10 <sup>13</sup>	175	0.04	47
3 - CO	2.2 × 10 <sup>13</sup>	216	14.4	42.8
1 - CH <sub>4</sub>	2.2 × 10 <sup>13</sup>	199	2.7	8.8
2 - CH <sub>4</sub>	2.2 × 10 <sup>13</sup>	234	7.6	68.4
3 - CH <sub>4</sub>	2.2 × 10 <sup>13</sup>	249	20.6	22.8

<sup>a</sup>The yield in the table indicates the relative amount (%) of each pool on a base of 100% for the considered pool.

Table 26: Kinetic parameters for Gaussian distribution. Main volatile species: ORL.

Precursor pool	A (s <sup>-1</sup> )	E <sub>0</sub> (kJ/mol)	σ (% of E <sub>0</sub> )	Yield <sup>a</sup> (100%)
1 - CO <sub>2</sub>	2.2 × 10 <sup>13</sup>	164	4.2	36.6
2 - CO <sub>2</sub>	2.2 × 10 <sup>13</sup>	182	1.1	30.8
3 - CO <sub>2</sub>	2.2 × 10 <sup>13</sup>	197	15.5	32.6
1 - CO	2.2 × 10 <sup>13</sup>	168	5.7	23.8
2 - CO	2.2 × 10 <sup>13</sup>	183	0.05	32.7
3 - CO	2.2 × 10 <sup>13</sup>	228	10.2	43.5
1 - CH <sub>4</sub>	2.2 × 10 <sup>13</sup>	201	3.5	10.1
2 - CH <sub>4</sub>	2.2 × 10 <sup>13</sup>	235	9.2	73.7
3 - CH <sub>4</sub>	2.2 × 10 <sup>13</sup>	282	17.1	16.2

<sup>a</sup>The yield in the table indicates the relative amount (%) of each pool on a base of 100% for the considered pool.

Table 27: Kinetic parameters for Gaussian distribution. Main volatile species: PS.

Precursor pool	A (s <sup>-1</sup> )	E <sub>0</sub> (kJ/mol)	σ (% of E <sub>0</sub> )	Yield <sup>a</sup> (100%)
1 - CO <sub>2</sub>	2.2 × 10 <sup>13</sup>	166	3.5	28.5
2 - CO <sub>2</sub>	2.2 × 10 <sup>13</sup>	184	0.9	27.0
3 - CO <sub>2</sub>	2.2 × 10 <sup>13</sup>	196	15.7	44.5
1 - CO	2.2 × 10 <sup>13</sup>	166	2.2	12
2 - CO	2.2 × 10 <sup>13</sup>	183	0.09	32
3 - CO	2.2 × 10 <sup>13</sup>	228	9.9	56
1 - CH <sub>4</sub>	2.2 × 10 <sup>13</sup>	205	3.3	18.4
2 - CH <sub>4</sub>	2.2 × 10 <sup>13</sup>	240	10	67.6
3 - CH <sub>4</sub>	2.2 × 10 <sup>13</sup>	281	13	14

<sup>a</sup>The yield in the table indicates the relative amount (%) of each pool on a base of 100% for the considered pool.

#### 4.4 CONCLUSIONS

Three agricultural residues, wheat straw, olive residues and peach stones, abundant in many regions of Europe, were tested using a TG-FTIR setup.

The materials underwent water leaching pre-treatment in order to remove alkali metals and chlorine which are known to create several problems in plant operation.

Table 28: Kinetic parameters for Gaussian distribution. Main volatile species: PSL.

Precursor pool	A (s <sup>-1</sup> )	E <sub>0</sub> (kJ/mol)	σ (% of E <sub>0</sub> )	Yield <sup>a</sup> (100%)
1 - CO <sub>2</sub>	2.2 × 10 <sup>13</sup>	167	3.2	38
2 - CO <sub>2</sub>	2.2 × 10 <sup>13</sup>	186	0.2	35.1
3 - CO <sub>2</sub>	2.2 × 10 <sup>13</sup>	204	11.5	26.9
1 - CO	2.2 × 10 <sup>13</sup>	167	1.7	10.6
2 - CO	2.2 × 10 <sup>13</sup>	185	0.9	31.8
3 - CO	2.2 × 10 <sup>13</sup>	230	9.8	57.6
1 - CH <sub>4</sub>	2.2 × 10 <sup>13</sup>	204	3.1	21.4
2 - CH <sub>4</sub>	2.2 × 10 <sup>13</sup>	242	9.6	52.2
3 - CH <sub>4</sub>	2.2 × 10 <sup>13</sup>	260	18	26.4

<sup>a</sup>The yield in the table indicates the relative amount (%) of each pool on a base of 100% for the considered pool.

The effect of such pre-treatments on quantity and quality of the ash-forming matter in these fuels was the subject of previous studies [72, 74, 75, 76, 77]. In this work the measurements of devolatilization reactivity showed that the leaching procedure increased the temperature of devolatilization and, consequently, the reaction rate, for all the tested fuels. Moreover, the residual char was reduced for all the samples more than the simple ash forming matter removal would have implied. However, the yield of light volatiles also decreases implying a higher yield of tars for all the samples.

The alkali metals contained in the samples, mostly K and Na, together with Cl, appeared to have an important catalytic effect in the pyrolysis process of such fuels, mostly when present in the form of minerals inclusions such as KCl and NaCl. It was shown how the most relevant effect of the leaching was on the WS sample which was also the sample with the highest chlorine content, while the effect on PS, the sample with the lowest amount of Cl, was almost absent. The catalytic effect can also be seen in the higher amount of tars released from the washed samples: the inorganic matters seems to favour their cracking.

The leaching process, thus, appears to have a beneficial effect not only in terms of quantity and quality of ash-forming matter in such fuels, but also increasing the energy density, increasing the amount of volatiles and increasing the reaction rate. On the other hand, higher yields of tars could be expected from the leached samples.

For more complex fuels, though, like peach stones or DDGS and chicken manure [163], the effect of water leaching on global reactivity appears to be limited.

The main products of pyrolysis, CO<sub>2</sub>, CO, CH<sub>4</sub> and H<sub>2</sub>O were analyzed by means of an FTIR. The release of such species followed the trends of the global devolatilization and the final yields were not sensibly influenced by the applied pre-treatments, unlike the results presented by Jensen et al. [195].

All the untreated samples presented a main reaction pathway at 176 kJ/mol which is consistent to what found in much different fuels like DDGS and chicken manure [163], indicating a common nature of this component among all the fuels. This constituent was assigned to cellulose decomposition. The hemi-cellulose component reacted with activation energies of about 165 kJ/mol – 170 kJ/mol. The leaching pre-treatment increased the activation energy of the main reaction up to 184 kJ/mol and, in the wheat straw sample, the number of reaction pathways was much higher in the untreated sample due to the catalytic effect of the alkali metals and mineral inclusions.





# 5

---

## QUANTITATIVE AND KINETIC TG – FTIR STUDY OF SLOW PYROLYSIS OF BIO-RESIDUES

---

*This chapter presents the results of a similar analysis to Chapter 4. However, the fuels analyzed here are DDGS and chicken manure. The higher nitrogen content of these fuels allowed for the detection of gaseous NO<sub>x</sub> precursors, such as NH<sub>3</sub>, HCN and HNCO, released during slow pyrolysis. A DAEM model was used to retrieve the kinetic parameters for the global devolatilization as well as for single N-volatile compounds. The effect of the water leaching pre-treatment was studied in terms of ash quantity, quality and effects on the devolatilization kinetics.*

The contents of this chapter were adapted from the work published in:  
J. Giuntoli, W. de Jong, S. Arvelakis, H. Spliethoff and A.H.M. Verkooijen,  
"Quantitative and kinetic TG-FTIR study of biomass residue pyrolysis: Dry distiller's grains with solubles (DDGS) and chicken manure."  
*J. Anal. Appl. Pyrolysis*, 85(2009) 301-312 ; DOI: 10.1016/jaap.2008.12.007  
© 2009 Elsevier. Reprinted with permission.

## 5.1 INTRODUCTION

Chapter 4 presented the results of a study on the reactivity of agricultural residues under slow pyrolysis conditions. The effects of a water leaching pre-treatment were also investigated. However, the detection of nitrogen volatile compounds was not possible because of the relatively low amount of fuel-N in the samples.

Therefore, in this chapter the focus is shifted on two different waste fuels with very high fuel-N content: a very novel material in terms of thermal applications, dry distiller's grains and solubles (DDGS), and chicken manure. This latter fuel is already used in pilot and commercial plants, mainly in gasification applications and in co-combustion with coal, but still problems related to  $\text{NO}_x$  emissions, slagging and fluidized bed agglomeration are encountered and they still need to be fully addressed [41, 65, 183]. Details on the origins and characteristics of the fuels are given in Chapter 3.

Both these materials contain considerable amounts of nitrogen embedded in different structures (mainly proteins for DDGS and urea and proteins for chicken manure) which could create issues related to  $\text{NO}_x$  emissions, but a deeper investigation is required to assess the real effects. For example, a high release of ammonia from the fuels could indeed favour reduction reactions and thus actually reduce the needs for  $\text{NO}_x$  removal technologies.

Furthermore, both these potential fuels are known not only to have a high amount of ash forming matter, mostly chicken manure, but also rich in such materials like K, P, Na and Cl that are problematic for plant operation as stated in earlier chapters. Water leaching has been quite successful in removing these elements in previous studies and thus, if successful again, could be implemented in a commercial way in order to enhance power plant operations and efficiency when dealing with troublesome waste fuels.

In this paper we characterized the thermal conversion behavior of these materials facing the above-mentioned drawbacks. By means of a Thermogravimetric Analyzer (TGA) we were able to generate fundamental data on the kinetics of pyrolysis of these secondary fuels which are, for the case of DDGS, so far completely missing in international literature. By coupling a Fourier Transform Infrared Spectrometer (FTIR) to the TGA we were able to characterize the different nitrogen compounds released during the process and their kinetic patterns. The kinetic data presented here are directly suitable for slow pyrolysis applications, like carbonization and biochar production, but also for modeling purposes using the appropriate tools (e.g. FG-Biomass). Finally, we applied the water leaching pre-treatment, developed by Arvelakis and Koukios [76], on the fuels and we studied its effects on pyrolytic conversion kinetics and product distribution.

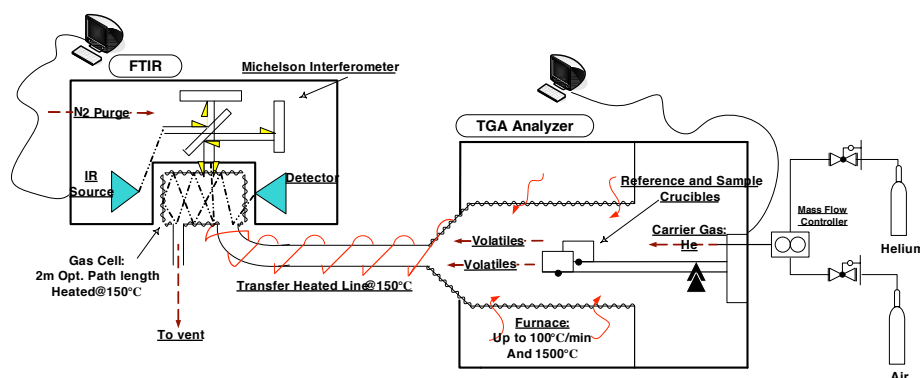


Figure 77: TG-FTIR set-up at Process and Energy Laboratory

## 5.2 EXPERIMENTAL

### 5.2.1 Equipment

The experimental work described in this paper was carried out using the TG-FTIR setup shown in Figure 108 and described in more details in Chapter 3. The apparatus for the evolved gas analysis was composed by a thermobalance SDT 2960 from TA Instruments coupled through a short stainless steel heated line (150 °C) to an FTIR spectrometer NEXUS manufactured by Thermo Nicolet.

Measurements were carried out under an inert atmosphere using Helium as a carrier gas with a flow of 100 mL/min controlled by a mass-flow controller. This flow had to be kept high enough to avoid long residence times in the oven and thus to prevent secondary reactions of the volatiles. However, it was low enough to guarantee well detectable concentrations of the species in the FTIR.

The inert gas carried the volatiles from the furnace, where they were released from the sample in the alumina crucible, to the gas cell of the FTIR which was also kept at 150 °C. This temperature was chosen high enough to avoid condensation of tars and ammonia adsorption [182] but not too high, to avoid thermal cracking of the released compounds.

The gas cell used in this work had an optical path length of 2 m, ZnSe windows, gold coated mirrors and an internal volume of 200 mL.

### 5.2.2 FTIR spectrometer

According to the vast experience acquired on this setup, the best compromise between signal-to-noise ratio and sampling time was obtained using a resolution of  $0.25\text{ cm}^{-1}$  co-adding 12 scans, for a total measurement time of 33.6 s.

The thermal history of the FTIR data could then be retrieved from the TGA data knowing the time delay due to the internal volume of the transfer line and gas cell. In our measurement this resulted in a delay of 1 minute that was then tuned by overlapping the curves.

A quantitative method on the FTIR was implemented by calibration for the following species: CO, CO<sub>2</sub>, CH<sub>4</sub>, H<sub>2</sub>O, NH<sub>3</sub>, HCN and HNCO. Details of the method can be found in [139] and in the appendixes of this thesis .

Some limitations in our quantitative method are the following: there are no calibration gases available for HNCO so that calibration lines can only be produced by means of urea decomposition following the procedure described in [139].

On the other hand, tests performed with an ammonia releasing salt (Tetraamminecopper(II) Sulfate monohydrate, CAS 10380-29-7) [379], have given mass balance closures within 5 % for NH<sub>3</sub> indicating the validity of our quantitative method for ammonia and the absence of significant adsorption phenomena in the transfer line.

It is important to understand, though, that eventual quantification uncertainties will affect only the absolute values of the mass balance of species, which is not our focus on this paper. Relative data and comparison between measurements and fuels will still hold since the same quantitative method was applied to all the measurements.

Moreover, the kinetic analysis will also not be influenced because it was based on the fit of the normalized conversion data and thus a homogeneous error on the absolute value of the concentration will not affect the main kinetic parameters at all. A non homogeneous error will also have a minor impact if compared to other intrinsic sources of errors.

### 5.2.3 *Samples and pre-treatments*

The fuels studied in this work were: chicken manure, provided from the Dutch company HoSt which uses it to feed a 2 MW<sub>th</sub> gasifier in Tzum, The Netherlands, and DDGS obtained from the company Abengoa from a plant in Spain converting barley seeds (*Hordeum Vulgare*) into ethanol with a dry-grind process.

As mentioned earlier, the composition of this material may vary slightly depending on the starting cereal used, but it will include everything that is not hydrolyzed in the process by the used enzymes. So, the hemicellulose, cellulose, lignin and protein fraction of the original cereal will be included in this material, as well as some residual starch and yeast. A detailed description of the composition of DDGS from corn can be found in Kim et al. [220], where it is possible to note the high amount of proteins, reaching 25 %wt<sub>d.b.</sub> of the sample.

Chicken manure originated from the hens bred for eggs and the manure was gathered directly from the floor of the cages where the animals are kept.

It consists mainly of manure, residual food and feathers from the chickens; no additional litter material was added. This manure was previously dried and sterilized at 70 °C for several hours.

Moreover, both the fuels underwent a pre-treatment of leaching in water according to the methodology described in Arvelakis and Koukios [76] and in Chapter 3.

Proximate and ultimate analysis of the fuels are summarized in Table 46. Ash elemental analysis is summarized in Table 30 for the most relevant compounds.

As can be seen from Table 46, the nitrogen content of all the fuels was very high, reaching almost 6 %wt<sub>d.b.</sub> (on a “dry basis”) for chicken manure, compared with values of around 0.3 %wt<sub>daf</sub> (on a “dry ash free” basis) for wood and 1 %wt<sub>d.b.</sub> for coal [147]. The leaching process appeared to affect, as expected, mainly the ash content of the fuels with a decrease of around 4.2 % and 7.1 % for DDGS and chicken manure, respectively. Moreover, a decrease of 3.4 % in the total N content of chicken manure was recorded, this was most probably due to the leaching of the ammonia dissolved in the manure. The results from FTIR measurements will confirm this supposition, showing a drastically reduced release of ammonia at low temperatures.

The heating value of the leached samples increased in both samples due to the removal of ash forming matter. Particularly significant appears the increase of 10.5 % for chicken manure.

From Table 30 it is noticeable that, alike other biomass fuels, DDGS ashes are rich in Si and K but also P is present in high percentage. Chicken manure presents, instead, a very high percentage of Ca, since limestone is fed on purpose to the animals to help them creating the egg-shells. Furthermore, the manure presents a high share of K and P. As explained earlier, higher concentrations of alkali metals in the ashes of biomass fuels are very critical for plant operation. Moreover, in the presence of Cl and sulfur, corrosion becomes a serious issue. The pre-treatment here proposed seems to affect, as expected, the content of Cl, S and Na, thus not only decreasing the quantity of the ashes but also increasing their quality. Phosphorous and calcium are not affected by the leaching, while potassium was expected to be removed in higher quantities but these results cannot confirm it. Potassium in biomass is associated mainly with chlorine. The large decrease in chlorine concentration observed in both cases after the leaching process indicates that a substantial amount of potassium has also been removed. However, in this case this could not be verified by the performed ash elemental analysis. This is probably due to the complex nature of the ash forming matter in the specific biomass samples as well as due to the used methodology for the determination of the relative concentrations. Characterization of the ash samples using SEM-EDX has shown that substantial removal of potassium is also taking place after the leaching treatment for both biomass samples. However, SEM-EDX provides

Table 29: Proximate and elemental<sup>a</sup> analysis of the fuels. Data are on a dry basis.

	DDGS	DDGS leached	Chicken manure	Chicken manure leached
Moisture <sup>b</sup>	8.9	8.5	20.2	9.4
Volatiles	78.2	76.2	67.9	65.7
Fixed Carbon	14.7	17	5.5	9.6
Ash <sup>c</sup>	7.1	6.8	26.6	24.7
C	49	48.8	39.6	37.2
H	6.3	6.3	4.1	5
N	4.5	4.5	5.9	5.6
S	0.4	0.4	0.7	0.8
O (by diff.)	32.7	33.2	23.2	26.7
HHV (MJ/kg)	19.8	20.5	13.3	14.7

<sup>a</sup>Performed with automatic procedure on a Carlo Erba EA 9010 manufactured by Fisons.

<sup>b</sup>as received basis.

<sup>c</sup>Ashed at 600 °C.

only semi-quantitative results and thus they cannot be used for an accurate estimation.

#### 5.2.4 Procedure

The fuels were manually ground using mortar and pestle and then placed in an alumina cup in amounts varying between 4 mg and 32 mg. They were kept at 50 °C for 45 min under a flow of 100 mL/min of helium in order to properly flush the oven and FTIR gas cell of atmospheric gases. After the isothermal period, the temperature was ramped at different heating rates (5 - 10 - 20 - 30 - 100 °C/min) up to 105 °C where it was kept for 15 min in order to dry the sample of the physically absorbed water (and ammonia for the chicken manure). Following the drying step, the temperature was raised up to 900 °C where it was kept isothermal for either 30 or 60 min.

Heat and mass transfer phenomena are known to affect kinetic analyses when using thermogravimetric techniques [68, 171, 195] so measurements were performed, for all the heating rates, with high mass (around 15 mg for chicken manure and 30 mg for DDGS) and with low mass samples (around 4 mg for both) in order to prove that the kinetics was not affected in its main parameters by such phenomena. Moreover the slower heating rates (10 - 20 - 30 °C/min) were used to retrieve the kinetic parameters from the measurements while the highest heating rate, 100 °C/min, was used as proof of the

Table 30: Elemental analysis of the ash forming matter. Data are on a dry basis.

	DDGS	DDGS Leached	CM	CM Leached
Al <sub>2</sub> O <sub>3</sub>	0.2	0.4	0.6	0.8
SiO <sub>2</sub>	22.4	24.9	4.2	5.6
CaO	2.9	3.9	29.1	35.6
MgO	7.3	8.2	6.1	6.0
Fe <sub>2</sub> O <sub>3</sub>	0.4	0.5	0.6	0.8
K <sub>2</sub> O	22.7	22.4	15.3	13.9
Na <sub>2</sub> O	2.7	1.8	2.9	1.6
TiO <sub>2</sub>	0.01	0.01	0.04	0.04
SO <sub>3</sub>	9.5	2.0	6.0	2.1
Cl <sup>b</sup>	2.9	0.9	1.5	0.1
P <sub>2</sub> O <sub>5</sub>	29.0	32.4	21.3	22.0

<sup>a</sup>0.125 g of dried sample was molten with 0.375 g of LiBO<sub>2</sub> and dissolved in HNO<sub>3</sub> and then analyzed with an ICP-AES. Analysis performed according to EPA 200.7.

<sup>b</sup>For analyses on Cl, the sample was sintered at 550 °C with Na<sub>2</sub>CO<sub>3</sub> + ZnO, leached with water and cleaned with a cation exchanger and subsequently analyzed with an ICP-SFMS. Analyses performed according to EPA method 200.8.

predictive capacity of the data; this will be shown in the proper section on kinetic analysis.

### 5.3 RESULTS AND DISCUSSION

#### 5.3.1 TG and DTG

Figure 78 presents the weight loss curves (TG) and the Differential Thermogravimetric curves (DTG) for the DDGS samples, both untreated and leached in water, as a function of temperature, at a heating rate of 10 °C/min.

The TG curves show no really relevant differences between the two samples with an overall weight loss of around 78 – 79 %wt<sub>a.r.</sub> at 900 °C for both samples. The decomposition is practically complete by 600 °C but the weight loss continues also during the isothermal period at 900 °C, leaving, after 60 minutes, a carbonaceous residue of 12.2 %wt<sub>daf</sub> and 10.3 %wt<sub>daf</sub> for the untreated and the leached samples, respectively.

The DTG curve of the untreated sample shows three distinct peaks (in addition to the one due to the drying step) at temperatures of 280 °C, 330 °C and 402 °C. The leached sample again does not show significant differences except for the first peak which is delayed at 289 °C. This behavior is well known

for lignocellulosic materials, where the first peak of decomposition is usually attributed to the rupture of the hemicellulose component while the second peak is due to the cellulose decomposition, with the lignin decomposing in a wider range of temperatures [68, 111, 159, 162, 171, 186, 195, 204, 366]. Jensen et al. [195] also studied the effect of adding KCl to cellulose and hemicellulose samples and found that the peak temperature of reaction of cellulose is not affected by the presence of additional salt, but the char yield is highly increased. For hemicellulose they also found that peak temperature is slightly reduced by the additional KCl. This can explain the shift of the first peak that we register on these samples, even though in Chapter 4 the main effect of the leaching appeared to be on the cellulose component. Moreover, the washing does not appear to have any significant impact on char formation since the residue is almost identical at zero holding time.

One can also observe a small irregularity appearing between the first two peaks at around 310 °C. This should be due to the decomposition of the residual starch from the main process; starch, in fact, has a structure resembling cellulose in its structural components (glucose units) but with different linkages [319] and is reported to react in this range of temperature in the literature [174, 186].

Figure 79 shows the same curves as in Figure 78 but relative to the chicken manure samples. This fuel presents four main peaks of reaction (plus the peak for the drying step and the last peak due to the decomposition of carbonates) at temperatures of 280 °C, 324 °C, 430 °C and 472 °C.

It appears evident that the first two components still represent the hemicellulosic and cellulosic components present in the fuel, due to non-digested food. The other two components are the ones most probably due to the decomposition of the manure, while the decomposition of carbonates appears important due to the high concentration of calcium in the manure. The chickens, in fact, are fed calcium stones on purpose in order to help them creating the eggshell.

The total weight loss of these samples is around 65 – 68 %wt<sub>a.r.</sub> at 900 °C. The weight loss continues during the isothermal step and the final residue, after 30 min, is around 26.5 %wt<sub>a.r.</sub> and 26.7 %wt<sub>a.r.</sub> for the untreated and leached sample, respectively. These values agree with the ones found in literature [139, 202, 361]. When considered on a dry and ash free basis, the residues of the untreated and leached sample are almost identical with a value of around 13.1 - 13.5 %wt<sub>daf</sub> at 900 °C, respectively. However, due to the high inhomogeneity of the sample, variations of 1 – 2 % in the ash content can be found, hindering the results when using “daf” basis. Surely enough, the composition of manure differs significantly from previous biomass materials studied, like agricultural residues, making direct comparison not an accurate estimate. Further and more specific measurements and analyses will be needed in order to assess the proper nature of the ash-forming matter in those waste materials.



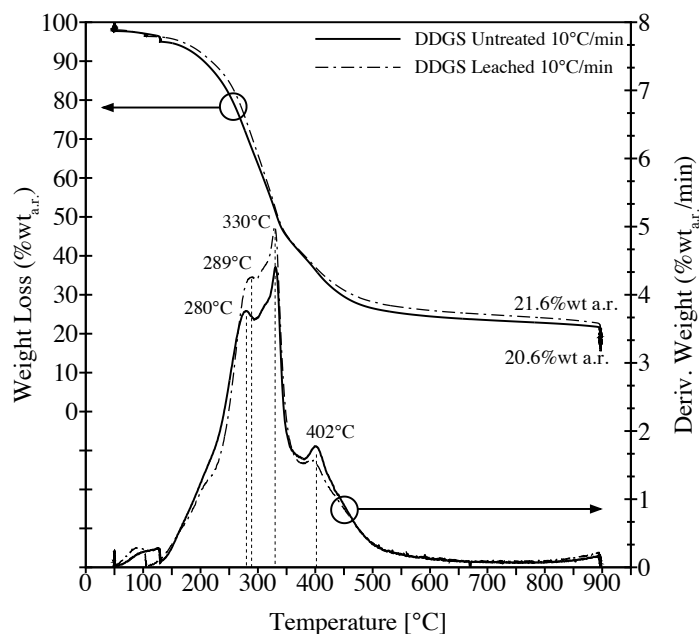


Figure 78: TG and DTG curves for DDGS untreated (-) and leached (- -); heating rate 10°C/min and He flow 100 mL/min. Data are on an "as received" basis.

### 5.3.2 FTIR

The light volatiles emitted during pyrolysis of the fuels were analyzed and quantified using an FTIR spectrometer. This let us investigate in details the mass loss behavior shown by TGA measurements.

For the DDGS sample, in the drying step, at 105°C, the physically absorbed moisture is released and the water that is released afterwards is only the pyrolytic water. From Figure 80 clearly appear some common and known features like the release of CH<sub>4</sub> at around 530°C, most likely due to the release of methoxyl groups from lignin decomposition [366]. The release of CO at high temperature due to secondary reactions of decomposition of the char has also been reported before [104, 139, 366] and detected in Chapter 4 as well.

From Figure 81 it can be observed that ammonia is the main N-compound released at low temperatures (<500°C) with a peak at around 319°C. At higher temperatures HCN plays a bigger role, with an increasing trend up to around 650°C. In between HNCO is also detected with a maximum at around 390°C. Figure 82 shows the FTIR spectra at the relevant temperatures. Known absorption bands for NO, NO<sub>2</sub> and N<sub>2</sub>O as reported by de Jong [200] are respectively: 1818 – 1937 cm<sup>-1</sup>, 1585 – 1600 cm<sup>-1</sup>, 2184 – 2202 cm<sup>-1</sup>. As it can

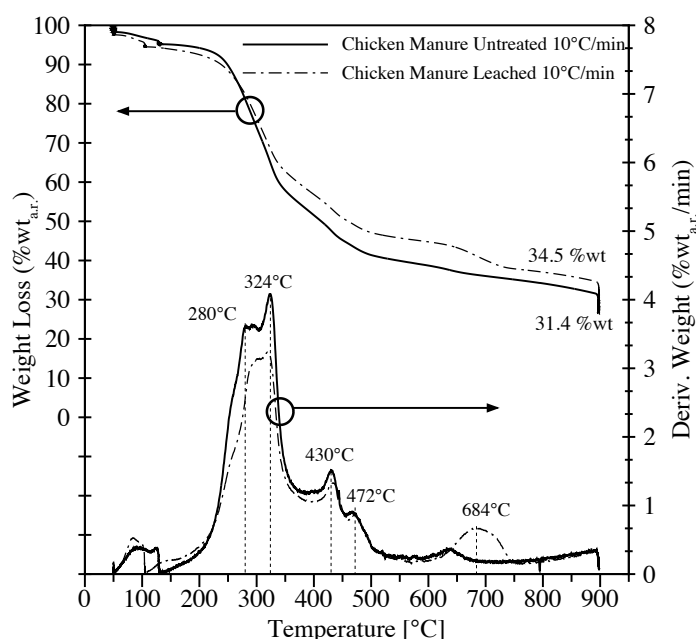


Figure 79: TG and DTG curves for chicken manure untreated (-) and leached (---); heating rate 10 °C/min and He flow 100 mL/min. Data are on an “as received” basis.

be seen from Figure 82, none of these compounds were clearly detected in the measurements with the DDGS sample.

This behavior is similar to what is reported in the literature and supports the theories expressed by other authors [182, 244, 180, 243, 245], which studied the pyrolytic decomposition behavior of single amino acids and polypeptides.

In Table 31 are reported results of TG–FTIR studies that can be found in the literature on free amino–acids or polypeptides, including the temperatures of maximum release for the nitrogen compounds. Results of this study, at heating rate of 20 °C/min, are also reported for comparison.

From Table 31 it appears that the release of ammonia for the DDGS sample, at 328 °C, happens in the temperature range of decomposition of the reference amino–acids. This can indicate that  $\text{NH}_3$  in the DDGS sample is released from deamination reactions of proteins and eventual free amino–acids present in the sample.

The trends of HCN and HNCO are quite similar to what is reported in the literature; for example Li et al. [244] show a release of HNCO with a peak at around 395 °C with a six fold decrease of intensity with respect to the peak of  $\text{NH}_3$ . That is in the range of our findings: 300 ppm<sub>v</sub> for ammonia and 50 ppm<sub>v</sub> for HNCO at its peak.

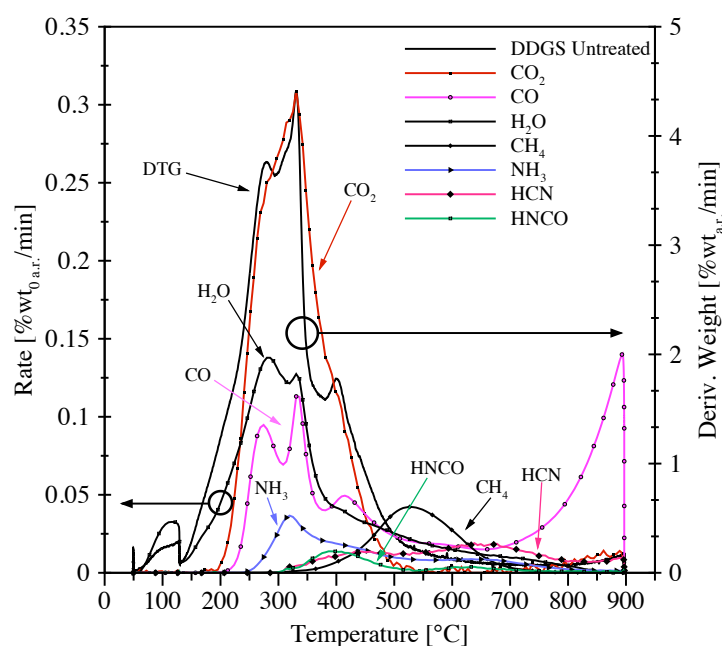


Figure 80: DDGS untreated: Superposition of DTG curve with the relative compounds analyzed by the FTIR; heating rate 10 °C/min and He flow of 100 mL/min. Data are on an “as received” basis.

Regarding HCN release, a similar trend as shown by Li et al. [244, 245] is found, showing an increasing release peaking at 664 °C. This temperature is somewhat lower than in the glycine and tyrosine measurements.

This sustains the mechanism proposed by Hansson et al. [180] explaining that the main route of reaction of the protein content in biomass passes through a first phase of deamination, followed by cyclization of the peptide or protein, with the formation of compounds called DiKetoPiperazines (DKP). These intermediate compounds then decompose at higher temperatures to produce HCN and HNCO, which can further split into HCN and CO, explaining the increasing trend of HCN release.

It appears, though, from Figure 81, that two consequential reactions take place at high temperature, the first releasing HNCO and HCN at around 395 °C but also another one releasing more HCN and HNCO and also giving rise to the ammonia release at around 664 °C. This could still be explained through the DKP decomposition, but it can also depend on some stronger nitrogen structures which could be found in the sample due to the presence of residual yeast. The DNA of the microorganisms contains other N-structures like pyridine and pyrrole heterocycles which could be responsible for this late release [180].

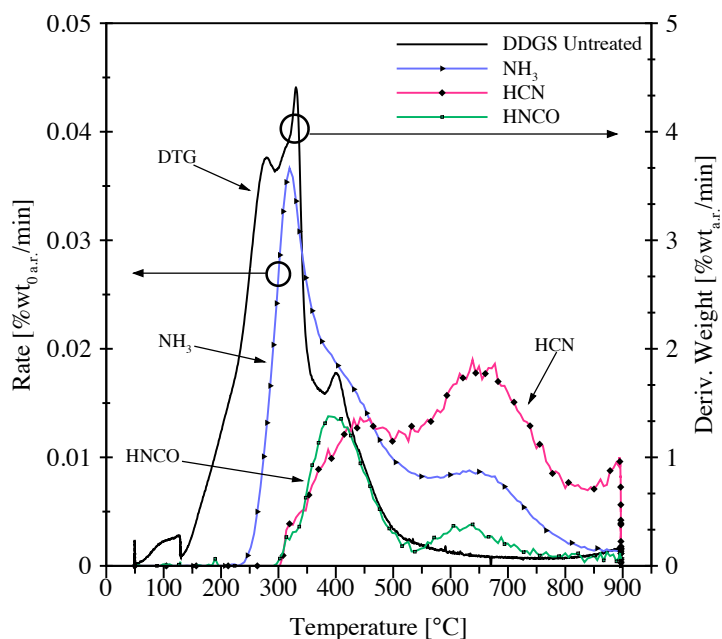


Figure 81: DDGS untreated: Re-scaling of Figure 80 for the main nitrogen compounds,  $\text{NH}_3$ , HCN and HNCO; heating rate  $10^\circ\text{C}/\text{min}$  and He flow of  $100\text{ mL}/\text{min}$ . Data are on an “as received” basis.

Table 31: TG–FTIR studies on amino acids decomposition found in the literature\*.

Author, year	Sample	$T_{\text{peak}} \text{NH}_3$ ( $^\circ\text{C}$ )	$T_{\text{peak}} \text{HCN}$ ( $^\circ\text{C}$ )	$T_{\text{peak}} \text{HNCO}$ ( $^\circ\text{C}$ )	Ref.
Li et al. (2006)	L-leucine	352	n.d.	n.d.	[243]
Li et al. (2007)	Glycine	282	717	395	[244]
Li et al. (2007)	Glycylglycine	250/352	717	395	[244]
Li et al. (2008)	Phenylalanine	291/406	406	406	[245]
Li et al. (2008)	Tyrosine	334/345	700	n.d.	[245]
This study	DDGS	328	664	407	-
This study	Chicken manure	443	455/477	443	-

\*Heating rate  $20^\circ\text{C}/\text{min}$

n.d.: Not detected in the referred study

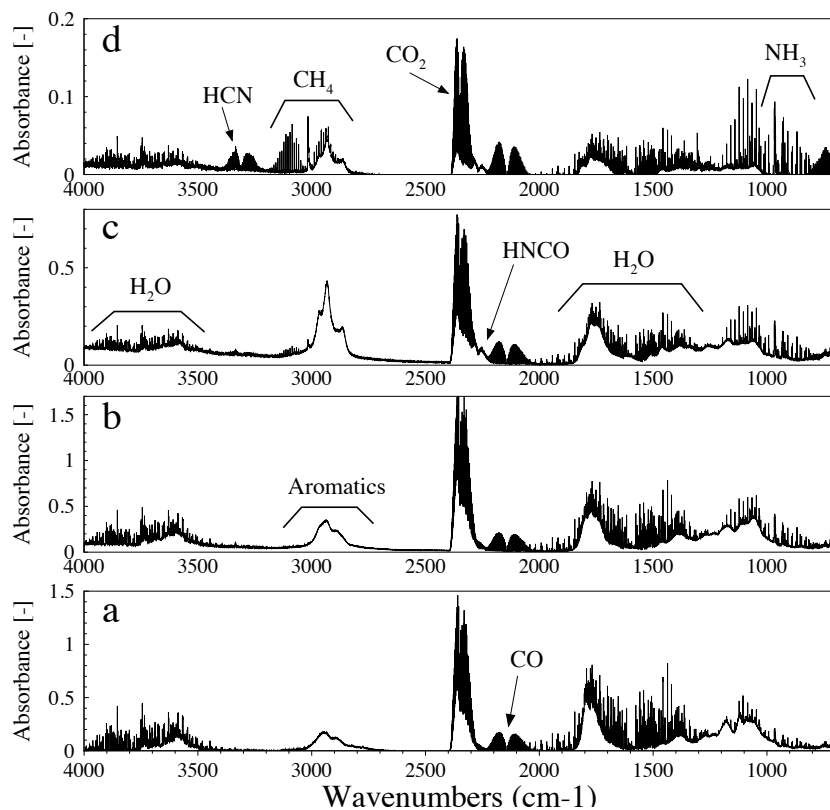


Figure 82: FTIR spectra from the DDGS untreated measurement at 10 °C/min; [a] spectrum at 280 °C, [b] spectrum at 330 °C, spectrum at 404 °C, spectrum at 650 °C.

Figure 83 and 84 show the results from FTIR measurements on chicken manure. In Figure 84 the nitrogen compounds are underlined and some remarkable differences appear with the behavior shown by DDGS. First of all a certain amount of ammonia is released already during the drying step at 105 °C without sensible release of any other N compound so that we can assume this to be physically absorbed  $\text{NH}_3$  contained in the manure. This component is also the one mostly affected by the leaching procedure: after the drying period, the untreated sample released 0.17 %wt<sub>d.b.</sub> of the initial weight as  $\text{NH}_3$ , while the leached sample only lost 0.05 %wt<sub>d.b.</sub> of its initial weight.

Furthermore, ammonia is released throughout all the measurement with a release rate similar to the one of DDGS but with a higher final yield of 3.1 %wt<sub>daf</sub> of the initial weight compared to 1.4 %wt<sub>daf</sub> released by the DDGS sample.

$\text{HNCO}$  shows a pronounced release at 430 °C, temperature at which also  $\text{HCN}$ ,  $\text{NH}_3$  and  $\text{CO}_2$  show a peak of reactivity. The same compounds are

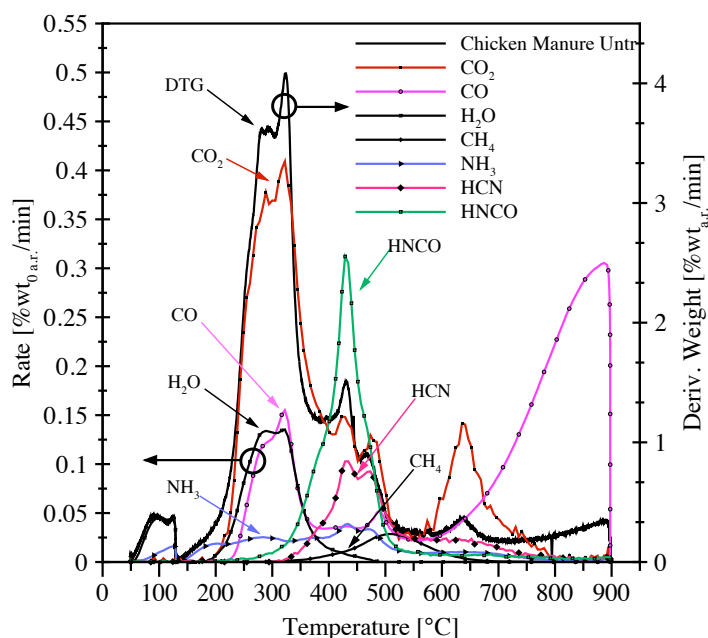


Figure 83: Chicken manure untreated: Superposition of DTG curve with the relative compounds analyzed by the FTIR; heating rate 10 °C/min and He flow of 100 mL/min. Data are on an “as received” basis.

emitted at 472 °C but HNCO has a decreasing trend at this temperature. It is worthy recalling that manure is mainly composed of undigested food matter and urine excretion from the chickens. As “Urine production and excretion is a vertebrate’s primary method for removal of nitrogen” [54], we expect most of the nitrogen in this sample to be in the form of ammonia or urea together with undigested proteins. Urea,  $\text{H}_2\text{N-CO-NH}_2$ , will decompose into HNCO and  $\text{NH}_3$  [368] while secondary reactions will produce more ammonia and HCN. However, also proteins will decompose in this range of temperature and could be responsible for the release of additional N-compounds as revealed by DDGS pyrolysis measurements.

When compared with literature, anyway, this behavior is comparable to the one shown by de Jong et al. [202]. They also present a double peak for ammonia, even though the sample studied in this paper reacts at higher temperatures: at 30 °C/min, 453 °C and 487 °C are the peak temperatures for our sample, compared with 380 °C and 495 °C for de Jong et al. [202]. HNCO too is expected to peak at around 495 °C according to de Jong et al. [202] while 450 °C is the peak temperature for our sample.

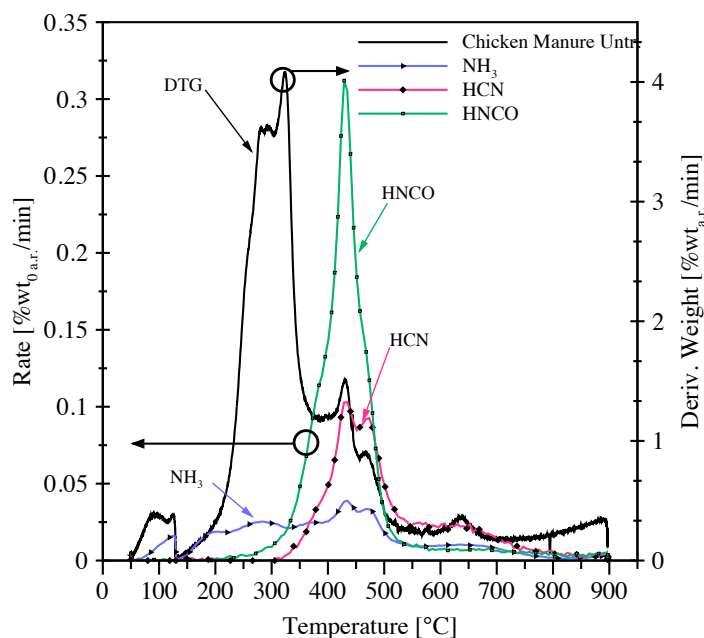


Figure 84: Chicken manure untreated: Re-scaling of Figure 83 for the main nitrogen compounds,  $\text{NH}_3$ , HCN and HNCO; heating rate  $10^\circ\text{C}/\text{min}$  and He flow of  $100\text{ mL}/\text{min}$ . Data are on an “as received” basis.

Table 32 summarizes the temperatures of maximum reaction rates for single species and the final yields measured by FTIR at  $900^\circ\text{C}$  at holding time equal to zero and after the isothermal step of 60 min. Considering the released molecules, some common features are underlined:  $\text{CO}_2$ , CO and  $\text{CH}_4$  are released in the same temperature range for all the fuels studied and comparable with the data available in the literature for model compounds [366].

It appears evident, comparing DDGS with chicken manure, that the nitrogen compounds have different origins. The nitrogen in DDGS is mainly in the form of proteins and we have shown how this could explain the release of  $\text{NH}_3$  at low temperatures and the following release of HCN and HNCO at higher temperatures. In chicken manure proteinic nitrogen is still present, mainly due to undigested food, and it is probably responsible for the continuous release of  $\text{NH}_3$  at lower temperatures. But manure has also a high concentration of nitrogen in the form of urea contained in the urines of the animals: this component is probably responsible for the high amount of HNCO that is released at around  $430^\circ\text{C}$ , in correspondence with the release of  $\text{NH}_3$  and HCN. In this sense, the appearance of the relative peak of  $\text{CO}_2$ , as can be seen

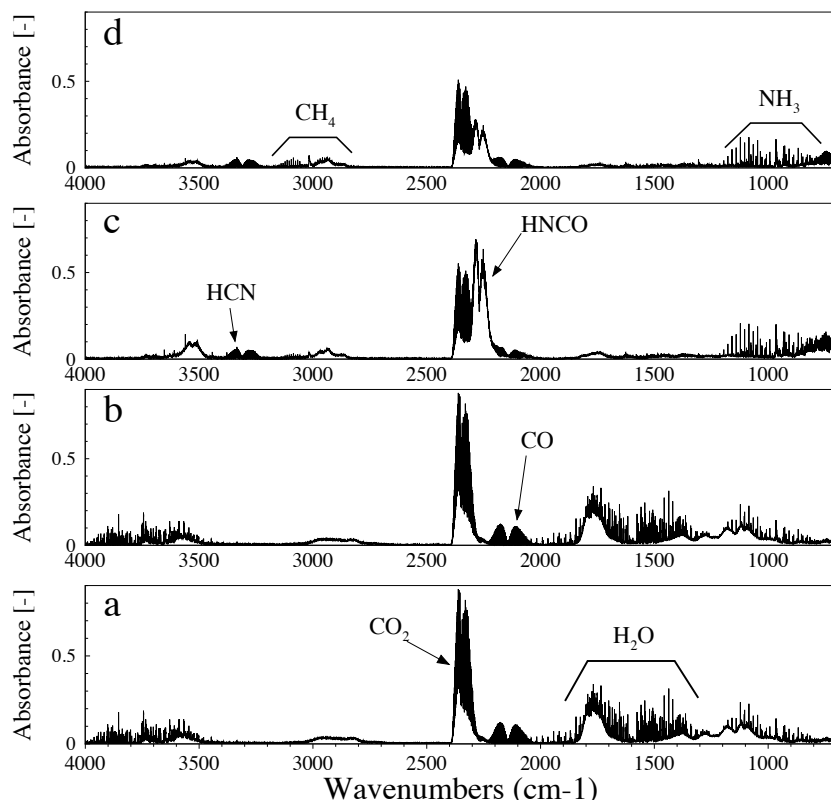


Figure 85: FTIR spectra from the chicken manure untreated measurements at 10 °C/min; [a] spectrum at 280 °C, [b] spectrum at 324 °C, spectrum at 430 °C, spectrum at 472 °C.

in Figure 83, reveals a possible decomposition of HNCO in NH<sub>3</sub> and CO<sub>2</sub> according to Yim et al. [368].

In terms of final yields, we can see that, as expected, more nitrogen is released by chicken manure and most of it is in the form of HNCO, even though, as explained earlier and in Chapter 3, quantification of HNCO is very difficult and this suggests that the absolute values should be considered more indicative than accurate. In relative terms, it is indubitable that the final yield from the manure samples is higher than for DDGS and that the washed chicken manure sample releases lower amounts of HNCO compared to the untreated sample.

Comparing the two fuels, even considering the limitations mentioned above, the mass recovery in the chicken manure appears higher, around 50 - 60 %wt<sub>daf</sub>, indicating a higher degree of decomposition and a very low amount of tars while for DDGS a higher amount of heavier aromatics are released, as illus-



Table 32: Temperatures at maximum release rates for a heating rate of 10 °C/min and maximum yields after holding times= 0s/60 min at isothermal conditions at 900 °C, on a dry and ash free basis of the original fuel.

Gas species	DDGS	DDGS leached	Chicken manure	Chicken manure leached
CO <sub>2</sub>	331	330	322	322
% wt <sub>daf</sub>	8.6/9.6	9.6/14.6	18.9/19.8	26.8/27.6
CO	331	330	322	322
% wt <sub>daf</sub>	7.2/18.1	8.3/26.4	18.0/35.3	18.3/42.9
CH <sub>4</sub>	526	526	507	506
% wt <sub>daf</sub>	1.5	1.5	1.1	1.0
H <sub>2</sub> O	280	290	322	316
% wt <sub>a.r.</sub>	5.2	2.3	3.3	2.8
NH <sub>3</sub>	319	318	434	439
% wt <sub>daf</sub>	1.4/1.5	1.8/1.9	3.1	3.9
HCN	638	659	434	434
% wt <sub>daf</sub>	1.3/1.4	1.8/2.6	4.1/4.2	3.8/4.1
HNCO	387	386	429	433
% wt <sub>daf</sub>	0.4	0.5	6.6	3.9

trated also in Figure 82 and 83. The total recovery for DDGS results in 20 - 24 %wt<sub>daf</sub>.

The leaching process appears to slightly increase the release of HCN and ammonia from the DDGS sample and in general the release of light volatiles at expenses of tars. Moreover, it appears to decrease abruptly the release of HNCO from chicken manure, most probably as consequence of urea removal but to increase tar release at expenses of light volatiles.

Moreover, the pre-treatment appears to greatly increase the release of CO<sub>2</sub> at high T in both fuels: this indicates that the removal of inorganics caused structural changes in the fuel so that some structures in the char were decomposed further than in the original fuel.

### 5.3.3 Kinetic analysis

There are many ways of approaching kinetic analysis of global complex reactions, as brilliantly reviewed by Burnham and Braun[119] and discussed in details in Chapter 3 of this dissertation.

In this work we chose to follow the latter line considering the previous works from our group [202, 139] and, mainly, the possible future applications of these data on an FG–Biomass model, which requires input data following a Gaussian kinetic [202, 318, 339].

The distributed activation energy model (DAEM) can be expressed as follows when it is applied to represent the change in the unreacted fraction of the sample:

$$x = \int_0^{\infty} \exp \left[ - \int_0^t k(T) dT \right] \cdot D(E) dE \quad (5.1)$$

Where  $k(T)$  obeys the Arrhenius equation and it is a function of time because of the applied temperature profile:

$$k(T) = A \cdot \exp \left( - \frac{E}{R \cdot T(t)} \right) \quad (5.2)$$

Here:

$$\int_0^{\infty} D(E) dE = 1 \quad (5.3)$$

The shape of the distribution  $D(E)$  is not known a priori and it depends on the composition and structure of the sample. As mentioned earlier, it is common practice to assume  $D(E)$  as a Gaussian distribution.

A valid alternative to this assumption is to choose a Discrete distribution of  $E$ , in which the integral in eq. 5.1 is substituted by a sum of a finite number of parallel reactions.

We chose this model because, even though the activation energies which are found and the actual reacting functional groups are not directly related [342], it provides a more effective visualization of the results and an additional degree of freedom to the method, as underlined by Miura[267].

For our analysis we used a FORTRAN based code, developed by A.K. Burnham and R.L. Braun, called KINETICS05 [113, 119] which can analyze, simultaneously, measurements performed at different heating rates and fit them with 25 first-order reactions sharing the same pre-exponential factor.

We chose to follow the common practice, anyway, and we fixed the pre-exponential factor at the value of  $2.2 \times 10^{13} \text{ s}^{-1}$  according to de Jong et al. [202] and Tsamba et al. [339], for the reasons explained in Chapter 3.

In this paper we decided to use a discrete distribution for the global devolatilization because we consider it more suitable to represent the hetero-

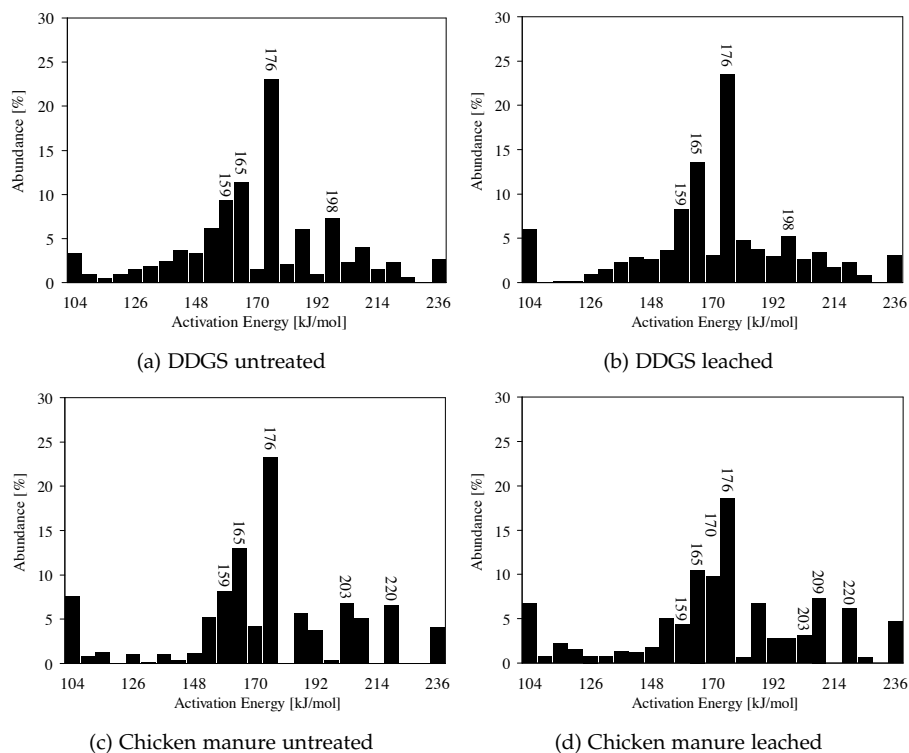


Figure 86: Distribution of activation energies using a pre-exponential factor  $A = 2.2 \times 10^{13} \text{ s}^{-1}$ .

geneous nature of the fuels, while we used one or more Gaussian distributions for the nitrogen species describing the pseudo - pools from which the compounds are released. We used the data at slower heating rates (10 – 20 – 30°C/min) to retrieve the kinetic parameters. The fitting of measurements with a high mass (around 15 mg for chicken manure and 30 mg for DDGS) and low mass (4 mg for both samples) gave the same discrete peaks, in terms of activation energy, and the absolute intensities of these peaks showed a standard deviation of around 7 % for both fuels.

In Figure 86 the results for the fit of the global devolatilization reactions of the untreated and pre-treated samples are shown. To relate this to its chemical meaning, Figure 87 shows the original DTG of DDGS untreated sample superposed with the 25 parallel first order reactions. It is then possible to recognize the hemicellulose decomposition through reactions with activation energies of 159 and 165 kJ/mol and the cellulose decomposition characterized by activation energy of 176 kJ/mol. These results are also in very good agreement with our previous study on agricultural residues shown in Chapter 4, underlining the presence of common structures among all these materials. The

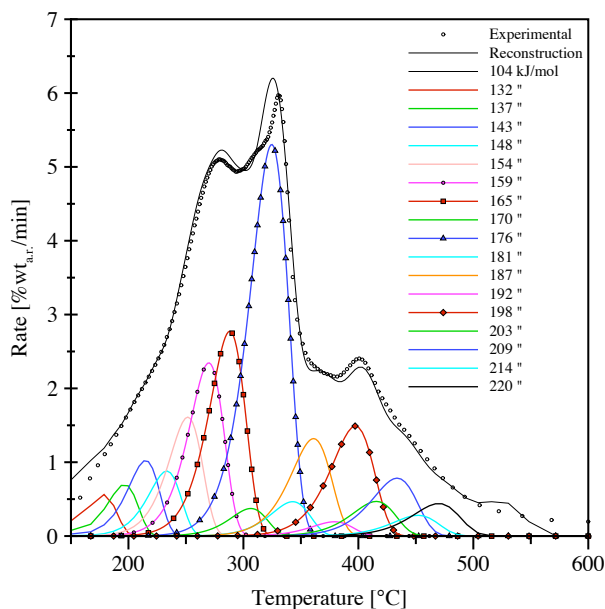


Figure 87: DDGS untreated at 10 °C/min, DTG and fit with 25 parallel first order reactions.

protein decomposition appears then as the component reacting with  $E$  equal to 198 kJ/mol.

Analyzing Figure 88, where the reactions are underlined for chicken manure untreated, we can see that there are common features in the reactions for hemicellulose and cellulose decomposition, while the additional peaks, composed by nitrogen compounds, appear for reactions with activation energies of 203 and 220 kJ/mol.

To test the predictive nature of the obtained kinetics and to guarantee that the right conditions were applied in the experiments (kinetic limited), we used the retrieved parameters to reconstruct the global devolatilization curve at a heating rate of 100 °C/min and we compared it to the experimental data.

Results are reported in Figure 89 and 90 for DDGS and chicken manure untreated, respectively. It appears evident that the kinetic parameters remain valid also at higher heating rates as long as the reaction mechanisms remain unchanged.

These results, thus, prove not only that the presented kinetic parameters constitute a valid basis for modeling purposes but they have also predictive value for slow pyrolysis applications like, for example, carbonization and biochar production [190].

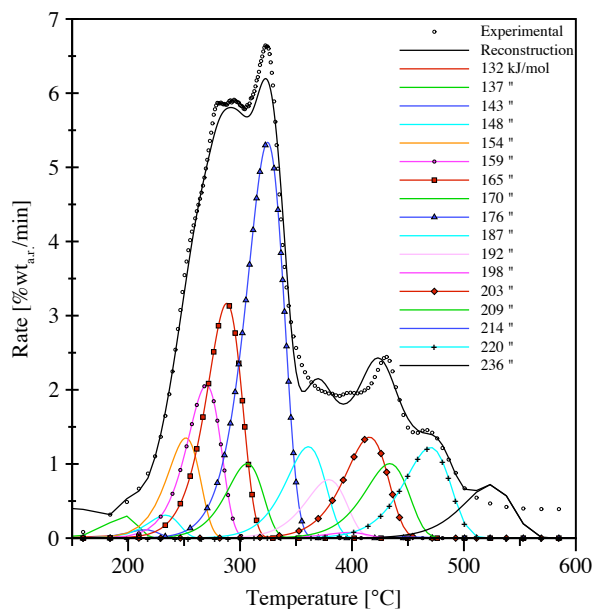


Figure 88: Chicken manure untreated at 10 °C/min, DTG and fit with 25 parallel first order reactions.

Table 33: Kinetic parameters for Gaussian distribution. Main nitrogen species: DDGS.

Precursor pool	A (s <sup>-1</sup> )	E <sub>0</sub> (kJ/mol)	σ (% of E <sub>0</sub> )	Yield <sup>a</sup> (100 %)
1 - NH <sub>3</sub>	2.2 × 10 <sup>13</sup>	173	0.1	10.9
2 - NH <sub>3</sub>	2.2 × 10 <sup>13</sup>	189	17	41.3
3 - NH <sub>3</sub>	2.2 × 10 <sup>13</sup>	255	43	47.8
1 - HCN	2.2 × 10 <sup>13</sup>	208	18	23.9
2 - HCN	2.2 × 10 <sup>13</sup>	277	31	67.8
3 - HCN	2.2 × 10 <sup>13</sup>	345	0.1	8.3
1 - HNCO	2.2 × 10 <sup>13</sup>	201	13	59.8
2 - HNCO	2.2 × 10 <sup>13</sup>	261	28	20.8
3 - HNCO	2.2 × 10 <sup>13</sup>	294	37	19.5

<sup>a</sup>The yield in the table indicates the relative amount (%) of each pool on a base of 100 % for the considered pool.

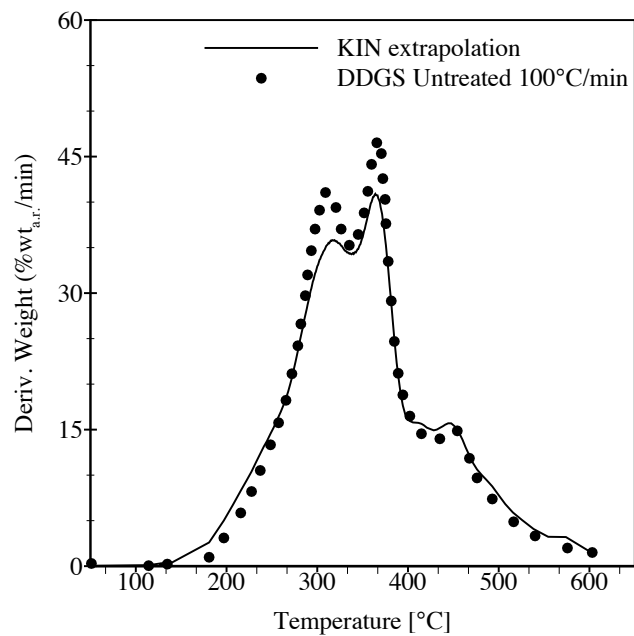


Figure 89: DDGS untreated experimental and reconstructed DTG at heating rate of 100°C/min. Discrete distribution was used for extrapolation.

Table 34: Kinetic parameters for Gaussian distribution. Main nitrogen species: DDGS leached.

Precursor pool	A (s <sup>-1</sup> )	E <sub>0</sub> (kJ/mol)	σ (% of E <sub>0</sub> )	Yield <sup>a</sup> (100 %)
1 - NH <sub>3</sub>	2.2 × 10 <sup>13</sup>	171	0.1	11.1
2 - NH <sub>3</sub>	2.2 × 10 <sup>13</sup>	181	21	49.7
3 - NH <sub>3</sub>	2.2 × 10 <sup>13</sup>	264	48	39.2
1 - HCN	2.2 × 10 <sup>13</sup>	207	19	23.0
2 - HCN	2.2 × 10 <sup>13</sup>	281	33	65.2
3 - HCN	2.2 × 10 <sup>13</sup>	345	0.1	11.8
1 - HNCO	2.2 × 10 <sup>13</sup>	200	13	61.4
2 - HNCO	2.2 × 10 <sup>13</sup>	267	36	35.4
3 - HNCO	2.2 × 10 <sup>13</sup>	338	4	3.2

<sup>a</sup>The yield in the table indicates the relative amount (%) of each pool on a base of 100% for the considered pool.

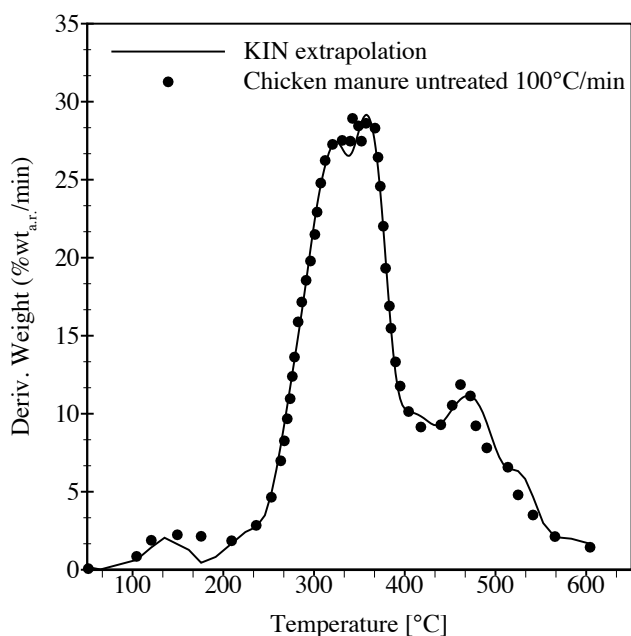


Figure 90: Chicken manure untreated experimental and reconstructed DTG at heating rate of 100 °C/min. Discrete distribution was used for extrapolation.

Table 35: Kinetic parameters for Gaussian distribution. Main nitrogen species: Chicken manure.

Precursor pool	A (s <sup>-1</sup> )	E <sub>0</sub> (kJ/mol)	σ (% of E <sub>0</sub> )	Yield <sup>a</sup> (100 %)
1 - NH <sub>3</sub>	2.2 × 10 <sup>13</sup>	159	24	40.4
2 - NH <sub>3</sub>	2.2 × 10 <sup>13</sup>	213	13	24
3 - NH <sub>3</sub>	2.2 × 10 <sup>13</sup>	251	52	35.6
1 - HCN	2.2 × 10 <sup>13</sup>	214	11	47.1
2 - HCN	2.2 × 10 <sup>13</sup>	222	0.1	1.4
3 - HCN	2.2 × 10 <sup>13</sup>	257	38	51.5
1 - HNCO	2.2 × 10 <sup>13</sup>	209	9	77.1
2 - HNCO	2.2 × 10 <sup>13</sup>	233	49	22.9

<sup>a</sup>The yield in the table indicates the relative amount (%) of each pool on a base of 100% for the considered pool.

Table 36: Kinetic parameters for Gaussian distribution. Main nitrogen species: Chicken manure leached.

Precursor pool	A (s <sup>-1</sup> )	E <sub>0</sub> (kJ/mol)	σ (% of E <sub>0</sub> )	Yield <sup>a</sup> (100 %)
1 - NH <sub>3</sub>	2.2 × 10 <sup>13</sup>	170	27	47.5
2 - NH <sub>3</sub>	2.2 × 10 <sup>13</sup>	214	8	20.6
3 - NH <sub>3</sub>	2.2 × 10 <sup>13</sup>	270	36	32.0
1 - HCN	2.2 × 10 <sup>13</sup>	208	0.1	1.4
2 - HCN	2.2 × 10 <sup>13</sup>	213	11	57.7
3 - HCN	2.2 × 10 <sup>13</sup>	253	48	41.0
1 - HNCO	2.2 × 10 <sup>13</sup>	206	26	47.7
2 - HNCO	2.2 × 10 <sup>13</sup>	209	5	52.3

<sup>a</sup>The yield in the table indicates the relative amount (%) of each pool on a base of 100% for the considered pool.

Table 33 to 36 indicate the precursor pools for the nitrogen species detected for the different fuels. Literature is available only for chicken manure sample [202] and agreement with those data is good.

From these data it appears that HCN and HNCO have components evolving at higher activation energies for the DDGS sample than from the chicken manure; this gives one more indication that they are either evolving from more stable structures, like DKP decomposition or heterocyclic N-structures, or that they are produced by secondary reactions.

The effect of leaching is again not relevant for the DDGS, while for chicken manure it has a slightly effect only on the release of HNCO for which the component at higher activation energy is removed by the pre-treatment and could be responsible for the lower final yield of HNCO registered by the FTIR.

#### 5.4 CONCLUSIONS

Thermogravimetric results were obtained for DDGS and chicken manure samples showing that, despite the different origin and heterogeneous nature of the materials, common features can be found in the decomposition of the hemicellulose and cellulose components despite the different fuels. Additional reactivity peaks, attributed to proteins decomposition, were detected at higher temperatures.

Water leaching pre-treatment was applied to both fuels. The pre-treatment had an effect both on quantity and quality of the ashes for both fuels. The amount of ashes was reduced and some problematic elements, like Cl, S, Na and K were removed. No significant effects appeared in the reactivity except



for a shift at higher temperatures for the hemicellulose component of both fuels. Chicken manure, due to its different origin and heterogeneous composition, appeared to behave differently than what seen in literature for more standard biomass fuels like straw. The effects of the leaching were minor compared to what observed in Chapter 4 for agricultural residues. The different composition of the inorganic matter could be responsible for this different behaviour.

The main  $\text{NO}_x$  precursors were detected and quantified for these fuels. DDGS mainly released  $\text{NH}_3$  and HCN with a minor release of HNCO. The main source of nitrogen appeared to be proteins. Chicken manure, instead, released mainly HNCO but also higher amounts of  $\text{NH}_3$  and HCN than DDGS. The sources of these compounds appeared to be both proteins and urea present in the urine of the animals. In this respect the leaching pre-treatment seemed to be effective in removing urea absorbed on the chicken manure sample highly reducing the release of HNCO.

The yields of other volatile species, like  $\text{CO}_2$  and CO, are for DDGS lower than for agricultural residues. The value for CO is quite close to values found in pyrolysis of agricultural residues, while the yield of methane is slightly higher. The values for chicken manure underline a lower yield of tars and carbonaceous residue compared to DDGS, with a higher degree of degradation of its forming structures. The leaching pre-treatment, as mentioned in Chapter 4, seems to have very little effect on the final residue, while it increases the yields of all volatile species, including volatile-N.

Kinetic parameters, valid for modeling purposes and slow pyrolysis applications, were retrieved both for global devolatilization and for the nitrogen compounds release. The parameters associated with hemicellulose and cellulose decomposition were the same for all the fuels despite their different origin and composition. They were also comparable with the parameters found for the agricultural residues analyzed in Chapter 4 in the same conditions.

HCN and HNCO showed components at higher activation energies for DDGS than for chicken manure indicating probably more strongly bound structures or secondary reactions. The leaching pre-treatment removed the component of HNCO at higher activation energies in the chicken manure sample.



# 6

---

## CHARACTERIZATION OF FAST PYROLYSIS OF DDGS AND PKC USING A HEATED FOIL REACTOR: NITROGEN CHEMISTRY AND REACTOR MODELING

---

*This chapter presents the results of fast pyrolysis studies of DDGS and PKC samples. The measurements were performed on a Heated foil-FTIR setup at conditions relevant to industrial applications. A numerical model of the heated foil reactor is introduced in the chapter and the results of the simulations performed are explained. The results of total weight loss of the fuels at high heating rates are compared with the data presented in Chapter 5. The main gaseous species and NO<sub>x</sub> precursors are detected and quantified by the FTIR and their yields and dependence on temperature are shown. Furthermore, the partitioning of fuel-bound nitrogen and carbon in the volatiles and in the solid char is presented. Finally, the effects of a water-leaching pre-treatment on the reactivity and volatiles yields of the fuels were studied.*

The contents of this chapter were adapted from the work submitted for publication in:

J. Giuntoli, J. Gout, A.H.M. Verkooijen, W. de Jong,

"Characterization of fast pyrolysis of dry distiller's grains and palm kernel cake using a heated grid reactor: Nitrogen chemistry and reactor modeling"

*Ind. Eng. Chem. Res.*, xx(xxxx) xx-xx ; DOI: xxx

Unpublished work © 2010 ACS. Reprinted with permission.

## 6.1 INTRODUCTION

The results introduced in this chapter have the purpose to help the characterization of the fast pyrolysis behaviour of biomass wastes with the focus on nitrogen partitioning. Two potential fuels with high N content, dry distiller's grains and solubles (DDGS) and palm kernel cake (PKC), were analyzed under fast pyrolysis conditions in a small-scale, heated foil reactor. In Chapter 5 we thoroughly studied the devolatilization behaviour of DDGS and chicken manure at slow heating rates and we were able to retrieve kinetic parameters and volatile composition. However, the conditions in real reactors are very different, with heating rates more in the order of magnitude of  $10^3$  to  $10^4$  °C/s. The heated foil reactor used in this work, which was introduced in Chapter 3, allowed the detection and quantification of volatile  $\text{NO}_x$  precursors, such as  $\text{NH}_3$  and HCN, released during pyrolysis at high heating rates, in the range of 500 to 1000 °C/s. The reactor allowed the study of the influence of temperature, heating rate and holding time on volatile composition, yields and weight loss. Moreover, the water leaching pre-treatment described by Arvelakis and Koukios [76] and in Chapter 3, was applied to the samples in order to remove the water soluble troublesome elements. Leached samples were investigated to test the influence of such pre-treatment on their thermal behavior.

Heated grid reactors have been extensively used in the last 40 years to study the fast devolatilization of coals [70, 140, 317] and, more recently, of biomass structures and samples [91, 140, 146, 176, 177, 200, 328, 329].

In addition to the experimental results from fast pyrolysis, this work introduces a numerical model of the reactor itself. Because of the architecture of the setup and the extreme speed of the phenomena involved, the possibilities for monitoring the experimental conditions are limited in the reactor, as opposed to a thermogravimetric analyzer [159, 163]. A numerical model is a good way to provide a better insight into the physical conditions in the reactor, such as temperature and velocity profiles. The findings from the model were validated against a non-contact temperature measurement. The results of these simulations complemented the experimental results by giving a clearer picture of the physical conditions in the reactor.

In a previous chapter, we investigated the slow pyrolysis of DDGS, both untreated and leached in water, in a TG-FTIR setup [163]. We reported that the main nitrogen compound to be released was  $\text{NH}_3$  at low temperatures, followed by HCN and HNCO at higher temperatures. The results also showed how the pyrolysis was complete at about 700 °C and that the final weight loss amounted to about 80 %wt<sub>a.r.</sub> at 900 °C. Moreover, the leaching pre-treatment appeared to have a limited effect on the reactivity and on the volatiles composition.

In another study from our group, Di Nola et al. [140] investigated the fast pyrolysis of coal, chicken manure and meat and bone meal. They found that

$\text{NH}_3$  was the main N-compound released at low temperatures with HCN yield increasing rapidly at higher temperatures.

Moreover, Becidan et al. [98, 99] investigated the fast pyrolysis of coffee waste, fiberboard and brewer spent grains. They showed how the amount of light gases released increased with temperature at the expenses of tars and residual char. However, they observed that  $\text{NH}_3$  was the main N-compound at all temperatures, even though the ratio  $\text{HCN} / \text{NH}_3$  was linearly increasing for all the samples. Furthermore, they found an increasing release of volatile-N compounds with temperature at the expenses of tar-N and char-N. In another work Becidan [95] underlined contradictory results found in literature with the main volatile-N species varying with heating rates, experimental equipments and, obviously, fuels. Tables 9 and 10 in Chapter 2, illustrate the results found in some previous works on volatile-N composition during slow and fast pyrolysis, respectively. Due to the very different nature of the materials analyzed and their nitrogen structures, a clear pattern does not appear from previous works. Generally it seems that ammonia is the main volatile released at slow heating rates, when the route of deamination of the protein chains is the main mechanism of release [180, 244, 245]. However, at high heating rates, closer to industrial conditions, HCN becomes more important, especially at high temperatures, indicating a different mechanism of release, including more secondary reactions in the gas phase [95, 180].

In order to obtain a definite picture of the behaviour of these materials, it is clear that a thorough characterization of each fuel, like the one presented in this paper, is necessary.

## 6.2 EXPERIMENTAL SECTION

### 6.2.1 *Integrated heated foil – FTIR setup*

The experimental work described in this paper was carried out on the setup illustrated in Figure 91. The apparatus has been slightly modified compared with the one described and used in previous works [139, 140]. The setup is described in more details in Chapter 3.

As it is shown in Figure 91, the setup consists of two different equipments: the actual heated foil reactor (HF) and a Fourier Transform InfraRed Spectrometer (FTIR) in which the reactor is inserted. The main part of the reactor consists of a stainless steel cylindrical chamber of 60 mm diameter and 65 mm of height. A grid, or foil in this work, is placed between two electrodes in the center of this chamber. An S-type (Pt/Pt-Rh) thermocouple (TC) of 0.01 mm diameter is placed underneath the foil, in contact with it. Finally, the sample is placed on the center of the foil. The reactor walls are heated with heating elements at a temperature of 110 °C, verified by an external K-type thermocouple, in order to avoid species condensation. When electric current is passed through the electrodes, the foil is heated via resistive heating at very

high rates of the order of  $1000\text{ }^{\circ}\text{C}/\text{s}$ . The control of the heating profile is done via the thermocouple and a fast acquisition card connected to a PC. The PC uses the TC reading as input for the control and adjusts the electrical current output so that the actual temperature profile follows the programmed one. The control is done via the software Testpoint and the thermal history can be customarily defined via the parameters of heating rate, final temperature and holding time at final temperature.

The choice in this work was to use a foil of stainless steel AISI 304 (18Cr 9Ni) with a thickness of 0.05 mm and a surface of  $8 \times 14\text{ mm}^2$ .

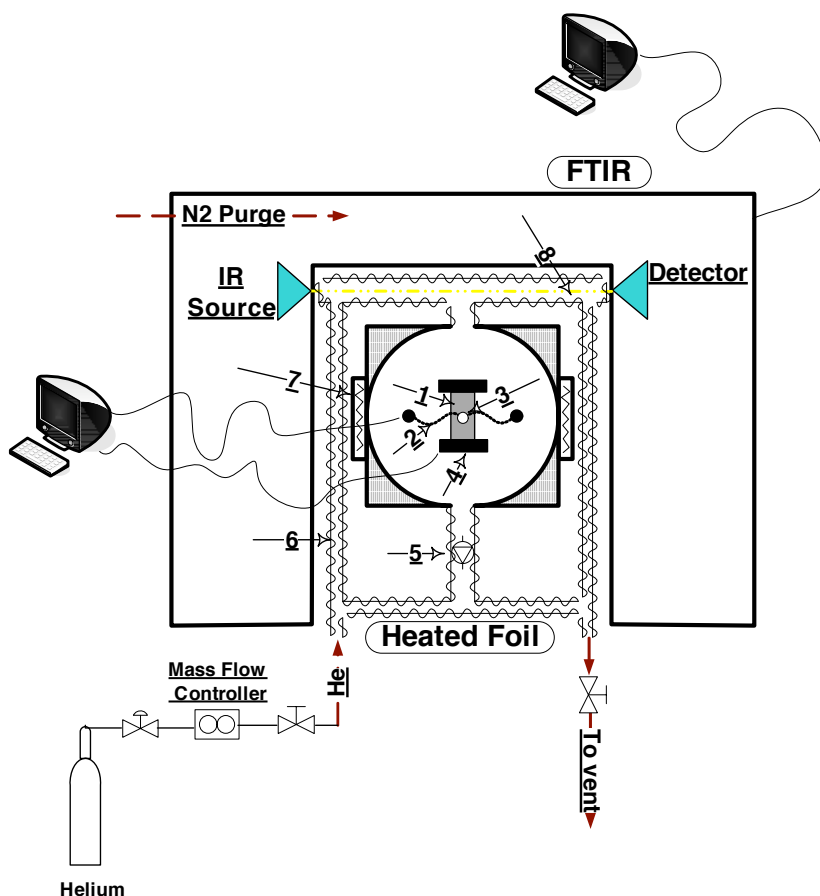
In the present measurement campaign, an amount of 5 to 7 mg of sample was weighted and then pressed into thin discs of approximately 0.7 mm thickness and 3 mm diameter. Once the sample was placed on the foil, the lid was sealed and the system was flushed with helium for a sufficient time to flush the chamber from atmospheric gases. Consequently, the inlet and outlet valves were closed to maintain an inert atmosphere in the reactor. After the valves were closed, the heating ramp was started and the sample was heated with a heating rate (HR) of  $600\text{ }^{\circ}\text{C}/\text{s}$  up to temperatures ranging between  $500\text{ }^{\circ}\text{C}$  and  $1300\text{ }^{\circ}\text{C}$ . The holding time (HT) at high temperature was usually kept equal to 10 s.

Once the gases are released from the sample, a volumetric pump, with a flow of  $2.6\text{ L}/\text{min}$ , circulates them from the hot zone into two transfer lines, heated at about  $110\text{ }^{\circ}\text{C}$ . The loop is closed by a final cylindrical tube encased among two ZnSe windows. This constitutes the actual gas cell of the FTIR and it has an optical path length of 0.2 m. The total volume of the reactor and circulation loop is  $200\text{ cm}^3$ .

A quantitative method was implemented on the FTIR via calibration of the following species: CO,  $\text{CO}_2$ ,  $\text{CH}_4$ ,  $\text{H}_2\text{O}$ ,  $\text{NH}_3$ , HCN and HNCO. The applied resolution for FTIR measurements was equal to  $0.25\text{ cm}^{-1}$  and the results of 3 scans were averaged for a total measurement time of 9 s. In order to guarantee a homogeneous distribution of the gases in the reactor volume, after the holding time at high temperature, the pyrolysis gases were circulated for about 2 minutes prior to the FTIR measurement. Sets of three measurements were performed; the reported values are the average of each series and the upper and lower values of the series are also reported as error bars.

### 6.2.2 Pyrometer

In order to validate the numerical model developed in this work, an InfraRed (IR) pyrometer was used. The pyrometer utilized here was a model IGA5 MB20 manufactured by Impac. Additional data can be found in Chapter 3. The pyrometer could measure the IR radiation of a spot of 1.1 mm diameter when placed at a distance of 90 mm from the target. The pyrometer measured temperatures in the range of  $250$  to  $2000\text{ }^{\circ}\text{C}$  in the wavelength range of  $1.45 - 1.8\text{ }\mu\text{m}$ . The pyrometer was mounted on two 25 mm travel motion



Helium

1	Foil	(Stainless steel 304)
2	S-type thermocouple	(0.01 mm)
3	Sample pill	
4	Electrodes	
5	Volumetric circulation pump	
6	Heated lines	(@110 °C)
7	Heating elements reactor walls	(@110 °C)
8	FTIR Gas cell	(0.2 m of length)

Figure 91: Heated foil setup

Table 37: Proximate and Elemental Analysis of the fuels. Data are on a dry basis.

	DDGS <sup>a</sup>	DDGS Leached <sup>a</sup>	PKC	PKC Leached
Moisture <sup>b</sup>	8.9	8.5	7.0	9.2
Volatiles	78.2	76.2	75.5	75.1
Fixed Carbon	14.7	17	18.4	19.5
Ash <sup>c</sup>	7.1	6.8	6.1	5.4
C	49.0	48.8	49.0	47.8
H	6.3	6.3	6.0	6.1
N	4.5	4.5	2.4	2.7
S	0.4	0.4	0.5	0.4
O (by diff.)	32.7	33.2	36.0	37.7
HHV (MJ/kg)	19.8	20.5	17.8	18.8

<sup>a</sup>Giuntoli et al. [163]<sup>b</sup>as received basis<sup>c</sup>Ashed at 550°C

control translation stages which could be adjusted on the horizontal x and y plane with a precision up to 25  $\mu\text{m}$ .

In order to minimize the influence of the surface properties of the foil on the actual emissivity of the material, before any series of measurements the “fresh” foil was heated up to 1100°C for 1 minute under helium atmosphere. The emissivity was found to be equal to 0.75 at a temperature of about 300°C.

### 6.2.3 Materials

The fuels analyzed in this work are: dry distiller’s grains and solubles and palm kernel cake. The proximate and ultimate analysis of all the fuels is given in Table 37 for the sake of clarity. More detailed information on the composition and origin of the fuels can be found in Chapter 3.

The two fuels studied here underwent a pre-treatment of leaching in water according to the methodology described in Chapter 3. The conditions of the pre-treatment are summarized in Table 38. The elemental analysis of the ash forming matter in the samples is illustrated in Table 39. Additional considerations on the pre-treatments and their effects on fuel properties and reactor operations can be found in previous chapters.



Table 38: Details of the pre-treatments applied to the fuels.

Sample	Particle Size Distribution	Water-to-Mass ratio	Time
Dry Distiller's Grains Solubles Leached	4 mm > D <sub>p</sub>	44.4 g/L	24 h
Palm Kernel Cake Leached	4 mm > D <sub>p</sub>	88.9 g/L	24 h

Table 39: Elemental analysis of the ash forming matter. Data are on a dry basis.

	DDGS <sup>a</sup>	DDGS Leached <sup>a</sup>	PKC	PKC Leached
Al <sub>2</sub> O <sub>3</sub>	0.2	0.4	4.4	5.2
SiO <sub>2</sub>	22.4	24.9	16.2	17.8
CaO	2.9	3.9	9.3	11.3
MgO	7.3	8.2	8.2	8.5
Fe <sub>2</sub> O <sub>3</sub>	0.4	0.5	11.5	12.4
K <sub>2</sub> O	22.7	22.4	14.0	12.3
Na <sub>2</sub> O	2.7	1.8	0.4	0.1
TiO <sub>2</sub>	0.01	-	0.1	0.2
SO <sub>3</sub>	9.5	2	9.2	2.4
Cl <sup>-</sup>	2.9	0.9	3.3	0.0
P <sub>2</sub> O <sub>5</sub>	29.0	32.4	23.7	25.4

<sup>a</sup>Giuntoli et al. [163]

#### 6.2.4 Numerical model

The numerical model introduced in this work was developed using the commercial finite elements code called Multiphysics version 3.5, developed by COMSOL. It was decided to model only the main reactor chamber of the setup and the geometry used is illustrated in Figure 92.

The equations implemented in the model were the following:

- General heat transfer equation, including conduction, convection and radiation. The specific equation used was the following:

$$\rho C_p \frac{\partial T}{\partial t} + \nabla \cdot (-k \nabla T) = Q + q_s T - \rho C_p \mathbf{u} \cdot \nabla T \quad (6.1)$$

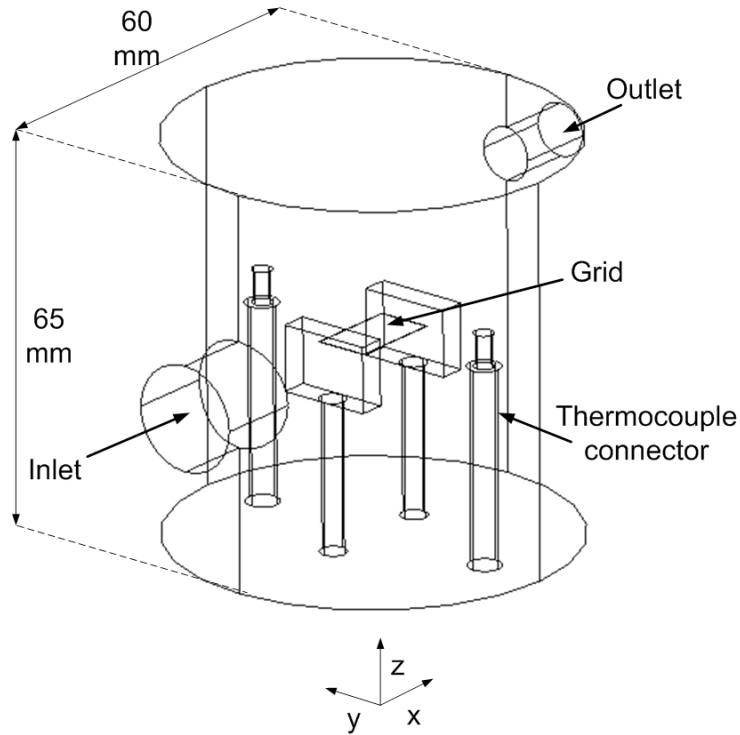


Figure 92: Geometry of the heated foil reactor used in the numerical model.

Table 40: Boundary conditions for the general heat transfer equation.

Boundary	Condition
Inlet	$T = T_0$
Outlet	$-\mathbf{n} \cdot (-k\nabla T) = 0$
External boundaries	$T = T_0$
Internal boundaries	$-\mathbf{n}_u \cdot (-k_u \nabla T_u) - \mathbf{n}_d \cdot (-k_d \nabla T_d) = 0$
Foil boundaries	$-\mathbf{n}_u \cdot (-k_u \nabla T_u) - \mathbf{n}_d \cdot (-k_d \nabla T_d) = \epsilon \sigma (T_{amb}^4 - T^4)$

The subscripts u and d stand for "up" and "down", that is the two sides of the surfaces

The meaning of the symbols used is given in the nomenclature.

The boundary conditions applied to this equations and the constant values used are summarized in Table 40 and 41.

- Conductive media equation, in order to model the resistive heating of the foil. The equation used was the following:

Table 41: Boundary constants for the general heat transfer equation.

Boundary	Temperature (°C)
Reactor walls	110
Reactor lid	95
Inlet	110

Table 42: Boundary constants for the conductive media equation.

Boundary	Equation
Electrode 1 bottom	$J_n = I(t)$
Electrode 2 bottom	$V = 0$
Other boundaries	$\mathbf{n} \cdot \mathbf{J} = \mathbf{0}$

$$-\nabla \cdot (\sigma_e \nabla V - \mathbf{J}^e) = Q_j \quad (6.2)$$

The boundary conditions applied to this equation are summarized in Table 42. The value of the input current,  $I(t)$ , was the actual current recorded during the measurements and illustrated in Figure 93.

- Weakly compressible Navier–Stokes equations to model the gas flow. The equations used were the following:

$$\rho \frac{\partial \mathbf{u}}{\partial t} + \rho \mathbf{u} \cdot \nabla \mathbf{u} = \nabla \cdot \left[ -p \mathbf{I} + \eta (\nabla \mathbf{u} + (\nabla \mathbf{u})^T) - \left( \frac{2\eta}{3} - \kappa \right) (\nabla \cdot \mathbf{u}) \mathbf{I} \right] + \mathbf{F} \quad (6.3)$$

$$\frac{\partial \rho}{\partial t} + \nabla \cdot (\rho \mathbf{u}) = 0 \quad (6.4)$$

The boundary settings applied to the weakly compressible Navier–Stokes equations are summarized in Table 43.

The following assumptions were applied:

- The temperature of the reactor walls, gas inlet and lid was assumed constant over time;
- Heat transfer via radiation was considered significant only for the foil and with effect only on the surrounding gases and not on the other reactor surfaces;
- The flow of the gases was laminar and incompressible since at the outlet of the reactor, where the velocities are maximum, the value of Reynolds

Table 43: Boundary conditions for the weakly compressible Navier–Stokes equations.

Boundary	Equation	Value
Inlet	$-(\mathbf{u}) = -\mathbf{U}_0 \cdot \mathbf{n}$	$U_0 = 0.218$
Outlet	$p = p_0$	$p_0 = 0$
Other boundaries	$\mathbf{u} = 0$	-

number was equal to approximately 40 and the Mach number was lower than 0.3;

- Buoyancy effects were accounted for using the Boussinesq approximation in the form of:

$$\mathbf{F} = (\rho - \rho_0) \mathbf{g} \quad (6.5)$$

This approximation holds when the flow can be considered incompressible and when the following condition holds:

$$\frac{\delta\rho}{\rho} = \alpha\delta T \ll 1$$

Due to the high gradients in the zone near the foil, this condition will not hold for the flow close to the foil. Such effect does not seem so relevant as to invalidate the results found.

- The physico–chemical properties of the materials and their relation with temperature were taken from the software’s own database.

The boundary conditions of the model were taken from the actual parameters of the real reactor. The model used as its main input the current input to the foil recorded during measurements on the real reactor, as shown in Figure 93. The other input used was the inlet velocity obtained from the volumetric flow of the pump.

## 6.3 RESULTS AND DISCUSSION

### 6.3.1 Numerical model: Temperature and velocity profiles

As mentioned before, the actual measurement of several important process parameters in the heated foil reactor is very difficult due to the speed of the phenomena involved and the small dimensions of the reactor. Therefore, the main goal of the numerical model presented in this work was to provide such important data as the temperature and velocity profiles in the reactor volume

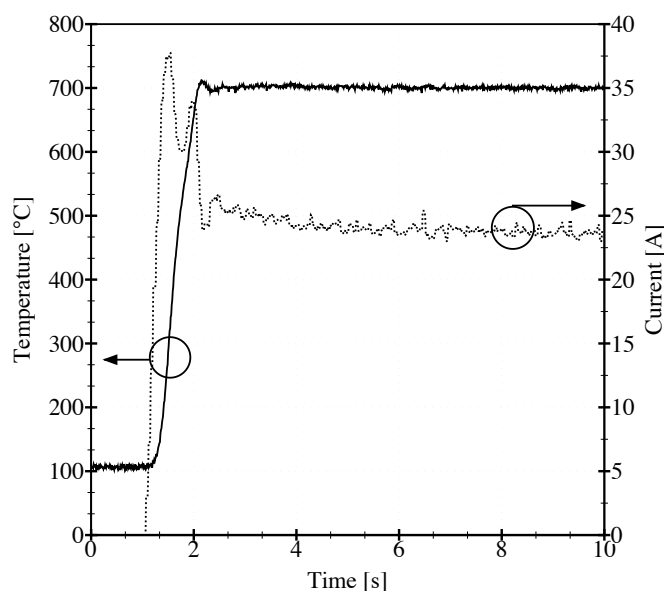


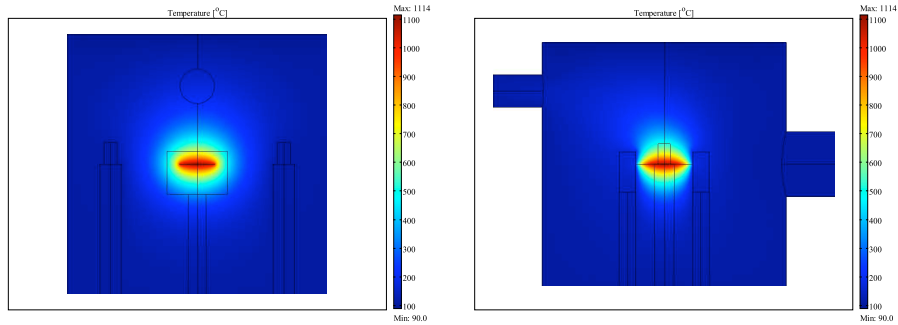
Figure 93: Experimental current intensity (dotted) and thermocouple reading (solid) with temperature setpoint=700 °C, HR=600 °C/s and HT=10 s.

and the temperature distribution on the foil. Knowing these data is of primary importance for a correct interpretation of the experimental results.

In order to quantify only the primary products of devolatilization, the gases released from the sample should be swept quickly into a cold zone of the reactor, the same way as it is done in other equipments such as thermogravimetric analyzers [163]. However, as it is shown in Figures 94 and 95, the real situation in a heated foil reactor is different. The gases, once released from the sample, are in a zone of low velocity and high temperature, so that secondary reactions in this area are likely to happen, especially at higher foil temperatures. As seen in Figure 94, even approximately 6 mm above the hot foil the temperature is still about 450 °C, sufficient for significant tar cracking [266].

Moreover, most of the gases are released within the first few seconds of the run and are then circulated by the pump. Considering the volumetric flow of the pump, a whole reactor volume is recirculated approximately every 5 s. This means that the gases released have the chance to flow once again through the hot zone above the foil. This might cause significant secondary decomposition of the tar volatiles [266].

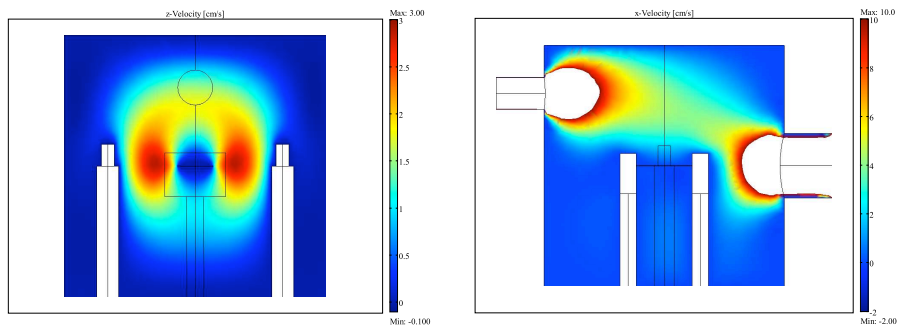
As it can be observed in Figure 95 and 96, the flow in the proximity of the foil is mostly driven by forced convection. The velocity in the x direction is approximately 1 cm/s at 3 mm above the hot surface and it quickly increases to 4 cm/s at a position 10 mm above the foil. The vertical velocity, in the z



(a) Distribution in the y-z plane

(b) Distribution on the x-z plane

Figure 94: Temperature distribution in the heated foil reactor for  $T_{TC}=1000\text{ }^{\circ}\text{C}$ ,  $HR=400\text{ }^{\circ}\text{C/s}$  and  $HT=10\text{ s}$ .



(a) Distribution in the y-z plane

(b) Distribution on the x-z plane\*

Figure 95: Velocity distribution in the heated foil reactor for  $T_{TC}=1000\text{ }^{\circ}\text{C}$ ,  $HR=400\text{ }^{\circ}\text{C/s}$  and  $HT=10\text{ s}$ .

\*The colourless areas in Figure 95b indicate zones in which the values of velocity are much higher than the maximum scale imposed in the plot for the sake of clarity.

direction, is instead approximately  $0.8\text{ cm/s}$  at a position  $5\text{ mm}$  above the foil and it peaks at  $1.8\text{ cm/s}$  at  $10\text{ mm}$ .

Figure 96 gives an illustration of the velocity magnitude and orientation over the centerline of the foil and the corresponding temperature. Remembering that the usual sample pill thickness is approximately  $0.7\text{ -}1\text{ mm}$ , when the temperature of the foil is set to  $1100\text{ }^{\circ}\text{C}$ , the volatile gases will encounter an

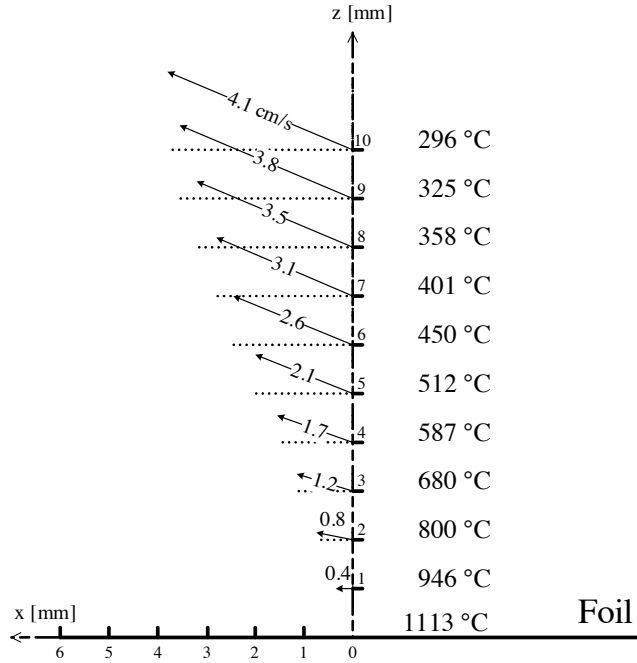


Figure 96: Velocity magnitude and direction over the foil. x-z plane for  $T_{TC}=1000\text{ }^{\circ}\text{C}$ ,  $HR=400\text{ }^{\circ}\text{C/s}$  and  $HT=10\text{ s}$ .

environment which is still very hot. Therefore, considering a worst case scenario, for which the gases are released without a vertical velocity at the top of the pill, such gases will have a residence time of about 1 s at  $800\text{ }^{\circ}\text{C}$  before they are transported out of the influence of the hot foil.

### 6.3.2 Numerical model: Temperature validation

Another very important parameter that can be analyzed thanks to the model is the actual temperature on the grid and its spatial distribution. It has been suggested in previous works, in fact, that measuring the grid / foil temperature with a thermocouple could introduce a significant error [175, 292]. Our model, as shown in Figure 94, also seems to indicate the actual temperature to be higher than the one recorded by the TC. This is due to several causes: the temperature drain introduced by the TC in the contact place, the heat loss via the tip and wires of the TC and, mostly, the non-perfect contact between the TC and the foil.

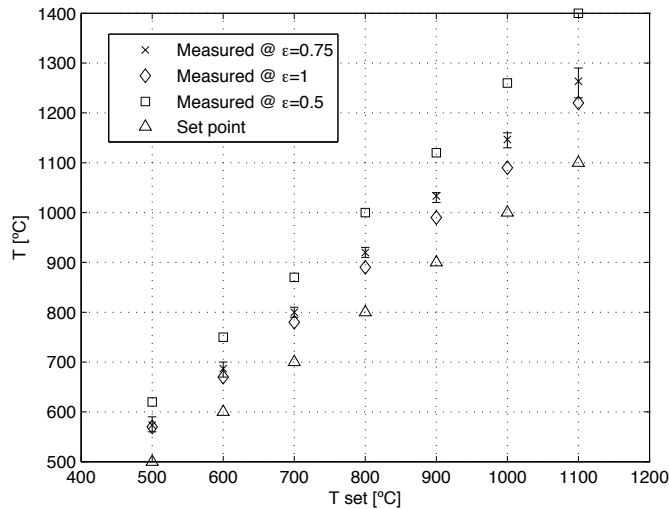


Figure 97: Temperature measured by thermocouple and IR pyrometer with different emissivity values

### 6.3.2.1 Actual foil temperature

Guo [175] simulated the heat loss via a thermocouple (TC) welded (thus in perfect contact) to the grid surface in a heated grid reactor and found out that, for a TC diameter of 0.1 mm already one could expect a difference equal to 2 to 5 % between the TC reading and the actual grid temperature. Prins et al. [292], using laser thermometry, found out that this difference ranged from 10% up to 25%.

As mentioned above, in the present work, it was chosen to analyze the foil temperature via an InfraRed pyrometer. After the foil was pre-treated in helium at 1100 °C for one minute, the pyrometer was used to measure the actual temperature on the foil surface; the results are shown in Figure 97.

The emissivity of the pre-treated foil was found to be equal to 0.75 at approximately 300 °C. In order to estimate the possible error introduced by this value, measurements were performed with assumed emissivity values equal to 0.5 and 1. As it can be seen from Figure 97, at all temperatures the reading of the pyrometer resulted in values higher than the actual TC setpoint, even considering an emissivity of 100%. Such difference resulted in approximately 70 to 110 °C above the TC reading at 500 °C and even higher differences at 1000 °C, of about 100 to 250 °C. The case with  $\epsilon = 0.5$  is to be considered, however, as an extreme case since the emissivity of the considered stainless steel AISI 304 is known to actually increase with temperature [303].

Considering all the elements of uncertainty regarding the temperature measurements, the model can help to point out the actual values. Figure 98 shows



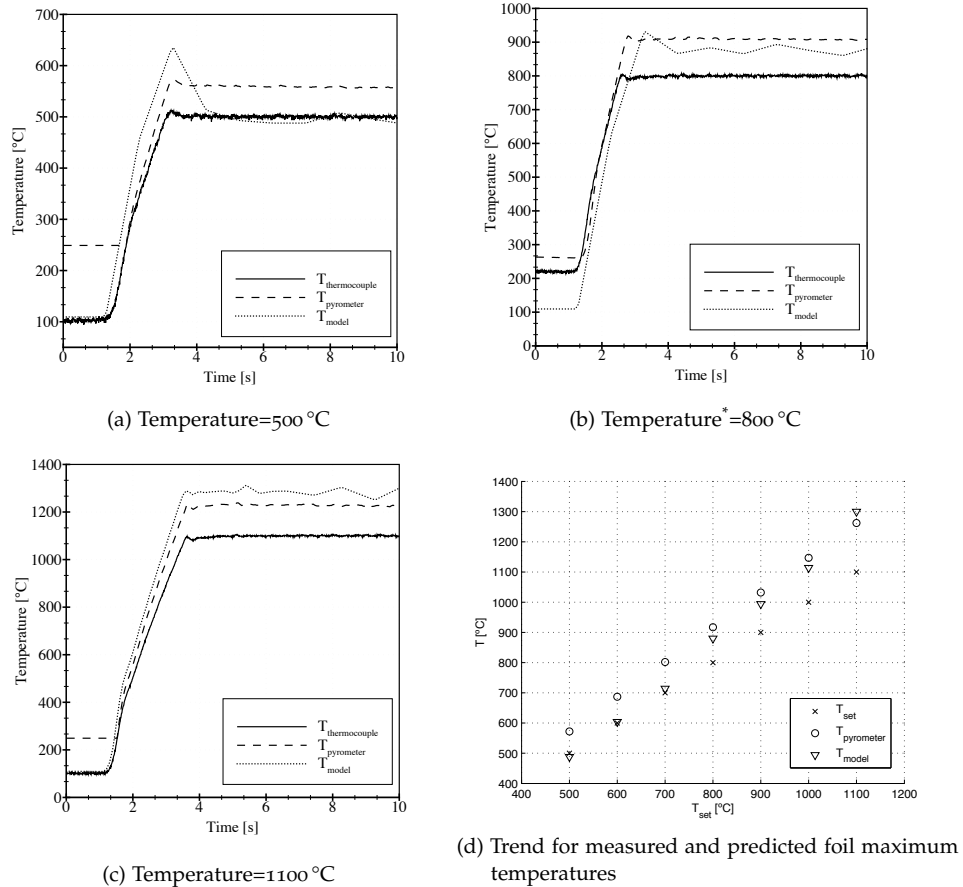


Figure 98: Measured and predicted temperatures of the foil at different setpoints at HR=600°C/s and HT=10s. The model uses an emissivity of  $\epsilon=0.75$  for the foil surface.

\*The TC signal in this case starts at a higher value due to thermal storage in the electrodes after a series of measurements

the comparison between the readings from the TC, the pyrometer and the predictions of the model at different setpoints. It is possible to see that at low temperatures, the model predicts values close to the temperature measured by the TC. At temperatures above 700°C, however, the model predictions follow the reading of the pyrometer much more closely, indicating temperatures much higher than the ones indicated from the TC.

Each of these trends has its pros and cons. The pyrometer reading, for example, is supposed to be very precise (within 1% of the spot temperature), but the actual emissivity influences the final measurement so as does the actual measurement point. The issues with the TC were mentioned above, while the model does not account for the actual surface conditions of the foil. Our view

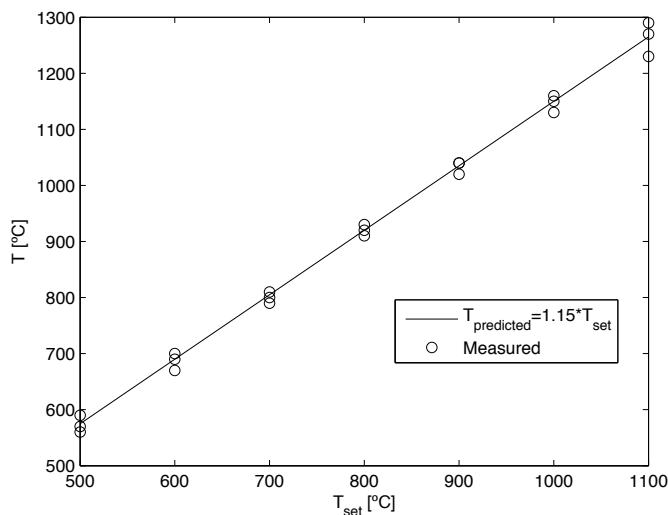


Figure 99: Relation between the temperature measured by the pyrometer with  $\epsilon = 0.75$  and the thermocouple

on this issue is that, while at low temperatures the emissivity of the foil does not play an important role (as shown in Figure 97), the pre-treated foil might have suffered some changes in its electrical and physical properties that are not accounted for in the model, explaining the lower value compared to the pyrometer measurement. At higher temperatures, instead, closer to the conditions at which the foil has been pre-treated, the pyrometer and the model give similar results and the differences should be attributed to small discrepancies in the values of emissivity. The model, in fact, uses a fixed value of  $\epsilon=0.75$ , while the emissivity of the actual foil might change with temperature.

In view of these results it was decided to use the pyrometer reading as the “correct” foil temperature and the relation shown in Figure 99 was found between the actual temperature and TC reading. The values of the setpoints used in the actual measurements were, therefore, modified to comply with the recorded difference of 15%.

### 6.3.2.2 Spatial distribution of temperature on the foil surface

Another important factor to consider in a heated grid reactor is the spatial distribution of temperature on the foil surface. Prins et al. [292] have shown a non-uniform distribution of temperature over their grid. This phenomenon could have a significant effect on the pyrolysis process since different part of the sample would be subjected to different heating rates and final temperatures.

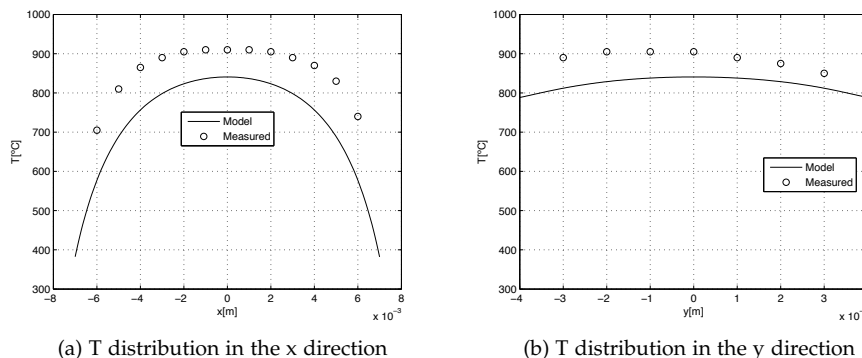


Figure 100: Temperature distribution over horizontal and vertical medians of the foil at  $T=800\text{ }^{\circ}\text{C}$ .

Figure 100 shows an example of the temperature distribution over the median lines of the foil along the  $x$  and  $y$  axis, as indicated in Figure 92, at a temperature of  $800\text{ }^{\circ}\text{C}$ .

Despite the difference in absolute values, that has been explained in the previous section, the model again agrees reasonably well with the pyrometer measurements. What can be noticed from these data is that the temperature is quite well homogeneously distributed in the longitudinal direction ( $x$ -axis) so that for the central  $6\text{ mm}$  of the foil the temperature is basically constant. This is also the case in the  $y$ -direction where, however, it is possible to notice an asymmetry on the right side due to a non-perfect contact of the foil with the electrode which caused a non-homogeneous current distribution. However, this did not seem to influence significantly the temperature distribution over the whole foil.

### 6.3.2.3 Practical recommendations

From such a simple numerical model as the one described above, it was possible to gather many useful practical recommendations.

- The presence of a hot zone above the heated foil is likely to cause the cracking of tars and other heavier volatiles as well as favour other homogeneous reactions: the volatiles detected should be, therefore, considered as products of primary and secondary devolatilization.
- The actual temperature of the foil and, consequently, of the sample, has to be considered higher than the actual temperature indicated by the control thermocouple: according to the present and previous works [175, 292] the difference between actual foil temperature and TC reading has to be considered in the order of 10 to 15 %.

- The temperature distribution on the surface of the foil appears to be more homogeneous than on a grid, as shown by Prins et al. [292]. The sample positioning on the foil, therefore, does not appear to be of extreme importance.

### 6.3.3 Experimental results

Once the physical conditions in the reactor were clarified thanks to the numerical model described above, the necessary corrections were applied to the equipment. The temperature indicated in the following plots should, therefore, be considered as the one measured by the IR pyrometer and not the one indicated by the control TC.

The weight loss of all the samples, on a dry and ash free basis, at different temperatures is shown in Figure 101. These data show that at high heating rates even at a relatively low temperature of 500 °C the carbonaceous residue amounts to about 26 %wt<sub>daf</sub>. Devolatilization proceeds significantly up to 900 °C where the char is reduced down to 11 - 14 %wt<sub>daf</sub>. Above 900 °C, there seems to be a plateau at 1000 °C and 1100 °C in which no more material is lost, while again some additional 2 - 3 % of material is lost between 1100 °C and 1300 °C. The final weight loss at very high temperature of 1300 °C is approximately 90 %wt<sub>daf</sub> for PKC and 92 %wt<sub>daf</sub> for DDGS.

These results differ significantly from what was obtained at slower heating rates. In a previous study we studied the devolatilization of DDGS and its leached sample at a heating rate of 10 °C/min [163] and found a weight loss equal to 77.5 %wt<sub>daf</sub> at 500 °C with a final weight loss of 83.1 %wt<sub>daf</sub> at 900 °C. Di Nola et al. [278], Di Nola et al. [140] found consistent results on weight loss between slow and fast pyrolysis measurements. Similar results were found by Becidan et al. [99] who also studied slow and fast pyrolysis of different biomass residues. They reported that the residual char for measurements with a heating rate of 10 °C/min and final temperature equal to 900 °C was much lower compared to the one obtained at high heating rates at the same reactor temperature.

It is quite commonly found in pyrolysis of biomass fuels [114, 115] that higher heating rates and high final temperatures maximize gas yield and minimize char residues, coherently with the results obtained here.

In terms of absolute values, the results obtained in this work appear to correspond to the ones reported by Di Nola et al. [140] who showed weight losses of about 87 - 95 %wt<sub>daf</sub> at 1000 °C for chicken litter and meat and bone meal samples and almost no carbonaceous residue for both samples at higher temperatures. Becidan et al. [99], found higher char residues of about 20 %wt<sub>daf</sub> at a temperature of 900 °C but, apart from the differences due to the different materials, the reactor configuration most probably played a major role: the reactor used by Becidan and coworkers, in fact, was a macro-TGA with a sample size of 75 g and, as shown in another work [97], actual heating rates

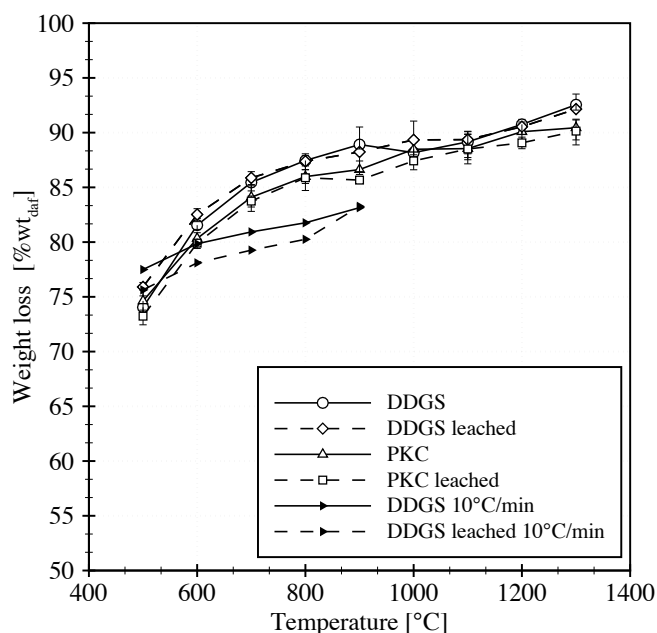


Figure 101: Weight loss in function of the foil temperature for all the samples at  $HR=600\text{ }^{\circ}\text{C/s}$  and  $HT=10\text{ s}$ .

of only about  $150\text{ }^{\circ}\text{C/min}$ . The combination of higher sample mass and lower heating rates, both conditions which favour char forming reactions, explains the difference with the present results. Stubington and Aiman [60, 328] in their work on sugar cane bagasse found higher differences when comparing results at slow and fast heating rates: a weight loss of about  $96\text{ } \%wt_{daf}$  at  $800\text{ }^{\circ}\text{C}$  and  $1000\text{ }^{\circ}\text{C/s}$  compared to  $86\text{ } \%wt_{daf}$  at  $800\text{ }^{\circ}\text{C}$  and  $5\text{ }^{\circ}\text{C/min}$ . Other works on fast pyrolysis of biomass samples on different reactors are consistent with the results presented here [146, 154, 279, 357].

### 6.3.3.1 Kinetic analysis

In the previous Chapters 3, 4 and 5 it was introduced the method used to obtain the kinetic parameters for slow pyrolysis processes.

The data retrieved under slow pyrolysis conditions for the reactivity of DDGS, as illustrated in Chapter 5 and summarized in Table 44, were extrapolated to a heating rate of  $600\text{ }^{\circ}\text{C/s}$ .

The result is illustrated in Figure 102. These results should be considered as preliminary since more measurement points are needed for an accurate evaluation.

However, from these data it is possible to conclude that the weight loss at high temperatures and high heating rates could be extrapolated from slow

Table 44: Activation energy distribution obtained at slow heating rates for DDGS.

Activation Energy (kJ/ mol )	Abundance (%)
104	3.4
110	0.9
115	0.4
121	1.0
126	1.5
132	1.9
136	2.4
143	3.7
148	3.3
154	6.2
159	9.3
165	11.4
170	1.6
176	23.1
181	2.1
187	6.1
192	0.9
198	7.3
203	2.4
209	4.0
214	1.5
220	2.4
225	0.7
231	0.0
236	2.7

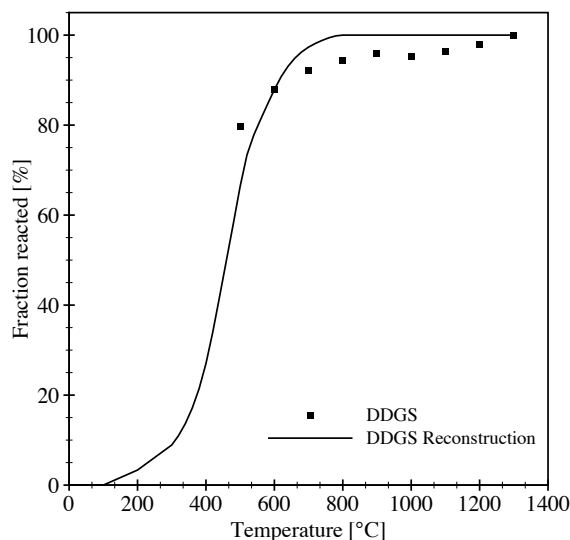


Figure 102: Kinetic reconstruction of the reactivity of DDGS sample using kinetic data retrieved on slow pyrolysis measurements

pyrolysis measurements. However, as it will be described in the following sections, the yields of volatile species, and especially volatile-N, seem to differ substantially from the ones retrieved from thermogravimetric experiments.

### 6.3.3.2 Product partitioning

Figure 103 shows the product distribution from all the samples tested at different final temperatures. At a temperature of 500 °C for all the samples most of the weight loss is due to tars and undetected light species, such as  $H_2$ , with yields of about 60 %wt<sub>daf</sub>. Light gases make up for only about 10 - 15 %wt<sub>daf</sub> of the initial mass and still approximately 25 %wt<sub>daf</sub> of char is left. These results are consistent with typical biomass pyrolysis applications: for moderate temperatures, high heating rates and low residence time of the vapours, Bridgwater [115] indicates typical oil yields of about 75 %wt<sub>dry</sub>. The maximum of tar content for the fuels studied is obtained at about 700 °C with a content of about 70 %wt<sub>daf</sub>. At this temperature the slopes of the light gases and char curves appear to change and while both tar and char decrease at higher temperatures, the yield of gases increases due to the final char evolution but also to the secondary reactions of tar cracking. Similar trends were reported in previous works [176, 279, 328], even though in the present work no actual plateau is reached for the species release, indicating probably severe secondary reactions at very high temperatures, as it will be shown later on.

At a temperature of 900 °C, typical for fluidized bed biomass combustion or gasification, the yield of light volatiles is around 24 - 27 %wt<sub>daf</sub>.

The differences among the untreated and leached samples are minimal as are the differences among DDGS and PKC which appear to have an almost identical product distribution.

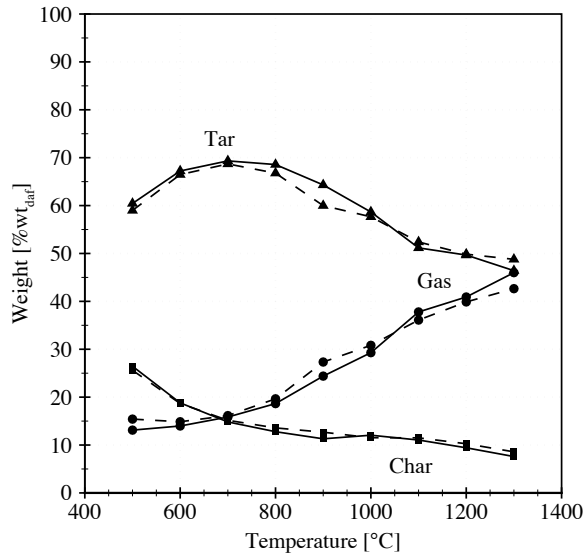
### 6.3.3.3 *Main volatile species release*

Figure 104 shows the release of the main volatile species from all the studied fuels. Analyzing these results, it is possible to see that CO<sub>2</sub> is the main light gas released at low temperatures starting from a yield of 9 - 11 %wt<sub>daf</sub> at 500 °C and reaching a steady value of about 15 - 16 %wt<sub>daf</sub> at 1100 °C. CO is only a minor compound for temperatures lower than 700 - 800 °C with yields of about 5 %wt<sub>daf</sub> but it increases greatly at higher temperatures to reach yields of about 20 - 25 %wt<sub>daf</sub>. This trend corresponds to the observed decrease in tar content, indicating that a partial source for CO might be the cracking of heavier volatiles in the hot zone surrounding the foil, as evidenced in the previous section. However, in a previous work, we have described how, even at low heating rates, a steep release of CO was recorded when the char was heated at 900 °C for 30 min [163]. This behaviour could be explained with an additional evolution of heavier structures that had re-condensed in the solid structure during the process of devolatilization. In slow pyrolysis tar cracking is not considered relevant since the gases are swept very quickly from the hot area via a large flow of a cold, inert carrier gas.

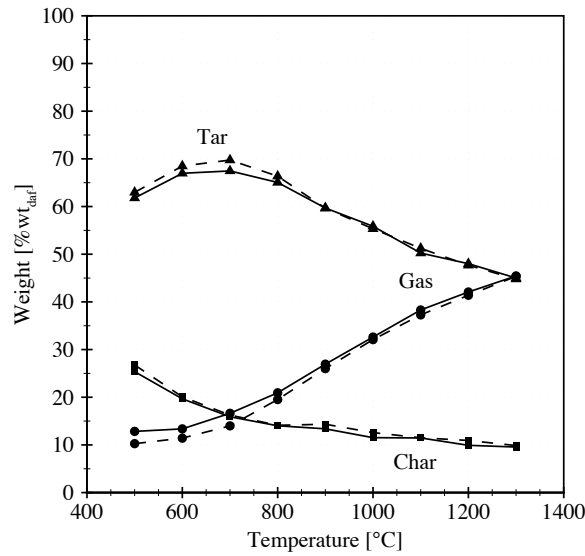
The yields of CH<sub>4</sub> are minor compared to other species. Most of the release of methane happens at temperatures higher than 900 °C. This was found also for experiments at lower heating rates in which CH<sub>4</sub> is usually released at higher temperatures than the other species [159, 163].

Table 45 summarizes some of the available studies on flash pyrolysis of biomass fuels. It appears evident that, despite the different techniques and materials, the release of main volatile species is quite consistent among the measurements, clearly indicating the common origin of these species. CO<sub>2</sub> release from pure cellulose does not appear to make up for the whole yield, as expected; decomposition of hemicellulose and lignin are also expected to release carbon dioxide when their sugar structures decompose. The behaviour of CO is also quite consistent among different materials with yields around 20 %wt<sub>daf</sub> and monotonous increase with increasing temperatures. In Table 45, moreover, results from slow pyrolysis are also reported. These data indicate that the yield of CO for DDGS is similar at 900 °C for very different heating rates, approximately 7 - 8 %wt<sub>daf</sub>, and that an isothermal period of 30 min after slow heating appears to have the same effect as an increase of final temperature at high heating rates. This might indicate indeed that the source of this yield is not only structural but comes from tar cracking, either inside the



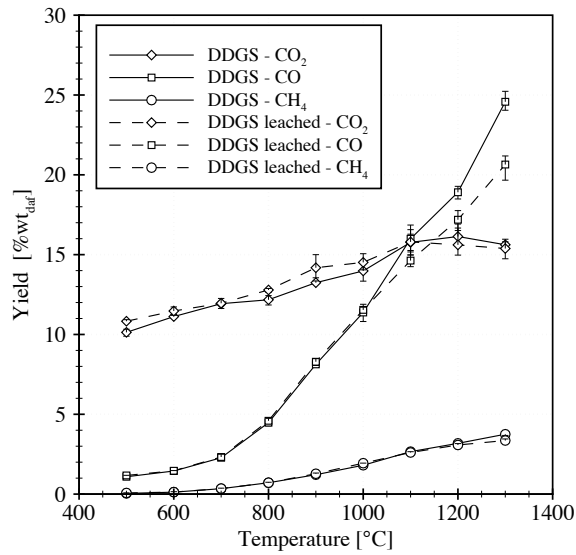


(a) DDGS untreated (solid) and leached (dashed)

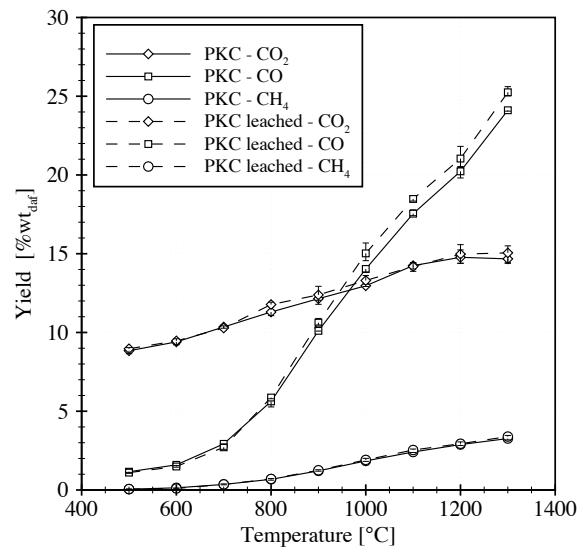


(b) PKC untreated (solid) and leached (dashed)

Figure 103: Product distribution for all samples at HR=600 °C/s and HT=10 s. Gas = Sum of yields of CO, CO<sub>2</sub>, CH<sub>4</sub>, NH<sub>3</sub>, HCN and pyrolytic water. Tar = Weight loss - char - gas.



(a) DDGS



(b) PKC

Figure 104: Yield of main gaseous species at HR=600 °C/s and HT=10 s.

char structure (in slow pyrolysis) or in the hot zone surrounding the foil (in fast pyrolysis).

Methane yield appears to be constant at around 3 %wt<sub>daf</sub> for many biomass fuels, a value which is almost double compared to what is found at slow heating rates [90, 159, 163], indicating also a possible origin from secondary tar decomposition.

Caballero et al. [121] showed that the yields of CO, CO<sub>2</sub> and H<sub>2</sub>O for fast pyrolysis of almond shells could actually be predicted from the yields of its main structural components (holocellulose and lignin). From their experiments it is possible to conclude that lignin is the main precursor for CO, CH<sub>4</sub> and water, while holocellulose and lignin share their contribution for CO<sub>2</sub> release. Methane release was, however, higher than the weighted sum of the release from the main components, indicating probably additional cracking due to the interaction among the components.

#### 6.3.3.4 Nitrogen volatile species release and partitioning

While data on the main gaseous species are available in literature, much less is known about the release of light nitrogen volatiles which, however, are fundamental for syngas quality and for NO<sub>x</sub> prediction in biomass combustion [164].

As mentioned above, DDGS and PKC present a high nitrogen content compared, for example, to woody biomasses [147, 204] and most of it is in the form of proteins. Among several devolatilization mechanisms, which are clearly illustrated in the work of Becidan [95] and in Chapter 2, the ones who are believed to be the most common in proteins pyrolysis are:

- Primary decarboxylation with the consequent formation of amines and CO<sub>2</sub> [295, 313]
- Dehydration with the formation of an intermediary cyclic amine, commonly 2,5-diketopiperazine (also called DKP) [180, 295, 310, 312, 313, 353].
- Cross-linking of proteins containing amino-acids with reactive side chains, e.g. lysine [302] was found to produce NH<sub>3</sub> and char-N [180].
- Another path relevant in slow pyrolysis of pure amino acids was found to be deamination or direct thermal loss of the final amino groups from free amino-acids or polypeptides[244, 245].

Secondary devolatilization of DKP, finally, is known to produce mainly HCN with minor amounts of HNCO and NH<sub>3</sub>, depending on the type of fuels and conditions. Hansson et al. [181], for example, reported more than 80% conversion of DKP to HCN at 1000 - 1100 °C under fast pyrolysis conditions.

This said, however, as shown in Tables 9 and 10 in Chapter 2, the relative amounts of HCN and ammonia vary greatly with process conditions and fuels.

Table 45: Yields of main light volatile species in flash pyrolysis conditions.

Sample	Setup	Heating rate	T (°C)	CO <sub>2</sub> (%wt <sub>daf</sub> )	CO (%wt <sub>daf</sub> )	CH <sub>4</sub> (%wt <sub>daf</sub> )	Ref.
Cellulose	Entrained flow	drop	900	6.5	65	7	[309]
Cellulose	Heated grid	1000 °C/s	1000	3 <sup>a</sup>	23 <sup>a</sup>	3 <sup>a</sup>	[176]
Maple wood	Entrained flow	drop	800	9	35	4.5	[309]
Sweet gum hardwood	Heated grid	1000 °C/s	1200	6.1 <sup>b</sup>	17 <sup>b</sup>	2.3 <sup>b</sup>	[279]
Wood chips	Packed bed	Isothermal	700	13.6	13.6	2.4	[138]
Wheat straw	Packed bed	Isothermal	700	18.2	10.4	2.4	[138]
Olive husks	Packed bed	Isothermal	700	18	7.7	2.6	[138]
Coffee waste	Macro-TGA	200 °C/min	900	32	20	6	[99]
Brewer spent grains	Macro-TGA	200 °C/min	900	18	20	6	[99]
Fiberboard	Macro-TGA	200 °C/min	900	20	25	6	[99]
Chicken litter	Heated grid	1000 °C/s	1200	28	25	3	[140]
Meat and bone meal	Heated grid	1000 °C/s	1200	17	14	4	[140]
DDGS	Heated foil	600 °C/s	1200	16	19	3	This work
PKC	Heated foil	600 °C/s	1200	15	20	3	This work
DDGS	TG-FTIR	10 °C/min	900	8-9 <sup>c</sup>	6-17 <sup>c</sup>	1.6-1.6 <sup>c</sup>	[163]

<sup>a</sup>as received basis<sup>b</sup>dry basis<sup>c</sup>holding time=0 min - holding time=30 min

Figure 105 shows the release of nitrogen species from the DDGS and PKC samples at 600 °C/s.

The first observation is that HCN is the main compound for all the fuels, with even no significant detection of NH<sub>3</sub> for PKC. A similar yield of HCN and ammonia is found at low temperatures for DDGS while, with increasing temperature, HCN increases largely while NH<sub>3</sub> only increases up to a value of 0.2 %wt<sub>daf</sub>. When compared on the relative basis of initial nitrogen, as shown in Figure 106, the release of HCN for PKC and DDGS and their washed samples is very similar up to 900 °C with a fuel-N conversion of about 7 - 8%. With increasing temperature, no difference is basically visible for the PKC and PKC leached sample, while the leaching appears to facilitate the conversion of fuel-N to HCN and ammonia for DDGS. At very high temperatures, the final conversion of fuel-N to HCN results to be around 20% for DDGS and 25% for the other samples. As mentioned above, no ammonia was detected for PKC, while around 3% of initial nitrogen in DDGS was converted to NH<sub>3</sub> and more than 5% for the leached sample. A possible explanation for the lower yield of ammonia from the PKC samples could reside in the much higher Fe content of these samples which could catalyze the decomposition of internally formed NH<sub>3</sub> to molecular N<sub>2</sub> [286].

Compared to the results obtained under slow pyrolysis conditions for DDGS and its washed sample [163], as indicated in Table 9 in Chapter 2, it is possible to see that at an equal temperature of 900 °C both the yields of ammonia and HCN are greatly lower at high heating rates. However, at higher temperatures, the final yield of HCN is higher than what measured at low heating rates with values of 1.9 %wt<sub>daf</sub> and 2.3 %wt<sub>daf</sub> for DDGS and DDGS leached, respectively. Even the total yield of NH<sub>3</sub> results lower than the one measured at low heating rates, indicating that the difference might not lay only in the different kinetics but in different mechanisms of reactions.

If one looks more carefully into the results of the slow pyrolysis measurements, as described in our previous work [163], one should notice that the release of ammonia was basically divided into two parts: a first peak at low temperatures with no other N-species associated and a second one at higher temperatures in correspondence with the release of HCN and HNCO. Such behaviour can be interpreted as a first step of deamination and dehydration of the protein chains with consequent formation of cyclic amines in the solid structure, followed by the secondary decomposition of DKP yielding HCN and HNCO. In case of fast pyrolysis, thus, it appears that the speed of the reaction does not allow the first step of deamination favouring thus instead the paths of decarboxylation and dehydration. This is sustained by previous works [198, 295, 310, 313] which have excluded a significant role of deamination during fast devolatilization of amino-acids and polypeptides.

The influence of the reactor configuration with possible catalytic decomposition of ammonia on the steel foil or absorption on the reactor walls cannot be completely excluded. However, the results obtained under combustion con-

ditions described in Chapter 7, indicate a lower fuel-N to NO conversion for DDGS compared to PKC which agrees with the present results: PKC releases much less ammonia than DDGS and the effect of the selective non-catalytic reduction of NO<sub>x</sub> is therefore limited.

The effect of the leaching on the DDGS sample appears to be consistent between slow and fast pyrolysis, increasing the yields of light N-species at all conditions. However, the measurement technique used in this campaign, the FTIR, cannot detect the release of molecular N<sub>2</sub> nor can it quantify tar-N, which implies that the higher yields of gaseous-N species could mean either less reduction of the volatile-N species to N<sub>2</sub>, which would be a negative effect for the overall process, or an improved decomposition of tar-N into lighter volatiles, which would instead be a favourable condition.

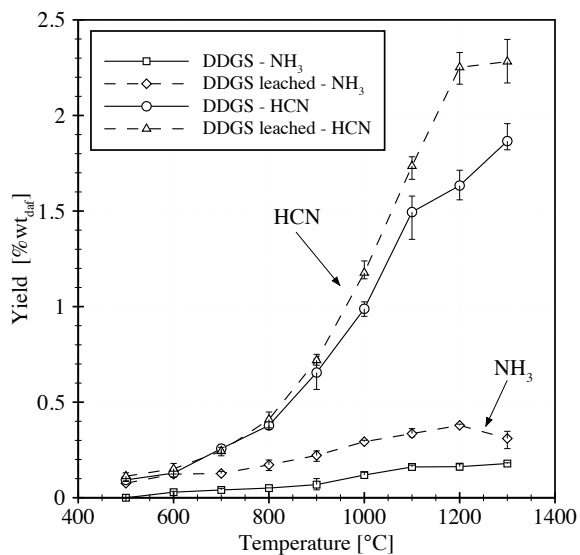
Compared to other works in the literature, as shown also in Table 10 in Chapter 2, the trends presented here are similar to the results illustrated by Di Nola et al. [140]. They found higher yields for HCN and NH<sub>3</sub> but this is not a surprise due to the much higher initial-N content of their studied fuels, chicken litter and meat and bone meal, and the different nature of their nitrogen structures. However, the trends they reported are very similar to our results with ammonia being the main compound at low temperatures but with HCN increasing steadily above 800 °C. Becidan et al. [98], instead, found quite different results, presenting ammonia as the main N-compound at every temperature up to 1000 °C. However, while the sample of brewer's spent grains should not differ much in composition compared to DDGS, the other samples, coffee wastes and fiberboard, are rich in caffeine and urea respectively, so a different devolatilization behaviour can be expected. Moreover, as mentioned above, the setup used in their work did not guarantee heating rates as high as in the present work (only in the range of 125 °C/min [97]) so that the process conditions actually seemed closer to slow pyrolysis than fast, thus not contradicting what was observed previously.

#### 6.3.3.5 Carbon and nitrogen partitioning

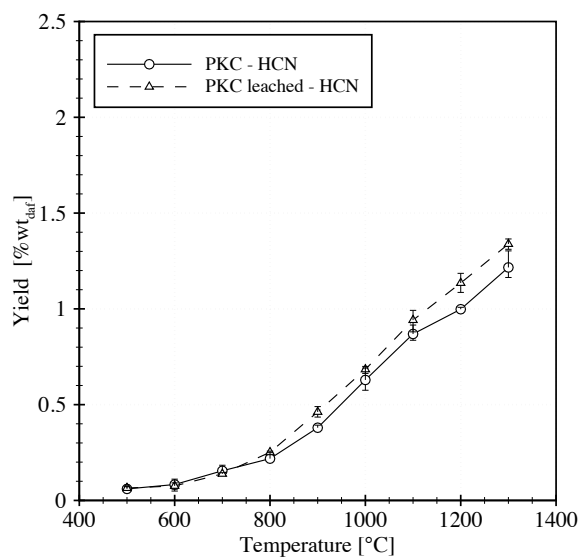
In order to better understand the actual evolution of C and N during flash pyrolysis, the partitioning of these elements was studied for DDGS and DDGS leached at two significant temperatures, as shown in Figure 107.

From Figure 107a, illustrating the C-partitioning, it is possible to substantiate the fact that tar cracking plays an important role at high temperatures: increasing the temperature from 900 °C to 1200 °C, the carbon content in the char only decreases about 3 - 4 % while the volatile-C increases by more than 10 - 14 %. As shown in the previous section, most of these increase is due to the CO released from the secondary cracking of tars.

The same can be deduced from Figure 107b, depicting the partitioning of nitrogen: for the DDGS sample, the char-N decrease amounts again to about 3 % while the volatile-N, especially in the form of HCN, increases by more



(a) DDGS



(b) PKC

Figure 105: Yield of nitrogen species at HR=600 °C/s and HT=10 s.

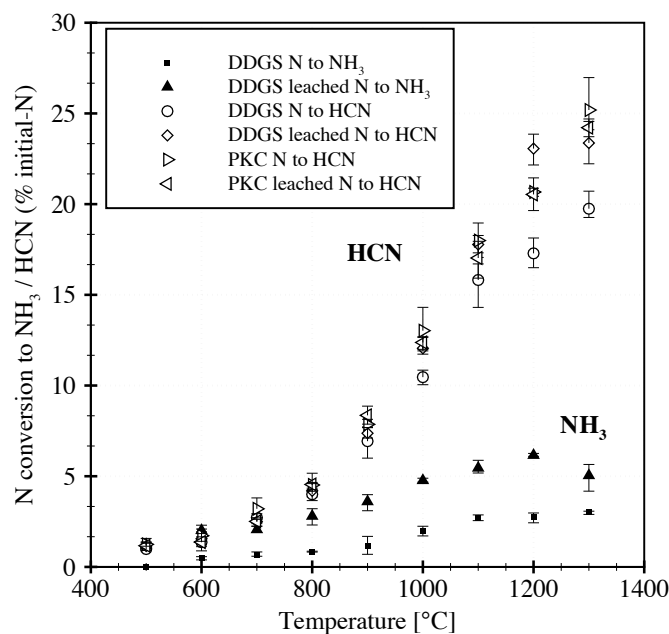


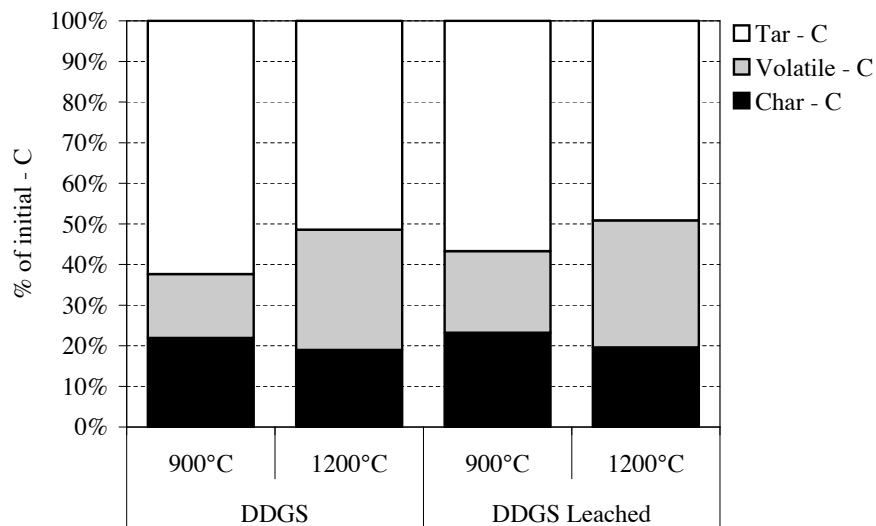
Figure 106: Fuel–N conversion to  $\text{NH}_3$  and HCN for all samples at  $\text{HR}=600\text{ }^\circ\text{C/s}$  and  $\text{HT}=10\text{ s}$ .

than 11%. This seems to suggest that most of the volatile–N release in these measurements originates from secondary reactions. As mentioned above, thus, the lower ammonia content compared to slow pyrolysis data can be explained with the lack of the deamination step which is apparently not possible at very high heating rates. Instead it is likely that a large part of the volatile–N is actually released as tar–N, including cyclic amines, which then decompose in gas phase reactions to release mostly HCN but also  $\text{NH}_3$  (linear amines).

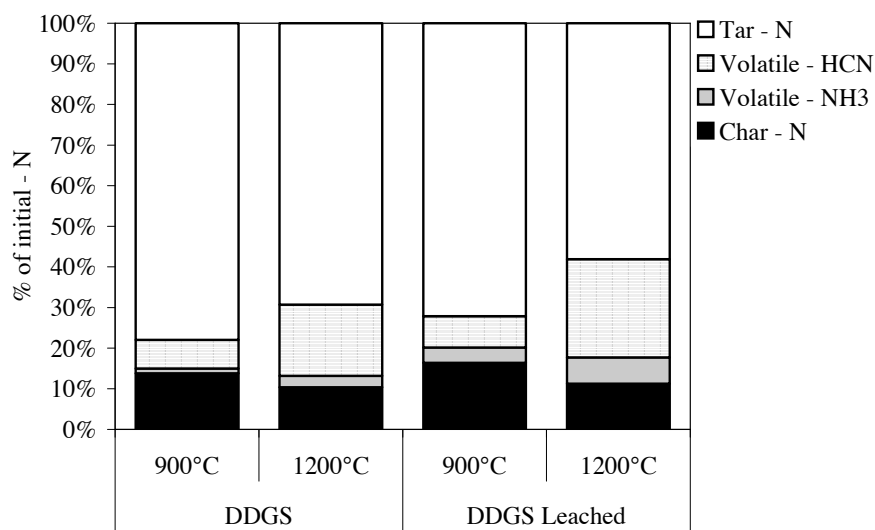
The presence of 10% of the initial nitrogen in the char structure even at high temperatures, indicates that a cross–linking reaction path exists favouring the formation of stable structures which are retained in the char. Such a mechanism was indeed observed in several works [180, 302] studying thermal decomposition of amino–acids; amino–acids (or proteins containing them) with reactive side chains tend to cross–link during pyrolysis and form char, as found, for example, for lysine [302].

The results for the washed sample of DDGS show that slightly more nitrogen is retained in the char compared to the untreated sample, especially at  $900\text{ }^\circ\text{C}$ , but mostly at the expense of tar–N (or molecular  $\text{N}_2$ ) since also the volatile–N part is higher than for untreated DDGS. As mentioned above, the current methodology does not allow to assess whether the leaching favours





(a) C-Partitioning



(b) N-Partitioning

Figure 107: Partitioning of carbon and nitrogen for DDGS and DDGS leached at HR=600 °C/s, HT=10 s and final temperatures of 900 °C and 1200 °C.

the decomposition of tar-N into lighter volatiles or if, instead, it inhibits the reduction of light volatiles to N<sub>2</sub>.

#### 6.4 CONCLUSIONS

A simple numerical model of a heated foil reactor was developed in this work. It was shown that a hot zone is created around the heating foil which is most likely to cause tar cracking especially at foil temperatures above 800 °C. The species detected in the measurements thus need to be considered a simultaneous contribution of primary and secondary devolatilization. Compared to other reactor types, however, the present configuration prevents serious interactions between the released volatiles and the remaining char.

The temperature of the foil was found to be approximately 15% higher than measured by the control thermocouple. Whenever using this type of reactor, therefore, a thorough investigation of the temperature field in the reactor and on the foil was found to be essential in order to accurately describe the experimental conditions.

The main gaseous species resulted to be CO<sub>2</sub> for all the samples at lower temperatures, while CO became important at temperatures higher than 1000 °C. The effect of the leaching in this respect appeared to be minimal for both DDGS and PKC, as it had been found also in slow pyrolysis conditions.

The main nitrogen compound released appeared to be HCN at every temperature, for both DDGS and PKC. Also NH<sub>3</sub> was detected from pyrolysis of DDGS but not from PKC. This difference could depend on the larger iron content in the PKC sample.

HCN resulted to be the most abundant nitrogen compound for all the samples, in contradiction with what was found at low heating rates. For slow pyrolysis conditions, thermal deamination of protein chains and amino-acids was found to be the main source of ammonia at low temperatures, followed by decomposition of cyclic amines and release of HCN, HNCO and NH<sub>3</sub> at higher temperatures. It appears that at higher heating rates, the first step is inhibited by the speed of the process, so that most of the nitrogen is released as cyclic amines which decompose successively in gaseous reactions into mainly HCN. This would explain the constant increase of HCN yield with temperature as tar-N decomposition becomes more important. Part of the NH<sub>3</sub> yield might also derive from gas phase reactions but cross-linking of proteins with reactive side groups is another likely source. This is supported by the presence of more than 10% of the initial nitrogen in the char of DDGS even at 1200 °C.

Preliminary results indicate that the global weight loss of DDGS could be reasonably predicted using kinetic parameters obtained at low heating rates. This was not valid for the yields of single volatile species.

The effect of leaching is negligible for PKC, while it appears to have a marked effect on the DDGS nitrogen partitioning. As it had been shown in slow pyrolysis experiments, the leached DDGS sample appears to yield more light volatiles than untreated DDGS but also more char-N. The higher content of nitrogen in stable char structures can partly explain the higher yields of

$\text{NH}_3$  recorded. However, the limitations in the measurement technique used do not allow to distinguish among two possible effects of the leaching: on one side it could improve tar-N decomposition into lighter volatiles but on the other side it could inhibit HCN and  $\text{NH}_3$  reduction to molecular nitrogen.

## NOMENCLATURE

- $C_p$  [kJ/kg\*K] = Specific heat capacity
- $F$  [N/m<sup>3</sup>] = Volume force
- $g$  [m/s<sup>2</sup>] = Gravity acceleration
- $I$  = Identity matrix
- $J^e$  [A/m<sup>2</sup>] = External current density vector
- $k$  [W/m\*K] = Thermal conductivity
- $n$  = Unity vector normal to the surface
- $p$  [Pa] = Pressure
- $q_s$  [W/m<sup>3</sup>\*K] = Production / absorption coefficient
- $Q$  [W/m<sup>3</sup>] = Heat source
- $Q_j$  [A/m<sup>3</sup>] = Current source
- $T$  [K] = Temperature
- $u$  [m/s] = Velocity vector
- $V$  [V] = Electric potential
- $\alpha$  [kg/m<sup>3</sup>\*K] = Coefficient of thermal expansion
- $\epsilon$  = Surface emissivity
- $\eta$  [Pa \* s] = Dynamic viscosity
- $\kappa$  [Pa \* s] = Dilatational viscosity
- $\rho$  [kg/m<sup>3</sup>] = Density of the fluid
- $\sigma$  = Stefan–Boltzmann constant =  $5.6707e - 8$  [W/m<sup>2</sup>\*K<sup>4</sup>]
- $\sigma_e$  [S/m] = Electric conductivity

# 7

---

## COMBUSTION CHARACTERISTICS OF BIOMASS RESIDUES: FATE OF FUEL-N

---

*After studying the detailed kinetic of slow pyrolysis (Chapters 4 and 5) and underlining the changes due to the higher heating rates encountered in industrial applications (Chapter 6), this chapter presents the results of measurements carried out under combustion conditions. The chapter introduces the results obtained from tests conducted in the SPR reactor at Åbo Akademi University. The experiments were carried out at conditions relevant for industrial applications such as fluidized-bed boilers. Commercially available analyzers were used to record the evolution of CO, CO<sub>2</sub> and NO from the samples. The characteristics of five different biomass wastes are compared and their fuel-N conversion to NO is analyzed.*

The contents of this chapter were adapted from the work published in:  
J. Giuntoli, W. de Jong, P. Piotrowska, M. Zevenhoven, A.H.M. Verkooijen  
and M. Hupa,

**"Combustion characteristics of biomass residues and bio-wastes: fate of  
fuel-N"**

*Energy & Fuels*, 24 (2010) 5309-5319 ; DOI: 10.1021/ef100571n.

© 2010 American Chemical Society. Reprinted with permission.

## 7.1 INTRODUCTION

In this chapter five biomass residues with high nitrogen content have been tested in a single-particle reactor to obtain fundamental data on their fuel N and their tendency to form NO. Under the usual conditions at which such fuels are combusted, in fact, the influence of thermal NO becomes irrelevant and all of the NO<sub>x</sub> emissions are caused by fuel-bound nitrogen, as explained in more details in Chapter 2. Therefore, a detailed knowledge of the nitrogen chemistry for such materials is essential for an efficient and cost-effective use.

Several studies have been conducted in the past on coal, peat and nitrogen model-compounds, as reported in details in Chapters 2 and 3 of this dissertation. More recently, interest has also shifted towards biomass samples and many studies are available on pyrolysis and combustion of different materials [98, 163, 165, 182, 202, 362, 278]. Such measurements generally show that NH<sub>3</sub> and HCN are the primary nitrogen products to be released in pyrolysis of coal and biomass. Their ratio varies greatly depending upon the nitrogen functionalities and operating conditions: coal and heterocyclic N compounds seem to decompose mostly through HCN, while amino acids and proteinic nitrogen appear to produce mostly ammonia. However, because of the many different structures in which N is present in biomass fuels, there is not yet enough knowledge on the nitrogen chemistry, and the results obtained vary with different fuels, setups and operating conditions [98]. Moreover, Munir et al. [270, 271] have shown how co-combustion of coal with several biomass residues, of even higher initial N content, could effectively reduce NO emissions in a 20 kW down-fired combustor. More information on the nitrogen chemistry during biomass pyrolysis can be found in Chapter 2. Therefore, the need for characterization of each single fuel is clear.

Three of the materials studied here are byproducts in different processes for the production of so-called first-generation liquid biofuels: dry distiller's grains and solubles (DDGS), palm kernel cake (PKC) and rapeseed cake (RC). Chicken manure (CM) is a waste of animal breeding, and the fermented sewage sludge (FSS) is a residue of the anaerobic digestion of the sewage sludge from wastewater treatment plants.

A detailed description on the origins and main composition of the studied fuels can be found in Chapter 3. Despite promising conditions, there is still a lack of fundamental data on the behaviour of DDGS under thermal conversion conditions. In the previous chapters and papers, we investigated the slow and fast pyrolysis of DDGS [161, 163]. The results indicated that under slow pyrolysis conditions, the main nitrogen compound released was NH<sub>3</sub>, followed by HCN and HNCO in minor amounts and at higher temperatures. The results obtained suggested that the main mechanism of release was the one indicated by Hansson et al. [180] stating that the main route of reaction of proteins in biomass passes through a first phase of deamination followed by cyclization of the peptide, or protein, with the formation of compounds called

DiketoPiperazines (DKP). These compounds decompose further at higher temperatures to produce HCN and HNCO. However, at higher heating rates, the mechanism seemed to change and the main compound released appeared to be HCN with minor amounts of ammonia. No HNCO was detected at high heating rates. It was suggested that the first step of deamination is inhibited at high heating rates, while most of the fuel-N is released as tar-N and consequently decomposes through secondary reactions into, mostly, HCN. The yield of  $\text{NH}_3$  is attributed to reactions of cross-linking of proteins with reactive side chains.

PKC and RC are residues of mechanical press of the oil from the seeds of palm fruits and rape. As explained in Chapter 3, these materials are rich in proteins and fibers [294] and mostly sold as feed for animals. As for DDGS, also for these materials, fundamental characterization of fuel N conversion in combustion is scarce. Eriksson et al. [149] investigated different combustion possibilities for rapeseed meal alone or in combination with bark, and they found that the concentration of NO in the flue gas increased when adding the rapeseed meal to bark. Nevalainen et al. [274] tested rapeseed expeller in a 50 kW circulating fluidized-bed boiler alone and in co-combustion with wood or bituminous coal; they too found greatly increased NO emissions with an increasing share of RC in the fuel. Moreover, the measurements with coal showed a lower concentration of NO but a higher presence of  $\text{N}_2\text{O}$  compared to the experiments with wood.

Chicken manure contains the excrement of the birds, undigested food, and organic parts of the birds themselves. CM has been used, for some years, in large-scale combustors, and data on pilot-scale facilities are available in the literature [217, 246, 378]. Li et al. [246] tested the co-combustion of CM with coal and found that NO emissions would increase with an increasing share of CM until 25 %wt, while the concentration of NO would drop again with a share of 50 %wt. They explained that the large amount of volatile N released by CM helped creating a  $\text{NO}_x$  reducing atmosphere around the particle, decreasing the total emissions. Zhu and Lee [378] tested the co-combustion of CM with natural gas in a swirling fluidized-bed combustor and they found increasing NO emissions when CM was added. Other studies have investigated more fundamental phenomena during CM slow and fast pyrolysis [140, 163, 202, 278]. In a previous work, presented also in Chapter 5, we tested the slow pyrolysis of CM in a TG – FTIR spectrometer setup [163] and found that  $\text{NH}_3$ , HCN and HNCO were the main nitrogen compounds released;  $\text{NH}_3$  was released throughout the whole range of temperatures because of the various forms in which it is found in the sample (inorganic and organic) [217], while HNCO and HCN were released at higher temperatures. In another study from our group, Di Nola et al. [140] investigated the fast pyrolysis of CM and found that no HNCO was detectable and that  $\text{NH}_3$  was indeed the main N compound at low temperatures (up to 600 °C) while HCN would

become the main compound at higher temperatures with an increasing trend up to 1300 °C.

Sewage sludge is formed during wastewater treatment. Werther and Ogada [359] gave a complete review of sludge composition and possible disposal techniques. As for CM, experience with sludge and FSS combustion and co-combustion is quite substantial, even though most of the data available rely on large-scale experiments and fundamental data are still lacking. Raw and digested sludges have been combusted for many years [359]. Leckner et al. [239] co-combusted up to 50 %<sub>th</sub> digested sludge with coal and wood on a nearly commercial-scale circulating fluidized bed. They reported no issues in operating the CFB in co-combustion, and they found that the emissions were below the legal limits for CO, NO, and SO<sub>2</sub> for shares up to 25 %<sub>th</sub> but a sharp increase in NO emissions was recorded with higher shares. Abelha et al. [56] pyrolyzed different biomass wastes and found that sludges released more HCN than the other materials. They also found that, when sludge was co-combusted with coal up to 35 %<sub>th</sub>, despite a much higher initial N content of the fuel mix, final emissions of NO<sub>x</sub> would not substantially increase. They explained this with the large part of fuel N released by the sludges during devolatilization and the following thermal De-NO<sub>x</sub> reactions. Korving et al. [227], moreover, found high N<sub>2</sub>O emissions during operations of a large-scale fluidized-bed combustor fed with FSS. They attributed this phenomenon to the oxidation of HCN, and they found that increasing the freeboard temperature and lowering the air/fuel ratio reduced N<sub>2</sub>O emissions by almost 8 times.

The results presented in this paper will help to gain some insight into the trends and fundamental mechanisms of fuel N to NO conversion of such fuels. The setup used in these measurements has been used for extensive investigation on black liquor combustion behavior [155, 156, 233, 234]. In the furnace, where only a few milligrams of fuel are combusted, the intrinsic chemistry of the fuel is explored, minimizing the influence of the reactor design. Each fuel was combusted under different conditions of temperature and oxidant atmosphere, and the release of CO, CO<sub>2</sub>, and NO was monitored with commercially available analyzers. The materials studied here retain a great potential as fuels, and some are already combusted as a way of disposal. However, a deeper knowledge of the fundamentals of nitrogen chemistry is needed if they are to be used efficiently and cost-effectively.

## 7.2 EXPERIMENTAL SECTION

The work described in this paper was performed using the setup shown in Figure 108 and described in Chapter 3. The setup consisted of a quartz tube reactor inserted in an electrically heated furnace. Feeding of the process gases was possible from the bottom and middle of the reactor. The flow of the gases was controlled by mass flow controllers, and the mixing of oxidizing (air) and inert (nitrogen) agents was performed directly in the reactor. The aver-



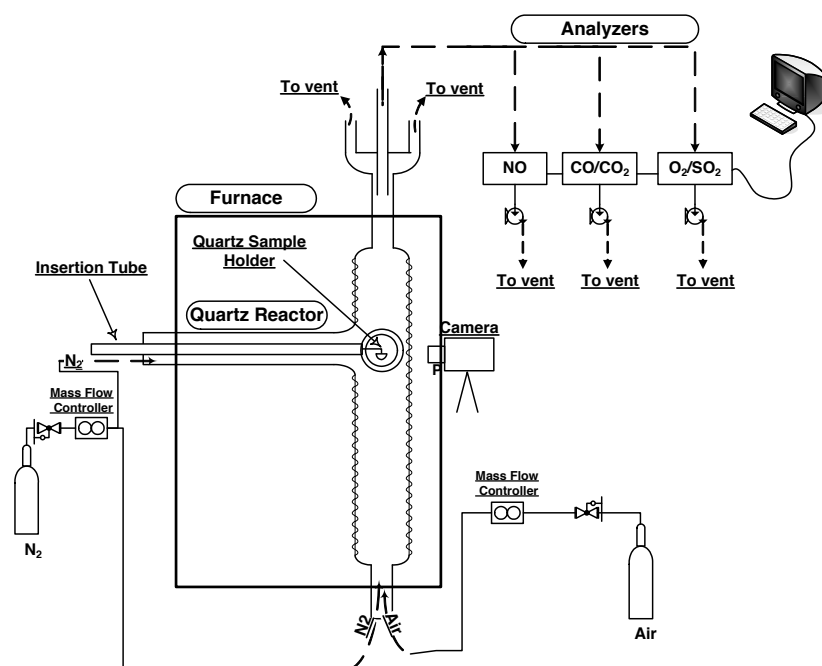


Figure 108: Single-particle furnace at Åbo Akademi University.

age residence time for the gases was around 20 s, while, if considering only the product gases from devolatilization/combustion of the fuel, the residence time at high temperature has to be considered about 4 s. The temperature in the reactor was measured with a thermocouple inserted in the ceramic wall of the furnace, close to the surface of the quartz reactor in the proximity of the sample placement point.

An insertion probe allowed the sample to be placed on the sample holder in a cold environment and then to be inserted, in a fraction of seconds, into the hot reactor. The sample holder used in the present work was made of quartz and had a porous bottom to allow the gases to flow through it.

The evolved gas analysis chain included three commercial analyzers for the measurement of  $O_2$ , CO,  $CO_2$ , NO, and  $SO_2$ . A chemiluminescence analyzer was used for NO detection; a non-dispersive infrared (NDIR) analyzer was used for CO +  $CO_2$  measurement; and a combined infrared + paramagnetic analyzer was used for  $SO_2$  and  $O_2$  detection, respectively. The different internal volumes of the analyzers introduced a bias in the measured signals, so that the NO signal appears to be delayed and wider than the signal obtained for CO and  $CO_2$ . This should not be attributed to a chemical phenomenon but rather to the longer residence time of the gases in the NO analyzer. However, the integral values of the released gases are not affected by this phenomenon,

and as it will be shown later, data can be compared after proper fitting of the curves.

### 7.2.1 Procedure

The fuels were manually ground with mortar and pestle and then placed on the sample holder in amounts ranging around 10–15 mg. The measurements were performed for all of the fuels at three different temperatures relevant for industrial applications: 800, 900, and 1000 °C. To test the fuels in different oxidant conditions, for each temperature, two different oxygen concentrations, 3 and 10%<sub>vol.</sub>, were used. Every measurement was repeated at least 3 times, and several sets of three measurements were compared.

As pointed out in the previous section, because of different internal volumes, a direct comparison between the behavior of CO + CO<sub>2</sub> and NO release was not possible. To overcome this issue and at the same time analyze the different contributions of volatile versus char emissions, the curves obtained from the analyzers were deconvoluted using a least-squares method fit with two Weibull-type distributions representing the devolatilization and char contributions.

### 7.2.2 Fuels

As mentioned above, the materials studied in this paper are not yet commonly used as fuels but are mostly byproducts or wastes from different processes. The proximate and ultimate analyses of all of the fuels are given in Table 46. Some of the fuels were studied in other papers, but their fundamentals of fuel N to NO conversion were not yet investigated.

## 7.3 RESULTS AND DISCUSSION

The different origins of the tested fuels are already clearly visible from the data reported in Table 46; DDGS, PKC, and RC present similar characteristics in terms of content of C, H, and O, while FSS and CM, because of their completely different origin, differ greatly in their main composition. In view of this division, in the rest of the paper, the group of DDGS, PKC, and RC will be referred to as residues, while the remaining materials, FSS and CM, will be defined as wastes. While the residues present a carbon content of around 50%<sub>wt<sub>d.b.</sub></sub>, comparable to other woody and agricultural biomass fuels [103, 159], the content of C in the wastes is much lower, about 40%<sub>wt<sub>d.b.</sub></sub> for CM and even lower than 30%<sub>wt<sub>d.b.</sub></sub> for FSS. Another great difference among these materials lays in the content of ash-forming matter; the residues present a content of inorganic matter of about 6–7%<sub>wt<sub>d.b.</sub></sub>, a value that is already much higher than for other common biomass fuels but still lower than many

Table 46: Proximate and Elemental Analysis of the Tested Fuels. Data are on a dry basis.

	DDGS <sup>a</sup>	PKC	RC <sup>b</sup>	FSS	CM <sup>a</sup>
Moisture <sup>c</sup>	8.9	7	2.1	7.4 <sup>d</sup>	20.2
Volatiles	78.2	75.5	74.7	43.3	67.9
Fixed Carbon	14.7	18.4	18.8	10.6	5.5
Ash <sup>e</sup>	7.1	6.1	6.5	46.1	26.6
C	49	49	49.9	26.5	39.6
H	6.3	6	6.9	5.9	4.1
N	4.5	2.4	5.1	3.2	5.9
S	0.4	0.5	0.7	1.2	0.7
Cl	0.2	0.2	0.3	0.1	0.4
O (by difference)	32.5	35.8	29.6	17	22.7
gross calorific value (MJ/kg)	19.8	17.8	22.2	11	13.3
g of CO <sub>2</sub> /MJ <sup>f</sup>	86	97	82	88	100

<sup>a</sup>From Giuntoli et al. [163].

<sup>b</sup>From Piotrowska et al. [290].

<sup>c</sup>as received basis.

<sup>d</sup>The sample was pre-dried in an oven before combustion tests.

<sup>e</sup>Ashed at 550 °C, except for CM, which was ashed at 6000 °C.

<sup>f</sup>Theoretical value for the complete oxidation of carbon content to CO<sub>2</sub> on gross calorific value basis.

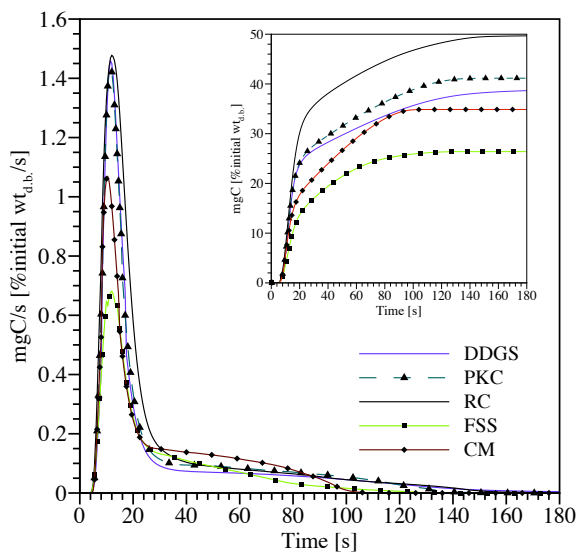
coals [147]. CM and FSS, instead, present an ash content of 26 and almost 47 %wt<sub>d.b.</sub>, respectively. This characteristic is, naturally, related to the origin of the fuels: CM is very rich in calcium, which is fed to the hens to give strength to the eggshells, while FSS includes all of the residues from the wastewater treatment and is additionally depleted of carbonaceous material during the digestion process. It is worth noticing, moreover, that the heating values of the residues are close or even higher than the values for clean and demolition wood [147, 338], making them quite good alternatives to woody biomass for thermal conversion, in this respect. The energy density of the wastes is, instead, hindered by their high content of inorganic materials and low C content; specific pretreatments for the removal of ash-forming matter prior to thermal conversion would indeed increase the efficacy of such fuels [163]. Finally, the content of nitrogen in all of the tested fuels is definitely higher than in other, more widely used, biomass materials, ranging from 2.4 to almost 6 %wt<sub>d.b.</sub> compared to values of 0.1 - 2 %wt<sub>d.b.</sub> for wood and agricultural res-

idues [147, 159]. Concerns for possible high  $\text{NO}_x$  emissions could, therefore, delay the use of such fuels on a large scale.

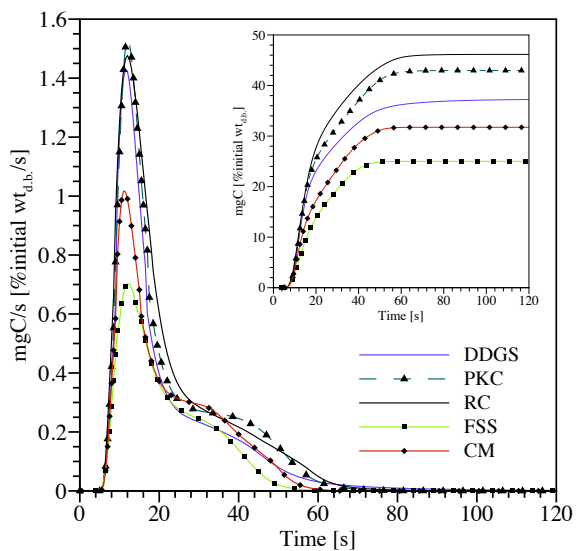
The original composition of the fuels has great relevance for their conversion characteristics [98, 182, 241]. As discussed previously, the residues generally consist of the typical constituents of woody biomass: hemicellulose, cellulose, and lignin, and nitrogen is mostly in the form of proteins. The CM sample, instead, together with the typical constituents of biomass, contains nitrogen in the form of urea, proteins, but also ammonium salts. The FSS sample, finally, contains the solid materials present in wastewater, which are mostly constituted by carbohydrates, fats, oils, and proteins. The main sources of nitrogen in wastewater are proteins and urea [359]. However, the FSS sample studied here is the residue of an anaerobic digestion process, and therefore, it is to be expected that the biodegradable fraction of the fuel has already been released together with the loose nitrogen. The residual material, thus, is mostly in the form of mono- and oligomers because of the effect of the action of the enzymes during the anaerobic digestion [358]. The main N compounds are therefore expected to be free amino acids.

### 7.3.1 Release profiles

Figure 109 illustrates the release profiles of carbon, measured as  $\text{CO} + \text{CO}_2$ , from all of the fuels included in this study at a reactor temperature of  $900^\circ\text{C}$  and oxidant concentrations of 3 and 10 % $_{\text{vol}}$ . In both plots, one can observe a first fast release because of the flash devolatilization and following homogeneous oxidation of the volatiles. This is followed by a slower slope because of the heterogeneous oxidation of the remaining char. The diverse nature of the two processes is also visible on the difference between the results at varying oxygen concentrations; the homogeneous oxidation of volatiles is not influenced by a higher concentration of  $\text{O}_2$ , and the conversion rate profiles are unchanged for all of the fuels. Moreover, despite the difference in absolute values, the release of volatiles follows very similar patterns for both residues and wastes, implying that a common approach could be used in modeling combustion processes of different biomass fuels. However, the effects of the oxidant concentration become evident in the heterogeneous char oxidation reactions. The behavior of the fuels, in this case, differs between residues and wastes, while in the 3 % $_{\text{vol}}$  case the residues present a slowly declining conversion rate which brings the total conversion time at approximately 3 min, the CM and FSS chars show a higher rate and a shorter conversion time (around 2 min). This effect is a combination of the much smaller amount of fixed carbon in these fuels and the catalytic effect of the high content of inorganic matter [107, 349, 372]. In an oxygen-rich atmosphere, the difference between materials is less evident and all of the fuels are completely combusted within around 80 s.

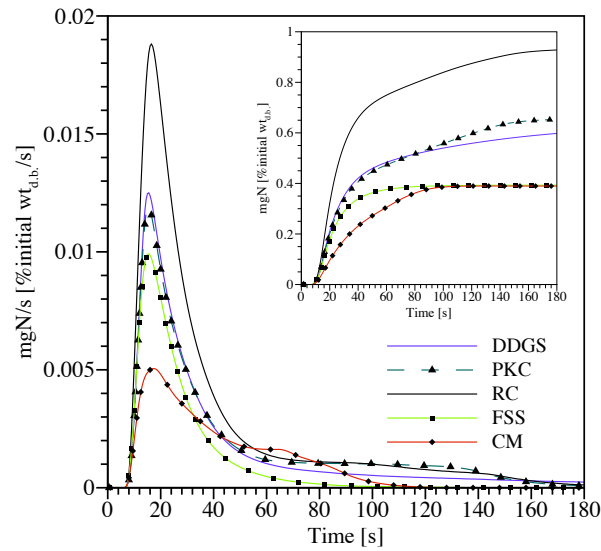


(a) 3%<sub>vol.</sub> O<sub>2</sub>.

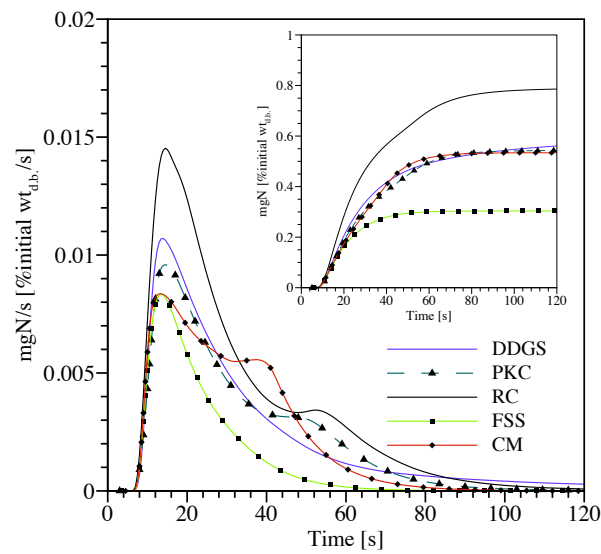


(b) 10%<sub>vol.</sub> O<sub>2</sub>.

Figure 109: Release of carbon as CO + CO<sub>2</sub> from all of the fuels at 900 °C: conversion rates (large plot) and cumulative data (small plot). Data are on a dry basis.



(a) 3 %<sub>vol.</sub> O<sub>2</sub>.



(b) 10 %<sub>vol.</sub> O<sub>2</sub>.

Figure 110: Release of nitrogen as NO from all of the fuels at 900 °C: conversion rates (large plot) and cumulative (small plot). Data are on a dry basis.

Figure 110 represents the release of nitrogen as NO from all of the fuels at 900 °C and 3 and 10 %<sub>vol.</sub>. It should be kept in mind that, because of the larger volume of the NO analyzer, the raw data cannot directly be overlapped with the carbon conversion, but fitting of the data is necessary, as will be explained in the following sections. The devolatilization phase, which is in reality a faster phenomenon, is transformed, by the transfer function of the analyzer, into a Weibull function trend, including a steep rise in the release followed by a tail created by the recirculation and dead volumes in the analyzer volume. In Figure 110a it can be seen that the first devolatilization phase is followed by a very long tail of nitrogen release because of the slow oxidation of the residual nitrogen present in the char; only for the chicken manure sample, the release of char N is faster and creates a secondary peak. The devolatilization behavior is, as for carbon, similar among all of the fuels, with the exception of CM. The char of this fuel, as seen also in Figure 109a, is very reactive; therefore, oxidation overlaps greatly with devolatilization, producing a broader release profile.

At higher oxygen concentrations, shown in Figure 110b, the char oxidation is faster for all of the fuels, while the devolatilization phases are almost unchanged. As shown in Figure 111, the conversion profiles during devolatilization maintain their shape for all of the fuels. As expected, the oxygen concentration has little effect on the homogeneous oxidation of the volatile NO precursors. The behavior of PKC and RC is readily understandable; the pyrolysis process is only slightly influenced by the different concentrations of oxidant, while the remaining nitrogen in the char is much more quickly oxidized to NO at higher oxygen concentrations. Despite its small amount of fixed C, CM is known to produce around 20 %wt<sub>daf</sub> of char under fast pyrolysis [140]; therefore, the oxidation of CM is very much improved at 10 %<sub>vol.</sub> and a superposition between volatile and char oxidation is detectable. This is most likely due to the high amount of ash-forming matter in the sample; while the conversion proceeds, the concentration of such minerals increases in the char, which is then quickly oxidized, while pyrolysis is still ongoing. FSS, as shown in Figure 111d and as will be described in the next sections, produces almost no char; therefore, the effect of the oxygen concentration is limited and only a slightly faster oxidation of volatiles is observed. DDGS seems to be the only exception to the behaviors described above; as shown in Figure 111a, the devolatilization profile is not influenced by the different atmospheres and, while char C appears to react faster (Figure 109b), char N follows the same slow oxidation as in the measurements at 3 %<sub>vol.</sub>

When looking at the cumulative release of N in Figure 110, it is possible to notice that RC is the fuel that releases the most NO, in agreement with the findings on large-scale boilers [149, 274]. The profiles of FSS resemble first-order reactions, hinting that the main release of nitrogen is from volatile matter. As mentioned above, FSS contains mostly free amino acids, which decompose very fast at such temperatures. The release of nitrogen for PKC,

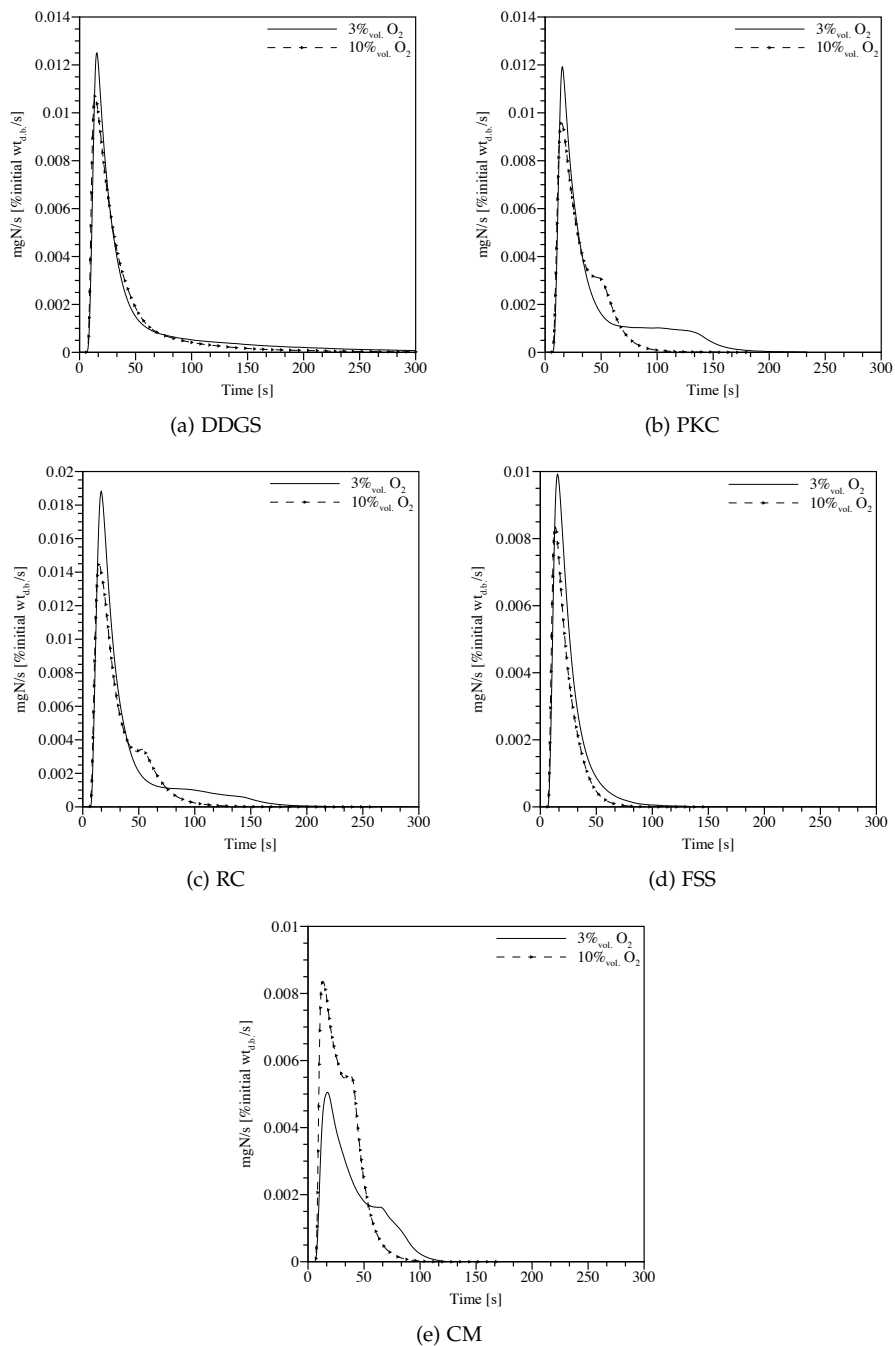


Figure 111: Nitrogen release profiles at 900 °C. Data are on a dry basis.



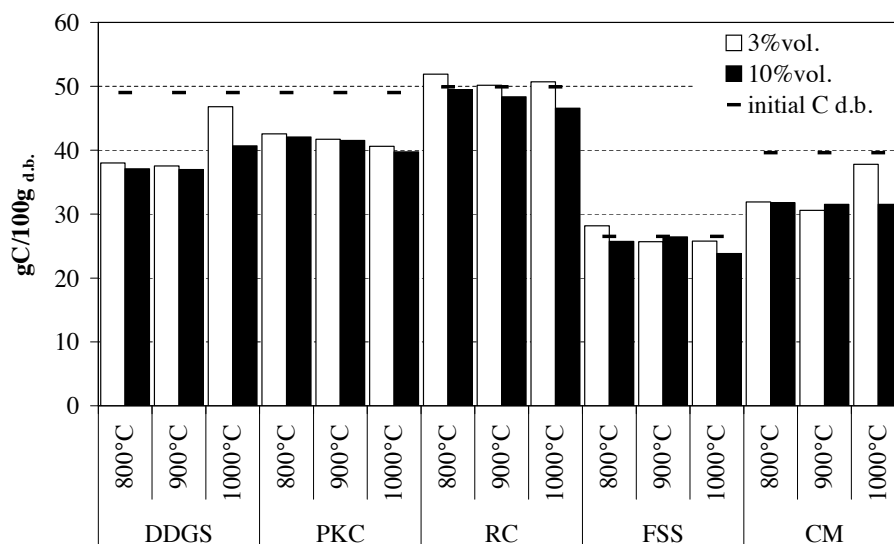


Figure 112: Total amount of carbon released as CO + CO<sub>2</sub> and initial C content. Data are on a dry basis.

DDGS, and RC, moreover, appears to be similar, deriving by the common nature of the structures contained in the fuels, mostly in the forms of proteins.

### 7.3.2 Total Release

After analyzing the general profiles of release from the different fuels at one temperature, in this and the next sections, the total release of carbon and nitrogen are analyzed as a function of the different conditions.

Figures 112 and 113 show the total release of carbon (as CO + CO<sub>2</sub>) and nitrogen (as NO) in all of the measurements performed in this study compared to their initial content. The release of carbon is, as expected, proportional to the initial content in the fuels, with mass balance closures between 80 and 100%; the difference in the mass balances was most likely due to the influence of the reactor geometry and the formation of soot. This is supported by the fact that most of the measurements indicate a higher recovery of C at oxygen-lean conditions, where the oxidation is slower and the volatiles can oxidize more completely. At higher oxygen contents, instead, the observed flame front presents the bright yellow color typical of soot formation, which would explain the lower recovery. However, assuming a complete combustion of the fuel C to carbon dioxide, it is interesting to observe the theoretical maximum amount of released CO<sub>2</sub> per megajoule produced by the fuel, because such values are becoming more and more crucial in the power sector subjected to GHG emissions regulations. From Table 46, it can be seen that the

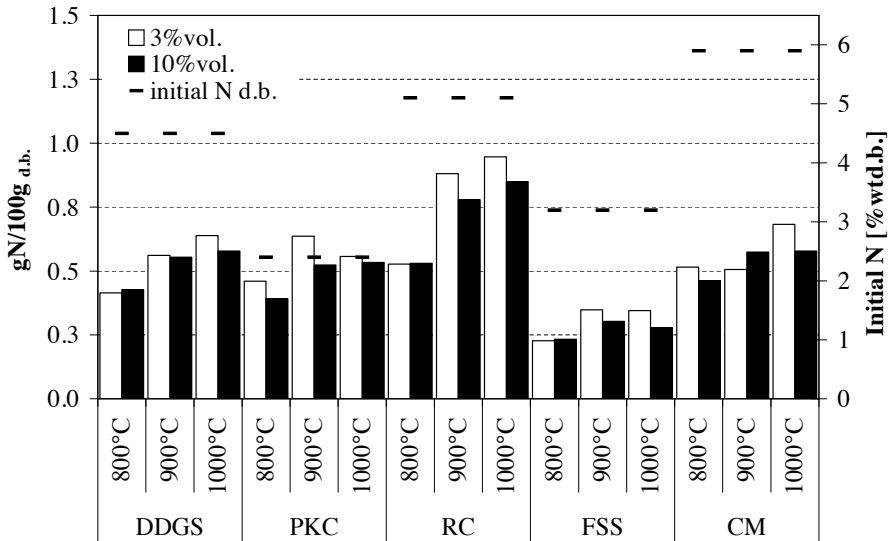


Figure 113: Total amount of nitrogen released as NO and initial N content. Data are on a dry basis.

values for these materials are comparable to the ones found in coals ( $\approx 90$ - $100$  g of  $\text{CO}_2/\text{MJ}$ ); efficiently co-firing such fuels with coal would, therefore, substitute fossil carbon with renewable  $\text{CO}_2$ , claiming an advantage in terms of emission rights without the need to apply a capture and storage process.

Figure 113 gives much information regarding these materials, showing the dependence of the released NO versus temperature, oxygen partial pressure, and fuel type. It must be noted that the data reported here as grams of N/100 g indicate the nitrogen released from the fuels as NO; the missing N to the mass balance is due to molecular  $\text{N}_2$  and possibly other compounds, such as  $\text{N}_2\text{O}$ , and unreacted NO precursors, such as HCN and  $\text{NH}_3$ , which could not be detected with the available analyzers but could be produced in the process [227, 362].

It is well-known that a temperature window exists in which  $\text{NH}_3$  reacts with NO to reduce it to  $\text{N}_2$  and water [211]; this effect is called thermal De- $\text{NO}_x$  and is currently used in commercial boilers as a primary means to reduce NO emissions directly in the reactor. The temperature window of maximum reduction, however, shifts depending upon the operation conditions (such as  $\text{O}_2$  partial pressure and radical concentrations) and so does the efficiency of such a process. Kasuya et al. [211] studied such dependencies and found that, at equal temperature, increasing the concentration of oxygen in the reactor would increase NO reduction. This effect, in addition to possible soot N formation because of the fast reactions, explains the lower NO release at 10% vol.  $\text{O}_2$  shown in all of the measurements in Figure 113.

Another effect that explains this behavior was underlined in the past by Kymäläinen et al. [234], who suggested that, at lower oxygen concentrations, the oxidation of ammonia is slow and, thus, happening far from the particle surface. Because of this,  $\text{NH}_3$  could not reduce the forming NO through the De- $\text{NO}_x$  reactions.

Additionally, it can still be seen in Figure 113 that the absolute amounts of N released as NO from DDGS, PKC, and CM are relatively similar, ranging around 0.5 - 0.6 g of N/100 g<sub>d.b.</sub>. RC, despite having similar structure and conversion profiles as the other residues, actually releases much higher amounts of NO, around 0.8 - 0.9 g of N/100 g<sub>d.b.</sub>. This would explain the steep increase in NO emissions measured by several studies [149, 274] when RC was co-fed in large-scale boilers. FSS is the material which releases less NO, in the range of 0.3 g of N/100 g<sub>d.b.</sub>. For comparison, these values are about 1 order of magnitude higher than the values obtained from black liquor combustion using a similar setup [234].

Among the variety of results achieved for different setups [98, 226, 362] in terms of nitrogen emissions from biomass samples, it appears that the results of this study fit quite well the predictions from previous studies. Winter et al. [362] tested several biomass fuels on a small-scale fluidized-bed boiler, measuring the release of nitrogen compounds under combustion conditions. They found that the final conversion of initial fuel N to NO diminished when the initial N content increased. The results from Winter et al. [362] are compared to the results of this study in Figure 114. It is very interesting to see that, despite the different setups, the trend holds validity also for the fuels analyzed in this study. PKC is the fuel with the lowest nitrogen content, and it releases more than 15% of its initial N as NO, whereas CM (5.9%wt<sub>d.b.</sub> initial N) is the fuel releasing the least amount of N as NO. This behavior can, again, be explained with the thermal De- $\text{NO}_x$  mechanism; a higher content of nitrogen in the fuel implies a higher concentration of  $\text{NH}_i$  radicals in the volatile matter, leading to a higher degree of NO reduction. The shown trend, thus, even though rough, seems to provide an easy tool for preliminary predictions of NO emissions from biomass materials. These results agree very well with the ones introduced in the previous chapter. In Chapter 6 it was shown that at high heating rates pyrolysis, DDGS releases slightly less of its initial-N as HCN than PKC, but more volatile-N species are available in absolute terms from DDGS for De $\text{NO}_x$  reactions. Moreover, another significant difference is the release of ammonia from DDGS, which is instead not recorded for PKC and that provides more promptly the needed  $\text{NH}_i$  radicals needed for NO reduction.

The dependence of N conversion with the temperature is shown in Figure 115. Such results are coherent with the predictions concerning the De- $\text{NO}_x$  temperature window. As mentioned above, at higher  $\text{O}_2$  concentrations, shown in Figure 115b, conversion is almost constant between 900 and 1000 °C indicating the approaching onset of the window of maximum reduction. At

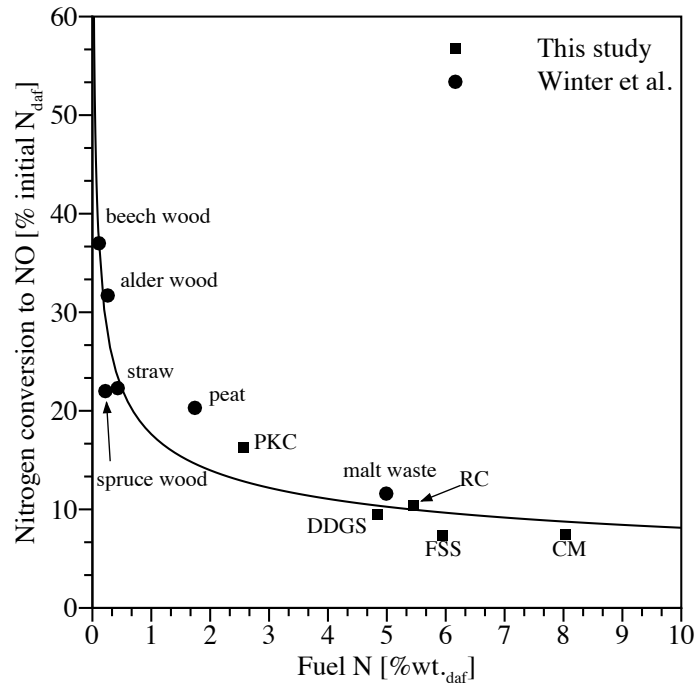


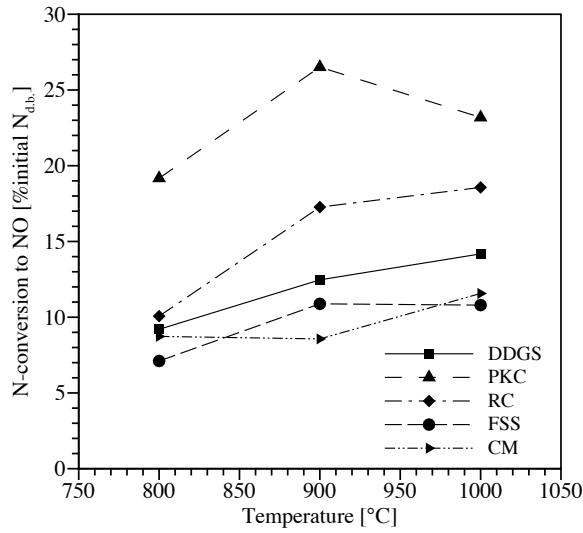
Figure 114: Conversion of fuel nitrogen to NO versus fuel nitrogen content. Data from this study and Winter et al. [362] are compared for measurements at 800 °C and 10%<sub>vol.</sub> O<sub>2</sub>.

lower oxygen partial pressure, shown in Figure 115a, most of the fuels show an increasing trend with an increasing temperature, indicating that the mechanism of reduction does not significantly change with the temperature under these conditions. However, PKC shows a clear maximum at 900 °C, indicating that the maximum De-NO<sub>x</sub> window is around this temperature.

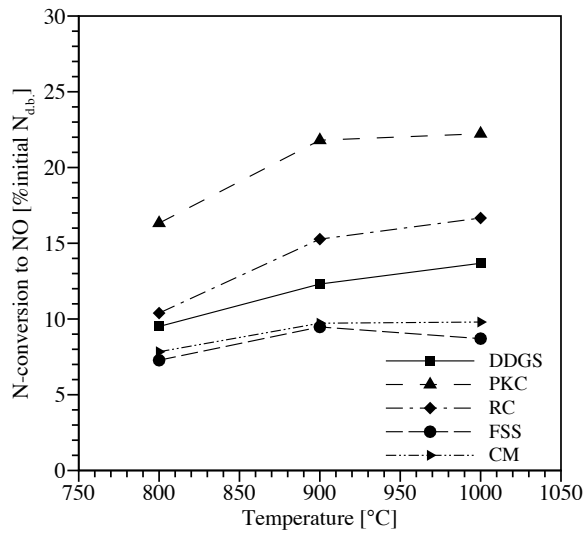
### 7.3.3 Devolatilization/Char partitioning

As mentioned in the previous sections, the partitioning of C and N between volatiles and char can help explain some of the data described above. For this purpose, the release profiles of carbon and nitrogen were fitted, by a least-squares method, with two Weibull-type curves representing devolatilization and char evolution.

The carbon partitioning, shown in Figure 116, shows quite a homogeneous behavior among the different fuels, with percentages of volatile carbon ranging from 55 to 60% for the wastes and up to 65 - 70% for the residue materials with higher carbon and volatile content. The influence of the final temperature and oxidant atmosphere is limited for all of the fuels, as expected. Figure 117



(a) Conversion of nitrogen to NO at 3% vol. O<sub>2</sub>.



(b) Conversion of nitrogen to NO at 10% vol. O<sub>2</sub>.

Figure 115: Nitrogen conversion to NO as a function of temperature.

instead depicts the partitioning for N release. It is clear that the different nitrogen functionalities in the different fuels play a crucial role. All of the fuels appear to release more volatile N at higher temperatures and higher oxygen concentrations, so that at 1000 °C, the release is almost complete during devolatilization for all of the fuels. Di Nola et al. [140] have shown that, in flash pyrolysis of biomass residues, the percentage of N released as light gases (NH<sub>3</sub> and HCN) increased with an increasing temperature at the expense of tar N, while char N stayed relatively constant at high temperatures. This seems to disagree with the present findings, in which the char N share is drastically reduced when increasing the reaction temperature. However, the different atmospheres (N<sub>2</sub> versus air) greatly affect the process; the interaction of oxygen with the char at severe conditions is substantial already during devolatilization.

Another very important point for modeling purposes is that, while at 800 °C and 3 %<sub>vol.</sub> O<sub>2</sub>, the release of C and N appears to be proportional for the residues, at more severe conditions this is not the case as evidenced also in previous studies [56]. It appears that, with an increasing temperature and oxygen concentration, there is a selective depletion of N from the char compared to C. FSS represents an exception among the fuels for several reasons: it is a preprocessed fuel; it has a very high content of minerals, including iron [359]; and, finally, it is known to release more HCN during pyrolysis than other biomass materials [56]. Being preprocessed, its structures are already decomposed to monomers and amino acids, allowing most of the N to be released in volatile form, as evidenced in Figure 117, and thus facilitating thermal De-NO<sub>x</sub> reactions. However, it is also likely that the iron in the sample would favor a catalytic decomposition of ammonia into N<sub>2</sub> and H<sub>2</sub>O, instead of oxidation to NO. Finally, HCN can oxidize not only to NO but also to N<sub>2</sub>O [56, 227], which was not measured in this study. The combination of such phenomena explains the off-trend position of FSS in Figure 114.

The nitrogen partitioning of the fuels in this study is, at mild conditions, comparable to previous studies [56, 362], reporting volatile N values in the range of 60 - 70 % for different types of biomass materials. Values reported for black liquor are also ranging around 60 - 80 % of volatile nitrogen [155].

It seems clear that the final amount of NO emissions from combustion or co-combustion of high-N biomass wastes is the result of a delicate balance among oxidation and reduction reactions of volatile N compounds, such as NH<sub>3</sub> and HCN since the percentage of char N seems almost not influential at industrial conditions. The results from this study can be useful to have a qualitative explanation of results found in the literature. For RC, for example, the results from this study do not indicate a clear difference in the partitioning of N release compared to the other fuels; however, the initial high content of N is responsible for higher final NO emissions. This explains why Nevalainen et al. [274] found increasing NO emissions when co-combusting RC with wood and coal. Li et al. [246] tested CM co-combustion with coal

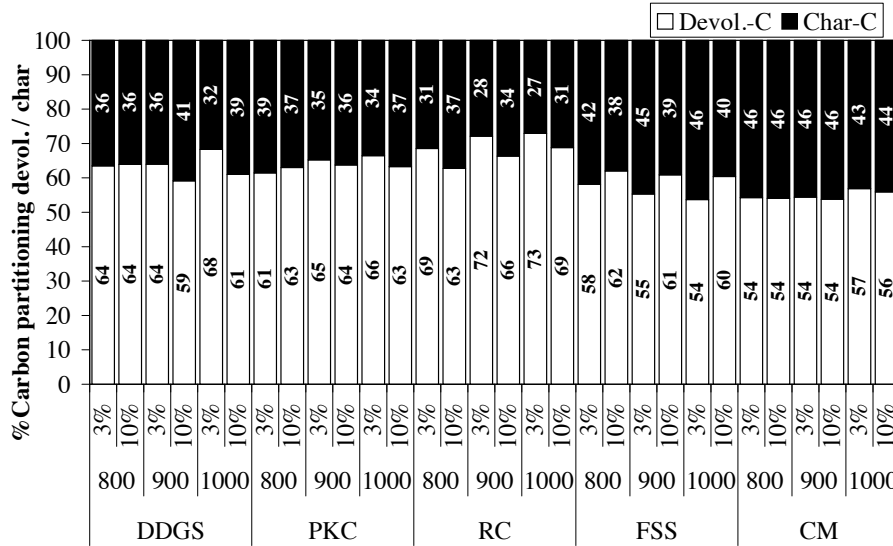


Figure 116: Carbon partitioning between devolatilization and char oxidation.

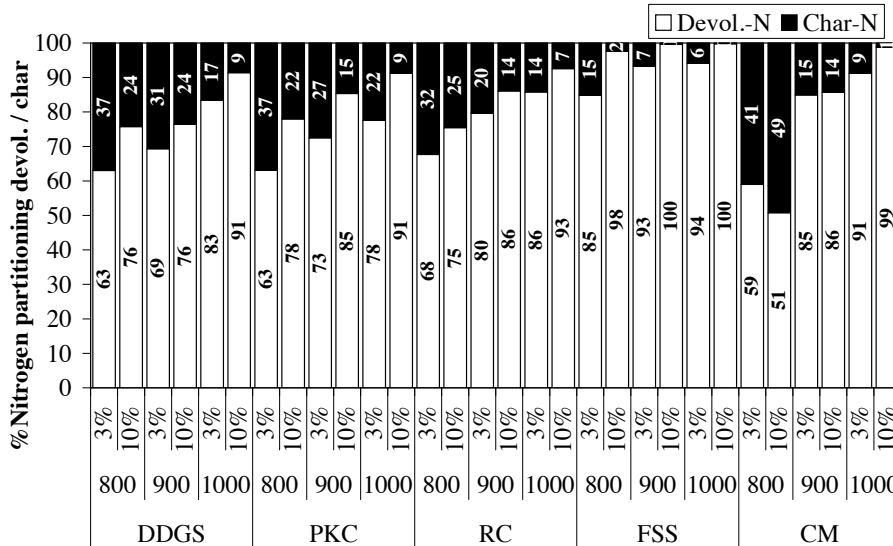


Figure 117: Nitrogen partitioning between devolatilization and char oxidation.

and found increasing NO emissions at lower shares of CM and decreasing NO emissions at higher shares of CM, despite the higher N content in CM compared to coal. The results from this study show that the conversion of fuel N to NO for CM is indeed lower than for all of the other fuels. Moreover, the high amount of volatile N released and the expected high concentration of NH<sub>3</sub> [140] could explain such results. With a lower share of CM, oxidation of NH<sub>3</sub> and HCN to NO would prevail, increasing the total NO emissions. However, with higher shares of CM and, thus, of volatile N around the particle, De-NO<sub>x</sub> reactions would prevail, decreasing the final NO emissions. Leckner et al. [239] found increasing NO emissions when co-combusting FSS with coal and wood. They found, however, that the increase in emissions was less than proportional to the increased N content of the fuel mixture for shares of FSS lower than 25 %<sub>th</sub> but drastically higher with additional FSS. The results presented here have shown that most of the NO from FSS is released during devolatilization. This would suggest that, with lower shares of FSS, thermal De-NO<sub>x</sub> reactions would help mitigate NO formation but, with an additional increase of such volatiles, oxidation reactions would overcome reduction and NO emissions would then increase sharply.

#### 7.4 CONCLUSIONS

In the work presented in this chapter, five biomass residue samples were tested under combustion conditions in a single-particle reactor. The tests were carried out in a quartz furnace at three different temperatures, 800, 900 and 1000 °C, and 3 and 10 %<sub>vol.</sub> O<sub>2</sub>. Following the release patterns of CO + CO<sub>2</sub> and NO, it was possible to determine the total release of C and N and, mostly, to analyze their fuel N to NO conversion and their partitioning between volatiles and char.

It was shown that, despite the different fuel characteristics, the devolatilization conversion profiles were similar among the fuels and were also not influenced by a higher oxygen concentration. It appears that, under combustion conditions, a common approach for modeling the devolatilization of different fuels could be adequate for a preliminary analysis. The same was found to be true for fuel N to NO conversion.

The total amount of CO<sub>2</sub>/MJ emitted by these fuels is comparable to the amounts released by coals. In the case of co-combustion in coal power plants, therefore, such materials could contribute to the substitution of fossil carbon with renewable carbon without the need for additional carbon-capture processes. The release of fuel N as NO was equal to around 0.5 - 0.6 g of N/100 g<sub>d.b.</sub> for DDGS, PKC, and CM, while it was higher for RC, around 0.8 - 0.9 g of N/100 g<sub>d.b.</sub>, and much smaller for FSS, 0.3 g of N/100 g<sub>d.b.</sub>. The conversion of fuel N to NO for the five biomass fuels investigated in the present work showed a power trend between the initial amount of fuel N and the final N to NO conversion, in agreement with what was suggested in previ-



ous studies. PKC, which contains the lowest amount of fuel N, was the fuel with the highest conversion of N to NO, and CM was the material with the lowest conversion. As a first approximation, such trend can even be used for NO prediction for several biomass fuels. Moreover, fuel N conversion to NO seemed to decrease with higher oxygen concentrations, in agreement with thermal De-NO<sub>x</sub> mechanisms. On the other hand, an increase in conversion was observed with an increasing temperature.

The partitioning between volatile and char C and N showed a proportionality between their release at 800 °C for all of the fuels, except FSS, which released most of its nitrogen in volatile form already at low temperatures. With increasing temperatures, it appears that a selective depletion of N undergoes from the char. At low temperatures, most of the fuels released around 60 - 70 % of their N as volatiles, while at higher temperatures, almost all of the initial nitrogen was released during devolatilization.

The data reported in this work help to explain some of the fundamental phenomena in NO formation during combustion of biomass residues and wastes. The measurements performed show how, despite the high nitrogen content of these fuels, most of the NO release happens in the few seconds of devolatilization, so that the reduction of NO with radicals from NH<sub>3</sub> and HCN is effective even when no air staging is applied. The data reported suggest that, with proper operational conditions, it should be possible to achieve low NO emissions even without additional gas-cleaning equipment.



# 8

---

## CONCLUDING REMARKS

---

*This final chapter summarizes the conclusions obtained from the current work. In light of such conclusions, recommendations are suggested for further research work.*

## 8.1 CONCLUSIONS

The main research question behind this work was the following:

“Which, how fast and how many nitrogen compounds are released during the thermal conversion of biomass wastes?”

The results presented in this dissertation give an important contribution to the deep understanding of the thermal conversion of biomass residues. The following points illustrate the general answers to the main and the collateral research questions:

- A detailed picture of the volatile-N species, namely HCN, NH<sub>3</sub> and HNCO, released during slow and fast pyrolysis and the kinetics of their release was obtained.  
The results of the present work substantiate the available literature on biomass and proteins pyrolysis: at slow heating rates, the devolatilization of protein chains is dominated by thermal deamination at low temperatures (300 °C) followed by the release of HCN and HNCO from the residual cyclical amides structures at higher temperatures (400 - 600 °C). At high heating rates, instead, the first step is not favoured due to the high speed of the heating process so that most of the nitrogen is released in large cyclical amides which then decompose further giving rise to high yields of HCN.  
These data are essential in order to clarify the mechanisms of fuel-N release under pyrolysis conditions making it possible to optimize process conditions for optimal NO<sub>x</sub> reduction.
- The characteristics of the conversion of fuel-N to NO under combustion conditions were observed for several biomass wastes.  
The final conversion of fuel-N to NO is found to strongly depend on the initial amount of nitrogen: with a high content of fuel-N, large concentrations of NH<sub>i</sub> radicals are available during combustion for reduction reactions of the already-formed NO back to molecular N<sub>2</sub>.  
These results are important to give a preliminary order of magnitude of the NO<sub>x</sub> emissions from these fuels;
- The weight loss profiles and kinetic parameters of slow devolatilization of some agricultural residues (such as wheat straw, olive residues and peach stones) and biomass wastes (such as dry distiller’s grains (DDGS) and chicken manure) were retrieved. Such data are available both for the initial fuels and for the volatile species released.  
Using a common approach for the analysis of all the fuels, common patterns of pyrolysis have appeared among all the samples indicating that the main structures of biomass actually react in similar ways even when contained in very different fuels.

These results are missing in published literature but they are essential for further modeling of the thermal conversion of these fuels;

- The effects of a water leaching pre-treatment were evaluated on devolatilization kinetics, product partitioning and species release. The leaching pre-treatment, in accordance with previous literature, has a significant effect on the ash quantity, composition and pyrolysis reactivity of wheat straw and olive residues; surprisingly, instead, it does not seem to affect the DDGS, chicken manure and peach stones samples. Moreover, the leaching appears to increase the yields of volatile-N species both at low and high heating rates. These results not only underline the important role of inorganic matter in thermal conversion of these fuels but also are the key for future deployment of the pre-treatment on an industrial scale;
- A numerical CFD model of the heated foil reactor was developed to give an improved insight into the physical conditions within the reactor and thus a better understanding of the experimental results. The simulation offers a deeper insight into the reactor conditions and several optimizations of the reactor design and experimental conditions have been possible thanks to them.

The following sections illustrate all the particular results obtained in each part of this work and enunciate the research questions that remain unanswered or that have arisen from the present work itself.

#### 8.1.1 *Slow pyrolysis measurements*

- The slow pyrolysis behavior of many different fuels, including wheat straw, olive residues, peach stones, dry distiller's grains with solubles (DDGS) and chicken manure, is similar in terms of reactivity and weight loss. At a heating rate of 10 °C/min, all the fuels present a main peak of reactivity, identified with the devolatilization of cellulose, at around 330 - 360 °C. Another reactivity peak or shoulder, usually identified with the decomposition of hemicellulose, is found for most of the fuels at temperatures of around 280 - 310 °C. The weight loss for all the fuels at a final temperature of 900 °C is between 70 and 87 %wt<sub>daf</sub>. DDGS and chicken manure present additional decomposition peaks at 400 °C and 430 - 470 °C, respectively, which are assigned to the decomposition of proteinic structures.
- The main light volatile species detected are always CO<sub>2</sub> and CO. At a heating rate of 10 °C/min, CO<sub>2</sub> yields range usually around 9 to 15 %wt<sub>d.b.</sub> with exception of chicken manure which presents higher yields due to its high content of calcium carbonates. CO yields are usually equal to 6 - 15 %wt<sub>d.b.</sub> but they increase drastically at temperatures higher than

650 °C and keep increasing when the sample is kept isothermal at high temperature. This phenomenon is most probably associated with the cracking of tarry compounds that have re-condensed in the char structure due to the slow speed of the devolatilization. CH<sub>4</sub> yields are always minor, with values ranging around 1 - 2 %wt<sub>d.b.</sub>; methane is usually found at temperatures higher than 400 - 500 °C as the main product of the decomposition of methoxyl groups from lignin.

- Detection of nitrogen compounds from wheat straw, olive residues and peach stones has not been possible with the present technique due to their relatively low nitrogen content. Higher-N fuels, like DDGS and chicken manure, instead, release easily detectable amounts of NH<sub>3</sub>, HCN and even HNCO. DDGS presents a steep release of ammonia at about 328 °C without other nitrogen species, indicating a first step of deamination of the proteinic chains in the fuel. Subsequently, at about 400 °C, the simultaneous release of NH<sub>3</sub>, HCN and HNCO indicates a further decomposition of proteins via the paths of dehydration, cyclization and final decomposition of cyclic amides (DKP) into mostly HCN, HNCO and, partly, ammonia. Another peak of release of HCN and NH<sub>3</sub> is found at very high temperature, 650 °C, with almost no corresponding weight loss: this could be assigned to previously condensed tar-N structures which decompose further at higher temperatures.

Chicken manure presents similar features to DDGS because of its protein content. However, differences are evident, for example, in the release of ammonia throughout all the temperature spectrum, even at very low temperatures, due to the loosely bound ammonia contained in the urines of the animals. Moreover, a much higher release of HNCO is detected because of the presence of high amount of urea in the sample.

During measurements at slow heating rates, DDGS presents similar yields of ammonia and HCN and lower values for HNCO. Chicken manure releases higher yields of nitrogen volatiles compared to DDGS. The main compound is HNCO while HCN yield is lower than HNCO but higher than ammonia.

- Applying a Distributed Activation Energy Model (DAEM) it is possible to retrieve kinetic parameter for the slow devolatilization of all the fuels. It is striking that, once the pre-exponential term is fixed into a physically meaningful value, most of the fuels present the same components: a first one at about 165 - 170 kJ/mol and another, the most relevant one, at 176 kJ/mol. This clearly indicates that, when analyzed with consistent techniques and methodologies, the main components of biomass, hemicellulose and cellulose, decompose with the same mechanism for a wide range of materials.

The exact kinetic parameters obtained for each volatile species can be

readily used as input data in pyrolysis modeling softwares such as FG-Biomass.

- The effects of the water-leaching are very peculiar. For the wheat straw and olive residues samples, most of the water solubles elements are removed in high percentages by the washing procedure. In terms of reactivity, the washed fuels decompose over a wider range of temperatures but the main reaction peak is shifted significantly to higher temperatures. The kinetic analysis suggests that while the hemicellulose component maintains its reactivity at about 170 kJ/mol, the cellulose structure reacts with an activation energy equal to 185 kJ/mol. The presence of alkali metals in the structure of biomass appears to have a clear catalytic effect for some materials, influencing mostly the reactivity of cellulose and increasing the number of possible reaction pathways. Different results, however, are found with more complicated fuels like peach stones, DDGS and chicken manure. For these fuels it appears indeed that the washing has a little effect on total ash content and even on the content of soluble alkalis. This minor effect is visible also in the reactivity which does not appear to significantly change for these samples. Deeper knowledge of the composition and structures in which the inorganic matter is included in such materials is required before conclusions can be drawn. Moreover, the leaching does not seem to have an effect on the reactivity of nitrogen compounds, but it has, however an effect on the yields of HCN and  $\text{NH}_3$  which increase for both DDGS and chicken manure. Due to the limitations of the measurement technique, however, it is not possible to distinguish the real source of this change: this could be the effect of both increased decomposition of N-containing structures or a decreased release of molecular  $\text{N}_2$  in favour of other volatile compounds.

#### 8.1.2 *Fast pyrolysis measurements*

- The fast pyrolysis behavior of DDGS and PKC is similar, due to the similarity in their composition. The weight loss is higher compared to the slow pyrolysis. The release of volatiles seems to proceed until about 900 °C after which, light gases still increase in yield but at the expense of heavier tars. The yield of tars is maximum at about 700 °C.
- $\text{CO}_2$  is again the main volatile species up to temperatures of about 900 °C, with a maximum yield of 15 %wt<sub>daf</sub> at 1200 °C for all the fuels. However, the yield of CO increases monotonically from a value of about 8 - 10 %wt<sub>daf</sub> at 900 °C to a value of almost 25 %wt<sub>daf</sub> at 1300 °C. This trend, as mentioned in the point above, is most likely due to the thermal cracking of formed tars in the hot area around the foil.  $\text{CH}_4$  is, again, a minor species, and its yield increases from values of about 1.2 %wt<sub>daf</sub>

at 900 °C to a maximum value of 3.2 - 3.8 %wt<sub>daf</sub> at 1200 °C. Methane is also a product of the cracking of aromatic structures.

- HCN is the main volatile-N species detected at all temperatures for all the fuels. Only minor yields of ammonia are recorded during pyrolysis of DDGS but not for PKC. HNCO is not detected for any of the samples. The yields of both NH<sub>3</sub> and HCN at 900 °C are lower than the ones recorded under slow heating rates, probably indicating a higher tar-N release. However, at a temperature of 1200 °C, HCN yield increases up to 1.2 - 2.2 %wt<sub>daf</sub> while ammonia yield still remains lower than 0.5 %wt<sub>daf</sub>. The mechanism of nitrogen release changes between slow and fast pyrolysis: with high heating rates, most of the protein chains are released in large molecules, most likely in the form of cyclic amides such as DKP. These amides, subsequently, decompose further into, mostly, HCN. The recorded yield of NH<sub>3</sub> can derive from three different mechanisms: thermal deamination, which is though not favoured at fast reaction speeds, from secondary decomposition of amines and amides or from the cross-linking of reactive proteins' side chains. This last route seems to be important because even at 1200 °C, approximately 10 % of the initial-N is still retained in the char of DDGS.
- The effects of leaching are, again, minimal regarding weight loss and product distribution. However, once again, the leaching seems to influence the volatile-N species favouring the formation of HCN and NH<sub>3</sub> over tar-N or molecular N<sub>2</sub>.

### 8.1.3 *Modeling of heated grid reactor*

- From the simulation of the temperature and velocity profiles in the reactor it is clear that there is an area of high temperature and low velocity around the hot foil. This is most likely the cause of the tar-cracking observed at high temperatures in fast pyrolysis experiments. The yields resulting from the fast pyrolysis measurements should, therefore, be considered as a contribution of primary and secondary devolatilization.
- A combination of simulations and measurements using a non-contact infrared pyrometer shows that the actual temperature of the foil is approximately 15 % (in degree Celsius) higher than the temperature measured by the control thermocouple.

### 8.1.4 *Combustion tests*

- The devolatilization profiles for carbon to CO + CO<sub>2</sub> and N to NO under combustion conditions are very similar for many, different, biomass fuels. Also oxygen concentration does not seem to affect this behaviour.



A common approach for the homogeneous release and oxidation of volatile gases seems, therefore, appropriate for the studied biomass wastes.

- Rapeseed cake is the sample with the higher absolute release of nitrogen as NO. The rest of the fuels, DDGS, PKC and chicken manure have comparable absolute values while the fermented sewage sludge is the fuel releasing the least amount of nitrogen as NO.
- The conversion of fuel-N to NO of the studied fuels decreases, following a power trend, with increasing initial nitrogen content. This behavior is attributed to the effect of the higher amount of  $\text{NH}_i$  radicals available in the gas phase around the particle when most of the nitrogen is released during devolatilization.  
For most of the fuels the conversion of fuel-N to NO increases with temperature and slightly decreases with higher oxygen concentration. The trend found in this study could be used as a preliminary mean for the prediction of N to NO conversion from several fuels.
- During the combustion of the tested fuels, the carbon partitioning between devolatilization and char oxidation does not change significantly among the fuels and at different conditions. The fraction of nitrogen released during devolatilization, instead, increases dramatically with temperature so that at 1000 °C almost all the nitrogen, which is released as NO, is released during the devolatilization stage. It appears that at lower temperatures the release of C and N from the fuel can be considered proportional, while the char is depleted of N faster than C at higher temperatures. The fermented sewage sludge sample behaves differently from the other fuels and it releases all of its N as NO during the pyrolysis phase. This is most likely due to its pre-processed nature and it also explains its lower conversion of fuel-N to NO.

## 8.2 RECOMMENDATIONS FOR FUTURE RESEARCH

### 8.2.1 *Slow pyrolysis research and kinetic modelling*

- The use of additional measurement techniques, such as micro-GC and in-situ Raman spectroscopy, connected on-line with the TG-FTIR setup would allow a better understanding of the nitrogen chemistry thanks to the detection of molecular  $\text{N}_2$  and possibly, tar-N compounds such as Diketopiperazines (DKP).
- Investigating the residual chars of different biomass samples and model compounds (e.g. Lysine for aliphatic amino acids and Bilirubin for heterocyclic-N compounds), prepared at different temperatures and conditions, using NMR techniques ( $^{15}\text{N}$  and  $^{13}\text{C}$ ) would greatly help in understanding the structural changes of char-N during pyrolysis. Difficulties

reside in the low natural abundance of  $^{15}\text{N}$  in the samples and consequently the low sensitivity of  $^{15}\text{N}$ -NMR measurements which makes it quite difficult and time consuming to achieve reliable results. With the progress of technology this should become possible in a near future, producing highly interesting results.

- A thorough investigation of biomass model compounds such as proteins, basic amino-acids, heterocyclic-N compounds and structural carbohydrates, on a TG-FTIR setup, using a consistent procedure would guarantee a better understanding of the mechanisms of volatile-N release from biomass samples. Some of these model compounds for nitrogen could range from aliphatic amino acids such as Lysine, to cyclic compounds such as Bilirubin or Diketopiperazines (DKP), while cellulose, xylan and lignin are commonly used to describe the structural carbohydrates found in biomass.
- The application of a consistent methodology for the kinetic analysis of the mentioned model compounds and biomass samples would guarantee a predictive capacity on pyrolysis kinetics. The results obtained in this work seem to suggest that using a consistent methodology, e.g. a Distributed Activation Energy Model and fixed pre-exponential factor equal to  $2.2 \times 10^{13} \text{ 1/s}$ , could reveal common patterns of devolatilization. Once detected, these patterns could be then related to the decomposition of model compounds such as cellulose and hemicellulose. Once that is established, knowing the initial amount of these basic structures would allow the prediction of slow pyrolysis kinetics without having to run the actual measurements. The role of inorganic matter on kinetics needs further investigation as well.

### 8.2.2 *Fast pyrolysis research and modelling*

- As for slow pyrolysis, the use of a micro-GC or in-situ Raman spectroscopy, able to detect molecular  $\text{N}_2$ ,  $\text{H}_2$  but also tar-N compounds such as Diketopiperazines (DKP), would greatly help understanding the nitrogen chemistry under high heating rates.
- The same goes for tar-N detection and analysis. The use of a tar-trap syringe to sample tars from heated grid measurements has already been developed by colleagues in the department and it should be used for more thorough investigation on the tar-N chemistry.
- The heated grid setup and the measurement methodology has already been improved during this work but more needs to be done in order to achieve a more reliable temperature control and decrease the influence of secondary reactions. The use of a pump with higher gas flow

would increase the velocity of the gases, thus limiting their residence time at high temperature and reducing the chances of secondary reactions. However, it seems unlikely to eliminate secondary reactions completely, this seems intrinsic to the design of the reactor.

- An infrared pyrometer could be used to measure the temperature of the surface of a sample reacting on the foil. However, in order for this measurement to be accurate, many factors need to be accounted for, like the infrared absorption of the volatiles' plume and the influence of background radiation of the foil on the radiation of the sample.
- An improved physical model of the particle, including accurate physical properties and a detailed surface/volume model, would help understanding the actual thermal history of the sample on the hot foil and therefore help the interpretation of the experimental data.
- The numerical model developed during this work provides a very good platform to implement further research. More detailed physical properties for the fuels should be measured and a more accurate surface expression should be implemented in the model; with those data, then, the thermal history of the sample could be accurately simulated. Consequently, detailed chemical kinetics should be implemented into the model. This will provide an excellent tool for the prediction of fast pyrolysis phenomena or for validation of the kinetics retrieved at slow pyrolysis conditions.

### 8.2.3 *Combustion research*

- Coupling an FTIR analyzer to the single-particle reactor would allow the detection of additional nitrogen species such as  $\text{NH}_3$ , HCN,  $\text{N}_2\text{O}$  and help to understand the overall nitrogen chemistry of the fuels. The addition of a micro-GC or Raman spectroscopy for the measurement of  $\text{N}_2$  and tar-N would, again, be very helpful.
- Simulation or measurement of the temperature and velocity profiles in the reactor would help in understanding the actual thermal history of the sample and of the gases released.

### 8.2.4 *Pre-treatments and fuels related research*

- Among the fuels studied in this research, detailed measurement campaigns on large-scale setups are largely missing. This is especially true for dry distiller's grains (DDGS) which has not been considered as a fuel for thermal conversion until very recently. Large-scale experiments under pyrolysis, gasification and combustion conditions would close the

final gap on the nitrogen chemistry of these fuels and confirm or deny the possibility of extrapolation of data from small-scale experiments.

- The leaching pre-treatment seems to have a positive effect on the reactivity and volatiles' composition of some fuels but not for others. A detailed study on the composition and the structures in which inorganic matter is bound in such fuels should be carried out in order to explain these effects.
- A detailed energetic and economic analysis for the use of water leaching on an industrial scale is required in order to promote it as a possible technology for real applications.

---

## BIBLIOGRAPHY

---

- [1] 'Our Common Future'. Technical report, World Commission on Environment and Development, Oxford (UK), 1987. (Cited on page 11.)
- [2] 'Disposal and Recycling Routes for Sewage Sludge'. Technical Report Brussels, European Commission, 2001. (Cited on page 57.)
- [3] 'Straw gasification for co-combustion in large CHP-Plants'. Technical report, International Energy Agency, 2001. (Cited on pages 81 and 85.)
- [4] 'Biomass Action Plan'. Technical Report COM(2005) 628, European Commission, Brussels, 2005. (Cited on page 16.)
- [5] 'De verwachte beschikbaarheid van biomassa in 2010'. Technical Report 2DEN05.16, SenterNovem, Den Haag (Netherlands), 2005. (Cited on page 38.)
- [6] 'How much bioenergy can Europe produce without harming the environment?' Technical Report 7/2006, European Environment Agency, Copenhagen, 2006. (Cited on page 19.)
- [7] 'World Energy Technology Outlook - WETO H<sub>2</sub>'. Technical Report EUR22038, European Commission - DG Research, Brussels, Belgium, 2006. (Cited on page 5.)
- [8] 'Biomass for Power Generation and CHP'. IEA Energy Technology Essentials, 2007. URL [www.iea.org/Textbase/techno/essentials.htm](http://www.iea.org/Textbase/techno/essentials.htm). (Cited on pages 26 and 27.)
- [9] 'Climate Change 2007: Synthesis Report'. Technical report, Intergovernmental Panel for Climate Change, 2007. (Cited on pages 12 and 13.)
- [10] 'Climate Change 2007: The Physical Science Basis'. Technical Report IPCC WG1 AR4, Intergovernmental Panel for Climate Change, 2007. (Cited on page 29.)
- [11] 'Commission staff working document: EU Energy Policy Data'. Technical Report SEC(2007) 12, European Commission, Brussels, 2007. (Cited on page 10.)
- [12] 'Deciding the Future: Energy Policy Scenarios to 2050'. Technical report, World Energy Council, London, UK, 2007. (Cited on page 5.)
- [13] 'An Energy Policy for Europe'. Technical Report COM(2007) 1, European Commission, Brussels, 2007. (Cited on pages 8, 15, and 16.)

- [14] 'A European Strategic Energy Technology Plan (SET-Plan): Towards a low carbon future'. Technical Report COM(2007) 723, European Commission, Brussels, 2007. (Cited on pages 15 and 16.)
- [15] 'Limiting Global Climate Change to 2 degrees Celsius. The way ahead for 2020 and beyond'. Technical Report COM(2007) 2, European Commission, Brussels, 2007. (Cited on pages 12 and 13.)
- [16] 'Renewable Energy Road Map. Renewable Energies in 21st century: building a more sustainable future'. Technical Report COM(2006) 848, European Commission, Brussels, 2007. (Cited on page 20.)
- [17] 'Towards a European Strategic Energy Technology Plan'. Technical Report COM(2006) 847, European Commission, Brussels, 2007. (Cited on pages 17 and 20.)
- [18] '20 20 by 2020: Europe's climate change opportunity'. Technical Report COM(2008) 30, European Commission, Brussels, 2008. (Cited on pages 15 and 16.)
- [19] 'Shell Energy Scenarios to 2050'. Technical report, Shell International BV, The Hague, The Netherlands, 2008. (Cited on page 5.)
- [20] 'The State of Food and Agriculture 2008. Biofuels: prospects, risks and opportunities'. Technical Report AD/I/I0290E/1/9.08/3000, FAO, Rome, Italy, 2008. (Cited on page 19.)
- [21] 'CO<sub>2</sub> emissions from fuel combustion - Highlights'. Technical report, International Energy Agency, Paris, France, 2009. (Cited on page 15.)
- [22] 'Greenhouse gas emission trends and projections in Europe 2009: Tracking progress towards Kyoto targets'. Technical Report 09/2009, European Environment Agency, Copenhagen, 2009. (Cited on pages 10, 11, 15, and 16.)
- [23] 'Investing in the Development of Low-Carbon Technologies'. Technical Report COM(2009) 519, European Commission, Brussels, 2009. (Cited on page 19.)
- [24] 'Investing in the Development of Low Carbon Technologies (SET-Plan): A Technology Roadmap'. Technical Report SEC(2009) 1295, European Commission, Brussels, 2009. (Cited on page 16.)
- [25] 'Key Energy Stats'. Technical report, International Energy Agency, 2009. (Cited on pages 6, 7, and 8.)
- [26] 'The Millennium Development Goals Report 2009'. Technical report, United Nations, New York City (US), 2009. (Cited on page 12.)

- 
- [27] 'Panorama of Energy: Energy statistics to support EU policies and solutions'. Technical report, Eurostat, Luxembourg, 2009. (Cited on pages 10 and 12.)
- [28] 'Technical status of biomass co-firing'. Technical Report 50831165, KEMA, Arnhem, The Netherlands, 2009. (Cited on page 27.)
- [29] 'World Energy Outlook 2009'. Technical report, International Energy Agency, 2009. (Cited on pages 5, 6, 7, 8, 12, 13, and 14.)
- [30] 'Biomass Combustion and Co-firing: An Overview'. <http://www.ieabcc.nl/>, 2010. (Cited on page 26.)
- [31] 'BK 7 schott glass'. 2010. URL <http://rmico.com/technical-notes/bk7-quartz-ge-si>. (Cited on page 103.)
- [32] 'CACHET-CO<sub>2</sub> project'. 2010. URL <http://www.cachetco2.eu/index.html>. (Cited on page 24.)
- [33] 'CATO-2 Project'. 2010. URL <http://www.co2-cato.nl/>. (Cited on page 24.)
- [34] 'DECARBit Project'. 2010. URL <http://decarbit.com/>. (Cited on page 24.)
- [35] 'Energy [r]evolution - A sustainable world energy outlook'. Technical Report JN330, EREC - Greenpeace, Brussels, Belgium, 2010. (Cited on page 5.)
- [36] 'Ethanol Industry Outlook 2010: Climate of Opportunity'. Technical report, Renewable Fuels Association, 2010. (Cited on page 86.)
- [37] 'European Biomass Industry Association'. 2010. URL <http://www.eubia.org/>. (Cited on page 88.)
- [38] 'Europe's Energy Portal'. 2010. URL <http://energy.eu/renewable>. (Cited on page 16.)
- [39] 'IEA Bioenergy Task 32: Biomass Combustion and Co-firing'. 2010. URL <http://www.ieabcc.nl/>. (Cited on pages 26 and 27.)
- [40] 'IEA Bioenergy Task 33: Thermal Gasification of Biomass'. 2010. URL <http://www.gastechnology.org/webroot/app/xn/xd.aspx?it=enweb&xd=iea/homepage.xml>. (Cited on page 24.)
- [41] 'Moerdijk power plant'. 2010. URL [http://www.bmcmoerdijk.nl/index.php?site\\_id=2](http://www.bmcmoerdijk.nl/index.php?site_id=2). (Cited on pages 89 and 142.)
- [42] 'PyNe - Pyrolysis network of IEA Bioenergy'. 2010. URL <http://www.pyne.co.uk>. (Cited on pages 22 and 23.)

- [43] 'The story of biodiesel in the village of Kinchlingi, India'. 2010. URL <http://www.theworkingcentre.org/wscd/ctx/story/story.html>. (Cited on page 114.)
- [44] 'Wikipedia: Cellulose'. 2010. URL <http://en.wikipedia.org/wiki/Cellulose>. (Cited on page 41.)
- [45] 'Wikipedia: Cotton'. 2010. URL <http://en.wikipedia.org/wiki/Cotton>. (Cited on page 41.)
- [46] 'Wikipedia: Lignin'. 2010. URL <http://en.wikipedia.org/wiki/Lignin>. (Cited on pages 43 and 44.)
- [47] 'Wikipedia: Nicotine'. 2010. URL <http://en.wikipedia.org/wiki/Nicotine>. (Cited on page 56.)
- [48] 'Wikipedia: Palm Oil'. 2010. URL [http://en.wikipedia.org/wiki/Palm\\_oil](http://en.wikipedia.org/wiki/Palm_oil). (Cited on page 88.)
- [49] 'Wikipedia: Peat'. 2010. URL <http://en.wikipedia.org/wiki/Peat>. (Cited on page 38.)
- [50] 'Wikipedia: Photosynthesis'. 2010. URL <http://en.wikipedia.org/wiki/Photosynthesis>. (Cited on page 41.)
- [51] 'Wikipedia: Starch'. 2010. URL <http://en.wikipedia.org/wiki/Starch>. (Cited on page 47.)
- [52] 'Wikipedia: Straw'. 2010. URL <http://en.wikipedia.org/wiki/Straw>. (Cited on page 81.)
- [53] 'Wikipedia: Strychnine'. 2010. URL <http://en.wikipedia.org/wiki/Strychnine>. (Cited on page 56.)
- [54] 'Wikipedia: Urine'. 2010. URL <http://en.wikipedia.org/wiki/Urine>. (Cited on page 154.)
- [55] Aarna, I. and Suuberg, E. M. 'A review of the kinetics of the nitric oxide-carbon reaction'. *Fuel*, 76(6): 475 – 491, 1997. (Cited on page 72.)
- [56] Abelha, P.; Gulyurtlu, I. and Cabrita, I. 'Release Of Nitrogen Precursors From Coal And Biomass Residues in a Bubbling Fluidized Bed'. *Energy & Fuels*, 22(1): 363–371, 2008. (Cited on pages 89, 204, and 218.)
- [57] Adouane, B. *Low NO<sub>x</sub> emissions from fuel-bound nitrogen in gas turbine combustors*. Ph.D. thesis, Delft University of Technology, Delft, The Netherlands, 2006. (Cited on page 26.)
- [58] Aggarwal, P. and Dollimore, D. 'A thermal analysis investigation of partially hydrolyzed starch'. *Thermochimica Acta*, 319(1-2): 17–25, 1998. (Cited on page 47.)



- [59] Aho, M. J.; Hämäläinen, J. P. and Tummavuori, J. L. 'Importance of solid fuel properties to nitrogen oxide formation through HCN and NH<sub>3</sub> in small particle combustion'. *Combustion and Flame*, 95(1-2): 22–30, 1993. (Cited on pages 61, 66, and 71.)
- [60] Aiman, S. and Stubington, J. 'The pyrolysis kinetics of bagasse at low heating rates'. *Biomass and Bioenergy*, 5(2): 113 – 120, 1993. (Cited on page 185.)
- [61] Al-Mansour, F. and Zuwala, J. 'An evaluation of biomass co-firing in Europe'. *Biomass and Bioenergy*, 34(5): 620 – 629, 2010. (Cited on page 27.)
- [62] Almendros, G.; Knicker, H. and González-Vila, F. J. 'Rearrangement of carbon and nitrogen forms in peat after progressive thermal oxidation as determined by solid-state <sup>13</sup>C- and <sup>15</sup>N-NMR spectroscopy'. *Organic Geochemistry*, 34(11): 1559–1568, 2003. (Cited on page 54.)
- [63] Alves, S. S. and Figueiredo, J. L. 'Kinetics of cellulose pyrolysis modelled by three consecutive first-order reactions'. *Journal of Analytical and Applied Pyrolysis*, 17(1): 37–46, 1989. (Cited on page 96.)
- [64] Åmand, L. E.; Leckner, B. and Andersson, S. 'Formation of nitrous oxide in circulating fluidized-bed boilers'. *Energy & Fuels*, 5(6): 815–823, 1991. (Cited on page 63.)
- [65] Annamalai, K.; Sweeten, J.; Mukhtar, S.; Thien, B.; Wei, G.; Priyadarsan, S.; Arumugam, S. and Heflin, K. 'Co-firing Coal: Feedlot and Litter Biomass (CFB and CLB) Fuels in Pulverized Fuel and Fixed Bed burners'. Technical report, National Energy Technology Laboratory, 2003. (Cited on page 142.)
- [66] Antal, M.; Várhegyi, G. and Jakab, E. 'Cellulose Pyrolysis Kinetics: Revisited'. *Ind. Eng. Chem. Res.*, 37(4): 1267–1275, 1998. (Cited on pages 42, 94, and 96.)
- [67] Antal, M. J. and Gronli, M. 'The Art, Science, and Technology of Charcoal Production'. *Industrial & Engineering Chemistry Research*, 42(8): 1619–1640, 2003. (Cited on pages 22 and 60.)
- [68] Antal, M. J. J. and Várhegyi, G. 'Cellulose Pyrolysis Kinetics: The Current State of Knowledge'. *Ind. Eng. Chem. Res.*, 34(3): 703–717, 1995. (Cited on pages 42, 94, 117, 125, 129, 133, 146, and 148.)
- [69] Anthony, D. and Howard, J. B. 'Coal devolatilization and hydrogastification'. *AIChE Journal*, 22(4): 625 – 656, 1976. (Cited on page 97.)
- [70] Anthony, D.; Howard, J. B.; Meissner, H. and Hottel, H. 'Apparatus for determining high pressure coal-hydrogen reaction kinetics under rapid

- heating conditions'. *Review of Scientific Instruments*, 45(8): 992 – 995, 1974. (Cited on pages 110 and 168.)
- [71] Aravind, P. *Studies on high efficiency energy systems based on Biomass Gasifiers and Solid Oxide Fuel Cells with Ni/GDC Anodes*. Dissertation, Delft University of Technology, Delft, The Netherlands, 2007. (Cited on pages 24 and 26.)
- [72] Arvelakis, S. *Improving the biomass gasification/combustion technology via appropriate physico-chemical pre-treatments of the raw material*. Ph.D. thesis, National Technical University of Athens, Athens, Greece, 2001. (Cited on pages 81, 82, 85, 114, 116, 118, 126, and 138.)
- [73] Arvelakis, S.; Gehrman, H.; Beckmann, M. and Koukios, E. G. 'Effect of leaching on the ash behavior of olive residue during fluidized bed gasification'. *Biomass and Bioenergy*, 22(1): 55–69, 2002. (Cited on pages 80 and 85.)
- [74] Arvelakis, S.; Gehrman, H.; Beckmann, M. and Koukios, E. G. 'Agglomeration problems during fluidized bed gasification of olive-oil residue: evaluation of fractionation and leaching as pre-treatments'. *Fuel*, 82(10): 1261–1270, 2003. (Cited on pages 25, 81, 114, 116, 121, and 138.)
- [75] Arvelakis, S.; Gehrman, H.; Beckmann, M. and Koukios, E. G. 'Preliminary results on the ash behavior of peach stones during fluidized bed gasification: evaluation of fractionation and leaching as pre-treatments'. *Biomass and Bioenergy*, 28(3): 331–338, 2005. (Cited on pages 81, 82, 85, 114, 116, 118, 119, 120, 122, and 138.)
- [76] Arvelakis, S. and Koukios, E. G. 'Physicochemical upgrading of agroresidues as feedstocks for energy production via thermochemical conversion methods'. *Biomass and Bioenergy*, 22(5): 331–348, 2002. (Cited on pages 48, 80, 81, 82, 114, 116, 118, 119, 120, 138, 142, 145, and 168.)
- [77] Arvelakis, S.; Vourliotis, P.; Kakaras, E. and Koukios, E. G. 'Effect of leaching on the ash behavior of wheat straw and olive residue during fluidized bed combustion'. *Biomass and Bioenergy*, 20(6): 459–470, 2001. (Cited on pages 80, 81, 85, 114, 116, and 138.)
- [78] Atimtay, A. T. 'Combustion of agro-waste with coal in a fluidized bed'. *Clean Technologies and Environmental Policy*, 12(1): 43 – 52, 2010. (Cited on page 85.)
- [79] Axworthy, A. E.; Dayan, V. H. and Martin, G. B. 'Reactions of fuel-nitrogen compounds under conditions of inert pyrolysis'. *Fuel*, 57(1): 29 – 35, 1978. (Cited on page 71.)

- [80] Bahng, M.-K.; Mukarakate, C.; Robichaud, D. J. and Nimlos, M. R. 'Current technologies for analysis of biomass thermochemical processing: A review'. *Analytica Chimica Acta*, 651(2): 117 – 138, 2009. (Cited on page 110.)
- [81] Balat, M. and Balat, H. 'Progress in biodiesel processing'. *Applied Energy*, 87(6): 1815 – 1835, 2010. (Cited on page 21.)
- [82] Balat, M.; Balat, M.; Kirtay, E. and Balat, H. 'Main routes for the thermoconversion of biomass into fuels and chemicals. Part 1: Pyrolysis systems'. *Energy Conversion and Management*, 50(12): 3147 – 3157, 2009. (Cited on pages 42, 43, 44, and 45.)
- [83] Balat, M.; Balat, M.; Kirtay, E. and Balat, H. 'Main routes for the thermoconversion of biomass into fuels and chemicals. Part 2: Gasification systems'. *Energy Conversion and Management*, 50(12): 3158 – 3168, 2009. (Cited on page 24.)
- [84] Barneto, A. G.; Carmona, J.; Alfonso, J. M. and Ferrer, J. A. C. 'Use of Thermogravimetry/Mass Spectrometry Analysis to Explain the Origin of Volatiles Produced during Biomass Pyrolysis'. *Industrial & Engineering Chemistry Research*, 48(15): 7430–7436, 2009. (Cited on pages 95 and 96.)
- [85] Bartels, M.; Lin, W.; Nijenhuis, J.; Kapteijn, F. and van Ommen, J. R. 'Agglomeration in fluidized beds at high temperatures: Mechanisms, detection and prevention'. *Progress in Energy and Combustion Science*, 34(5): 633–666, 2008. (Cited on pages 25 and 80.)
- [86] Bartle, K.; Perry, D. and Wallace, S. 'The functionality of nitrogen in coal and derived liquids: An XPS study'. *Fuel Processing Technology*, 15: 351 – 361, 1987. Coal Characterisation for Conversion Processes. (Cited on page 54.)
- [87] Basiuk, V. A. 'Pyrolysis of valine and leucine at 500 °C: identification of less-volatile products using gas chromatography-Fourier transform infrared spectroscopy-mass spectrometry'. *Journal of Analytical and Applied Pyrolysis*, 47(2): 127 – 143, 1998. (Cited on pages 67 and 68.)
- [88] Basiuk, V. A. and Douda, J. 'Pyrolysis of poly-glycine and poly-alanine: analysis of less-volatile products by gas chromatography/Fourier transform infrared spectroscopy/mass spectrometry'. *Journal of Analytical and Applied Pyrolysis*, 55(2): 235 – 246, 2000. (Cited on pages 68 and 69.)
- [89] Basiuk, V. A. and Douda, J. 'Analysis of less-volatile products of poly-valine pyrolysis by gas chromatography/Fourier transform infrared spectroscopy/mass spectrometry'. *Journal of Analytical and Applied Pyrolysis*, 60(1): 27 – 40, 2001. (Cited on pages 68 and 69.)

- [90] Bassilakis, R.; Carangelo, R. M. and Wójtowicz, M. A. 'TG-FTIR analysis of biomass pyrolysis'. *Fuel*, 80(12): 1765–1786, 2001. (Cited on pages 40, 74, 95, 96, 123, 126, and 191.)
- [91] Bastiaans, R.; Toland, A.; Holten, A. and de Goey, L. 'Kinetics of CO release from bark and medium density fibreboard pyrolysis'. *Biomass and Bioenergy*, 34(5): 771 – 779, 2010. (Cited on pages 110 and 168.)
- [92] Bauen, A.; Berndes, G.; Junginger, M.; Londo, M. and Vuille, F. 'Bioenergy - A Sustainable and Reliable Energy Source. A review of status and prospects'. Technical Report IEA BIOENERGY: ExCo: 2009:06, International Energy Agency, 2009. (Cited on pages 7, 8, 28, and 39.)
- [93] Baxter, L. 'Biomass-coal co-combustion: opportunity for affordable renewable energy'. *Fuel*, 84(10): 1295 – 1302, 2005. Special Issue Dedicated to Professor Terry Wall. (Cited on page 27.)
- [94] Baxter, L. L. 'Ash deposition during biomass and coal combustion: A mechanistic approach'. *Biomass and Bioenergy*, 4(2): 85–102, 1993. (Cited on pages 39 and 80.)
- [95] Becidan, M. *Experimental Studies on Municipal Solid Waste and Biomass Pyrolysis*. Ph.D. thesis, Norwegian University of Science and Technology, Trondheim, Norway, 2007. (Cited on pages 49, 50, 55, 56, 63, 66, 67, 68, 69, 70, 72, 169, and 191.)
- [96] Becidan, M.; Skreiberg, Ø. and Hustad, J. E. 'An experimental study of nitrogen species release during municipal solid waste (MSW) and biomass pyrolysis and combustion'. In A. V. Bridgwater and D. G. B. Boocock (editors), 'Proceedings of the Science in Thermal and Chemical Biomass Conversion Conference', volume 2, pages 1443 – 1455. CPL Press, Victoria, BC, Canada, 2004. (Cited on page 75.)
- [97] Becidan, M.; Skreiberg, Ø. and Hustad, J. E. 'Experimental study on pyrolysis of thermally thick biomass residues samples: Intra-sample temperature distribution and effect of sample weight ("scaling effect")'. *Fuel*, 86(17-18): 2754 – 2760, 2007. (Cited on pages 184 and 194.)
- [98] Becidan, M.; Skreiberg, Ø. and Hustad, J. E. 'NO<sub>x</sub> and N<sub>2</sub>O Precursors (NH<sub>3</sub> and HCN) in Pyrolysis of Biomass Residues'. *Energy & Fuels*, 21(2): 1173–1180, 2007. (Cited on pages 55, 63, 74, 75, 169, 194, 202, 208, and 215.)
- [99] Becidan, M.; Skreiberg, Ø. and Hustad, J. E. 'Products distribution and gas release in pyrolysis of thermally thick biomass residues samples'. *Journal of Analytical and Applied Pyrolysis*, 78(1): 207 – 213, 2007. (Cited on pages 169, 184, and 192.)

- 
- [100] Becidan, M.; Várhegyi, G.; Hustad, J. E. and Skreiberg, Ø. 'Thermal Decomposition of Biomass Wastes. A Kinetic Study'. *Industrial & Engineering Chemistry Research*, 46(8): 2428–2437, 2007. (Cited on page 95.)
- [101] Beis, S. H.; Onay, Ö. and Koçkar, Ö. M. 'Fixed-bed pyrolysis of safflower seed: influence of pyrolysis parameters on product yields and compositions'. *Renewable Energy*, 26(1): 21 – 32, 2002. (Cited on page 63.)
- [102] Benson, S. W. *Thermochemical Kinetics*. John Wiley & Sons, London (England), 1st edition, 1968. (Cited on page 99.)
- [103] Biagini, E.; Barontini, F. and Tognotti, L. 'Devolatilization of Biomass Fuels and Biomass Components Studied by TG/FTIR Technique'. *Ind. Eng. Chem. Res.*, 45(13): 4486–4493, 2006. (Cited on pages 22, 42, 43, 44, 94, 95, and 206.)
- [104] Biagini, E.; Fantei, A. and Tognotti, L. 'Effect of the heating rate on the devolatilization of biomass residues'. *Thermochimica Acta*, 472(1-2): 55–63, 2008. (Cited on pages 126 and 149.)
- [105] Biagini, E.; Guerrini, L. and Nicoletta, C. 'Development of a Variable Activation Energy Model for Biomass Devolatilization'. *Energy & Fuels*, 23(6): 3300–3306, 2009. (Cited on page 40.)
- [106] Biermann, U.; Friedt, W.; Lang, S.; Lühs, W.; Machmüller, G.; Metzger, J. O.; Klass, M. R.; Schäfer, H. J. and Schneider, M. P. 'New Syntheses with Oils and Fats as Renewable Raw Materials for the Chemical Industry'. In B. Kamm; P. R. Gruber and M. Kamm (editors), 'Biorefineries - Industrial Processes and Products Vol. 2', volume 2, chapter 8, pages 253 – 290. Wiley-VCH, 2006. (Cited on page 47.)
- [107] Blasi, C. D. 'Combustion and gasification rates of lignocellulosic chars'. *Progress in Energy and Combustion Science*, 35(2): 121 – 140, 2009. (Cited on pages 59, 60, and 208.)
- [108] Blasi, C. D.; Branca, C. and D'Errico, G. 'Degradation characteristics of straw and washed straw'. *Thermochimica Acta*, 364(1-2): 133 – 142, 2000. (Cited on page 65.)
- [109] von Blottnitz, H. and Curran, M. A. 'A review of assessments conducted on bio-ethanol as a transportation fuel from a net energy, greenhouse gas, and environmental life cycle perspective'. *Journal of Cleaner Production*, 15(7): 607–619, 2007. (Cited on pages 18 and 19.)
- [110] Bothast, R. and Schlicher, M. 'Biotechnological processes for conversion of corn into ethanol'. *Applied Microbiological Biotechnology*, 67: 19 – 25, 2005. (Cited on pages 47 and 86.)

- [111] Branca, C.; Albano, A. and Blasi, C. D. 'Critical evaluation of global mechanisms of wood devolatilization'. *Thermochimica Acta*, 429(2): 133 – 141, 2005. (Cited on pages 96 and 148.)
- [112] Braun, R. L. and Burnham, A. K. 'Analysis of chemical reaction kinetics using a distribution of activation energies and simpler models'. *Energy Fuels*, 1(2): 153–161, 1987. (Cited on pages 96 and 97.)
- [113] Braun, R. L. and Burnham, A. K. 'KINETICS: A Computer Program to Analyze Chemical Reaction Data'. Technical report, Lawrence Livermore National Laboratory, 1994. (Cited on pages 98, 129, and 158.)
- [114] Bridgwater, A. V. (editor). *Progress in Thermochemical Biomass Conversion*. Wiley-Blackwell, 1st edition, 2001. (Cited on pages 22, 32, 59, and 184.)
- [115] Bridgwater, A. V. 'Renewable fuels and chemicals by thermal processing of biomass'. *Chemical Engineering Journal*, 91(2-3): 87 – 102, 2003. (Cited on pages 22, 23, 24, 25, 184, and 187.)
- [116] Bridgwater, A. V. and Peacocke, G. V. C. 'Fast pyrolysis processes for biomass'. *Renewable and Sustainable Energy Reviews*, 4(1): 1 – 73, 2000. (Cited on page 22.)
- [117] Bryers, R. W. 'Fireside slagging, fouling, and high-temperature corrosion of heat-transfer surface due to impurities in steam-raising fuels'. *Progress in Energy and Combustion Science*, 22(1): 29 – 120, 1996. (Cited on page 25.)
- [118] Buckley, A. N. 'Nitrogen functionality in coals and coal-tar pitch determined by X-ray photoelectron spectroscopy'. *Fuel Processing Technology*, 38(3): 165 – 179, 1994. (Cited on page 54.)
- [119] Burnham, A. K. and Braun, R. L. 'Global Kinetic Analysis of Complex Materials'. *Energy Fuels*, 13(1): 1–22, 1999. (Cited on pages 98, 127, 129, 157, and 158.)
- [120] Caballero, J. A. and Conesa, J. A. 'Mathematical considerations for non-isothermal kinetics in thermal decomposition'. *Journal of Analytical and Applied Pyrolysis*, 73(1): 85–100, 2005. (Cited on page 96.)
- [121] Caballero, J. A.; Font, R. and Marcilla, A. 'Comparative study of the pyrolysis of almond shells and their fractions, holocellulose and lignin. Product yields and kinetics'. *Thermochimica Acta*, 276: 57 – 77, 1996. (Cited on page 191.)
- [122] Carroll, A. and Somerville, C. 'Cellulosic biofuels'. *Annual Review of Plant Biology*, 60: 165 – 182, 2009. (Cited on page 21.)

- [123] Clo, A. 'Compagnie petrolifere: mutamenti strutturali e risposte strategiche'. *Energia*, 3: 36 – 46, 2007. (Cited on page 5.)
- [124] Coats, A. W. and Redfern, J. P. 'Kinetic Parameters from Thermogravimetric Data'. *Nature*, 201: 68 – 69, 1964. (Cited on page 95.)
- [125] Conesa, J. A.; Marcilla, A.; Caballero, J. A. and Font, R. 'Comments on the validity and utility of the different methods for kinetic analysis of thermogravimetric data'. *Journal of Analytical and Applied Pyrolysis*, 58-59: 617-633, 2001. (Cited on page 96.)
- [126] Dale, B. E. and Kim, S. 'Biomass Refining Global Impact - The Biobased Economy of the 21st Century'. In B. Kamm; P. R. Gruber and M. Kamm (editors), 'Biorefineries - Industrial Processes and Products Vol. 1', volume 1, chapter 2, pages 41 – 66. Wiley-VCH, 2006. (Cited on page 51.)
- [127] Das, P.; Ganesh, A. and Wangikar, P. 'Influence of pretreatment for deashing of sugarcane bagasse on pyrolysis products'. *Biomass and Bioenergy*, 27(5): 445 – 457, 2004. (Cited on page 114.)
- [128] Davidson, R. M. 'Nitrogen in coal'. Technical Report IEAPER/o8, IEA Coal Research, 1994. (Cited on page 71.)
- [129] Defoort, F.; Thiery, S.; Puech, A.; Castelli, P.; Masson, E. and Dufour, A. 'Naphthalene, a tar measured on line by FTIR in biomass pyrolysis gas'. In '18th European Biomass Conference and Exhibition: From Research to Industry and Market', Lyon, France, 2010. (Cited on page 92.)
- [130] Demirbas, A. 'Progress and recent trends in biofuels'. *Progress in Energy and Combustion Science*, 33(1): 1 – 18, 2007. (Cited on page 21.)
- [131] Demirbas, A. 'Biorefineries: Current activities and future developments'. *Energy Conversion and Management*, 50(11): 2782 – 2801, 2009. (Cited on page 21.)
- [132] Demirbas, A. 'Political, economic and environmental impacts of biofuels: A review'. *Applied Energy*, 86(Supplement 1): S108 – S117, 2009. Bio-fuels in Asia. (Cited on page 21.)
- [133] Demirbas, A. 'Sustainable Charcoal Production and Charcoal Briquetting'. *Energy Sources, Part A: Recovery, Utilization, and Environmental Effects*, 31(19): 1694 – 1699, 2009. (Cited on page 22.)
- [134] DeNevers, N. *Air pollution control engineering*. Chemical engineering series. McGraw - Hill, Boston, 2000. (Cited on pages 28 and 29.)
- [135] Devezas, T. C. and Corredine, J. T. 'The biological determinants of long-wave behavior in socioeconomic growth and development'. *Technological Forecasting and Social Change*, 68(1): 1 – 57, 2001. (Cited on pages 2 and 4.)

- [136] Devezas, T. C. and Corredine, J. T. 'The nonlinear dynamics of technoeconomic systems: An informational interpretation'. *Technological Forecasting and Social Change*, 69: 317 – 357, 2002. (Cited on page 4.)
- [137] Devezas, T. C.; LePoire, D.; Matias, J. C. O. and Silva, A. M. P. 'Energy scenarios: Toward a new energy paradigm'. *Futures*, 40(1): 1–16, 2008. (Cited on pages 3, 4, and 5.)
- [138] Di Blasi, C.; Signorelli, G.; Di Russo, C. and Rea, G. 'Product Distribution from Pyrolysis of Wood and Agricultural Residues'. *Industrial & Engineering Chemistry Research*, 38(6): 2216–2224, 1999. (Cited on page 192.)
- [139] Di Nola, G. *Biomass fuels characterization for NOx emissions in co-firing applications*. Phd dissertation, Delft University of Technology, Delft, The Netherlands, 2007. (Cited on pages 27, 32, 54, 58, 62, 63, 72, 92, 93, 94, 95, 97, 100, 101, 107, 110, 116, 126, 144, 148, 149, 158, 169, 268, 269, and 270.)
- [140] Di Nola, G.; de Jong, W. and Spliethoff, H. 'The fate of main gaseous and nitrogen species during fast heating rate devolatilization of coal and secondary fuels using a heated wire mesh reactor'. *Fuel Processing Technology*, 90(3): 388–395, 2009. (Cited on pages 27, 40, 58, 63, 75, 100, 110, 168, 169, 184, 192, 194, 203, 211, 218, and 220.)
- [141] Dixon, T.; Mann, A.; Plaza, F. and Gilfillan, W. 'Development of advanced technology for biomass combustion—CFD as an essential tool'. *Fuel*, 84(10): 1303 – 1311, 2005. Special Issue Dedicated to Professor Terry Wall. (Cited on page 100.)
- [142] Dong, L.; Gao, S.; Song, W. and Xu, G. 'Experimental study of NO reduction over biomass char'. *Fuel Processing Technology*, 88(7): 707–715, 2007. (Cited on page 72.)
- [143] Doughty, A. and Mackie, J. C. 'Kinetics of pyrolysis of a coal model compound, 2-picoline, the nitrogen heteroaromatic analogue of toluene. 2. The 2-picoly radical and kinetic modeling'. *The Journal of Physical Chemistry*, 96(25): 10339–10348, 1992. (Cited on page 71.)
- [144] Doughty, A. and Mackie, J. C. 'Kinetics of pyrolysis of the isomeric butenenitriles and kinetic modeling'. *The Journal of Physical Chemistry*, 96(1): 272–281, 1992. (Cited on page 71.)
- [145] van der Drift, A. and Boerrigter, H. 'Synthesis gas from biomass for fuels and chemicals'. Technical Report ECN-C-06-001, Energy research Centre of the Netherlands (ECN), Petten, The Netherlands, 2006. (Cited on page 24.)
- [146] Drummond, A.-R. F. and Drummond, I. W. 'Pyrolysis of Sugar Cane Bagasse in a Wire-Mesh Reactor'. *Industrial & Engineering Chemistry Research*, 35(4): 1263–1268, 1996. (Cited on pages 110, 168, and 185.)



- [147] ECN. 'Phyllis Database for Biomass and Wastes'. 2010. URL <http://www.ecn.nl/phyllis/>. (Cited on pages 22, 30, 38, 40, 46, 48, 51, 145, 191, 207, and 208.)
- [148] El Boushy, A. R.; Klaassen, G. J. and Ketelaars, E. H. 'Biological Conversion of Poultry and Animal Waste to a Feedstuff for Poultry'. *World's Poultry Science Journal*, 41: 133 – 145, 1985. (Cited on page 51.)
- [149] Eriksson, G.; Hedman, H.; Boström, D.; Pettersson, E.; Backman, R. and Öhman, M. 'Combustion Characterization of Rapeseed Meal and Possible Combustion Applications'. *Energy & Fuels*, 23(8): 3930–3939, 2009. (Cited on pages 203, 211, and 215.)
- [150] Escobar, J. C.; Lora, E. S.; Venturini, O. J.; Yáñez, E. E.; Castillo, E. F. and Almazan, O. 'Biofuels: Environment, technology and food security'. *Renewable and Sustainable Energy Reviews*, 13(6-7): 1275 – 1287, 2009. (Cited on page 19.)
- [151] Eurostat. 'European Statistics'. 2010. URL <http://epp.eurostat.ec.europa.eu/portal/page/portal/eurostat/home/>. (Cited on page 9.)
- [152] Faaij, A. P. 'Bio-energy in Europe: changing technology choices'. *Energy Policy*, 34(3): 322 – 342, 2006. (Cited on pages 23, 25, 26, and 27.)
- [153] Fenimore, C. 'Formation of nitric oxide in premixed hydrocarbon flames'. *Symposium (International) on Combustion*, 13(1): 373 – 380, 1971. Thirteenth symposium (International) on Combustion, Thirteenth symposium (International) on Combustion. (Cited on page 61.)
- [154] Figueiredo, J.; Valenzuela, C.; Bernalte, A. and Encinar, J. 'Pyrolysis of holm-oak wood: influence of temperature and particle size'. *Fuel*, 68(8): 1012 – 1016, 1989. (Cited on page 185.)
- [155] Forssén, M.; Hupa, M. and Hellström, P. 'Liquor-to-liquor differences in combustion and gasification processes: Nitrogen oxide formation tendency'. *Tappi Journal*, 82(3): 221 – 227, 1998. (Cited on pages 111, 204, and 218.)
- [156] Forssén, M.; Hupa, M. and Pettersson, R. 'Nitrogen oxide formation during black liquor char combustion and gasification'. *Journal of Pulp and Paper Science*, 23(9): 439 – 446, 1997. (Cited on pages 111 and 204.)
- [157] Friedman, H. J. *Polym. Science: Part C.*, 6: 183, 1964. (Cited on page 95.)
- [158] Friedman, T. L. *Hot, Flat and Crowded: Why the world needs a Green Revolution and how we can renew our global future*. Penguin Group Publisher, London (England), 2008. (Cited on pages 11 and 12.)

- [159] Giuntoli, J.; Arvelakis, S.; Spliethoff, H.; de Jong, W. and Verkooyen, A. H. M. 'Quantitative and Kinetic Thermogravimetric Fourier Transform Infrared (TG-FTIR) Study of Pyrolysis of Agricultural Residues: Influence of Different Pretreatments'. *Energy & Fuels*, 23(11): 5695–5706, 2009. (Cited on pages 22, 42, 43, 58, 85, 95, 148, 168, 188, 191, 206, and 208.)
- [160] Giuntoli, J.; Gout, J.; Verkooyen, A. H. M. and de Jong, W. 'Characterization of fast pyrolysis of biomass fuels using a heated grid reactor: Nitrogen chemistry and reactor modeling'. In '18th European Biomass Conference and Exhibition: From Research to Industry and Market', Lyon, France, 2010. (Cited on page 75.)
- [161] Giuntoli, J.; Gout, J.; Verkooyen, A. H. M. and de Jong, W. 'Characterization of fast pyrolysis of dry distiller's grains (DDGS) and palm kernel cake using a heated foil reactor: nitrogen chemistry and reactor modeling', 2010. Submitted on 29/07/2010. (Cited on page 202.)
- [162] Giuntoli, J.; de Jong, W.; Arvelakis, S.; Spliethoff, H. and Verkooyen, A. H. M. 'Influence of pre-treatments on thermal conversion of agricultural residues: effects on nitrogen chemistry during pyrolysis'. In 'Proceedings 16th European Biomass Conference and Exposition', Berlin, Germany, 2007. (Cited on pages 117 and 148.)
- [163] Giuntoli, J.; de Jong, W.; Arvelakis, S.; Spliethoff, H. and Verkooyen, A. H. M. 'Quantitative and kinetic TG-FTIR study of biomass residue pyrolysis: Dry distiller's grains with solubles (DDGS) and chicken manure'. *Journal of Analytical and Applied Pyrolysis*, 85(1-2): 301–312, 2009. (Cited on pages 22, 42, 43, 48, 58, 74, 95, 114, 116, 117, 125, 126, 129, 131, 138, 139, 168, 172, 173, 177, 184, 188, 191, 192, 193, 202, 203, and 207.)
- [164] Giuntoli, J.; de Jong, W.; Verkooyen, A. H. M.; Piotrowska, P.; Zevenhoven, M. and Hupa, M. 'Combustion characteristics of biomass residues and bio-wastes: fate of fuel-N'. *Energy & Fuels*, 2010. Accepted for publication. (Cited on pages 48, 76, and 191.)
- [165] Glarborg, P.; Jensen, A. D. and Johnsson, J. E. 'Fuel nitrogen conversion in solid fuel fired systems'. *Progress in Energy and Combustion Science*, 29(2): 89 – 113, 2003. (Cited on pages 30, 61, 63, 69, 71, 72, and 202.)
- [166] Glazer, M. *Alkali Metals in combustion of biomass with coal*. Ph.D. thesis, Delft University of Technology, Delft, 2007. (Cited on pages 26, 80, and 81.)
- [167] Glazer, M. P.; Khan, N. A.; de Jong, W.; Spliethoff, H.; Schurmann, H. and Monkhouse, P. 'Alkali Metals in Circulating Fluidized Bed Combustion of Biomass and Coal: Measurements and Chemical Equilibrium Analysis'. *Energy & Fuels*, 19(5): 1889–1897, 2005. (Cited on page 80.)

- [168] Gómez Díaz, C. J. *Understanding Biomass Pyrolysis Kinetics: Improved Modeling Based on Comprehensive Thermokinetic Analysis*. Ph.D. thesis, Universitat Politècnica de Catalunya, Barcelona, Spain, 2006. (Cited on page 96.)
- [169] Gout, J. *Product characterization of fast pyrolysis of dry distillers grains with solubles and palm kernel cake using a heated grid reactor*. Master's thesis, Delft University of Technology, The Netherlands, 2010. (Cited on page 100.)
- [170] Griffiths, P. R. and De Haseth, J. A. *Fourier transform infrared spectrometry*. John Wiley & Sons, New York, USA, 1986. (Cited on page 94.)
- [171] Grønli, M.; Antal, M. and Varhegyi, G. 'A Round-Robin Study of Cellulose Pyrolysis Kinetics by Thermogravimetry'. *Ind. Eng. Chem. Res.*, 38(6): 2238–2244, 1999. (Cited on pages 42, 94, 117, 133, 146, and 148.)
- [172] Grønli, M.; Varhegyi, G. and Di Blasi, C. 'Thermogravimetric Analysis and Devolatilization Kinetics of Wood'. *Ind. Eng. Chem. Res.*, 41(17): 4201–4208, 2002. (Cited on page 95.)
- [173] Gröll, D. R.; Jetxinger, F.; Kozich, M.; Wastyn, M. M. and Wittenberger, R. 'Industrial Starch Platform - Status quo of Production, Modification and Application'. In B. Kamm; P. R. Gruber and M. Kamm (editors), 'Biorefineries - Industrial Processes and Products Vol. 2', volume 2, chapter 2, pages 61 – 96. Wiley-VCH, 2006. (Cited on page 47.)
- [174] Guinesi, L. S.; da Róz, A. L.; Corradini, E.; Mattoso, L. H. C.; Teixeira, E. d. M. and Curvelo, A. A. d. S. 'Kinetics of thermal degradation applied to starches from different botanical origins by non-isothermal procedures'. *Thermochimica Acta*, 447(2): 190–196, 2006. (Cited on pages 47, 94, and 148.)
- [175] Guo, J. *Pyrolysis of wood powder and gasification of wood-derived char*. Ph.D. thesis, Eindhoven University of Technology, Eindhoven, The Netherlands, 2004. (Cited on pages 103, 104, 105, 179, 180, and 183.)
- [176] Hajaligol, M. R.; Howard, J. B.; Longwell, J. P. and Peters, W. A. 'Product compositions and kinetics for rapid pyrolysis of cellulose'. *Industrial & Engineering Chemistry Process Design and Development*, 21(3): 457–465, 1982. (Cited on pages 104, 110, 168, 187, and 192.)
- [177] Hajaligol, M. R.; Howard, J. B. and Peters, W. A. 'An experimental and modeling study of pressure effects on tar release by rapid pyrolysis of cellulose sheets in a screen heater'. *Combustion and Flame*, 95(1-2): 47 – 60, 1993. (Cited on pages 110 and 168.)

- [178] Hämäläinen, J. P. and Aho, M. J. 'Conversion of fuel nitrogen through HCN and NH<sub>3</sub> to nitrogen oxides at elevated pressure'. *Fuel*, 75(12): 1377 – 1386, 1996. (Cited on page 29.)
- [179] Hämäläinen, J. P.; Aho, M. J. and Tummavuori, J. L. 'Formation of nitrogen oxides from fuel-N through HCN and NH<sub>3</sub>: a model-compound study'. *Fuel*, 73(12): 1894 – 1898, 1994. (Cited on page 71.)
- [180] Hansson, K.-M.; Åmand, L.-E.; Habermann, A. and Winter, F. 'Pyrolysis of poly-L-leucine under combustion-like conditions'. *Fuel*, 82(6): 653–660, 2003. (Cited on pages 51, 55, 63, 67, 68, 69, 150, 151, 169, 191, 196, and 202.)
- [181] Hansson, K.-M.; Samuelsson, J.; Åmand, L.-E. and Tullin, C. 'The temperature's influence on the selectivity between HNCO and HCN from pyrolysis of 2,5-diketopiperazine and 2-pyridone'. *Fuel*, 82(18): 2163–2172, 2003. (Cited on pages 69 and 191.)
- [182] Hansson, K.-M.; Samuelsson, J.; Tullin, C. and Åmand, L.-E. 'Formation of HNCO, HCN, and NH<sub>3</sub> from the pyrolysis of bark and nitrogen-containing model compounds'. *Combustion and Flame*, 137(3): 265–277, 2004. (Cited on pages 63, 64, 66, 67, 92, 143, 150, 202, and 208.)
- [183] Hara, T.; Shinguu, H.; Shiishara, K.; Nakagawa, T. and Yoshikawa, K. 'Performance demonstration of a gasification and power generation facility for chicken manure by a long-term continuous operation'. In 'Proceedings 7th High Temperature Air Combustion and Gasification International Symposium', Phuket, Thailand, 2008. (Cited on page 142.)
- [184] van Haveren, J.; Scott, E. and Sanders, J. 'Bulk chemicals from biomass'. *Biofuels, Bioproducts and Biorefining*, 2(1): 41 – 57, 2008. (Cited on page 21.)
- [185] Heikkinen, J. *Characterisation of Supplementary fuels for Co-combustion with Pulverised Coal*. Dissertation, Delft University of Technology, Delft, The Netherlands, 2005. (Cited on pages 47, 94, and 100.)
- [186] Heikkinen, J. M.; Hordijk, J. C.; de Jong, W. and Spliethoff, H. 'Thermogravimetry as a tool to classify waste components to be used for energy generation'. *Journal of Analytical and Applied Pyrolysis*, 71(2): 883 – 900, 2004. (Cited on pages 42, 43, 44, 49, 95, and 148.)
- [187] Hoppesteyn, P. *Application of Low Calorific Value Gaseous Fuels in gas turbine combustors*. Ph.D. thesis, Delft University of Technology, Delft, The Netherlands, 1999. (Cited on page 26.)
- [188] Huber, G.; Iborra, S. and Corma, A. 'Synthesis of transportation fuels from biomass: Chemistry, Catalysts and Engineering'. *Chemical Review*, 106: 4044 – 4098, 2006. (Cited on page 21.)

- [189] Ikeda, E.; Nicholls, P. and Mackie, J. C. 'A kinetic study of the oxidation of pyridine'. *Proceedings of the Combustion Institute*, 28(2): 1709 – 1716, 2000. (Cited on page 71.)
- [190] Ioannidou, O. and Zabaniotou, A. 'Agricultural residues as precursors for activated carbon production–A review'. *Renewable and Sustainable Energy Reviews*, 11(9): 1966 – 2005, 2007. (Cited on pages 115 and 160.)
- [191] Jakab, E.; Faix, O. and Till, F. 'Thermal decomposition of milled wood lignins studied by thermogravimetry/mass spectrometry'. *Journal of Analytical and Applied Pyrolysis*, 40-41: 171 – 186, 1997. PYROLYSIS '96. (Cited on page 94.)
- [192] Jakab, E.; Faix, O.; Till, F. and Székely, T. 'Thermogravimetry/mass spectrometry study of six lignins within the scope of an international round robin test'. *Journal of Analytical and Applied Pyrolysis*, 35(2): 167 – 179, 1995. (Cited on page 94.)
- [193] Jenkins, B. M.; Bakker, R. R. and Wei, J. B. 'On the properties of washed straw'. *Biomass and Bioenergy*, 10(4): 177–200, 1996. (Cited on pages 48, 81, 85, and 114.)
- [194] Jenkins, B. M.; Baxter, L. L.; Miles, T. R. and Miles, T. R. 'Combustion properties of biomass'. *Fuel Processing Technology*, 54(1-3): 17 – 46, 1998. (Cited on page 48.)
- [195] Jensen, A.; Dam-Johansen, K.; Wojtowicz, M. and Serio, M. 'TG-FTIR Study of the Influence of Potassium Chloride on Wheat Straw Pyrolysis'. *Energy & Fuels*, 12(5): 929–938, 1998. (Cited on pages 42, 81, 85, 94, 114, 117, 121, 123, 125, 126, 127, 129, 133, 139, 146, and 148.)
- [196] Jensen, P. A.; Sander, B. and Dam-Johansen, K. 'Pretreatment of straw for power production by pyrolysis and char wash'. *Biomass and Bioenergy*, 20(6): 431–446, 2001. (Cited on page 81.)
- [197] Johnson, D. L. 'The Corn Wet Milling and Corn Dry Milling Industry - A Base for Biorefinery Technology Developments'. In B. Kamm; P. R. Gruber and M. Kamm (editors), 'Biorefineries - Industrial Processes and Products Vol. 1', volume 1, chapter 15, pages 345 – 356. Wiley-VCH, 2006. (Cited on page 47.)
- [198] Johnson, W. R. and Kan, J. C. 'Mechanisms of hydrogen cyanide formation from the pyrolysis of amino acids and related compounds'. *The Journal of Organic Chemistry*, 36(1): 189–192, 1971. (Cited on pages 69 and 193.)
- [199] Johnsson, J. E. 'Formation and reduction of nitrogen oxides in fluidized-bed combustion'. *Fuel*, 73(9): 1398 – 1415, 1994. (Cited on page 63.)

- [200] de Jong, W. *Nitrogen compounds in pressurized fluidized bed gasification of biomass and fossil fuels*. Dissertation, Delft University of Technology, Delft, The Netherlands, 2005. (Cited on pages 23, 25, 26, 29, 32, 63, 94, 95, 100, 110, 149, 168, and 269.)
- [201] de Jong, W. 'Sustainable Hydrogen Production by Thermochemical Biomass Processing'. In R. Gupta (editor), 'Hydrogen Fuel: Production, Transport and Storage', chapter 6, pages 185 – 225. Taylor & Francis group, USA, 1st edition, 2009. (Cited on pages 23, 24, and 25.)
- [202] de Jong, W.; Di Nola, G.; Venneker, B.; Spliethoff, H. and Wójtowicz, M. 'TG-FTIR pyrolysis of coal and secondary biomass fuels: Determination of pyrolysis kinetic parameters for main species and NO<sub>x</sub> precursors'. *Fuel*, 86(15): 2367–2376, 2007. (Cited on pages 32, 48, 58, 63, 74, 95, 97, 99, 100, 129, 132, 148, 154, 158, 164, 202, and 203.)
- [203] de Jong, W. and Marcotullio, G. 'Overview of Biorefineries based on Co-Production of Furfural, Existing Concepts and Novel Developments'. *International Journal of Chemical Reactor Engineering*, 8(A69), 2010. (Cited on page 43.)
- [204] de Jong, W.; Pirone, A. and Wójtowicz, M. A. 'Pyrolysis of Miscanthus Giganteus and wood pellets: TG-FTIR analysis and reaction kinetics'. *Fuel*, 82(9): 1139–1147, 2003. (Cited on pages 32, 40, 74, 95, 97, 99, 133, 148, and 191.)
- [205] Kambara, S.; Takarada, T.; Yamamoto, Y. and Kato, K. 'Relation between functional forms of coal nitrogen and formation of nitrogen oxide (NO<sub>x</sub>) precursors during rapid pyrolysis'. *Energy & Fuels*, 7(6): 1013–1020, 1993. (Cited on page 54.)
- [206] Kamm, B.; Gruber, P. R. and Kamm, M. (editors). *Biorefineries - Industrial Processes and Products Vol. 1*. Wiley-VCH-Verl., Weinheim, 2006. (Cited on page 24.)
- [207] Kamm, B.; Gruber, P. R. and Kamm, M. (editors). *Biorefineries - Industrial Processes and Products Vol. 2*. Wiley-VCH, Weinheim, 2006. (Cited on page 21.)
- [208] Kamm, B.; Kamm, M.; Schmidt, M.; Hirth, T. and Schulze, M. 'Lignocellulose-based Chemical Products and Product Family Trees'. In B. Kamm; P. R. Gruber and M. Kamm (editors), 'Biorefineries - Industrial Processes and Products Vol. 2', volume 2, chapter 3, pages 97 – 149. Wiley-VCH, 2006. (Cited on pages 41, 42, and 46.)
- [209] Karekezi, S.; Lata, K. and Teixeira Coelho, S. 'Traditional Biomass Energy. Improving its Use and Moving to Modern energy use'. Technical report, 2004. (Cited on page 7.)

- [210] Kastanaki, E.; Vamvuka, D.; Grammelis, P. and Kakaras, E. 'Thermogravimetric studies of the behavior of lignite-biomass blends during devolatilization'. *Fuel Processing Technology*, 77-78: 159–166, 2002. (Cited on page 85.)
- [211] Kasuya, F.; Glarborg, P.; Johnsson, J. E. and Dam-Johansen, K. 'The thermal DeNO<sub>x</sub> process: Influence of partial pressures and temperature'. *Chemical Engineering Science*, 50(9): 1455 – 1466, 1995. (Cited on page 214.)
- [212] Kaynak, B.; Topal, H. and Atimtay, A. T. 'Peach and apricot stone combustion in a bubbling fluidized bed'. *Fuel Processing Technology*, 86(11): 1175 – 1193, 2005. (Cited on page 85.)
- [213] Kelemen, S.; Freund, H.; Gorbaty, M. and Kwiatek, P. 'Thermal Chemistry of Nitrogen in Kerogen and Low-Rank Coal'. *Energy Fuels*, 13(2): 529–538, 1999. (Cited on page 54.)
- [214] Kelemen, S.; Gorbaty, M.; Kwiatek, P.; Fletcher, T.; Watt, M.; Solum, M. and Pugmire, R. 'Nitrogen Transformations in Coal during Pyrolysis'. *Energy Fuels*, 12(1): 159–173, 1998. (Cited on page 54.)
- [215] Kelemen, S. R.; Afeworki, M.; Gorbaty, M. L.; Kwiatek, P. J.; Sansone, M.; Walters, C. C. and Cohen, A. D. 'Thermal Transformations of Nitrogen and Sulfur Forms in Peat Related to Coalification'. *Energy & Fuels*, 20(2): 635–652, 2006. (Cited on page 54.)
- [216] Kelemen, S. R.; Gorbaty, M. L. and Kwiatek, P. J. 'Quantification of Nitrogen Forms in Argonne Premium Coals'. *Energy & Fuels*, 8(4): 896–906, 1994. (Cited on page 54.)
- [217] Kelleher, B. P.; Leahy, J. J.; Henihan, A. M.; O'Dwyer, T. F.; Sutton, D. and Leahy, M. J. 'Advances in poultry litter disposal technology - a review'. *Bioresource Technology*, 83(1): 27–36, 2002. (Cited on pages 89 and 203.)
- [218] Khan, A.; de Jong, W.; Jansens, P. and Spliethoff, H. 'Biomass combustion in fluidized bed boilers: Potential problems and remedies'. *Fuel Processing Technology*, 90(1): 21 – 50, 2009. (Cited on pages 25, 27, 29, 39, 48, 80, and 85.)
- [219] Kilpinen, P. and Hupa, M. 'Homogeneous N<sub>2</sub>O chemistry at fluidized bed combustion conditions: A kinetic modeling study'. *Combustion and Flame*, 85(1-2): 94–104, 1991. (Cited on page 63.)
- [220] Kim, Y.; Mosier, N. S.; Hendrickson, R.; Ezeji, T.; Blaschek, H.; Dien, B.; Cotta, M.; Dale, B. and Ladisch, M. R. 'Composition of corn dry-grind ethanol by-products: DDGS, wet cake, and thin stillage'. *Bioresource Technology*, 99(12): 5165 – 5176, 2008. (Cited on pages 46, 51, 86, and 144.)

- [221] Kissinger, H. 'Variation of Peak Temperature with Heating rate in differential thermal analysis'. *Journal of Research of the National Bureau of Standards*, 57(4): 217 – 221, 1956. (Cited on page 96.)
- [222] Kissinger, H. E. 'Reaction Kinetics in Differential Thermal Analysis'. *Analytical Chemistry*, 29(11): 1702 – 1706, 1957. (Cited on pages 95 and 96.)
- [223] Knicker, H.; Almendros, G.; González-Vila, F. J.; Martin, F. and Lázdemann, H. D. '<sup>13</sup>C- and <sup>15</sup>N-NMR spectroscopic examination of the transformation of organic nitrogen in plant biomass during thermal treatment'. *Soil Biology and Biochemistry*, 28(8): 1053 – 1060, 1996. (Cited on page 54.)
- [224] Knicker, H.; Fründ, R. and Lüdemann, H.-D. 'The Chemical Nature of Nitrogen in Native Soil Organic Matter'. *Naturwissenschaften*, 80: 219 – 221, 1993. (Cited on page 54.)
- [225] Knoef, H. *Handbook Biomass Gasification*. BTG (Biomass Technology Group), Enschede, The Netherlands, 2005. (Cited on page 32.)
- [226] Konttinen, J.; Hupa, M.; Kallio, S.; Winter, F. and Samuelsson, J. 'NOx formation Tendency Characterization for Biomass Fuels'. In ASME (editor), '18th International Conference on Fluidized Bed Combustion', ASME, Toronto, Ontario, Canada, 2005. (Cited on pages 76 and 215.)
- [227] Korving, L. D.; Schilt, C. and de Jong, W. 'Reduction of nitrous oxide emissions by a smaller air to fuel ratio in a large-scale sewage sludge fluidized bed combustor'. In 'Fifth International Conference on Waste Management and the Environment', Wessex Institute of Technology, Tallinn, Estonia, 2010. (Cited on pages 89, 204, 214, and 218.)
- [228] Koutinas, A. A.; Wang, R.-H. and Webb, C. 'The biochemurgist - Bioconversion of agricultural raw materials for chemical production'. *Biofuels, Bioproducts and Biorefining*, 1(1): 24 – 28, 2007. (Cited on pages 21, 51, and 88.)
- [229] Kramlich, J. C. and Linak, W. P. 'Nitrous oxide behavior in the atmosphere, and in combustion and industrial systems'. *Progress in Energy and Combustion Science*, 20(2): 149 – 202, 1994. (Cited on page 63.)
- [230] Kripp, T. C. 'Biobased Consumer Products for Cosmetics'. In B. Kamm; P. R. Gruber and M. Kamm (editors), 'Biorefineries - Industrial Processes and Products Vol. 2', volume 2, chapter 15, pages 409 – 441. Wiley-VCH, 2006. (Cited on page 47.)
- [231] Kruse, A. 'Supercritical water gasification'. *Biofuels, Bioproducts and Biorefining*, 2(5): 415 – 437, 2008. (Cited on pages 48 and 57.)



- [232] van Kuijk, H. *Grate Furnace Combustion: A Model for Solid Fuel Layer*. Ph.D. thesis, Eindhoven University of Technology, Eindhoven, The Netherlands, 2008. (Cited on page 26.)
- [233] Kymäläinen, M.; Forssén, M.; Jansson, M. and Hupa, M. 'The Fate of Nitrogen in the chemical recovery process in a kraft pulp mill. Part IV: Smelt Nitrogen and its formation in Black Liquor Combustion'. *Journal of Pulp and Paper Science*, 28(5): 152 – 158, 2002. (Cited on pages 111 and 204.)
- [234] Kymäläinen, M.; Forssén, M.; Kilpinen, P. and Hupa, M. 'Nitrogen oxide formation in Black Liquor single droplet combustion'. *Nordic Pulp and Paper Research Journal*, 16(4): 346 – 354, 2001. (Cited on pages 111, 204, and 215.)
- [235] Ladisch, M.; Mosier, N.; Youngmi, K.; Ximenes, E. and Hogsett, D. 'Converting cellulose to biofuels'. *Chemical Engineering Progress*, 106(3): 56 – 63, 2010. (Cited on page 21.)
- [236] Lang, T.; Jensen, A. and Jensen, P. 'Retention of Organic Elements during Solid Fuel Pyrolysis with Emphasis on the Peculiar Behavior of Nitrogen'. *Energy Fuels*, 19(4): 1631–1643, 2005. (Cited on pages 63 and 65.)
- [237] Lange, J.-P. 'Lignocellulose conversion: An introduction to chemistry, process and economics'. *Biofuels, Bioproducts and Biorefining*, 1(1): 39 – 48, 2007. (Cited on page 21.)
- [238] Lappas, A.; Bezergianni, S. and Vasalos, I. 'Production of biofuels via co-processing in conventional refining processes'. *Catalysis Today*, 145(1-2): 55 – 62, 2009. CATALYSIS FROM ART TO SCIENCE: Special Issue in Honour of the Contribution of Julian Ross to the Advancement of Catalysis Science. (Cited on page 21.)
- [239] Leckner, B.; Åmand, L. E.; Lücke, K. and Werther, J. 'Gaseous emissions from co-combustion of sewage sludge and coal/wood in a fluidized bed'. *Fuel*, 83(4-5): 477–486, 2004. (Cited on pages 40, 89, 204, and 220.)
- [240] Leppälahti, J. 'Formation of NH<sub>3</sub> and HCN in slow-heating-rate inert pyrolysis of peat, coal and bark'. *Fuel*, 74(9): 1363–1368, 1995. (Cited on pages 71, 72, and 74.)
- [241] Leppälahti, J. and Koljonen, T. 'Nitrogen evolution from coal, peat and wood during gasification: Literature review'. *Fuel Processing Technology*, 43(1): 1–45, 1995. (Cited on pages 51, 52, 56, 63, and 208.)
- [242] Li, C.-Z. and Tan, L. L. 'Formation of NO<sub>x</sub> and SO<sub>x</sub> precursors during the pyrolysis of coal and biomass. Part III. Further discussion on the formation of HCN and NH<sub>3</sub> during pyrolysis'. *Fuel*, 79(15): 1899–1906, 2000. (Cited on pages 71, 74, and 75.)

- [243] Li, J.; Wang, Z.; Yang, X.; Hu, L.; Liu, Y. and Wang, C. 'Decomposing or subliming? An investigation of thermal behavior of l-leucine'. *Thermochimica Acta*, 447(2): 147–153, 2006. (Cited on pages 53, 94, 150, and 152.)
- [244] Li, J.; Wang, Z.; Yang, X.; Hu, L.; Liu, Y. and Wang, C. 'Evaluate the pyrolysis pathway of glycine and glycyglycine by TG-FTIR'. *Journal of Analytical and Applied Pyrolysis*, 80(1): 247–253, 2007. (Cited on pages 53, 67, 68, 94, 150, 151, 152, 169, and 191.)
- [245] Li, J.; Yuwen, L.; Jingyan, S.; Zhiyong, W.; Ling, H.; Xi, Y. and Cunxin, W. 'The investigation of thermal decomposition pathways of phenylalanine and tyrosine by TG-FTIR'. *Thermochimica Acta*, 467(1-2): 20–29, 2008. (Cited on pages 53, 67, 94, 150, 151, 152, 169, and 191.)
- [246] Li, S.; Wu, A.; Deng, S. and Pan, W.-p. 'Effect of co-combustion of chicken litter and coal on emissions in a laboratory-scale fluidized bed combustor'. *Fuel Processing Technology*, 89(1): 7–12, 2008. (Cited on pages 89, 203, and 218.)
- [247] Lichtenthaler, F. W. 'The Key Sugars of Biomass: Availability, Present Non-Food Uses and Potential Future Development Lines'. In B. Kamm; P. R. Gruber and M. Kamm (editors), 'Biorefineries - Industrial Processes and Products Vol. 2', volume 2, chapter 1, pages 3 – 60. Wiley-VCH, 2006. (Cited on page 43.)
- [248] Lin, W.; Dam-Johansen, K. and Frandsen, F. 'Agglomeration in bio-fuel fired fluidized bed combustors'. *Chemical Engineering Journal*, 96(1-3): 171 – 185, 2003. (Cited on pages 25 and 80.)
- [249] Llorente, M. F.; Laplaza, J. M.; Cuadrado, R. E. and García, J. C. 'Ash behaviour of lignocellulosic biomass in bubbling fluidised bed combustion'. *Fuel*, 85(9): 1157 – 1165, 2006. (Cited on pages 25 and 80.)
- [250] Loison, R. and Chauvin, R. 'Fast pyrolysis of coal'. *La Chimica e l'Industria*, 91: 269 – 275, 1964. (Cited on page 110.)
- [251] van Loo, S. and Koppejan, J. (editors). *The Handbook of Combustion & Co-firing*. Earthscan, Stirling, UK, 2008. (Cited on pages 27 and 32.)
- [252] Lynd, L.; Wyman, C. and Gerngross, T. 'Biocommodity engineering'. *Biotechnology Progress*, 15(5): 777 – 793, 1999. (Cited on page 21.)
- [253] Mackie, J. C.; Colket, M. B. and Nelson, P. F. 'Shock tube pyrolysis of pyridine'. *The Journal of Physical Chemistry*, 94(10): 4099–4106, 1990. (Cited on page 71.)

- [254] Mamman, A. S.; Lee, J.-M.; Kim, Y.-C.; Hwang, I. T.; Park, N.-J.; Hwang, Y. K. and Chang, H. J.-S., J.-S. 'Furfural: Hemicellulose / xylose-derived biochemical'. *Biofuels, Bioproducts and Biorefining*, 2(5): 438 – 454, 2008. (Cited on page 43.)
- [255] Manya, J.; Velo, E. and Puigjaner, L. 'Kinetics of Biomass Pyrolysis: a Reformulated Three-Parallel-Reactions Model'. *Ind. Eng. Chem. Res.*, 42(3): 434–441, 2003. (Cited on page 94.)
- [256] Marchetti, C. 'Primary Energy Substitution Models: On the Interaction between Energy and Society'. *Technological Forecasting and Social Change*, 10: 345 – 356, 1977. (Cited on pages 2 and 3.)
- [257] Marchetti, C. 'Fifty-year pulsation in human affairs : Analysis of some physical indicators'. *Futures*, 18(3): 376 – 388, 1986. (Cited on page 2.)
- [258] Marcotullio, G.; Krisanti, E.; Giuntoli, J. and de Jong, W. 'Selective production of hemicellulose derived carbohydrates from wheat straw using dilute HCl or FeCl<sub>3</sub> solutions under mild conditions. (Part 1) Thermogravimetric analysis of the solid residues.', 2010. Submitted to *Biore-source Technology*. (Cited on page 85.)
- [259] Martoprawiro, M.; Bacskay, G. B. and Mackie, J. C. 'Ab Initio Quantum Chemical and Kinetic Modeling Study of the Pyrolysis Kinetics of Pyrrole'. *The Journal of Physical Chemistry A*, 103(20): 3923–3934, 1999. (Cited on page 71.)
- [260] Matsumura, Y.; Minowa, T.; Potic, B.; Kersten, S. R.; Prins, W.; van Swaaij, W. P.; van de Beld, B.; Elliott, D. C.; Neuenschwander, G. G.; Kruse, A. and Jr., M. J. A. 'Biomass gasification in near- and super-critical water: Status and prospects'. *Biomass and Bioenergy*, 29(4): 269 – 292, 2005. (Cited on pages 48 and 57.)
- [261] Meier, D. and Faix, O. 'State of the art of applied fast pyrolysis of lignocellulosic materials – a review'. *Bioresource Technology*, 68(1): 71 – 77, 1999. *Bioprocessing and Characterization of Lignocellulosics*. (Cited on page 23.)
- [262] Meszaros, E.; Várhegyi, G.; Jakab, E. and Marosvolgyi, B. 'Thermogravimetric and Reaction Kinetic Analysis of Biomass Samples from an Energy Plantation'. *Energy & Fuels*, 18(2): 497–507, 2004. (Cited on page 96.)
- [263] Miles, T. R.; Miles, T. R., Jr.; Baxter, L. L.; Bryers, R. W.; Jenkins, B. M. and Oden, L. L. 'Boiler deposits from firing biomass fuels'. *Biomass and Bioenergy*, 10(2-3): 125 – 138, 1996. (Cited on pages 25 and 80.)
- [264] Miller, J. A. and Bowman, C. T. 'Mechanism and modeling of nitrogen chemistry in combustion'. *Progress in Energy and Combustion Science*, 15(4): 287 – 338, 1989. (Cited on pages 61, 63, 64, and 66.)

- [265] Miller, J. A. and Glarborg, P. 'Modeling the thermal De-NO<sub>x</sub> process: Closing in on a final solution'. *International Journal of Chemical Kinetics*, 31(11): 757 – 765, 1999. (Cited on page 64.)
- [266] Milne, T. A.; Evans, R. J. and Abatzoglou, N. 'Biomass Gasifier "Tars": Their Nature, Formation, and Conversion'. Technical Report NREL/TP-570-25357, National Renewable Energy Laboratory, Colorado, USA, 1998. (Cited on pages 26, 59, and 177.)
- [267] Miura, K. 'A New and Simple Method to Estimate f(E) and ko(E) in the Distributed Activation Energy Model from Three Sets of Experimental Data'. *Energy Fuels*, 9(2): 302–307, 1995. (Cited on pages 97, 98, and 158.)
- [268] Mohan, D.; Pittman, C. U. and Steele, P. H. 'Pyrolysis of Wood/Biomass for Bio-oil: A Critical Review'. *Energy & Fuels*, 20(3): 848–889, 2006. (Cited on pages 22, 23, 42, 43, 45, 46, and 58.)
- [269] Mullins, O.; Mitra-Kirtley, S.; Van Elp, J. and Cramer, S. 'Molecular Structure of Nitrogen in Coal from XANES Spectroscopy'. *Applied Spectroscopy*, 47(8): 1268 – 1275, 1993. (Cited on page 54.)
- [270] Munir, S.; Nimmo, W. and Gibbs, B. M. 'Co-combustion of agricultural residues with coal: Turning waste into energy'. *Energy & Fuels*, 24(3): 2146 – 2153, 2010. (Cited on page 202.)
- [271] Munir, S.; Nimmo, W. and Gibbs, B. M. 'Shea meal and cotton stalk as potential fuels for co-combustion with coal'. *Bioresource Technology*, 101(19): 7614 – 7623, 2010. (Cited on page 202.)
- [272] Muzio, L. J. and Quartucy, G. C. 'Implementing NO<sub>x</sub> control: Research to application'. *Progress in Energy and Combustion Science*, 23(3): 233 – 266, 1997. (Cited on page 63.)
- [273] Narayan, R. and Antal, M. 'Thermal Lag, Fusion, and the Compensation Effect during Biomass Pyrolysis'. *Ind. Eng. Chem. Res.*, 35(5): 1711–1721, 1996. (Cited on page 99.)
- [274] Nevalainen, H.; Leino, T.; Tourunen, A.; Hiltunen, M. and Coda Zabetta, E. 'Deposits and emissions during the co-combustion of biodiesel residue with coal and biomass in a CFB pilot'. In '9th International Conference on Circulating Fluidized Beds', Hamburg, 2008. (Cited on pages 203, 211, 215, and 218.)
- [275] Nielsen, H. P.; Frandsen, F. J.; Dam-Johansen, K. and Baxter, L. L. 'The implications of chlorine-associated corrosion on the operation of biomass-fired boilers'. *Progress in Energy and Combustion Science*, 26(3): 283 – 298, 2000. (Cited on pages 25, 48, and 80.)

- [276] Niven, R. 'Ethanol in gasoline: environmental impacts and sustainability review article'. *Renewable and Sustainable Energy reviews*, 9: 535 – 555, 2005. (Cited on page 19.)
- [277] Nogami, H. 'Pulverized coal combustion simulation'. In T. Miura (editor), 'Advanced Coal Combustion', Nova Science, Huntington, USA, 2001. (Cited on page 57.)
- [278] di Nola, G.; de Jong, W. and Spliethoff, H. 'TG-FTIR characterization of coal and biomass single fuels and blends under slow heating rate conditions: Partitioning of the fuel-bound nitrogen'. *Fuel Processing Technology*, 91(1): 103 – 115, 2010. (Cited on pages 27, 42, 43, 44, 58, 184, 202, and 203.)
- [279] Nunn, T. R.; Howard, J. B.; Longwell, J. P. and Peters, W. A. 'Product compositions and kinetics in the rapid pyrolysis of sweet gum hardwood'. *Industrial & Engineering Chemistry Process Design and Development*, 24(3): 836–844, 1985. (Cited on pages 185, 187, and 192.)
- [280] Oasmaa, A. and Czernik, S. 'Fuel Oil Quality of Biomass Pyrolysis Oils State of the Art for the End Users'. *Energy & Fuels*, 13(4): 914–921, 1999. (Cited on page 23.)
- [281] Oasmaa, A.; Kuoppala, E. and Solantausta, Y. 'Fast Pyrolysis of Forestry Residue. 2. Physicochemical Composition of Product Liquid'. *Energy & Fuels*, 17(2): 433–443, 2003. (Cited on page 23.)
- [282] Oasmaa, A.; Peacocke, C.; Gust, S.; Meier, D. and McLellan, R. 'Norms and Standards for Pyrolysis Liquids. End-User Requirements and Specifications'. *Energy & Fuels*, 19(5): 2155–2163, 2005. (Cited on page 23.)
- [283] Ollero, P.; Serrera, A.; Arjona, R. and Alcantarilla, S. 'The CO<sub>2</sub> gasification kinetics of olive residue'. *Biomass and Bioenergy*, 24(2): 151–161, 2003. (Cited on page 40.)
- [284] Olsson, J. G.; Jaglid, U.; Pettersson, J. B. C. and Hald, P. 'Alkali Metal Emission during Pyrolysis of Biomass'. *Energy & Fuels*, 11(4): 779–784, 1997. (Cited on page 117.)
- [285] Orfao, J. J. M.; Antunes, F. J. A. and Figueiredo, J. L. 'Pyrolysis kinetics of lignocellulosic materials—three independent reactions model'. *Fuel*, 78(3): 349–358, 1999. (Cited on pages 94, 95, and 96.)
- [286] Pelka, R.; Moszyńska, I. and Arabczyk, W. 'Catalytic ammonia decomposition over Fe/Fe<sub>4</sub>N'. *Catalysis Letters*, 128(1-2): 72 – 76, 2009. (Cited on page 193.)

- [287] Pels, J. R.; Kapteijn, F.; Moulijn, J. A.; Zhu, Q. and Thomas, K. M. 'Evolution of nitrogen functionalities in carbonaceous materials during pyrolysis'. *Carbon*, 33(11): 1641–1653, 1995. (Cited on pages 49 and 54.)
- [288] Petrus, L. and Noordermeer, M. 'Biomass to biofuels, a chemical perspective'. *Green chemistry*, 8: 861 – 867, 2006. (Cited on page 21.)
- [289] Pettersson, A.; Zevenhoven, M.; Steenari, B.-M. and Åmand, L.-E. 'Application of chemical fractionation methods for characterisation of biofuels, waste derived fuels and CFB co-combustion fly ashes'. *Fuel*, 87(15-16): 3183–3193, 2008. (Cited on page 48.)
- [290] Piotrowska, P.; Zevenhoven, M.; Davidsson, K.; Hupa, M.; Åmand, L.-E.; Barišić, V. and Coda Zabetta, E. 'Fate of Alkali Metals and Phosphorus of Rapeseed Cake in Circulating Fluidized Bed Boiler Part 1: Cocombustion with Wood'. *Energy & Fuels*, 24(1): 333–345, 2009. (Cited on page 207.)
- [291] Pokol, G. and Várhegyi, G. 'Kinetic Aspects of Thermal Analysis'. *Critical Reviews in Analytical Chemistry*, 19(1): 65 – 93, 1988. (Cited on page 99.)
- [292] Prins, M. J.; Lindén, J.; Li, Z. S.; Bastiaans, R. J. M.; van Oijen, J. A.; Aldén, M. and de Goey, L. P. H. 'Visualization of Biomass Pyrolysis and Temperature Imaging in a Heated-Grid Reactor'. *Energy & Fuels*, 23(2): 993–1006, 2009. (Cited on pages 104, 105, 179, 180, 182, 183, and 184.)
- [293] Pye, E. K. 'Industrial Lignin Production and Applications'. In B. Kamm; P. R. Gruber and M. Kamm (editors), 'Biorefineries - Industrial Processes and Products Vol. 2', chapter 5, pages 165 – 200. Wiley-VCH, 2006. (Cited on page 44.)
- [294] Ramachandran, S.; Singh, S. K.; Larroche, C.; Soccol, C. R. and Pandey, A. 'Oil cakes and their biotechnological applications - A review'. *Biore-source Technology*, 98(10): 2000–2009, 2007. (Cited on pages 51, 88, and 203.)
- [295] Ratcliff, M. A.; Medley, E. E. and Simmonds, P. G. 'Pyrolysis of amino acids. Mechanistic considerations'. *The Journal of Organic Chemistry*, 39(11): 1481–1490, 1974. (Cited on pages 67, 191, and 193.)
- [296] Rausch, K. and Belyea, R. 'The Future of Coproducts from Corn Processing'. *Applied Biochemistry and Biotechnology*, 128: 47 – 86, 2006. (Cited on page 86.)
- [297] Raveendran, K.; Ganesh, A. and Khilar, K. C. 'Influence of mineral matter on biomass pyrolysis characteristics'. *Fuel*, 74(12): 1812 – 1822, 1995. (Cited on pages 114 and 117.)

- [298] Raveendran, K.; Ganesh, A. and Khilar, K. C. 'Pyrolysis characteristics of biomass and biomass components'. *Fuel*, 75(8): 987–998, 1996. (Cited on pages 114 and 133.)
- [299] Ren, Q.; Zhao, C.; Wu, X.; Liang, C.; Chen, X.; Shen, J. and Wang, Z. 'Formation of NO<sub>x</sub> precursors during wheat straw pyrolysis and gasification with O<sub>2</sub> and CO<sub>2</sub>'. *Fuel*, 89(5): 1064 – 1069, 2010. (Cited on page 63.)
- [300] Rodante, F.; Fantauzzi, F. and Catalani, G. 'Thermal analysis of a series of dipeptides having [alpha]-alanine as the first term. Mutual influence of structures'. *Thermochimica Acta*, 284(2): 351 – 365, 1996. (Cited on pages 53, 67, and 94.)
- [301] Rodante, F.; Marrosu, G. and Catalani, G. 'Thermal analysis of different series of dipeptides'. *Thermochimica Acta*, 197(1): 147 – 160, 1992. (Cited on pages 67 and 94.)
- [302] Rodante, F.; Marrosu, G. and Catalani, G. 'Thermal analysis of some alpha-amino acids with similar structures'. *Thermochimica Acta*, 194: 197 – 213, 1992. (Cited on pages 53, 67, 94, 191, and 196.)
- [303] Roger, C.; Yen, S. and Ramanathan, K. 'Temperature variation of total hemispherical emissivity of stainless steel AISI 304'. *Journal of the Optical Society of America*, 69(10): 1384 – 1390, 1979. (Cited on pages 105 and 180.)
- [304] Sander, B. 'Properties of Danish biofuels and the requirements for power production'. *Biomass and Bioenergy*, 12(3): 177 – 183, 1997. Biomass Quality for Power Production. (Cited on page 81.)
- [305] Sanders, J.; Scott, E.; Weusthuis, R. and Mooibroek, H. 'Bio-Refinery as the Bio-Inspired Process to Bulk Chemicals'. *Macromolecular Bioscience*, 7(2): 105–117, 2007. (Cited on page 21.)
- [306] Sanger, M.; Werther, J. and Ogada, T. 'NO<sub>x</sub> and N<sub>2</sub>O emission characteristics from fluidised bed combustion of semi-dried municipal sewage sludge'. *Fuel*, 80(2): 167 – 177, 2001. (Cited on page 89.)
- [307] Scharlemann, J. and Laurance, W. 'How Green Are Biofuels?' *Science*, 319: 43 – 44, 2008. (Cited on page 19.)
- [308] Schmidt, L. and Dauenhauer, P. 'Chemical engineering: Hybrid routes to biofuels'. *Nature*, 447(7147): 914 – 915, 2007. (Cited on page 21.)
- [309] Scott, D. S.; Piskorz, J.; Bergougnou, M. A.; Graham, R. and Overend, R. P. 'The role of temperature in the fast pyrolysis of cellulose and wood'. *Industrial & Engineering Chemistry Research*, 27(1): 8–15, 1988. (Cited on page 192.)

- [310] Sharma, R. K.; Chan, W. G. and Hajaligol, M. R. 'Product compositions from pyrolysis of some aliphatic [alpha]-amino acids'. *Journal of Analytical and Applied Pyrolysis*, 75(2): 69 – 81, 2006. (Cited on pages 67, 191, and 193.)
- [311] Sharma, R. K.; Chan, W. G.; Seeman, J. I. and Hajaligol, M. R. 'Formation of low molecular weight heterocycles and polycyclic aromatic compounds (PACs) in the pyrolysis of [alpha]-amino acids'. *Journal of Analytical and Applied Pyrolysis*, 66(1-2): 97 – 121, 2003. (Cited on page 94.)
- [312] Sharma, R. K.; Chan, W. G.; Wang, J.; Waymack, B. E.; Wooten, J. B.; Seeman, J. I. and Hajaligol, M. R. 'On the role of peptides in the pyrolysis of amino acids'. *Journal of Analytical and Applied Pyrolysis*, 72(1): 153 – 163, 2004. (Cited on pages 67, 94, and 191.)
- [313] Simmonds, P. G.; Medley, E. E.; Ratcliff, M. A. and Shulman, G. P. 'Thermal decomposition of aliphatic monoaminomonocarboxylic acids'. *Anal. Chem.*, 44(12): 2060–2066, 1972. (Cited on pages 67, 68, 69, 191, and 193.)
- [314] Sjöström, E. *Wood chemistry : fundamentals and applications*. Academic Press, San Diego ; Toronto, 1993. (Cited on pages 30, 39, and 42.)
- [315] Skreiberg, Ø.; Kilpinen, P. and Glarborg, P. 'Ammonia chemistry below 1400 K under fuel-rich conditions in a flow reactor'. *Combustion and Flame*, 136(4): 501–518, 2004. (Cited on pages 64 and 66.)
- [316] Solomon, P.; Serio, M. and Suuberg, E. 'Coal Pyrolysis: Experiments, kinetic rates and mechanisms'. *Prog. Energy Combust. Sci*, 18: 133 – 220, 1992. (Cited on pages 59 and 94.)
- [317] Solomon, P. R. and Colket, M. B. 'Evolution of fuel nitrogen in coal devolatilization'. *Fuel*, 57(12): 749 – 755, 1978. (Cited on pages 110 and 168.)
- [318] Solomon, P. R.; Hamblen, D. G.; Carangelo, R. M.; Serio, M. A. and Deshpande, G. V. 'General model of coal devolatilization'. *Energy & Fuels*, 2(4): 405–422, 1988. (Cited on pages 97, 99, 100, 115, 133, and 158.)
- [319] Solomons, T. and Fryhle, C. *Organic Chemistry*. Wiley International Edition, 8th edition, 2004. (Cited on pages 39, 46, 49, 55, 56, and 148.)
- [320] Solum, M. S.; Altmann, K. L.; Strohmeier, M.; Berges, D. A.; Zhang, Y.; Facelli, J. C.; Pugmire, R. J. and Grant, D. M. '<sup>15</sup>N Chemical Shift Principal Values in Nitrogen Heterocycles'. *Journal of the American Chemical Society*, 119(41): 9804–9809, 1997. (Cited on page 54.)
- [321] Sørensen, C. O.; Johnsson, J. E. and Jensen, A. 'Reduction of NO over Wheat Straw Char'. *Energy & Fuels*, 15(6): 1359–1368, 2001. (Cited on page 72.)



- [322] Sorrell, S.; Speirs, J.; Bentley, R.; Brandt, A. and Miller, R. 'An Assessment of the evidence for a near-term peak in global oil production'. Technical report, UK Energy research Centre, 2009. (Cited on page 7.)
- [323] Speight, J. G. (editor). *The chemistry and technology of coal*. CRC Press, 2nd edition, 1994. (Cited on page 38.)
- [324] Stenseng, M. *Pyrolysis and combustion of biomass*. Ph.D. thesis, Technical University of Denmark, Lyngby, Denmark, 2001. (Cited on page 65.)
- [325] Stenseng, M.; Jensen, A. and Dam-Johansen, K. 'Investigation of biomass pyrolysis by thermogravimetric analysis and differential scanning calorimetry'. *Journal of Analytical and Applied Pyrolysis*, 58-59: 765-780, 2001. (Cited on page 117.)
- [326] Stern, N. 'The Economics of Climate Change'. Technical report, Cambridge (UK), 2006. (Cited on pages 12 and 13.)
- [327] Stevens, D. J. 'Hot Gas Conditioning: Recent Progress With Larger-Scale Biomass Gasification Systems'. Technical Report NREL/SR-510-29952, National Renewable Energy Laboratory (NREL), Richland, Washington, USA, 2001. (Cited on page 26.)
- [328] Stubington, J. F. and Aiman, S. 'Pyrolysis kinetics of bagasse at high heating rates'. *Energy & Fuels*, 8(1): 194-203, 1994. (Cited on pages 48, 110, 168, 185, and 187.)
- [329] Tamboer, R. *Fast pyrolysis of biomass in a heated wire mesh & FTIR laboratory setup*. Master's thesis, Delft University of Technology, The Netherlands, 2007. (Cited on pages 100, 101, 107, 110, 168, 268, and 270.)
- [330] Tan, L. L. and Li, C.-Z. 'Formation of NO<sub>x</sub> and SO<sub>x</sub> precursors during the pyrolysis of coal and biomass. Part I. Effects of reactor configuration on the determined yields of HCN and NH<sub>3</sub> during pyrolysis'. *Fuel*, 79(15): 1883-1889, 2000. (Cited on page 71.)
- [331] Terentis, A.; Doughty, A. and Mackie, J. C. 'Kinetics of pyrolysis of a coal model compound, 2-picoline, the nitrogen heteroaromatic analog of toluene. 1. Product distributions'. *The Journal of Physical Chemistry*, 96(25): 10334-10339, 1992. (Cited on page 71.)
- [332] Tian, F.-J.; Li, B.-Q.; Chen, Y. and Li, C.-Z. 'Formation of NO<sub>x</sub> precursors during the pyrolysis of coal and biomass. Part V. Pyrolysis of a sewage sludge'. *Fuel*, 81(17): 2203 - 2208, 2002. (Cited on page 63.)
- [333] Tian, F.-J.; Yu, J.; McKenzie, L.; Hayashi, J.-i. and Li, C.-Z. 'Conversion of Fuel-N into HCN and NH<sub>3</sub> during the Pyrolysis and Gasification in Steam: A Comparative Study of Coal and Biomass'. *Energy Fuels*, 21(2): 517-521, 2007. (Cited on page 75.)

- [334] Tiffany, D. G.; Morey, R. V. and De Kam, M. 'Use of distillers by-products and corn stover as fuels for ethanol plants'. In 'Farm Foundation Conference on Transition to a Bioeconomy: Integration of Agricultural and Energy Systems', Atlanta, Georgia, 2008. (Cited on pages 86 and 88.)
- [335] Tiffany, D. G.; Morey, R. V. and De Kam, M. 'Economics of Biomass Gasification / Combustion at Fuel Ethanol Plants'. *Applied Engineering in Agriculture*, 25(3): 391 – 400, 2009. (Cited on page 86.)
- [336] Tillman, D. A. 'Biomass cofiring: the technology, the experience, the combustion consequences'. *Biomass and Bioenergy*, 19(6): 365 – 384, 2000. (Cited on pages 27 and 85.)
- [337] Torres, W.; Pansare, S. S. and Goodwin Jr., J. G. 'Hot gas removal of tars, ammonia, and hydrogen sulfide from biomass gasification gas'. *Catalysis Reviews - Science and Engineering*, 49(4): 407 – 456, 2007. (Cited on page 26.)
- [338] Tortosa Masía, A.; Buhre, B.; Gupta, R. and Wall, T. 'Characterising ash of biomass and waste'. *Fuel Processing Technology*, 88: 1071 – 1081, 2007. (Cited on pages 40, 48, and 207.)
- [339] Tsamba, A. J.; Yang, W.; Blasiak, W. and Wójtowicz, M. A. 'Cashew Nut Shells Pyrolysis: Individual Gas Evolution Rates and Yields'. *Energy & Fuels*, 21(4): 2357–2362, 2007. (Cited on pages 97, 99, 129, 133, and 158.)
- [340] Turn, S. Q.; Kinoshita, C. M. and Ishimura, D. M. 'Removal of inorganic constituents of biomass feedstocks by mechanical dewatering and leaching'. *Biomass and Bioenergy*, 12(4): 241–252, 1997. (Cited on page 48.)
- [341] Ucar, S. and Ozkan, A. R. 'Characterization of products from the pyrolysis of rapeseed oil cake'. *Bioresource Technology*, 99(18): 8771–8776, 2008. (Cited on page 40.)
- [342] Ungerer, P. and Pelet, R. 'Extrapolation of the kinetics of oil and gas formation from laboratory experiments to sedimentary basins'. *Nature*, 327: 52 – 54, 1987. (Cited on pages 98 and 158.)
- [343] Vamvuka, D.; Pasadakis, N.; Kastanaki, E.; Grammelis, P. and Kakaras, E. 'Kinetic Modeling of Coal/Agricultural By-Product Blends'. *Energy Fuels*, 17(3): 549–558, 2003. (Cited on pages 40, 85, and 99.)
- [344] Várhegyi, G.; Antal, M. J.; Jakab, E. and Szabo, P. 'Kinetic modeling of biomass pyrolysis'. *Journal of Analytical and Applied Pyrolysis*, 42(1): 73–87, 1997. (Cited on pages 94 and 96.)

- [345] Várhegyi, G.; Antal, M. J.; Szekely, T. and Szabo, P. 'Kinetics of the thermal decomposition of cellulose, hemicellulose, and sugarcane bagasse'. *Energy Fuels*, 3(3): 329–335, 1989. (Cited on pages 42, 43, 94, and 95.)
- [346] Varhegyi, G.; Antal, M. J.; Szekely, T.; Till, F. and Jakab, E. 'Simultaneous thermogravimetric-mass spectrometric studies of the thermal decomposition of biopolymers. 1. Avicel cellulose in the presence and absence of catalysts'. *Energy & Fuels*, 2(3): 267–272, 1988. (Cited on pages 95, 114, 121, 125, and 127.)
- [347] Várhegyi, G.; Antal, M. J.; Szekely, T.; Till, F.; Jakab, E. and Szabo, P. 'Simultaneous thermogravimetric-mass spectrometric studies of the thermal decomposition of biopolymers. 2. Sugarcane bagasse in the presence and absence of catalysts'. *Energy & Fuels*, 2(3): 273–277, 1988. (Cited on pages 95, 114, 117, and 125.)
- [348] Várhegyi, G.; Jakab, E.; Till, F. and Szekely, T. 'Thermogravimetric-mass spectrometric characterization of the thermal decomposition of sunflower stem'. *Energy & Fuels*, 3(6): 755–760, 1989. (Cited on pages 95 and 127.)
- [349] Várhegyi, G.; Mészáros, E.; Antal, M. J.; Bourke, J. and Jakab, E. 'Combustion Kinetics of Corncob Charcoal and Partially Demineralized Corncob Charcoal in the Kinetic Regime'. *Industrial & Engineering Chemistry Research*, 45(14): 4962–4970, 2006. (Cited on page 208.)
- [350] Várhegyi, G.; Szabo, P.; Jakab, E. and Till, F. 'Least squares criteria for the kinetic evaluation of thermoanalytical experiments. Examples from a char reactivity study'. *Journal of Analytical and Applied Pyrolysis*, 57(2): 203–222, 2001. (Cited on pages 96 and 133.)
- [351] Vassilev, S. V.; Baxter, D.; Andersen, L. K. and Vassileva, C. G. 'An overview of the chemical composition of biomass'. *Fuel*, 89: 913 – 933, 2010. (Cited on page 48.)
- [352] de Velden, M. V.; Baeyens, J.; Brems, A.; Janssens, B. and Dewil, R. 'Fundamentals, kinetics and endothermicity of the biomass pyrolysis reaction'. *Renewable Energy*, 35(1): 232 – 242, 2010. (Cited on pages 22 and 23.)
- [353] Voorhees, K. J.; Zhang, W.; Hendricker, A. D. and Murugaverl, B. 'An investigation of the pyrolysis of oligopeptides by Curie-point pyrolysis–tandem mass spectrometry'. *Journal of Analytical and Applied Pyrolysis*, 30(1): 1 – 16, 1994. (Cited on pages 67 and 191.)
- [354] Wallace, S.; Bartle, K. D. and Perry, D. L. 'Quantification of nitrogen functional groups in coal and coal derived products'. *Fuel*, 68(11): 1450 – 1455, 1989. (Cited on page 54.)

- [355] Wang, M.; Saricks, C. and Santini, D. 'Effects of Fuel Ethanol Use on Fuel-Cycle Energy and Greenhouse Gas Emissions'. Technical report, US DOE, Argonne National Laboratory, 1999. (Cited on page 41.)
- [356] Wang, M.; Wu, M. and Huo, H. 'Life-cycle energy and greenhouse gas emission impacts of different corn ethanol plant types'. *Environmental Research Letters*, 2(2): 024001, 2007. (Cited on page 88.)
- [357] Wei, L.; Xu, S.; Zhang, L.; Zhang, H.; Liu, C.; Zhu, H. and Liu, S. 'Characteristics of fast pyrolysis of biomass in a free fall reactor'. *Fuel Processing Technology*, 87(10): 863 – 871, 2006. (Cited on page 185.)
- [358] Weiland, P. 'Biogas production: current state and perspectives'. *Applied Microbiological Biotechnology*, 85: 849 – 860, 2010. (Cited on page 208.)
- [359] Werther, J. and Ogada, T. 'Sewage sludge combustion'. *Progress in Energy and Combustion Science*, 25(1): 55–116, 1999. (Cited on pages 48, 89, 204, 208, and 218.)
- [360] Werther, J.; Saenger, M.; Hartge, E. U.; Ogada, T. and Siagi, Z. 'Combustion of agricultural residues'. *Progress in Energy and Combustion Science*, 26(1): 1 – 27, 2000. (Cited on pages 25, 27, 48, 80, and 85.)
- [361] Whitely, N.; Ozao, R.; Artiaga, R.; Cao, Y. and Pan, W.-P. 'Multi-utilization of Chicken Litter as Biomass Source. Part I. Combustion'. *Energy Fuels*, 20(6): 2660–2665, 2006. (Cited on pages 89 and 148.)
- [362] Winter, F.; Wartha, C. and Hofbauer, H. 'NO and N<sub>2</sub>O formation during the combustion of wood, straw, malt waste and peat'. *Bioresource Technology*, 70(1): 39–49, 1999. (Cited on pages xxiv, 76, 202, 214, 215, 216, and 218.)
- [363] Wójtowicz, M. A.; Bassilakis, R.; Smith, W. W.; Chen, Y. and Carangelo, R. M. 'Modeling the evolution of volatile species during tobacco pyrolysis'. *Journal of Analytical and Applied Pyrolysis*, 66(1-2): 235–261, 2003. (Cited on pages 95 and 97.)
- [364] Xu, X. G.; Li, S. Q.; Li, G. D. and Yao, Q. 'Effect of Co-firing Straw with Two Coals on the Ash Deposition Behavior in a Down-Fired Pulverized Coal Combustor'. *Energy & Fuels*, 24(1): 241–249, 2009. (Cited on page 85.)
- [365] Yaman, S. 'Pyrolysis of biomass to produce fuels and chemical feedstocks'. *Energy Conversion and Management*, 45(5): 651–671, 2004. (Cited on pages 22 and 23.)
- [366] Yang, H.; Yan, R.; Chen, H.; Lee, D. H. and Zheng, C. 'Characteristics of hemicellulose, cellulose and lignin pyrolysis'. *Fuel*, 86(12-13): 1781–1788, 2007. (Cited on pages 42, 43, 44, 94, 125, 126, 148, 149, and 155.)

- [367] Yee, K. F.; Tan, K. T.; Abdullah, A. Z. and Lee, K. T. 'Life cycle assessment of palm biodiesel: Revealing facts and benefits for sustainability'. *Applied Energy*, 86(Supplement 1): S189 – S196, 2009. Bio-fuels in Asia. (Cited on page 19.)
- [368] Yim, S. D.; Kim, S. J.; Baik, J. H.; Nam, I.; Mok, Y. S.; Lee, J.-H.; Cho, B. K. and Oh, S. H. 'Decomposition of Urea into NH<sub>3</sub> for the SCR Process'. *Industrial & Engineering Chemistry Research*, 43(16): 4856–4863, 2004. (Cited on pages 154 and 156.)
- [369] Zanzi, R.; Sjöström, K. and Björnbom, E. 'Rapid pyrolysis of agricultural residues at high temperature'. *Biomass and Bioenergy*, 23(5): 357 – 366, 2002. (Cited on page 65.)
- [370] Zeldovich, Y. B.; Sadovnikov, P. Y. and Frank-Kamenetskii, D. A. 'The oxidation of nitrogen in combustion and explosions'. *Acta Physicochem USSR*, 21: 577 – 628, 1946. (Cited on page 60.)
- [371] Zelkowski, J. *Kohleverbrennung: Brennstoff, Physik, Theori und Technik (Coal combustion, fuel, physics, theory and technology)*. VGB, Essen, 1986. (Cited on page 62.)
- [372] Zevenhoven, R. and Hupa, M. 'The reactivity of chars from coal, peat and wood towards NO, with and without CO'. *Fuel*, 77(11): 1169–1176, 1998. (Cited on pages 72 and 208.)
- [373] Zevenhoven-Onderwater, M. *Ash-forming Matter in Biomass Fuels*. Ph.D. thesis, Åbo Akademi University, Turku, Finland, 2001. (Cited on page 80.)
- [374] Zevenhoven-Onderwater, M.; Backman, R.; Skrifvars, B.-J. and Hupa, M. 'The ash chemistry in fluidised bed gasification of biomass fuels. Part I: predicting the chemistry of melting ashes and ash-bed material interaction'. *Fuel*, 80(10): 1489–1502, 2001. (Cited on page 80.)
- [375] Zevenhoven-Onderwater, M.; Backman, R.; Skrifvars, B. J.; Hupa, M.; Liliendahl, T.; Rosén, C.; Sjöström, K.; Engvall, K. and Hallgren, A. 'The ash chemistry in fluidised bed gasification of biomass fuels. Part II: Ash behaviour prediction versus bench scale agglomeration tests'. *Fuel*, 80(10): 1503 – 1512, 2001. (Cited on pages 80 and 114.)
- [376] Zevenhoven-Onderwater, M.; Blomquist, J. P.; Skrifvars, B. J.; Backman, R. and Hupa, M. 'The prediction of behaviour of ashes from five different solid fuels in fluidised bed combustion'. *Fuel*, 79(11): 1353–1361, 2000. (Cited on page 80.)
- [377] Zhou, H.; Jensen, A. D.; Glarborg, P. and Kavaliauskas, A. 'Formation and reduction of nitric oxide in fixed-bed combustion of straw'. *Fuel*, 85(5-6): 705–716, 2006. (Cited on pages 63 and 72.)

#### BIBLIOGRAPHY

---

- [378] Zhu, S. and Lee, S. W. 'Co-combustion performance of poultry wastes and natural gas in the advanced Swirling Fluidized Bed Combustor (SFBC)'. *Waste Management*, 25(5): 511–518, 2005. (Cited on pages 89 and 203.)
- [379] Zivkovic, Z. D. 'The kinetics and mechanism of the thermal decomposition of tetramminecopper(II) sulphate monohydrate'. *Thermochimica Acta*, 203: 251–257, 1992. (Cited on pages 94 and 144.)

# A

---

## QUANTIFICATION METHOD FOR THE FTIR IN COMBINATION WITH TGA

---

*This section introduces the specific parameters of the quantification method used to quantify the gaseous species in the FTIR when used in combination with TGA during the measurements described in Chapters 4 and 5.*

A.1 GENERAL

The quantification method used in this work and described in this section was implemented on the software package from the manufacturer of the FTIR, Thermo Nicolet, called Quant Setup and applicable with the other software OMNIC.

Many of the parameters used in the measurements are described either in the previous Chapters 3, 4 and 5 or in the previous works of our section, namely the PhD Dissertation of Dr. Gianluca Di Nola [139]. Also the calibration data used in the present work are the same as the ones retrieved and described in previous works [139, 329].

Since in the present work, however, several details of the quantification method were modified, the purpose of this section is to give such specific details which differ from other works.

A.2 SPECIES AND SPECTRAL REGIONS

Tables 47, 48 summarize the limits of validity of the calibration lines and the spectral regions and specific windows used for each quantified species. Table 49, moreover, illustrates the eventual interferences between the calibration spectra that the software will take into account.

A.3 CALIBRATION LINES

Figures 118 till 126 show the actual calibration curve for the species most commonly used in TG-FTIR measurements together with the parameters of the curve and the relative error after calibration is applied.

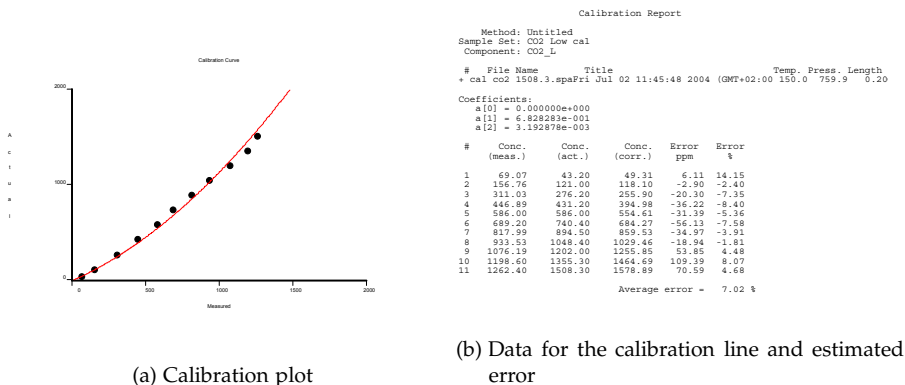
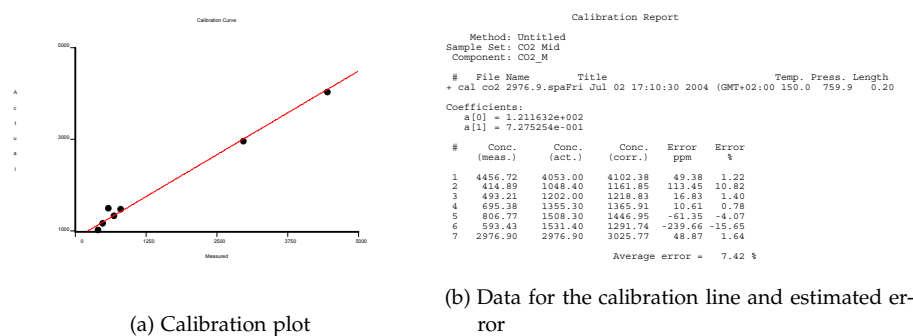


Figure 118: Calibration line plot and data for the species: CO<sub>2</sub> Low.



Table 47: Calibration range of the different species.

Species	Concentration limits [ppm <sub>v</sub> ]		Calibration standard [ppm <sub>v</sub> ]
	Low	High	
CO <sub>2</sub> Low	43.2	1508.3	586
CO <sub>2</sub> Mid	1048	4053	2976.9
CO <sub>2</sub> High	1202	29210	24686
CO <sub>2</sub> Very High	29210	165747	154044
CO Low	181	6384	2178.4
CO Mid	4830	17912	6384
CO Very High	14846	90964	88723
CH <sub>4</sub> Low	199	1801	1443
CH <sub>4</sub> High	1801	19683	14521
HCN	41	920	662
NH <sub>3</sub>	41	920	920
HNCO	225	371	371
H <sub>2</sub> O	481	1630	1140.7
H <sub>2</sub> O Very High	1141	6146	2674.5

Figure 119: Calibration line plot and data for the species: CO<sub>2</sub> Mid.

Additional information on calibration techniques and calibration spectra can be found in the works of de Jong [200] and Di Nola [139] and in the Chapters 4 and 5.

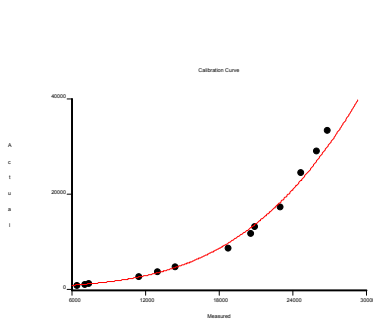
Table 48: Spectral regions and windows for the different species.

Species	Regions [cm <sup>-1</sup> ]		Windows [cm <sup>-1</sup> ]	
	Start	End	Start	End
CO <sub>2</sub> Low	2378.2	2386.8	2378.2	2380.0
			2385.2	2386.8
CO <sub>2</sub> Mid	2378.2	2383.7	2378.2	2381.1
			2382.0	2383.7
CO <sub>2</sub> High	2372.3	2387.9	2372.3	2377.7
			2385.7	2387.9
CO <sub>2</sub> Very High	2392.4	3516.8	2392.4	2394.9
			3515.7	3516.8
CO Low	2107.5	2131.7	2107.5	2131.7
CO Mid	2107.4	2131.8	2107.4	2131.8
CO Very High	2096.9	2101.8	2096.9	2097.7
			2101.0	2101.8
CH <sub>4</sub> Low	3056.8	3166.4	3056.8	3166.4
CH <sub>4</sub> High	2998.7	3131.0	2998.7	3028.9
			3048.0	3131.0
HCN	3273.0	3278.7	3273.0	3278.7
NH <sub>3</sub>	881.0	899.0	881.0	899.0
HNCO	2250.1	2274.2	2250.1	2252.3
			2271.4	2274.2
H <sub>2</sub> O	3700.0	3919.0	3700.0	3919.0
H <sub>2</sub> O Very High	3970.0	3975.5	3970.0	3973.2
			3973.6	3975.5

For the measurements on the heated foil setup, a detailed description of the quantification method can be found in the works of Tamboer [329] and Di Nola [139].

Table 49: Calibration matrix to account for mutual overlapping. S=Sample, I=Interference.

Species	Region [cm <sup>-1</sup> ]		Components in regions															
	Start	End	CO <sub>2</sub> Low	CO <sub>2</sub> Mid	CO <sub>2</sub> High	CO <sub>2</sub> V. High	CO Low	CO Mid	CO High	CO V. High	CH <sub>4</sub> Low	CH <sub>4</sub> High	HCN	NH <sub>3</sub>	H <sub>2</sub> O	H <sub>2</sub> O V. High	HNCO	
CO <sub>2</sub> Low	2378.2	2386.8	S	-	-	-	-	-	-	-	-	-	-	-	-	-	-	-
CO <sub>2</sub> Mid	2378.2	2383.7	-	S	-	-	-	-	-	-	-	-	-	-	-	-	-	-
CO <sub>2</sub> High	2372.3	2387.9	-	-	S	-	-	-	-	-	-	-	-	-	-	-	-	-
CO <sub>2</sub> Very High	2392.4	3516.8	-	-	-	S	-	-	-	-	-	-	-	-	-	-	-	-
CO Low	2107.5	2131.7	-	-	-	-	S	-	-	-	-	-	-	-	-	-	-	-
CO Mid	2107.4	2131.8	-	-	-	-	-	S	-	-	-	-	-	-	-	-	-	-
CO Very High	2096.9	2101.8	-	-	-	-	-	-	S	-	-	-	-	-	-	-	-	-
CH <sub>4</sub> Low	3056.8	3166.4	-	-	-	-	-	-	-	S	-	-	-	-	-	-	-	-
CH <sub>4</sub> High	2998.7	3131.0	-	-	-	-	-	-	-	-	S	-	-	-	-	-	-	-
HCN	3273.0	3278.7	-	-	-	-	-	-	-	-	-	-	S	-	-	-	-	-
NH <sub>3</sub>	881.0	899.0	-	-	-	-	-	-	-	-	-	-	-	S	-	-	-	-
H <sub>2</sub> O	3700.0	3919.0	-	-	-	-	-	-	-	-	-	-	-	-	S	-	-	-
H <sub>2</sub> O Very High	3970.0	3975.5	-	-	-	-	-	-	-	-	-	-	-	-	-	S	-	-
HNCO	2250.1	2274.2	I	I	I	I	I	I	I	-	-	-	-	-	-	-	-	S



(a) Calibration plot

Calibration Report

Method: Untitled  
 Sample Set: CO2 High cal  
 Component: CO2\_H

# File Name Title Temp. Press. Length  
 + cal co2 1202.spa Fri Jul 02 11:59:49 2004 (GMT+02:00) 150.0 759.9 0.20

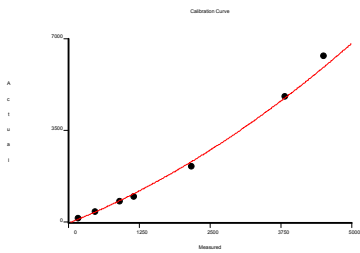
Coefficients:  
 a[0] = 0.000000e+000  
 a[1] = 2.874327e-001  
 a[2] = -2.038136e-004  
 a[3] = 1.121107e-007

#	Conc. (meas.)	Conc. (act.)	Conc. (corr.)	Error ppm	Error %
1	26860.50	33461.00	30128.41	-3332.59	-9.96
2	18778.56	3023.00	10007.62	-884.62	-10.91
3	20583.33	11926.00	13156.62	1230.62	10.32
4	23910.20	11445.00	11800.38	355.38	2.64
5	23035.52	17585.00	18584.95	999.95	5.69
6	24686.00	24686.00	23073.36	-1612.64	-6.53
7	25967.30	29210.00	27065.92	-2144.08	-7.34
8	14453.10	5036.00	4874.50	-161.50	-3.21
9	12989.31	4053.00	3765.68	-287.32	-7.09
10	11449.70	2976.90	2866.83	-110.07	-3.70
11	7374.45	1508.30	1450.52	-57.98	-3.83
12	7051.54	1355.30	1379.29	23.99	1.77
13	6453.55	1202.00	1257.16	55.16	4.59

Average error = 6.64 %

(b) Data for the calibration line and estimated error

Figure 120: Calibration line plot and data for the species: CO<sub>2</sub> High.



(a) Calibration plot

Calibration Report

Method: Untitled  
 Sample Set: CO Low cal  
 Component: CO\_L

# File Name Title Temp. Press. Length  
 + cal co 6384.spa Mon Jul 12 16:44:56 2004 (GMT+02:00) 150.0 759.9 0.20

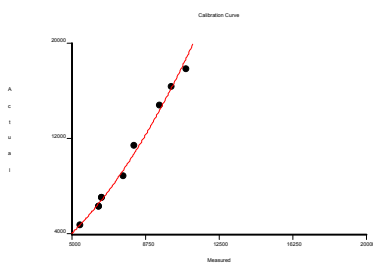
Coefficients:  
 a[0] = 0.000000e+000  
 a[1] = 8.517672e-001  
 a[2] = 7.291173e-004

#	Conc. (meas.)	Conc. (act.)	Conc. (corr.)	Error ppm	Error %
1	2178.40	2178.40	2342.95	164.55	7.55
2	182.16	181.00	158.67	-22.43	-12.39
3	477.78	434.30	430.41	-3.89	-0.90
4	908.03	836.70	858.12	21.42	2.56
5	1158.70	1038.30	1124.85	86.55	8.34
6	3820.35	4830.00	4753.29	-76.71	-1.59
7	4515.06	6384.00	5939.87	-444.13	-6.96

Average error = 6.95 %

(b) Data for the calibration line and estimated error

Figure 121: Calibration line plot and data for the species: CO Low.



(a) Calibration plot

Calibration Report

Method: Untitled  
 Sample Set: CO Medium cal  
 Component: CO\_M

# File Name Title Temp. Press. Length  
 + cal co 16410.spa Tue Jul 13 12:42:28 2004 (GMT+02:00) 150.0 759.9 0.20

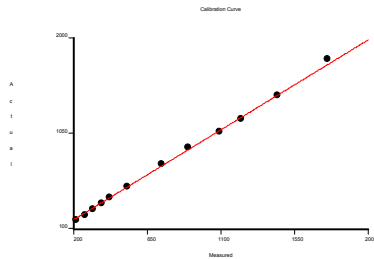
Coefficients:  
 a[0] = 0.000000e+000  
 a[1] = 4.861268e-002  
 a[2] = 1.100925e-003

#	Conc. (meas.)	Conc. (act.)	Conc. (corr.)	Error ppm	Error %
1	7631.43	8979.00	9404.15	425.15	4.73
2	5402.45	4830.00	4789.62	-40.38	-0.84
3	6384.00	6384.00	6631.75	247.75	3.88
4	6539.60	7197.00	6951.22	-245.78	-3.41
5	10828.98	17912.00	18715.17	803.17	4.48
6	6384.00	6384.00	6631.75	247.75	3.88
7	6539.60	7197.00	6951.22	-245.78	-3.41
8	8168.68	11511.00	10746.91	-764.09	-6.64
9	9479.75	14846.00	14399.50	-446.50	-3.01
10	10069.45	16410.00	16216.26	-193.74	-1.18

Average error = 3.89 %

(b) Data for the calibration line and estimated error

Figure 122: Calibration line plot and data for the species: CO Mid.



(a) Calibration plot

Calibration Report

Method: Untitled  
 Sample Set: CH4 Low cal  
 Component: CH4\_L

# File Name Title Temp. Press. Length  
 + cal ch4 1801.spa Wed Aug 18 15:46:53 2004 (GMT+02:00) 150.0 759.9 0.20

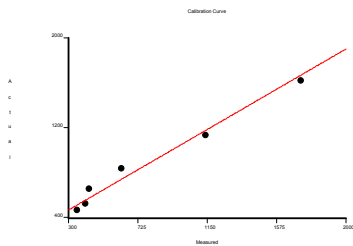
Coefficients:  
 a[0] = 0.000000e+000  
 a[1] = 9.915440e-001

#	Conc. (meas.)	Conc. (act.)	Conc. (corr.)	Error ppm	Error %
1	213.64	198.90	211.83	12.93	6.50
2	269.94	254.70	267.27	12.57	4.93
3	315.90	310.40	313.23	2.83	0.91
4	372.67	366.10	369.52	3.42	0.93
5	419.58	421.70	416.04	-5.66	-1.34
6	525.52	532.80	521.07	-11.73	-2.20
7	734.20	754.10	738.00	-26.10	-3.46
8	898.17	919.50	890.58	-28.92	-3.15
9	1088.18	1084.00	1078.98	-5.02	-0.46
10	1221.12	1204.00	1210.79	6.79	0.56
11	1443.00	1443.00	1430.80	-12.20	-0.85
12	1753.04	1801.00	1738.21	-62.79	-3.49

Average error = 3.03 %

(b) Data for the calibration line and estimated error

Figure 123: Calibration line plot and data for the species: CH<sub>4</sub> Low.



(a) Calibration plot

Calibration Report

Method: Untitled  
 Sample Set: H2O cal  
 Component: H2O

# File Name Title Temp. Press. Length  
 + cal h2o 1630.7.spaThu Jan 13 16:35:23 2005 (GMT+01:00) 150.0 759.9 0.20

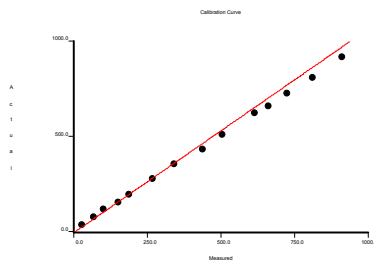
Coefficients:  
 a[0] = 3.145657e+001  
 a[1] = 8.402868e-001

#	Conc. (meas.)	Conc. (act.)	Conc. (corr.)	Error ppm	Error %
1	355.34	480.90	521.86	40.96	8.52
2	402.52	531.70	561.51	29.81	5.61
3	425.21	663.20	580.58	-82.62	-12.46
4	623.21	849.30	746.95	-102.35	-12.05
5	1140.70	1140.70	1181.79	41.09	3.60
6	1724.31	1630.70	1672.19	41.49	2.54

Average error = 8.41 %

(b) Data for the calibration line and estimated error

Figure 124: Calibration line plot and data for the species: H<sub>2</sub>O.



(a) Calibration plot

Calibration Report

Method: Untitled  
 Sample Set: HCN cal  
 Component: HCN

# File Name Title Temp. Press. Length  
 + cal hcn 815.spa Fri Nov 05 14:10:39 2004 (GMT+01:00) 150.0 759.9 0.20

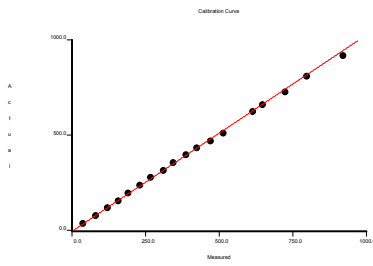
Coefficients:  
 a[0] = 0.000000e+000  
 a[1] = 1.064958e+000

#	Conc. (meas.)	Conc. (act.)	Conc. (corr.)	Error ppm	Error %
1	910.41	920.00	969.55	49.55	5.39
2	28.75	41.10	30.62	-10.48	-25.50
3	68.72	82.30	73.18	-9.12	-11.08
4	102.89	123.20	109.57	-13.63	-11.06
5	150.35	163.80	160.12	-3.68	-2.23
6	187.90	204.00	200.11	-3.89	-1.91
7	269.02	283.50	286.50	3.00	1.06
8	340.40	361.70	362.51	0.81	0.22
9	438.94	439.00	467.46	28.46	6.48
10	503.89	514.00	536.62	22.62	4.40
11	616.46	626.00	656.51	30.51	4.87
12	662.00	662.00	705.00	43.00	6.50
13	724.28	731.00	771.33	40.33	5.52
14	811.75	815.00	864.48	49.48	6.07

Average error = 8.98 %

(b) Data for the calibration line and estimated error

Figure 125: Calibration line plot and data for the species: HCN.



(a) Calibration plot

Calibration Report

Method: Untitled  
 Sample Set: NH3 cal  
 Component: NH3

# File Name Title Thu Nov 04 17:35:56 2004 (GMT+01:00) 150.0 759.9 0.20  
 + cal nh3 815.spa

Coefficients:  
 a[0] = 0.000000e+000  
 a[1] = 1.027757e+000

#	Conc. (meas.)	Conc. (act.)	Conc. (corr.)	Error ppm	Error %
1	920.00	920.00	945.54	25.54	2.78
2	38.99	41.10	40.07	-1.03	-2.50
3	80.84	82.30	83.08	0.78	0.95
4	122.76	123.20	126.17	2.97	2.41
5	153.01	163.80	163.42	-0.38	-0.23
6	191.53	204.00	196.85	-7.15	-3.51
7	230.12	243.90	236.51	-7.39	-3.03
8	267.65	283.50	275.08	-8.42	-2.97
9	312.94	322.70	321.62	-1.08	-0.33
10	343.84	361.70	353.38	-8.32	-2.30
11	389.79	400.30	400.61	0.31	0.08
12	424.96	438.60	436.76	-1.84	-0.42
13	472.03	476.60	485.13	8.53	1.79
14	513.85	514.00	528.11	14.11	2.75
15	614.76	626.00	631.83	5.83	0.93
16	647.58	662.00	665.55	3.55	0.54
17	724.62	731.00	744.73	13.73	1.88
18	796.73	815.00	818.84	3.84	0.47

Average error = 2.00 %

(b) Data for the calibration line and estimated error

Figure 126: Calibration line plot and data for the species: NH<sub>3</sub>.

---

## NOMENCLATURE

---

### Latin Symbols

A	Pre-exponential factor	[s <sup>-1</sup> ]
c <sub>j</sub>	Weight factor	-
D(E)	Distribution of activation energy	-
D <sub>p</sub>	Diameter of the particle	[m]
E	Activation Energy	[kJ/mol]
E <sub>0</sub>	Mean activation energy	[kJ/mol]
f(x)	Generic function of the unreacted initial material	-
H <sub>r</sub>	Heating rate	[°C/min]
k(T)	General Arrhenius expression	[s <sup>-1</sup> ]
m	Weight data from TGA run	[%]
n	Reaction order	-
R	Universal gas constant	[kJ/(K * mol)]
T	Temperature	[K]
t	Time	[s]
x	Unreacted fraction of the initial material	-

### Greek Symbols

α	Generic integer coefficient	-
α <sub>j</sub>	Reacted fraction for pseudo-components	-
β	Generic integer coefficient	-
c	Generic constant	-
ε	Surface radiative emissivity	-
F	Fraction of the market penetrated	[%]
σ	Variance	[%]

**Acronyms**

a.r.	as received
BAU	Business as Usual
BFB	Bubbling Fluidized Bed
CCS	Carbon Capture and Storage
CDM	Clean Development Mechanism
CFB	Circulating Fluidized Bed
CFD	Computational Fluid Dynamics
CHP	Combined Heat and Power
DAEM	Distributed Activation Energy Model
daf	dry and ash free
d.b.	dry basis
DDGS	Dry Distiller's Grains with Solubles
DKP	DiKetoPiperazines
DNA	DeoxyriboNucleic Acid
DSC	Differential Scanning Calorimeter
DTG	Differential Thermogravimetric curve
EEA	European Environment Agency
EFR	Entrained Flow Reactor
EU-15	European Union including member states up to 1 May 2004
EU-27	European Union including member states up at least to 1 September 2010
FFF	Fluid Fossil Fuels
FSS	Fermented Sewage Sludge
FTIR	Fourier Transform InfraRed
GC	Gas Chromatography
GCV	Gross Calorific Value
GHG	Greenhouse Gases



GWP	Global Warming Potential
HF	Heated Foil
HHV	Higher Heating Value
HR	Heating Rate
HT	Holding Time
ICE	Internal Combustion Engine
IEA	International Energy Agency
IGCC	Integrated Gasification and Combined Cycle
IGFC	Integrated Gasification and Fuel Cell
IGGT	Integrated Gasification and Gas Turbine
IPCC	Intergovernmental Panel for Climate Change
IR	InfraRed
LCA	Life Cycle Analysis
LHV	Low Heating Value
MCFC	Molten Carbonate Fuel Cell
MHV	Medium Heating Value
MSW	Municipal Solid Waste
NDIR	Non Dispersive InfraRed
NMR	Nuclear Magnetic Resonance
OECD	Organization for Economic Co-operation and Development
OPEC	Organization of the Petroleum Exporting Countries
ORC	Organic Rankine Cycle
ORFL	Olive Residue Fractionated + Leached
ORF	Olive Residue Fractionated
ORL	Olive Residue Leached
OR	Olive Residues
P-BFB	Pressurized - Bubbling Fluidized Bed
P-CFB	Pressurized - Circulating Fluidized Bed

## NOMENCLATURE

---

PKC	Palm Kernel Cake
PSL	Peach Stones Leached
PS	Peach Stones
RC	Rapeseed Cake
RDF	Refuse Derived Fuel
RES	Renewable Energy Sources
RNA	RiboNucleic Acid
SEM-EDX	Scanning Electron Microscopy – Energy Dispersive X-ray spectroscopy
SET	Strategic Energy Technology
SOFC	Solid Oxide Fuel Cell
SPR	Single Particle Reactor
TC	ThermoCouple
TGA	Thermogravimetric Analyzer
TPES	Total Primary Energy Supply
UNFCCC	United Nations Framework Convention on Climate Change
U.N.	United Nations
U.S.	United States
WEO	World Energy Outlook
WSL	Wheat Straw Leached
WS	Wheat Straw
XANES	X-ray Absorption Near Edge Structure spectroscopy
XPS	X-ray Photoelectron Spectroscopy

---

## ACKNOWLEDGEMENTS

---

The book you just finished to read or browsed through is filled with the sweat of four years of hard work and headaches which would have been close to unbearable if it had not been for the help and support of many people that I want to acknowledge at this point.

First of all, I would like to thank from the bottom of my heart my supervisor Wiebren de Jong. From the first e-mail that I sent you asking information about an opening advertised two years earlier (and this says a lot about our section's website!) you have always been supportive of me and my work, coping with my frequent outbursts, whether of joy or despair, and always bringing a rational side into the discussion even when my irrational side was clouding my mind. You have taught me a lot about chemistry, engineering and research and I think we have been a very good team during all these years! I really wish we will be able to collaborate again on many projects!

Secondly, I want to express my sincere gratitude to my promotor Ad Verkooijen. Together with precious scientific advises, you have always supported and shared my "social" view of energy and biomass and I have relished our discussions about nuclear Iran, peak oil and whether biomass was any better than photovoltaic! Thank you for entrusting me with the responsibility of giving a lecture in your course: the first time was not the best but the second still stands out as one of my best presenting performances so far! In the first years of my PhD you have pushed me many times to be more self confident and to trust my skills and my research and I cannot express how much this has meant to me and it permanently forged the scientist I am today; I hope that now, four years later I have changed your mind and maybe made you a little proud of our work. If I pass by Mango please have ready a bottle of your wine!

A special *kiitos* to Professor Mikko Hupa and Maria Zevenhoven for welcoming me at the Process chemistry centre at Åbo Akademi and for their personal and scientific support in the months I spent in Finland. I believe the work we have done together is of high quality but what I will really never forget are the "delicious" berry wines of Finland! The next time you will happen to be around Florence I will treat you to some very different flavours!

A special thank goes to Duco Bosma. Many times people say "I couldn't have done it without him" and yet in a few times like this one, this is actually true! Without your constant help on the TGA, FTIR and even heated grid even though you did not work with us anymore!, I would have either given up or simply smashed the whole thing with an hammer! So, thank you, thank you, thank you!

I would also like to acknowledge the very productive collaboration with Dr. Stelios Arvelakis who provided us interesting ideas and fuels during the project.

An obvious but sincere thank goes to the European Commission for funding my research and for employing me afterwards! To all the Marie Curie INECSE fellows: I think it will be hard to find more entertaining project meetings than the ones we managed to arrange, good luck to you all and we will for sure meet again!

I want to acknowledge the “main characters” of the best working environment that could possibly be found: Aylin, Bart, Christian, Elif, Jelan, John, Richard and of course the Italian crew, Gianluca, Mattia e Stefano, you made working at P&E feeling like a holiday and of course, with a sip of White Russian working days magically seemed so short...!

Many thanks go surely to old and new office mates: Calim, Eleonora, Emiliano, Hans, Marcin, Martina, Miguel and Ryan; thanks for listening to my almost constant complaints about Dutch lifestyle and for not bothering me when I was not in the right mood!

Deep thanks to all the rest of the P&E: Eveline and Judith, Leslie and Helma, Aravind, Ernesto Marta, Michel, Richard, Xiangmei, Zuopeng, the guys in the workshop, I assure you you all have left a deep memory in me! A good luck to Michel and all the “new ones” with their projects!

I would like also to express my appreciation for my student Jeroen Gout; you worked hard and well on the heated grid and the numerical model and I am sure that I would have struggled much to finish that work if it had not been for your help, good luck with your future career!

A special thank to Francesco Montella and Dr. Ferioli who freed me from the hell of Zusterlaan and brought me to the paradise of Schipluiden: you probably saved my mental health!

To my good friends Andrea, Eduardo, Muneeb and Edite: your friendship lifted my spirit and brightened up many dark days; even if life is bringing us far and keeping us busy with a lot of “adult” issues, you should know that you have a place in my thoughts.

Per gli amici che ancora resistono in Italia: siamo rimasti pochi ma buoni! Ale, Gabri, Gianluca e Jo, non ho certo bisogno di dottorarmi per esprimervi i miei sentimenti e ringraziamenti per essere sempre li’ quando ne ho bisogno...se non lo avete ancora capito dopo piu’ di dieci anni allora non so che farci! La mia speranza e’ che un giorno i nostri figli possano giocare insieme senza dover prendere un aereo per vedersi...

Grazie mille a Chiara per aver messo uno splendido tocco artistico in questo, altrimenti arido, lavoro scientifico.

An ironic acknowledgement goes to Peter Jansens; even if everything else in the management of the department was not exactly perfect, you hired the love of my life and for this I will always remember you!

Last but not least I have to express my fondest *merci* to my lovely Mahsa: since the first moment you entered into my life that night at the Persian restaurant, I knew you would never leave my heart. We had to tame each other in the years but I could not possibly see my life without you. Thanks for bringing in my life that balance that had been missing for the previous 26 years. Our love is a praise to the power of Negroni!

Caro Leo, adesso che hai finalmente trovato la tua strada sono sicuro che in 6 anni saremo a festeggiare la tua laurea...per adesso non mi abbandonare su Xbox Live senno' mi uccidono subito!

Cari babbo, mamma, nonne, zii, Greta e Matteino: la vita da emigrato e' gia' difficile di suo ma il pensiero di vivere una vita lontano da casa e da voi e' ancora peggio...resistete ancora qualche anno poi cerchero' di rimediare anche a questo. Nel frattempo grazie per non esservi ancora dimenticati di me, per quella speciale capacita' di farmi sentire adulto e bambino al tempo stesso e per l'aiuto costante ad affrontare le responsabilita' della vita...senza il vostro supporto sarei crollato molto tempo fa.

And finally let me thank God, Allah, Vishnu, Fate or however you want to name it for my strength and my luck.



---

## SELECTED PUBLICATIONS

---

### JOURNAL PAPERS

- J. Giuntoli, W. de Jong, S. Arvelakis, H. Spliethoff and A. H. M. Verkooyen, 'Quantitative and kinetic TG-FTIR study of biomass residue pyrolysis: Dry distiller's grains with solubles (DDGS) and chicken manure'. *Journal of Analytical and Applied Pyrolysis*, 85(1-2): 301-312, 2009.
- J. Giuntoli, S. Arvelakis, H. Spliethoff, W. de Jong and A. H. M. Verkooyen, 'Quantitative and Kinetic Thermogravimetric Fourier Transform Infrared (TG-FTIR) Study of Pyrolysis of Agricultural Residues: Influence of Different Pre-treatments'. *Energy & Fuels*, 23(11): 5695-5706, 2009.
- J. Giuntoli, W. de Jong, A. H. M. Verkooyen, P. Piotrowska, M. Zevenhoven and M. Hupa, 'Combustion characteristics of biomass residues and bio-wastes: fate of fuel-N'. *Energy & Fuels*, 24: 5309-5319, 2010.
- J. Giuntoli, J. Gout, A. H. M. Verkooyen and W. de Jong, 'Characterization of fast pyrolysis of dry distiller's grains (DDGS) and palm kernel cake using a heated foil reactor: nitrogen chemistry and reactor modeling'. *Ind. Eng. Chem. Res.*, 2010. Submitted for publication.
- G. Marcotullio, E. Krisanti, J. Giuntoli and W. de Jong, 'Selective production of hemicellulose derived carbohydrates from wheat straw using dilute HCl or FeCl<sub>3</sub> solutions under mild conditions. Thermo-gravimetric analysis of the solid residues'. *Bioresource Technology*, 2010. Submitted for publication.

### INTERNATIONAL CONFERENCE PAPERS:

#### *Oral presentations*

- J. Giuntoli, W. de Jong, S. Arvelakis, H. Spliethoff and A. H. M. Verkooyen, 'Influence of pre-treatments on thermal conversion of agricultural residues: effects on nitrogen chemistry during pyrolysis'. *Proceedings of the 16<sup>th</sup> European Biomass Conference and Exhibition*. Berlin, Germany, May 7 - 11, 2007.
- J. Giuntoli, W. de Jong, S. Arvelakis, H. Spliethoff and A. H. M. Verkooyen, 'Quantitative and kinetic TG-FTIR study of biomass residue pyrolysis: Dry distiller's grains and solubles (DDGS) and chicken manure'.

*Proceedings of the 18<sup>th</sup> International Symposium on Analytical and Applied Pyrolysis*. Lanzarote, Spain, May 18 - 23, 2008.

- J. Giuntoli, W. de Jong, M. Zevenhoven, P. Piotrowska, E. Monedero, M. Hupa and A. H. M. Verkooijen, 'NO<sub>x</sub> release during combustion of bio-fuel by-products: Dry Distiller's Grains with Solubles (DDGS) and Palm Kernel Cake'. *Proceedings of the 6<sup>th</sup> International Biofuels Conference*. New Delhi, India, March 4 - 5, 2009.
- J. Giuntoli, J. Gout, A. H. M. Verkooijen and W. de Jong, 'Characterization of fast pyrolysis of biomass fuels using a heated grid reactor: Nitrogen chemistry and reactor modeling'. *Proceedings of the 18<sup>th</sup> European Biomass Conference and Exhibition*. Lyon, France, May 3 - 7, 2010.

*Poster presentations*

- J. Giuntoli, S. Arvelakis, W. de Jong, H. Spliethoff and A. H. M. Verkooijen, 'Effects of pre-treatments on the nitrogen behaviour in pyrolysis of agricultural residues'. *Proceedings of the conference Biomass for Energy*. Bruges, Belgium, September 25 - 26, 2006.
- J. Giuntoli, S. Arvelakis, W. de Jong, H. Spliethoff and A. H. M. Verkooijen, 'Characterization of pre-treated biomass waste under pyrolysis conditions: Nitrogen chemistry and kinetic analysis'. *Proceedings of the 7<sup>th</sup> Netherlands Process technology Symposium (NPS7)*. Veldhoven, The Netherlands, October 29 - 30, 2007.

INDEPENDENT COLLABORATIONS WITH THE INTERNET PORTAL AGI ENERGIA

- J. Giuntoli, 'L' energia da biomassa' (*Energy from biomass*), published online on 18/12/2007.  
URL: <http://83.216.172.76/AGIEnergia/Notizia.aspx?idd=89&id=58&ante=0>
- J. Giuntoli, 'Emissioni di gas serra dai trasporti: esistono soluzioni o tutti in bicicletta?' (*Greenhous gas emissions from the transport sector: are there any solutions of shall we all get a bike?*), published online on 17/02/2009.  
URL: <http://83.216.172.76/AGIEnergia/Notizia.aspx?idd=313&id=20&ante=0>
- J. Giuntoli, 'Trasformare la crisi in opportunità: il G20 e la ripresa sostenibile' (*Transforming crisis in opportunity: the G20 meeting and sustainable recovery*), published online on 22/09/2009.  
URL: <http://83.216.172.76/AGIEnergia/Notizia.aspx?idd=397&id=25&ante=0>



---

## CURRICULUM VITAE

---

The author Jacopo Giuntoli was born on June 10, 1981 in Florence, Italy. He completed his high school studies at the “Liceo Scientifico Coluccio Salutati” in Montecatini Terme, Italy, in the year 2000 with the highest grade. In the same year he enrolled at “Politecnico di Milano” where he obtained his Bachelor degree with honors in Mechanical Engineering in the year 2003. He then continued his studies at “Politecnico di Milano” obtaining his Master degree with honors in Energy Engineering in the year 2005. For his final master thesis he worked during an internship at the refinery ENI in Sannazzaro de’ Burgondi, Italy, where he assisted the process technology engineer in the startup of a plant for the desulfurization of gasoline from catalytic cracking. In 2006 he was appointed as a PhD promovendum at Delft University of Technology in the Energy Technology section, 3mE Faculty, under the supervision of Professor Ad Verkooijen and Dr. Ir. Wiebren de Jong. During this period he also worked as a visiting researcher in the group of Process Chemistry Centre at Åbo Akademi University, Turku (Finland), under the supervision of Professor Mikko Hupa. The results of his doctoral research have been published in various high-ranking international journals and presented at several international conferences and symposia in the field of renewable energies and fuel characterization.

Currently, Jacopo is employed as a PostDoc Grantholder at the Joint Research Centre - Institute for Energy, where he carries out research on biomass for energy in support of various European Commission policies.